PROCESSED KIMBERLITE – WATER INTERACTIONS IN DIAMOND MINE WASTE, EKATI DIAMOND MINE, N.W.T., CANADA

by

Hugh Andrew Rollo

A thesis submitted to the Department of Geological Sciences and Geological Engineering
in conformity with the requirements for the degree of
Master of Science

Queen's University
Kingston, Ontario, Canada

July 2003

Abstract

The Ekati Diamond Mine is located approximately 300 km northeast of Yellowknife in the Canadian Arctic. Processed kimberlite ore is stored in a modified lake basin that has been isolated from the local drainage system by an ice-core dam. Surficial deposition of crushed kimberlite increases the potential for reaction of the minerals in the waste, resulting in an increase in dissolved solids in the storage facility water. Low total dissolved solids and little buffering capacity characterize the local surface water, the ultimate recipient of discharge from the storage facility.

The goals of this project are to chemically and mineralogically define the components of the mineral-water system that exists within the processed kimberlite containment facility, and to use major element water chemistry to determine the minerals and processes controlling the water chemistry observed. Both solid and water samples were collected from the processed kimberlite containment facility, from 2000 to 2002, in order to define and characterize the chemical and physical components of the system. Reaction path and inverse computer modeling, together with water and mineral data, have been used to deduce the minerals and processes most important in controlling water chemistry and to predict how these processes will affect the evolution of the system.

The kimberlite ore is dominated by volcaniclastic kimberlite with lenses and blocks of epiclastic sediments throughout the pipe. The mineralogy is predominantly serpentine and forsteritic olivine, with lesser calcite, spinel, pyroxene, garnet, phlogopite, pyrite, and smectite. Minor sulphate and sulphide minerals are indicated to be concentrated in mud xenoclasts found throughout the kimberlite. Major dissolved constituents in containment facility water include SO_4, Mg, Ca, Na, K, and HCO_3 with the first three dominating the system. Water pH is approximately neutral, total Fe concentrations do not exceed 3 mg/L, and iron oxide staining is not present in the processed kimberlite. These data suggest that oxidation of sulphide minerals is not significant at present and that dissolution of SO_4-bearing minerals, although volumetrically minor, is one of the most significant contributions to water quality. Reaction path and inverse modeling indicate that evaporation, and reactions occurring during mineral processing are the most significant controls on water chemistry in the containment facility.

Acknowledgements

I would like to thank Jim Millard, John Witteman, Tom Unka, Matthew Otto, Mike Tanguay, Rob MacLean, Camille Douglas, and all personnel of the Ekati Environment Department for their technical and logistical support of this research. Without their help much of this work would not have been possible.

I would also like to thank my family for their emotional, and sometimes financial, support throughout my degree. Their love and encouragement have meant more to me than they know, and for this I am forever grateful.

Most importantly, I would like to acknowledge my supervisor, Dr. Heather Jamieson, for her unending support and confidence. She made me feel like a colleague, while providing me with the invaluable guidance and encouragement of an advisor. Her enthusiasm has been a motivation to me throughout this project and she has made my Masters everything that I hoped it would be, and more. For this I am sincerely grateful. Thank you Heather.

Finally, I would like to dedicate this thesis to my Grandfather, Hugh Redpath. He showed me the satisfaction of taking on a challenge and the pride that comes from working hard.

Table of Contents

List of Figures

List of Tables

List of Abbreviations

(aq)	aqueous
(l)	liquid
(s)	solid
a	activity
ABA	acid-base accounting
AMD	acid mine drainage
AP	acid generating potential
BCMWLAP	British Columbia Ministry of Water, Land, and Air Protection
D.D.H.	diamond drill hole
DIC	dissolved inorganic carbon
DOC	dissolved organic carbon
EDS	energy dispersive spectroscopy
EMPA	electron microprobe analysis
FOV	field of view
HDPE	high density polyethylene
HMS	heavy medium separation
HPGR	high pressure grinding rolls
IAP	ion-activity product
k_{sp}	solubility product
LLCF	Long Lake Containment Facility
LLNL	Lawrence Livermore National Laboratory
m	molality (moles solute/ kg solution)
NGSO	National Guidelines and Standards Office
NP	neutralization potential
NPR	neutralization potential ratio
PVC	polyvinyl chloride
QA/QC	quality assurance/quality control
SI	saturation index
WQD	water quality guideline
XRD	X-ray diffraction
$\delta^{34}S$	stable sulphur isotopic ratio - measured in permil (‰)

1 Introduction

Since the 1991 discovery of the first economically viable diamondiferous kimberlites in the Canadian Arctic, diamond mining has become one of Canada's newest mining sectors (Baker et al., 2003). Operations began at Canada's first diamond mine, Ekati, in August 1998, while the second fully operational diamond mine, Diavik, began operations in January 2003. It is estimated that the combined production at these two mines will account for approximately 10% to 15% of the world diamond production by value by the end of 2003 (Baker et al., 2003) making the diamond mining sector a significant contributor to the northern economy and Canada as a whole.

The Arctic environment is characterized by an extreme climate with short cool summers and long extremely cold winters. As well, surface waters of the region are relatively pristine with low total dissolved solids and little buffering capacity. This study is concerned with the investigation of the waste produced from Canada's first operating diamond mine and its potential effects on the environment.

The Ekati Diamond Mine is located within the Lac de Gras drainage basin, which forms the headwaters of the Coppermine River that flows north to the Arctic Ocean. Waste kimberlite and process water, produced from mining and processing kimberlite ore, is stored in an engineered containment facility, formerly two lake basins. Water from the processed kimberlite containment facility is discharged to the receiving environment, provided it meets regulatory requirements stipulated in the Ekati Water License agreement. Surficial deposition of crushed kimberlite material increases the potential for reaction and dissolution of the minerals in the waste resulting in an increase in dissolved solids in the storage facility water, which will then be released to the environment. Diamond mining in the Canadian Arctic is in its infancy and as a result, few studies have been conducted to investigate the behaviour of diamond mine waste, specifically in the Arctic environment.

As one of the first field-based investigations of diamond mine waste in the Canadian Arctic, the objectives of this research are: 1) to chemically and mineralogically define the components of the mineral-water system that exists within the processed kimberlite containment facility, and 2) to use major element water chemistry to determine the minerals and processes most significantly controlling the water chemistry observed in the processed kimberlite containment facility. This project is the first in a series of studies concerned with the investigation of the geochemical behaviour of diamond mine waste, with the ultimate goal of developing criteria to help predict the long-term downstream water quality that results from diamond mining operations.

1.1 Ekati Diamond Mine

1.1.1 Location

The Ekati mine is located approximately 300 km northeast of Yellowknife, N.W.T. in Canada's Northwest Territories (Figure 1.1). Access to the mine is possible by air all year as well as by an ice-road, from Yellowknife, during the mid-winter months. The Ekati claim block contains kimberlite pipes that are part of the Lac de Gras kimberlite field. The mine is approximately 200 km south of the Arctic Circle in the area of continuous permafrost (Rescan Environmental Services Inc., 1996b).

1.1.2 Climate

The Ekati mine is in the Low Arctic Ecoclimate region where summers are short and cool and winters are long and extremely cold (Rescan Environmental Services Inc., 1996b). The mean annual temperature in the region is –11.8°C with summer (July to August) temperatures up to 20°C, and winter temperatures as low as –35°C. The mean annual precipitation ranges from approximately 250 mm to 300 mm and is split almost evenly between rain and snowfall water equivalent. Most of the precipitation occurs between late August and early October, but some precipitation falls all year long. As well, the average annual open-water evaporation is approximately 200mm to 350 mm (Rescan Environmental Services Inc., 1996b).

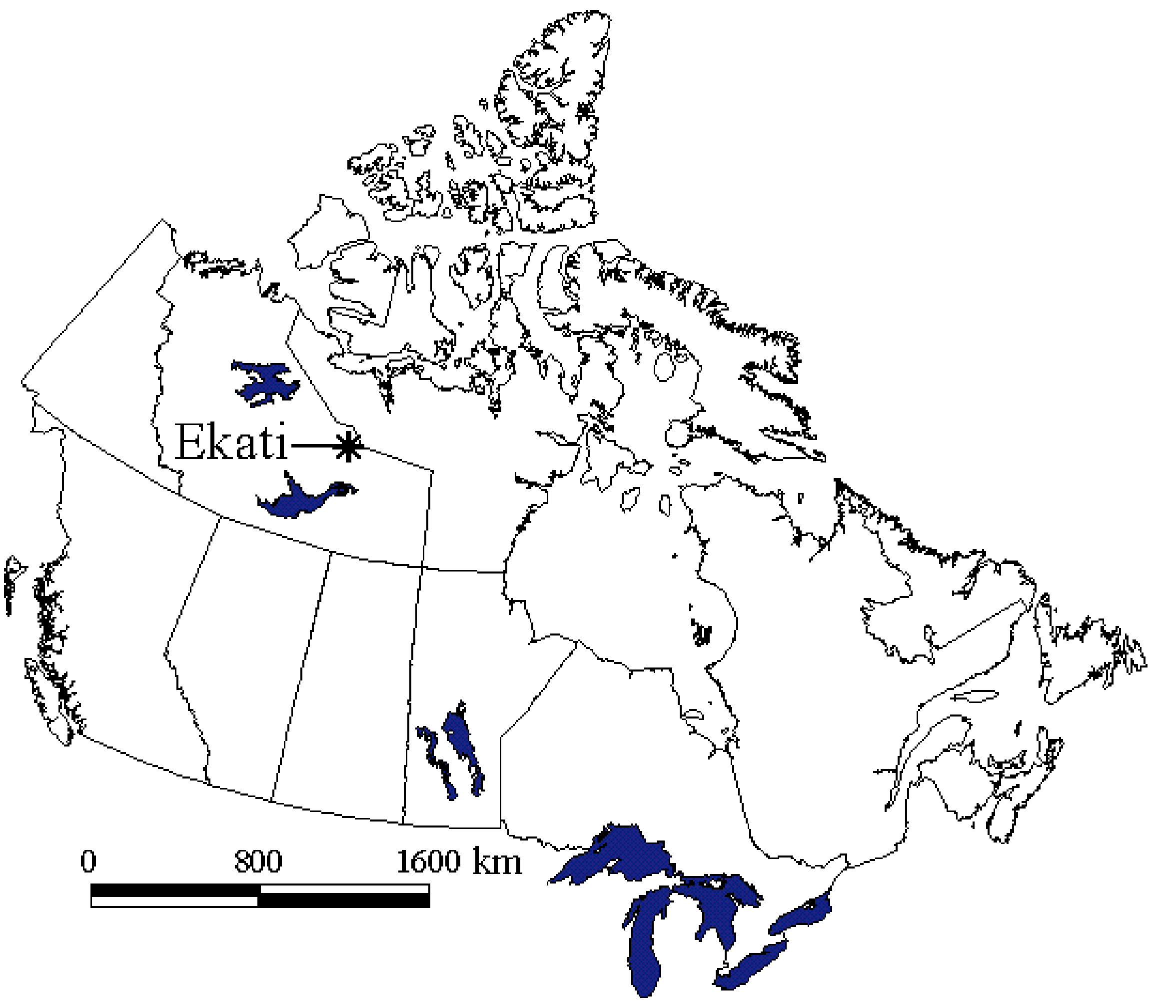

Figure 1.1: Map of Canada showing the location of the Ekati mine

1.1.3 Geological Setting

The Ekati Diamond Mine is located in the central Lac de Gras region of the Slave Geological Province (Figure 1.2), which is an Archean portion of the North American Craton. The Slave is a relatively small craton (about 213 000 km^2) (Pell, 1997a) that contains some of the world's oldest rocks dated at 3.96 Ga (Isachsen and Bowring, 1994). The Slave is composed predominantly of polydeformed 2.7 Ga metasedimentary and subordinate metavolcanic rocks of the Yellowknife Supergroup intruded by large volumes of 2.6 Ga granitoid rocks (Hoffman, 1989; Pell, 1997a) (Figure 1.3), and is divided into three main Archean domains: a) the ancient crustal Anton Terrane to the west, b) the younger juvenile Hackett River Arc domain to the east, and c) the central accretionary Contwoyto Terrane (Kusky, 1989) (Figure 1.2). The Sleepy Dragon Terrane, indicated in Figure 1.2, is thought to be a basement nappe related to the Anton Terrane to the west (Kusky, 1989).

1.1.4 Regional Geology

The diamondiferous pipes of the Lac de Gras kimberlite field are located in a northwest trending zone in the central accretionary Contwoyto domain (Carlson et al., 1998; Kjarsgaard et al., 2002) (Figure 1.2). The main lithologies found in the Lac de Gras region are metasedimentary schists, migmatites, and various syn- and post-tectonic intrusive complexes, all of which are Archean in age (Carlson et al., 1995). There are also five different Proterozoic dyke swarms varying in age from 2.4 Ga to 1.27 Ga that crop out around the property (Carlson et al., 1995). Kimberlites are the only Phanerozoic

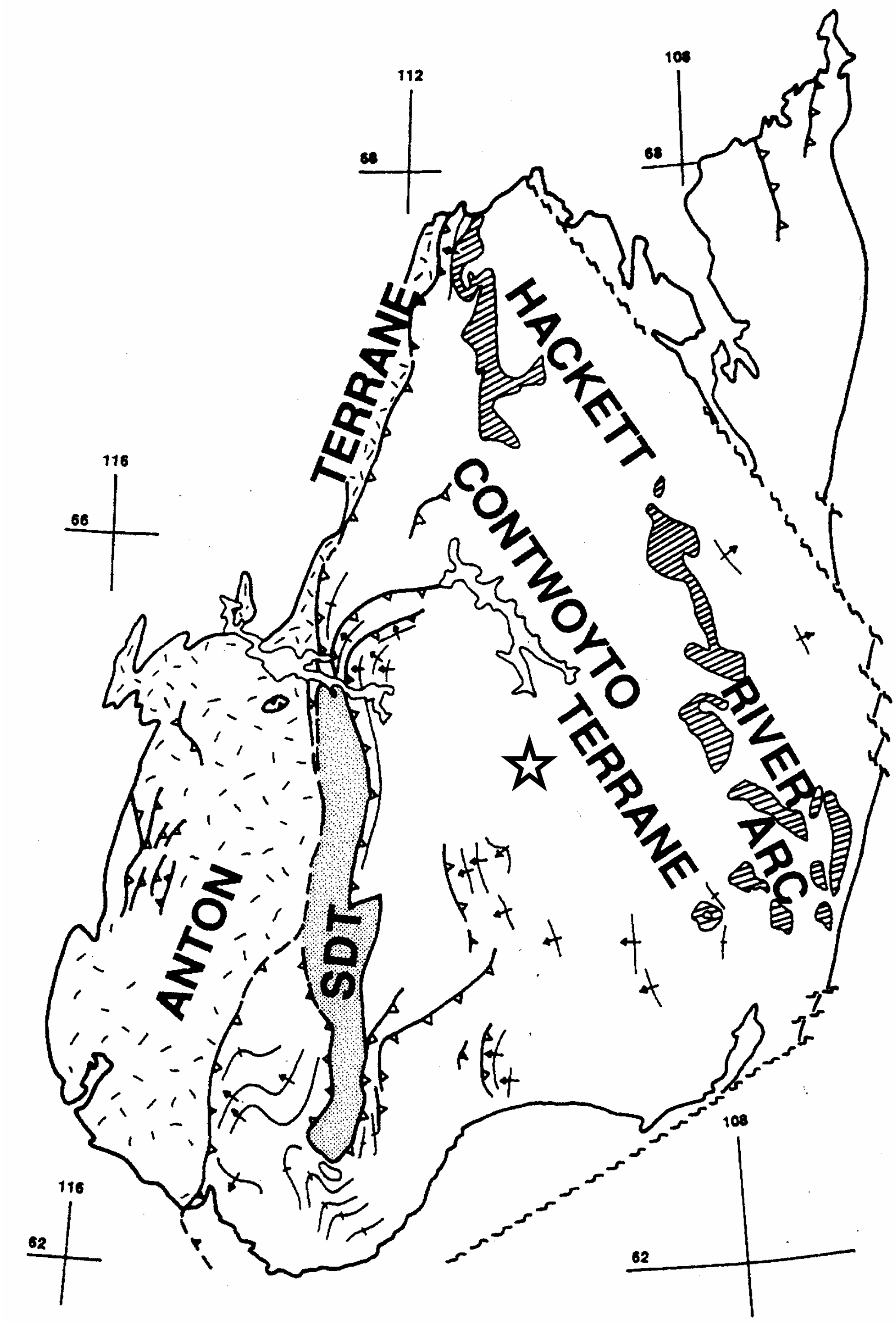

Figure 1.2: Map of the Slave Craton, indicating the location of the Anton Terrane, Sleepy Dragon Terrane (SDT), Contwoyto Terrane, and the Hacket River Arc. Cross hairs indicate location of lines of longitude and latitude for scale (modified from Kusky, 1989). The star indicates the approximate location of the Ekati Diamond Mine in the central Contwoyto Terrane

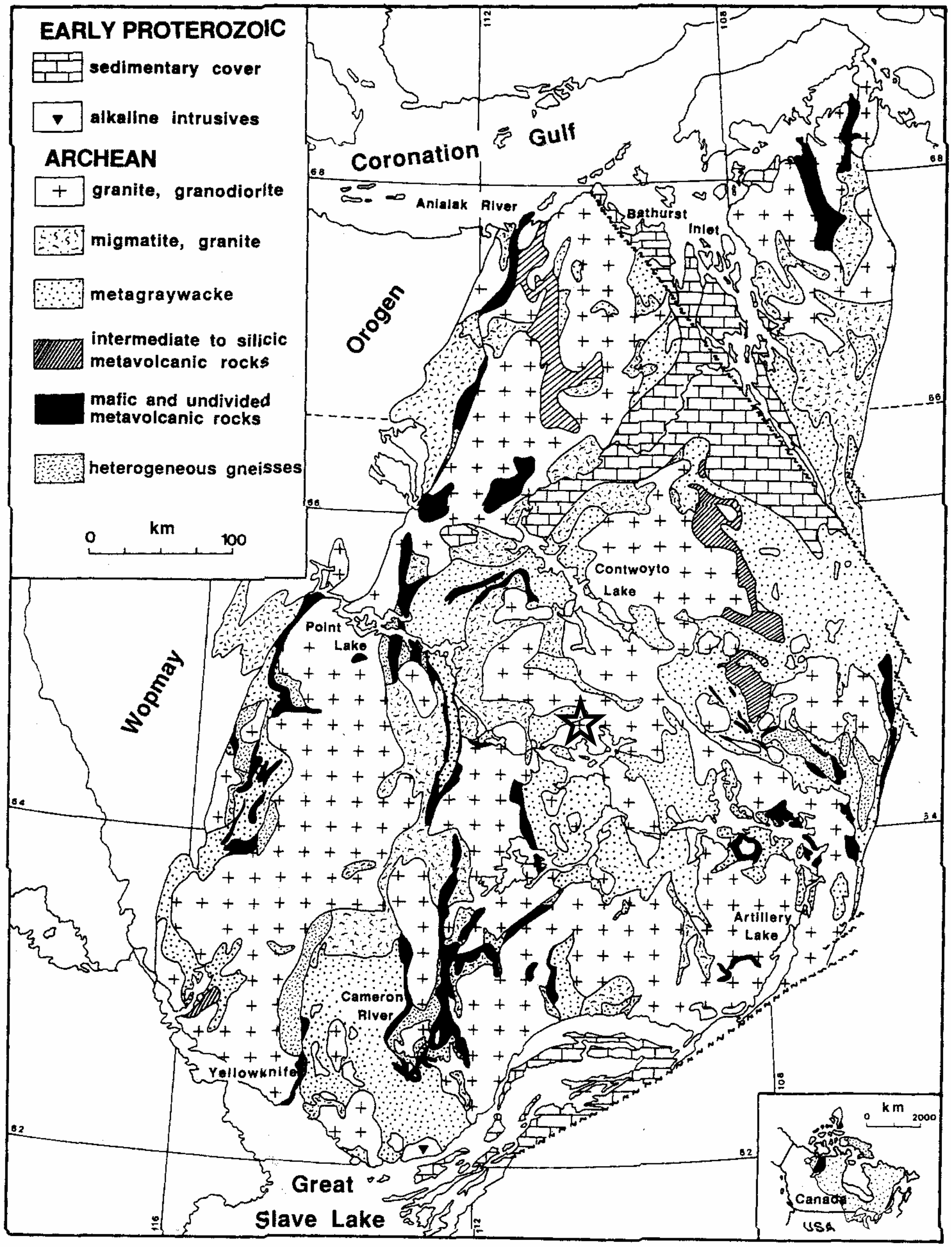

Figure 1.3: Geology of the Slave Geological Province (modified from Kusky, 1989). The star indicates the location of Ekati, just north of Lac de Gras.

age rocks known in the Lac de Gras area. However, fossiliferous mudstone xenoliths found within many kimberlites of the region indicate the presence of a thin cover of Phanerozoic age sediments during emplacement of the Lac de Gras kimberlites, which has been eroded away since their intrusion. Dinoflagellate and fish fossils found within the mudstone are of marine origin suggesting that the Western Interior Seaway extended over the Slave, for at least a short time, during the Upper Cretaceous (Doyle et al., 1998; Field and Scott-Smith, 1998; Nassichuk and Dyke, 1998; Nassichuk and McIntyre, 1995). Fossils found within Lac de Gras kimberlites range in age from 97 Ma to 56 Ma (Nassichuk and McIntyre, 1995).

There appear to have been two phases of kimberlite emplacement in this region occurring at 74-67 Ma and 58-46 Ma respectively (Kjarsgaard et al., 2002). Rb/Sr age-dating of an Ekati kimberlite yielded an age of 52 +/- 1.2 Ma (Carlson et al., 1995), which is in good agreement with paleontological constraints.

Lac de Gras kimberlites are typically steep-sided conical shaped pipes 2 to 12 hectares in surface area; however most do not crop out at the surface but are found as erosional features underlying many of the lakes in the region (Pell, 1997b; Wright, 1999). Crater facies kimberlite dominate the Lac de Gras field, but minor amounts of diatreme and massive hypabyssal facies kimberlite have been documented as well (Wright, 1999). Two main lithotypes are found : 1) medium to light green volcaniclastic kimberlite breccia, and 2) medium green to black, olivine macrocrystal kimberlite (Pell, 1997b). Crater facies kimberlite is typified by volcaniclastic and epiclastic breccias with occasional well defined layering. Diatreme facies has both lithotypyes present and hypabyssal facies kimberlite is massive with 50% olivine macrocrysts set in a uniform groundmass (Pell, 1997b).

Volcaniclastic material includes pyroclastic ash tuffs, lapilli tuffs, and olivine crystal-rich tuffs. Epiclastic material includes mudstones, siltstones, sandstones, and, rarely, conglomerates, some of which are thought to be of kimberlitic origin (Carlson et al., 1998). Diatreme and hypabyssal kimberlites, when present, are sometimes found cross-cutting volcaniclastic kimberlite phases and less typically appear to completely replace diatreme and crater facies materials (Berg and Carlson, 1998).

1.1.5 Panda Kimberlite

The processed kimberlite studied as part of this investigation was derived from the top portion of the Panda Kimberlite, the first pipe to be mined at Ekati. The host rock of the Panda kimberlite is a white to grey, medium to coarse-grained, weakly foliated to massive biotite granodiorite with an average composition of 40% quartz, 45% feldspar, and 15% biotite. The Panda host rock is relatively unaltered, but weakly altered zones are present and contain 1% to 3% epidote (Kjarsgaard et al., 2002; Rescan Environmental Services Inc., 1996b).

The Panda kimberlite, like all kimberlites at Ekati, originally occupied the bottom of a small lake, which has been drained, and the overlying 15 m to 25 m of glacial and lacustrine sediments have been stripped. The original pre-mining surface area of the Panda pipe was approximately 3.1 hectares (Carlson et al., 1998).

Like many kimberlites of the Lac de Gras area, the Panda kimberlite is dominated by crater facies to a depth of approximately 300 metres. The main rock types found in the

Panda kimberlite are volcaniclastic (olivine crystal tuffs, lapilli tuffs, and tuff breccias) in origin, but epiclastic sediments are also present as lenses and blocks throughout the pipe (Carlson et al., 1998). The units of the Panda pipe commonly have well-defined, centimeter scale beds of variable thickness that are continuous over tens of metres and are typically flat lying in the central regions of the pipe, but become more steeply dipping towards the margins of the pipe (Carlson et al., 1998).

The olivine crystal tuff is characterized by a pelletal texture with an abundance of olivine macrocrysts ranging in sizes up to 1 cm (Carlson et al., 1998). Garnet, chrome diopside, and chromite are also present as xenocrysts set in a very fine-grained altered matrix. The lapilli are typically composed of olivine macrocrysts with rims (<0.2 mm) of altered magmatic kimberlite. Serpentine, carbonate, and clay minerals dominate the fine-grained matrix material of this unit (Carlson et al., 1998).

The lapilli tuff displays a range in olivine grain sizes (0.5mm to 1.5 cm), olivine concentrations (20% to 90%), ash content, and degree of sorting. The mudstone xenoclasts typically found in this unit are highly fissile and irregularly shaped, ranging in size from 2 mm to 50 mm. It is common to find olivine crystals embedded into the margin of these clasts (Carlson et al., 1998).

Tuff breccia units within the Panda kimberlite are clast-supported with coarse olivine macrocrysts ranging in size from 6 mm to 20 mm (Carlson et al., 1998). This unit typically contains a high concentration (15% to 30%) of xenoliths, which include mudstone, granite, quartz sandstone, limestone, and mantle nodule fragments and is commonly found to be intergradational with coarse-grained lapilli tuff. The two units are thought to be different size fractions of a single volcaniclastic accumulation (Carlson et al., 1998).

1.1.6 Ore Processing

The extraction of diamonds from the kimberlite ore is carried out by a complex sequence of steps involving crushing, washing, sorting, and concentration of the diamonds. Water for the processing circuit is pumped from a water-reclaim barge, located within the processed kimberlite containment facility (section 3.2.1.3). The following discussion is an overview of the steps involved in mineral processing and ore waste generation at Ekati as described in the Environmental Impact Statement prepared for Ekati by Rescan Environmental Services Inc.(Rescan Environmental Services Inc., 1996a). Figure 1.4 is a flowchart illustrating the various steps involved in mineral processing at Ekati to be referred to during the following discussion.

Kimberlite ore is mined by open pit and hauled to the process plant as large boulder-sized material. The first step in the processing circuit is to crush the run-of-mine ore to a particle size of 150 mm and 300 mm, which is sent to the coarse-ore stockpile warehouse, located adjacent to the processing plant. The kimberlite ore is taken from the stockpile warehouse, by conveyor, to the mineral processing plant. Immediately before entering the process plant a secondary crushing reduces the 150 mm to 300 mm diameter ore particles to <75 mm in diameter.

The crushed ore is conveyed to a primary scrubber and sizer that uses water to disaggregate and remove soft fines and clay particles from the crushed ore as well as sort the ore into <4 mm and >4mm size fractions.

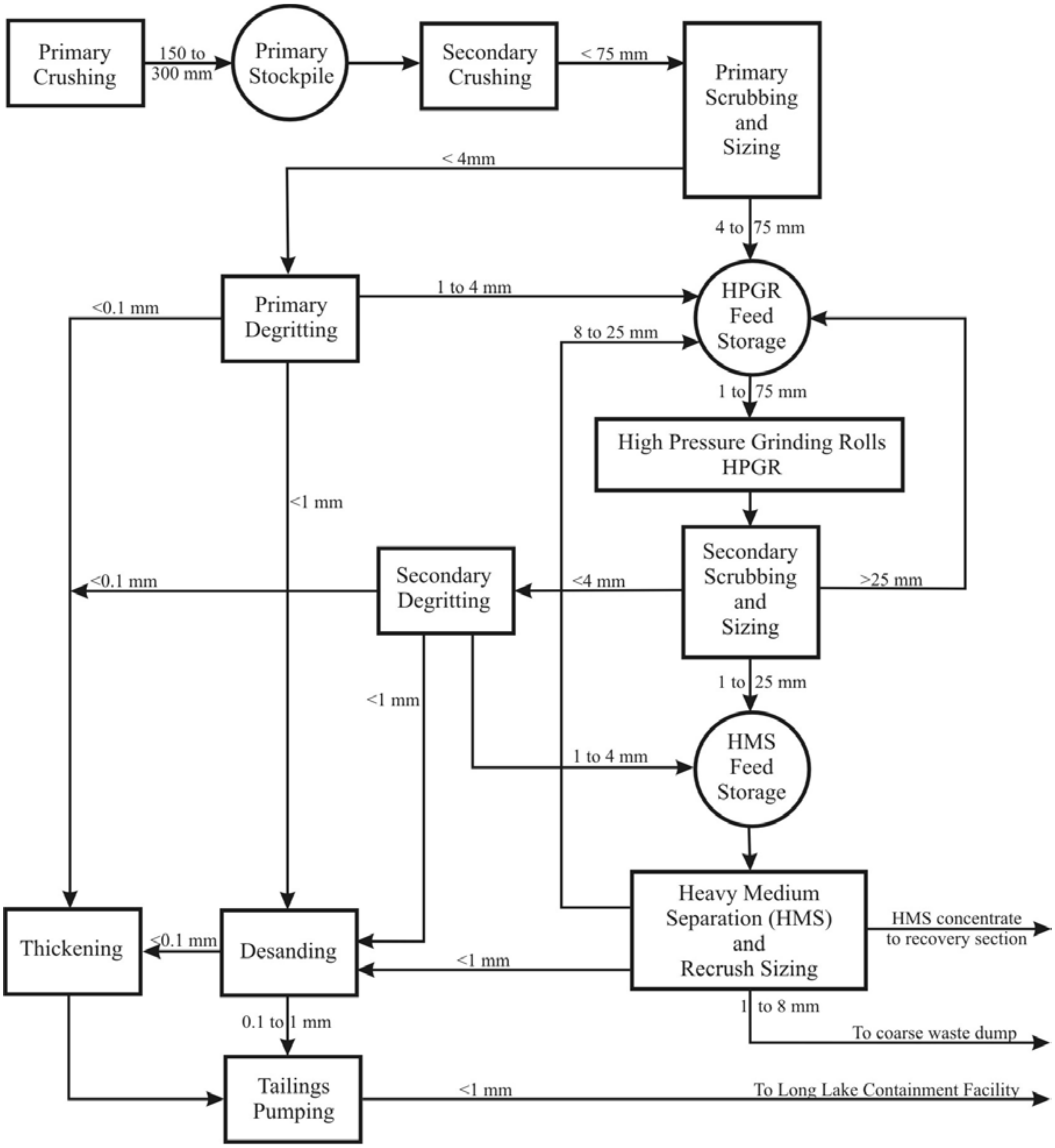

Figure 1.4: Flowchart of the primary concentration step of the mineral processing circuit at Ekati.

The >4 mm size fraction continues on to the high pressure grinding rolls (HPGR) while the <4 mm size fraction is sent to the primary degritting station. Degritting and desanding is used in the mineral processing circuit to help remove fine-grained material from the products of the various crushing, cleaning, and separating stages. From the primary degritting step, all material that is 1 to 4 mm is sent to the HPGR rolls while all material < 1mm is sent to the settling tank to be pumped to the processed kimberlite fines containment facility.

The feed to the HPGR is the sized material (1 to 75 mm) from the primary scrubbing and primary degritting sections as well as 8 to 25 mm material from the heavy medium separation section (to be discussed later). The purpose of the HPGR is to crush the ore without destroying any diamonds. The material produced during this step is then conveyed to a secondary scrubbing and sizing section to help break-up the compacted cake produced by the HPGR.

The secondary sizing step separates the ore into three size fractions: 1) <4 mm, 2) >25mm, and 3) 4 to 25 mm. The <4 mm size fraction is sent to the secondary degritting section where it is cleaned of all material <1mm, which is sent to the processed kimberlite containment facility. The >25 mm ore size fraction is sent back through the HPGR to ensure that all material passing on to the next step in the circuit is <25 mm. The 4 to 25 mm size fraction is sent on to the heavy medium separation step.

Heavy medium separation (HMS) is a gravity ore concentration step that uses water charged with fine-grained ferrosilicon to create a density divide between low-density (non-diamond bearing) material and the high-density (diamond bearing) material. High-density material sinks to the bottom of the HMS unit while the low-density material floats to the top and is removed. This step produces a small volume of highly concentrated ore that is then suitable for the final diamond recovery steps of the mineral processing circuit. The low-density material removed at this step is sent to a sizing screen to be divided into three size fractions: a) 8 to 25 mm, b) 1 to 8 mm, and c) < 1 mm. The 8 to 25 mm fraction is sent back through the HPGR processing step, the 1 to 8 mm fraction becomes coarse tailings that is hauled to the coarse kimberlite reject pile, and the <1 mm size fraction is sent to the kimberlite containment facility.

The final recovery of diamonds from the high-density fraction of the HMS is carried out by magnetic and X-ray separation techniques. Unlike the crushing, scrubbing, and sizing steps of primary ore concentration, the final recovery of diamonds is a dry process with a very small amount of solid waste produced.

1.1.7 Ore Waste

Two fractions of waste are produced at Ekati: a) 1 to 8 mm sized material (coarse kimberlite reject material), and b) <1 mm sized material (processed kimberlite fines).

The coarse kimberlite waste produced during the HMS step of the mineral processing circuit accounts for approximately 10 to 20 weight percent of the total waste produced at Ekati. This material is dewatered and subsequently conveyed to a pile located adjacent to the process plant (Figure 1.5A). From this point, the coarse kimberlite reject material is hauled by truck to a subaerial disposal site immediately adjacent to the main mine site.

The processed kimberlite fines, produced by the degritting and desanding steps of the mineral processing circuit, accounts for approximately 80 to 90 weight percent of the total waste produced at Ekati. Kimberlite fines are thickened in the process plant before

A)

B)

Figure 1.5: **A)** Coarse kimberlite reject pile adjacent to the mineral processing plant. From here, this material is hauled to a sub-aerial disposal site. **B)** Spigot discharging kimberlite fines and process water from the mineral processing plant to the kimberlite containment facility. The fines are hydraulically pumped at a solids content of approximately 40% to 50%.

being pumped to the kimberlite fines containment facility at a solids content of approximately 45 percent by weight. To assist in the settling of fine particles from the process water, a coagulant and flocculant are added to the processed kimberlite fines slurry before it enters the thickening tank. The dose of coagulant (PERCOL 368) and flocculant (PERCOL E-10) added to the Panda fines slurry is approximately 35 g and 120 g per tonne of ore processed, respectively (EBA Engineering Consultants Ltd., 1998).

1.1.8 Processed Kimberlite Fines Containment Facility

After thickening, the processed kimberlite fines are hydraulically pumped from the process plant to the processed kimberlite fines containment facility, known as the Long Lake Containment Facility (LLCF) (Figure 1.5B). The Long Lake Containment Facility is located approximately three kilometers west of the main Ekati mine site. Two basins, formerly lakes, underlie the LLCF: Nancy Lake in the north and Long Lake in the south (Figure 1.6). The containment facility is divided into a series of four cells (B, C, D, and E) that are separated by three pervious filter dykes (dykes B, C, and D) designed to help reduce turbidity in the LLCF runoff (EBA Engineering Consultants Ltd., 1995) (Figure 1.7).

The core of the filter dykes is composed of gravel to boulder sized waste granite material, obtained during mining operations, and the upstream side of each dyke has a covering of till obtained from the initial stripping of overburden in open-pit preparation (EBA Engineering Consultants Ltd., 1995). This poorly sorted cover material acts as a filter that helps to slow water flow within the LLCF, thereby allowing fine suspended material an opportunity to settle out of the water column on the face of each dyke. An

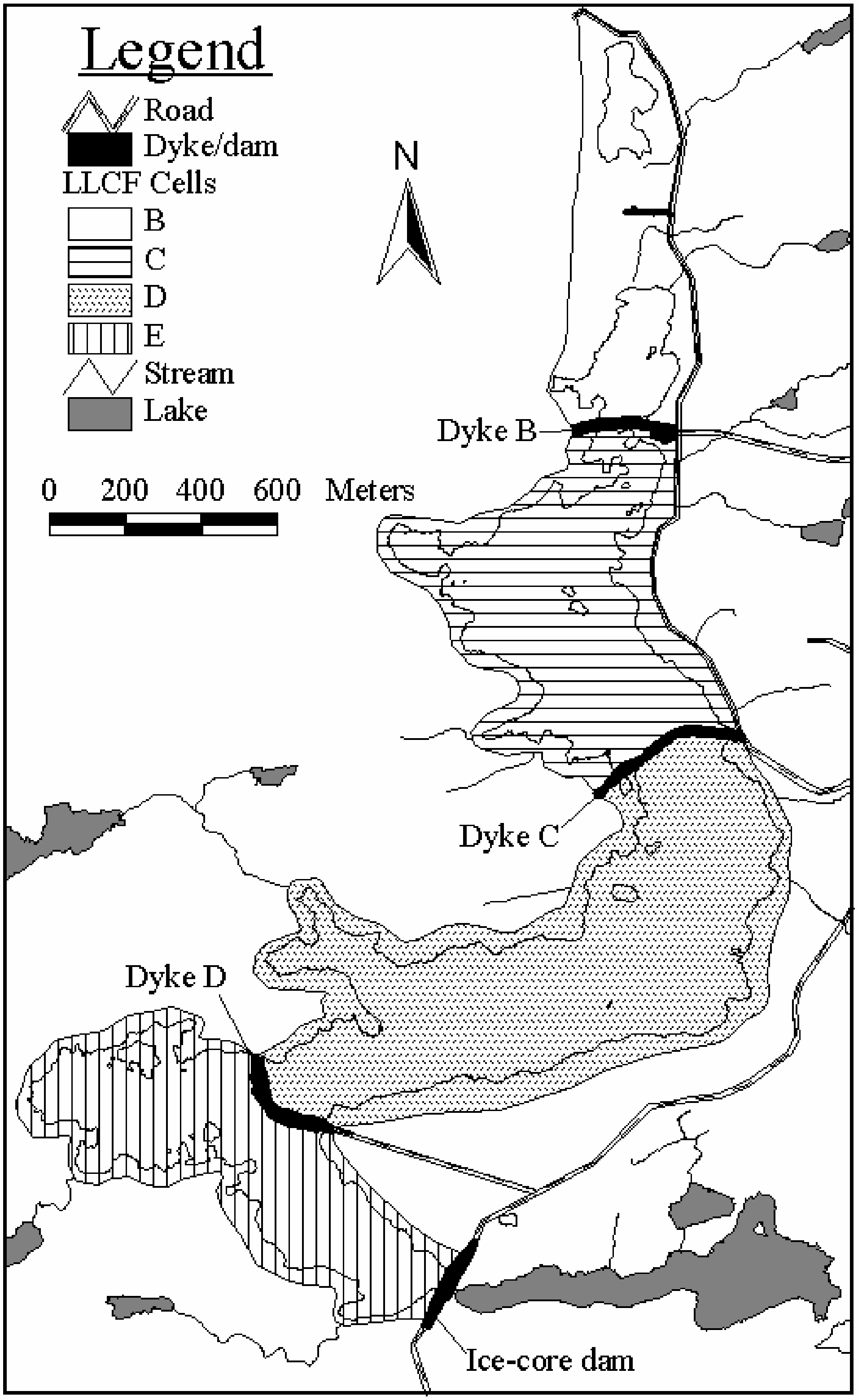

Figure 1.6: Long Lake Containment Facility.

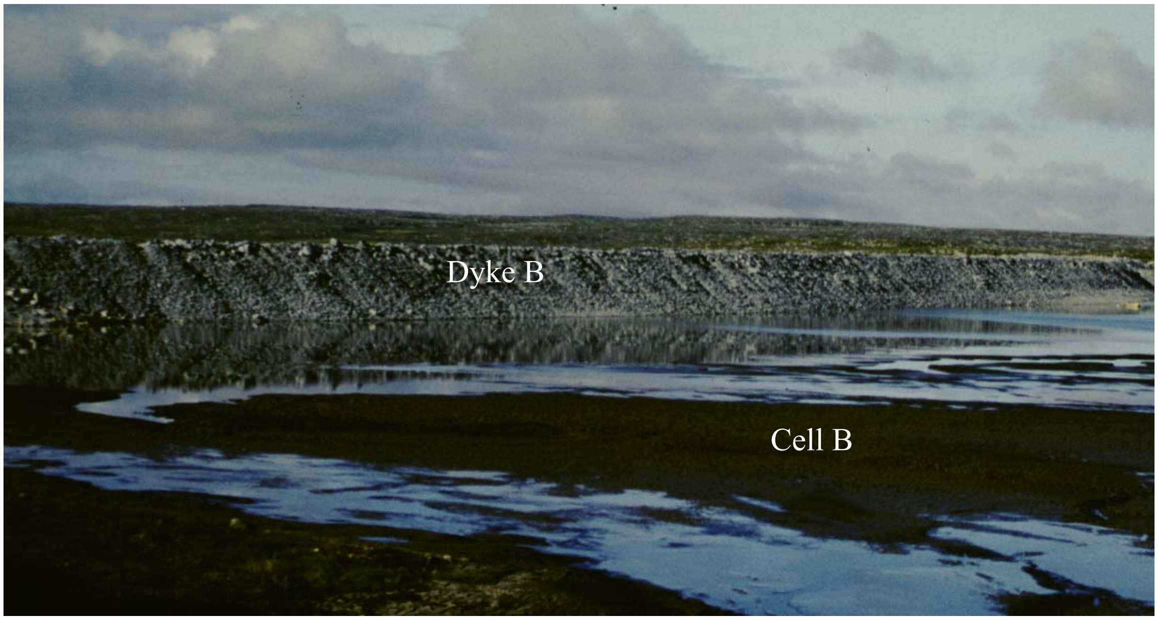

Figure 1.7: View (looking southwest) of Dyke B. This is an example of the pervious filter dykes constructed in the LLCF to help reduce turbidity in the LLCF discharge from Cell E.

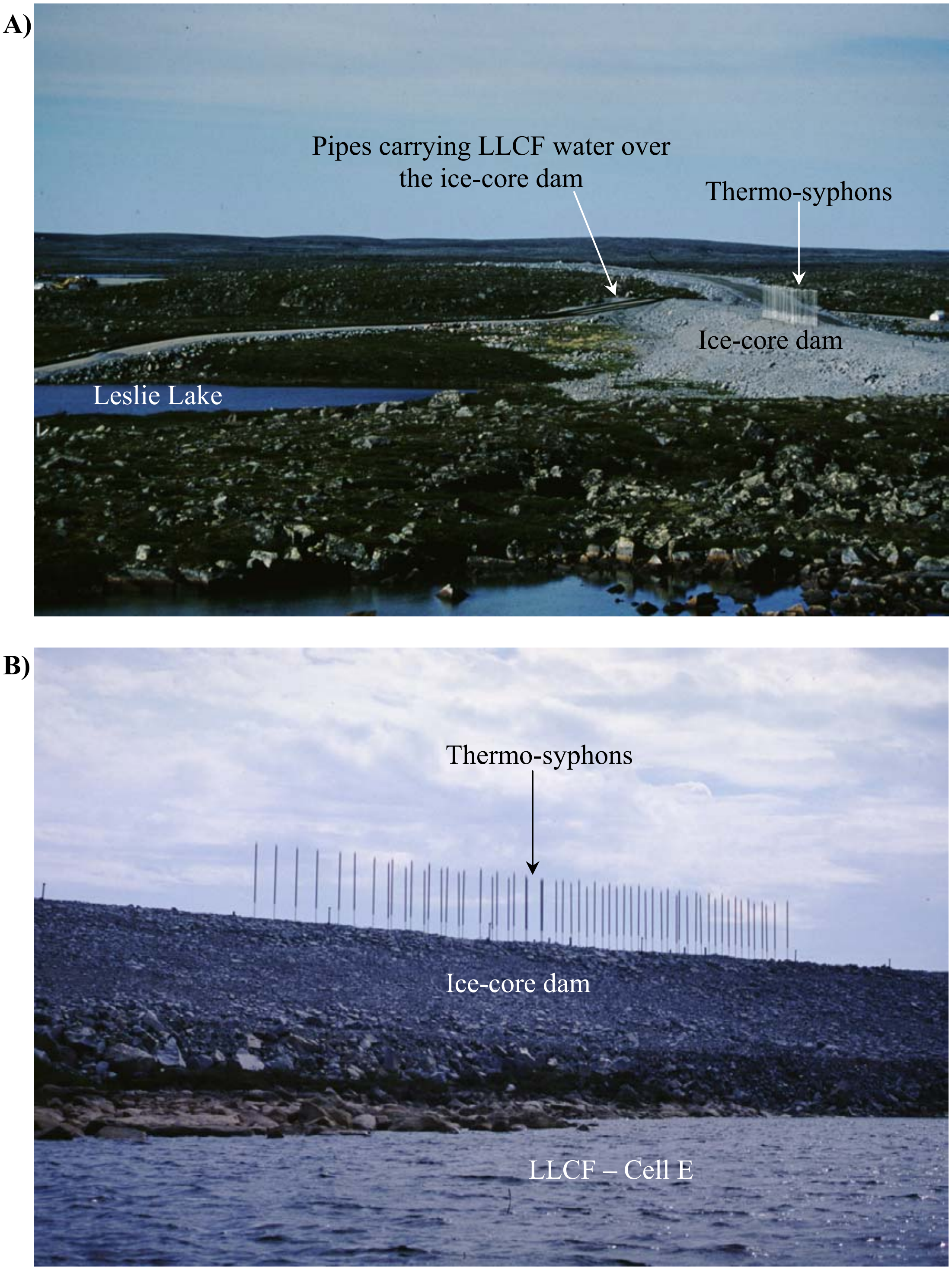

Figure 1.8: **A)** View (looking west) of the ice-core dam at the southern end of the LLCF. A diesel powered water pump sends discharge water from the LLCF into Leslie Lake through a set of pipes running over the dam. **B)** Close-up view (looking south) of the ice-core dam and Thermo-syphons.

impermeable ice-core dam has been constructed at the south end of cell E (outlet dam) (Figure 1.8). This dam was constructed in the winter months in order to create a solid ice-core. Long pipes containing liquid carbon dioxide, called Thermo-syphons, were installed into the ice-core during construction of the dam. The liquid carbon-dioxide sinks to the bottom of the pipe. Heat in the ice-core is absorbed by the liquid carbon dioxide causing it to vaporize and rise to the top of the pipes that emerge from the top of the dam (Figure 1.8). Wind blowing through the pipes cools the carbon dioxide, which condenses and drips back down to the bottom of the pipe to remove more heat from the ice-core (EBA Engineering Consultants Ltd., 1995). This passive refrigeration system ensures that the ice-core remains frozen even during the summer months. The purpose of this dam is to isolate the containment facility from the natural drainage of the region, thus allowing control over the discharge of LLCF water to the surrounding environment. Any water leaving the LLCF has to be pumped over the outlet dam to the receiving environment (Leslie Lake).

Each cell within the LLCF is filled with processed kimberlite discharge, in order from north to south, starting with Cell B. Therefore, the first processed kimberlite fines discharged to the LLCF were deposited in the northernmost portion of Cell B.

1.1.9 Long Lake Containment Facility Stratigraphy

Drilling of the LLCF fines was conducted in March 2001 in order to obtain information for this project on the vertical structure of kimberlite fines within the facility. The drilling was carried out using a Cold Region Research Engineering Laboratory (CCREL) barrel and a split spoon sampler (Figure 1.9). The CRREL barrel was used in

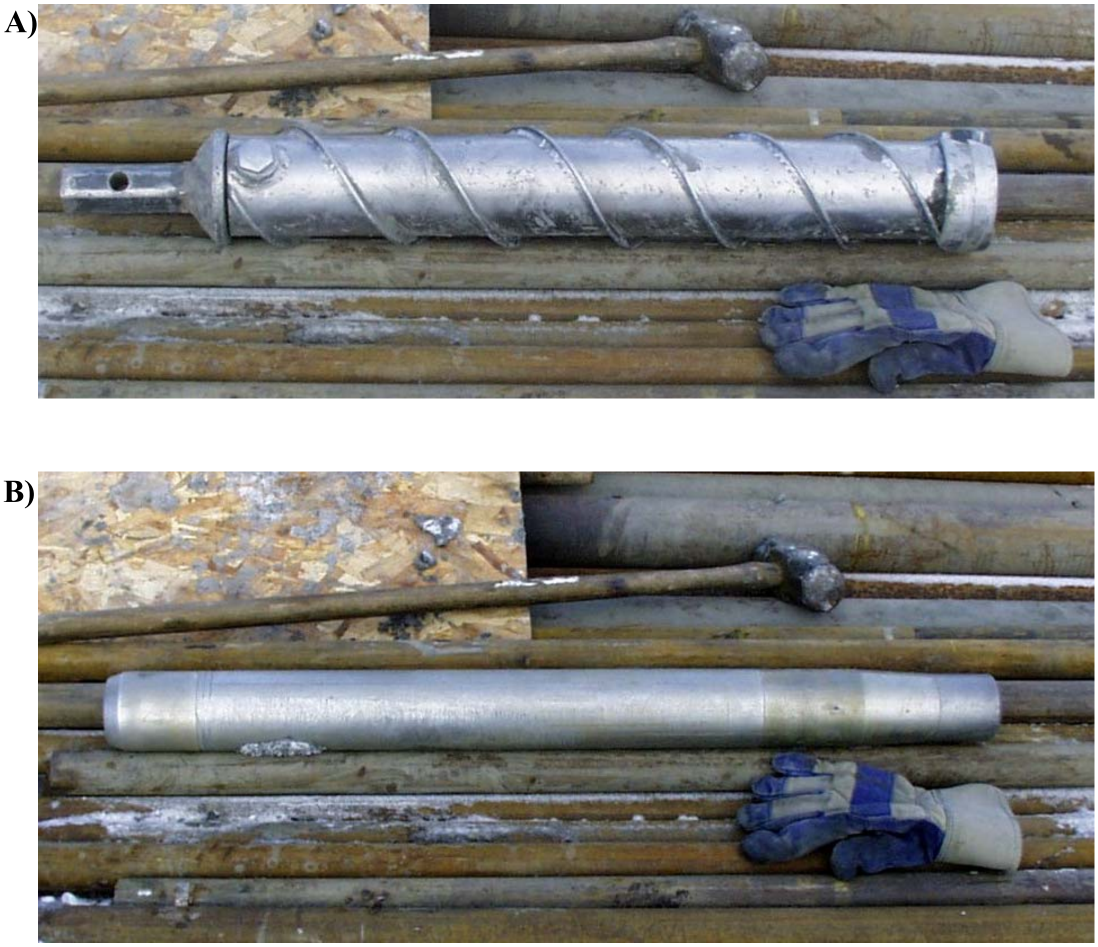

Figure 1.9: A) CRREL barrel used to sample the LLCF fines during the winter 2001 drilling program. Core samples produced are approximately 600 cm in length and 7.6 cm in diameter. **B)** Split spoon sampler used in the winter 2001 drilling program. Note that the bottom of the sampler is on the left of the photo. This sampler was pounded into the ground using a drop hammer attached to the drill head. The core samples were collected in a cellulose acetate butyrate sleeve that was inserted into the split spoon before it was driven into the ground. Dimensions of the core collected with this sampler are 6.4 cm by 600 cm.

the uppermost three to four metres where the ground was very cold and the split spoon sampler was used for the remainder of the hole.

Once collected, CRREL samples were extruded from the barrel, logged, wrapped in plastic film, placed in plastic sample bags, and kept outside to ensure they remained frozen. The split spoon was fitted with a cellulose acetate butyrate liner that received the kimberlite fines as the sampler was pounded into the ground. Once collected, the liner containing the sample was removed from the split spoon, logged, capped, and placed outside to ensure that it remained frozen as well.

Figure 1.10 is a cross section of the northern portion of cell B showing the stratigraphy of the kimberlite fines. Three distinct units are present in the northern portion of cell B. The upper layer extends to approximately 1 m below the surface and is characterized by dense, ice-bonded kimberlite fines with a distinctive lack of visible ice layers or lenses. This represents the active layer that develops during the warm summer months. There are no ice lenses or layers in this unit because as the active layer develops in the summer any ice that was present melts and drains from the fines. All pore-water samples reported in this study have been collected from this layer during the summer season when the active layer has thawed.

The boundary between the first and second layer is very sharp at approximately 1 m depth with the second layer extending to approximately 5 m below the surface of the fines. This zone is typified by centimetre-scale rhythmic layering of kimberlite fines and ice that is reminiscent of glacial-lacustrine varves. Each of the rhythmic layers is composed of fines with little to no ice, grading upwards to solid ice with little to no fines. This unit is frozen, but as the base of this layer is approached the fines become softer and

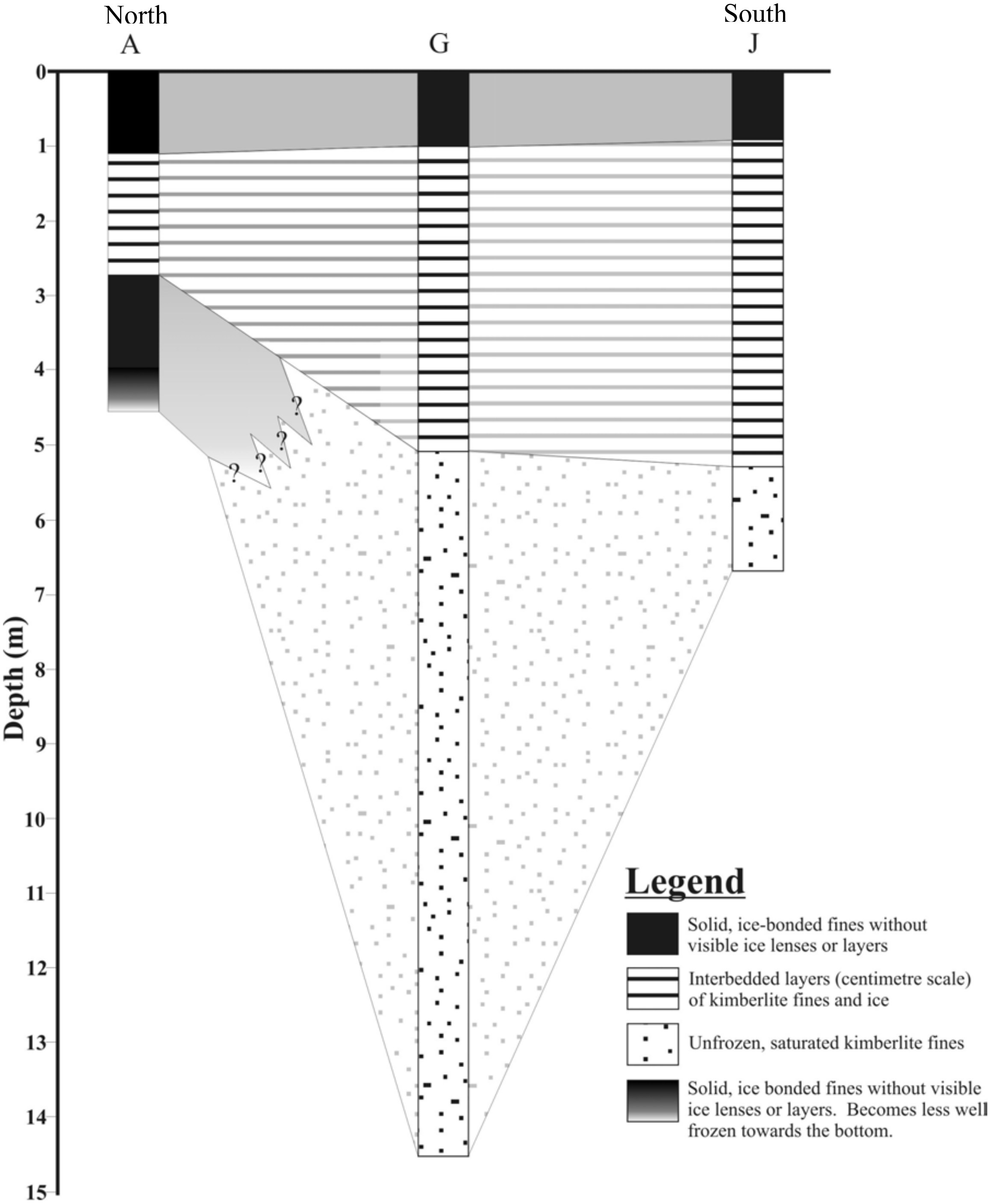

Figure 1.10: North-south cross-section through the northern portion of the LLCF (Cell B) showing the stratigraphy of the processed kimberlite fines as determined from drill core collected in March 2001. Refer to figure 3.2 for March 2001 drilling locations.

less well frozen until the kimberlite fines become completely unfrozen at a depth of approximately 5 m. This banded layer is interpreted to represent winter deposition of kimberlite fines. A low angle fan forms around the discharge point with the discharge stream meandering across the surface, allowing fines to settle out of suspension while the water drains on top (Figure 1.11). In the summer this water flows downstream over and through the fan deposits. However, during winter deposition it is cold enough (approximately –30^{o}C) for the water to freeze within a few hours. As the stream of fines and water from the discharge spigot flows over the frozen substrate, the fines settle out first with the water freezing on top. This process happens repeatedly, preserving the graded layers observed in drill core.

The third unit extends from the frozen-unfrozen interface at 5 m depth to the bottom of the containment facility. This zone is composed of completely saturated unfrozen processed kimberlite fines.

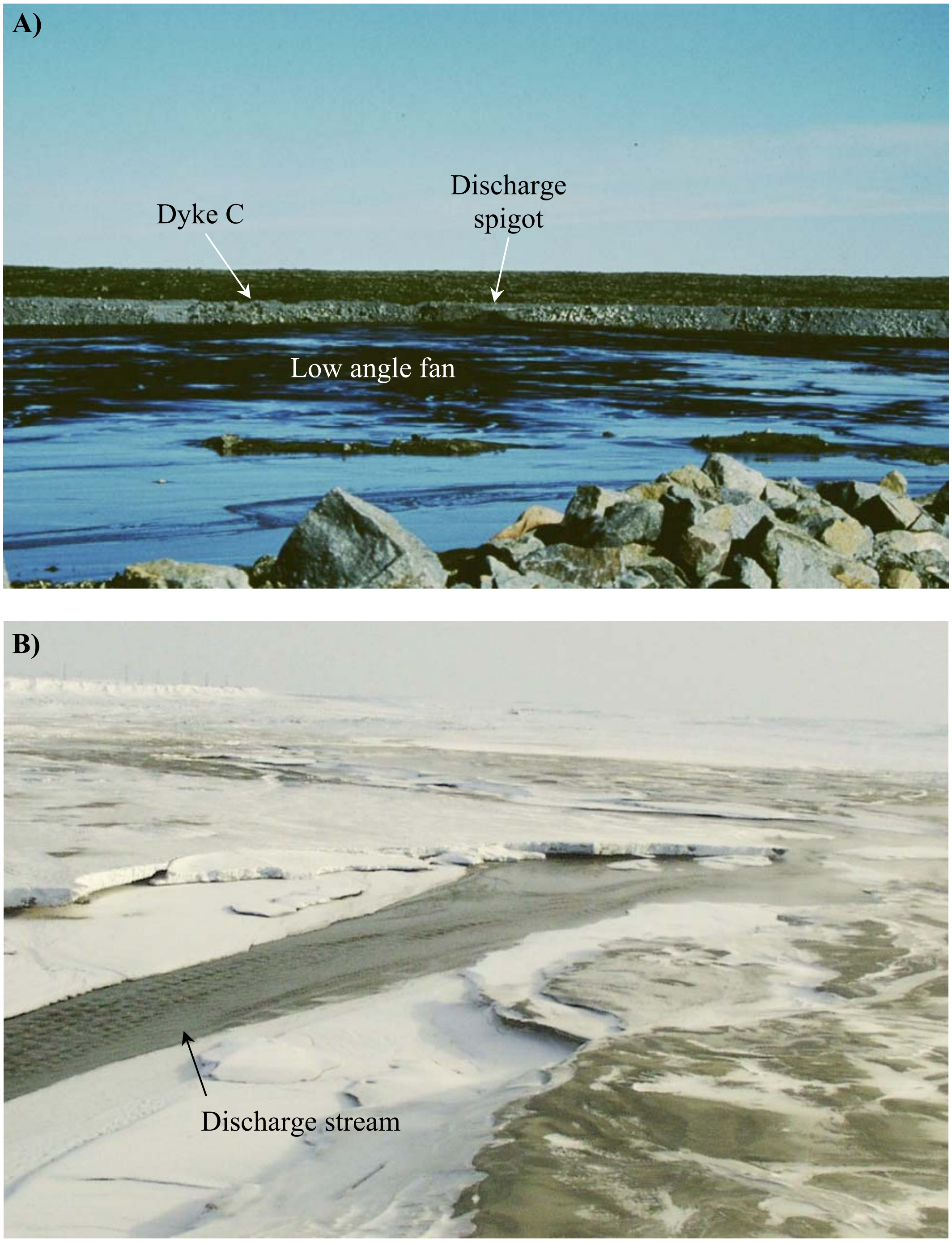

Figure 1.11: **A)** View (looking northwest) of Dyke C, in July 2001. The arrow indicates the location of the discharge spigot. Note the low angle fan created by the processed kimberlite fines discharging into the LLCF. Also note the water that is flowing over the fan. **B)** View (looking south from Dyke C) of the discharge stream from spigot in March 2001. Note how the stream spreads over the surface of the fan in the upper part of the photo.

2 Literature Review

2.1 Acid Mine Drainage

One of the most significant concerns associated with mine waste is the generation of acid mine drainage (AMD). Therefore, any discussion of sulphide-bearing mine waste should discuss the basic principles of AMD and AMD prediction.

AMD occurs when sulphide-bearing mine waste is oxidized on exposure to air and water (Mine Environment Neutral Drainage (MEND) Project, 1991). Oxidation of sulphide minerals, the most common of which is pyrite (FeS_2), results in the generation of acidity as well as Fe, Mn, Al, and SO_4 (Evangelou and Zhang, 1995). Often, this drainage becomes extremely acidic with pH values as low as -3.6 reported (Nordstrom et al., 2000). This low pH discharge is an environmental concern because aquatic biota and plant life are negatively affected at pH's under approximately 5.6, and are unable to survive under more acidic conditions (Drever, 1997; Evangelou and Zhang, 1995; Jambor et al., 2002). Another environmental concern associated with AMD is that potentially toxic elements such as Pb, Hg, Cd, Ni, Zn, Cu, and As tend to be associated with pyrite and are much more soluble at low pH, oxidizing conditions (Drever, 1997).

2.1.1 Pyrite Oxidation

Pyrite oxidation is a complex process involving chemical, biological, and electrochemical reactions (Evangelou and Zhang, 1995). The reactions controlling pyrite oxidation are (Evangelou and Zhang, 1995; Singer and Stumm, 1970):

$$FeS_2 + 7/2\,O_2 + H_2O \longrightarrow Fe^{2+} + 2SO_4^{2-} + 2H^+, \qquad (1)$$

$$FeS_2 + 14Fe^{3+} + 8H_2O \longrightarrow 15Fe^{2+} + 16H^+ + 2SO_4^{2-}, \qquad (2)$$

$$Fe^{2+} + 1/4\,O_2 + H^+ \longrightarrow Fe^{3+} + 1/2\,H_2O, \qquad (3)$$

$$Fe^{3+} + 3H_2O \longrightarrow Fe(OH)_{3(s)} + 3H^+. \qquad (4)$$

As can be seen from the above reactions, O_2 and Fe^{3+} are the major oxidants of pyrite. The Fe^{2+} produced from the oxidation of pyrite by equation (1) or (2) is oxidized to Fe^{3+} following equation (3), which can be microbially catalyzed by the iron oxidizing bacteria *Acidithiobacillus ferrooxidans*. Finally, Fe^{3+} may be removed from solution through the precipitation of Fe-oxyhydroxides if the pH increases (Evangelou and Zhang, 1995). It should also be noted that the hydrolysis of Fe^{3+} is also a potential source of acid generation (equation 4).

At pH<4.5, Fe^{3+} is the most effective pyrite oxidant and the resulting rate of pyrite oxidation is dependant on the rate of Fe^{3+} production (Evangelou and Zhang, 1995). Therefore, under low pH conditions, reaction (3) becomes the rate limiting step and oxidation of pyrite can be represented by equations (2) and (3).

At circumneutral pH, the rate of abiotic Fe^{2+} oxidation increases rapidly, but the Fe^{3+} concentration in solution decreases due to the precipitation of $Fe(OH)_3$ through equation (4) above (Evangelou and Zhang, 1995). Because there is very little bacterially mediated oxidation of pyrite at neutral to alkaline pH values, some researchers have suggested that O_2 is a more important oxidant than Fe^{3+} in such environments (Evangelou and Zhang, 1995).

The effect of temperature on the rate of pyrite oxidation can be described using the Arrhenius equation:

$$k = A\exp\left[\frac{-E_a}{RT}\right],$$

where k is the rate constant, E_a is the activation energy, A is the pre-exponential factor referred to as the Arrhenius factor, R is the universal gas constant, and T is temperature in degrees Kelvin (Nicholson, 1994). The equation above indicates that as the temperature decreases, so does the corresponding rate constant. Since the rate of a chemical reaction is directly proportional to the rate constant for the reaction, as the rate constant decreases, so does the rate of the reaction (Nicholson, 1994). This is consistent with investigations of pyrite oxidation in the Canadian arctic which indicate that acid generation in sulphide-rich tailings is retarded in this environment (Elberling et al., 2000; Meldrum et al., 2001).

2.1.2 Prediction of Acid Mine Drainage

There are two main techniques used in the prediction of AMD: static tests and kinetic tests (Jambor et al., 2002).

2.1.2.1 Static Tests

Static tests, also known as acid-base accounting (ABA), is a one-time measurement of the total acid generating potential (AP) and the total neutralization potential (NP) of the waste material (Steffen Robertson and Kirsten Inc., 1989). This method is based on the assumption that all the acid generated by the primary acid-producing minerals (sulphides) will be neutralized by the main acid neutralizing minerals (carbonates). An accounting technique is used to determine if the sample contains enough carbonate material to neutralize the acid that could potentially be generated from the rock (Mine Environment

Neutral Drainage (MEND) Project, 1991). The benefit of this technique is that it provides rapid results inexpensively. However, static tests do not provide information on the rates or identities of reactions occurring within the sample (Jambor et al., 2002).

The generation of acid in mine waste is predominantly by the oxidation of sulphide minerals (section 2.1.1.). Therefore, the AP of a rock is estimated by determining its sulfide-S content, which is assumed to be present as pyrite (Jambor et al., 2002). The sample is analyzed for its total-S and sulphate-S. The amount of sulphide-S in the sample is then determined by subtracting the sulphate-S concentration from the total-S concentration.

The NP of a mine waste is determined by reacting a known weight of finely ground sample with a known amount of HCl. The amount of acid consumed by the sample is then expressed in equivalent kilograms of calcium carbonate per tonne of waste (Mine Environment Neutral Drainage (MEND) Project, 2000).

In order to facilitate the accounting technique used, both AP and NP are reported in comparable and consistent units of kg $CaCO_3$/tonne of rock or tailings (Mine Environment Neutral Drainage (MEND) Project, 1991). The oxidation of pyrite produces acid, by the following net reaction,

$$FeS_{s(s)} + 15/4\,O_{2(g)} + 7/2\,H_2O \longrightarrow Fe(OH)_{3(s)} + 4H^+ + 2SO_4^{2-}, \qquad (5)$$

which is the sum of reactions 1, 3, and 4. The acid produced by reaction 5 is neutralized by calcite following the reaction,

$$CaCO_{3(s)} + 2H^+ \longrightarrow Ca^{2+} + 2H^+ + CO_3^{2-}. \qquad (6)$$

The two reactions listed above indicate that the 2 moles of acid generated per mole of sulphur in pyrite is neutralized by 1 mole of calcite (Mine Environment Neutral Drainage

(MEND) Project, 2000). If calculated on a weight basis, 1 g of S is neutralized by 3.125 g of calcite. Therefore, since sulphur concentrations are usually reported as a weight percent, 1% sulphide-S requires 31.25 kg $CaCO_3$ per tonne of waste material. In other words:

$$AP = [\text{sulphide-S (wt. \%)}] \times [31.25 \text{ kg } CaCO_3/\text{tonne rock}]$$

The net neutralization potential (NNP) is then calculated by:

$$NNP = NP - AP.$$

A positive NNP value indicates that the waste is not net-acid producing, while a negative NNP indicates that the waste will probably become acid generating (Mine Environment Neutral Drainage (MEND) Project, 2000). Alternatively, the neutralization potential ratio (NPR) is used to predict the acid generating potential of mine waste. The NPR is calculated by:

$$NPR = NP/AP.$$

In the case of NPR, a value greater than 1 indicates that the waste will not be acid generating, while a value less than 1 indicates that acid generation is potentially an issue.

Both NNP and NPR calculations are valid methods used to calculate the acid generating potential of mine waste, but the NPR method is preferred since it gives an indication of the relative abundance of NP or AP (Mine Environment Neutral Drainage (MEND) Project, 2000).

2.1.2.2 Kinetic Tests

Kinetic methods of AMD prediction are essentially dissolution tests conducted to aid in the prediction of drainage quality from mine waste rock and tailings material (Lapakko, 2003). The most common type of kinetic test is the humidity cell, which is intended to simulate the unsaturated environment of waste rock piles and tailings impoundments (Drever, 1997).

Approximately 1 kg of the rock to be tested is crushed so that 100% is less than 0.6 cm in diameter and placed on a filter inside a plastic chamber, approximately 10 cm in diameter. The contents of the cell are subjected to moist air for three days (approximately 95% relative humidity) followed by dry air for three days (< 10% relative humidity). The contents of the cell are then leached with 500 mL or 1000 mL of distilled de-ionized water on the seventh day (Drever, 1997; Lapakko, 2003). The volume of water used to leach the cell at the end of a week cycle is arbitrary, but for consistency the volume should be decided on prior to the beginning of testing (Lapakko, 2003). The purpose of the leaching step is to recover any readily soluble products that have formed due to mineral dissolution or sulphide oxidation in order to determine the dissolved load contributed from the previous week's test. The leachate is then analyzed for pH, and the solutes of interest. Humidity cell tests are usually run for a minimum of 20 cycles (weeks), but it is usually more desirable to continue testing until the rates of SO_4 generation and metal leaching have stabilized, which can take up to 120 weeks or more (Lapakko, 2003). The results from this type of testing are then used to estimate the rate of acid generation and metal release to the environment on a weekly basis.

2.2 Previous Work on Panda Kimberlite

2.2.1 Acid-Base Accounting and Metal Release Rates

In 1997, Norecol Dames and Moore Consultants geochemically characterized and investigated the AMD potential of rock types and simulated processed kimberlite fines from Ekati (Norecol Dames and Moore, 1997). Both static and kinetic testing were conducted to help determine acid generation and neutralization potential of the rock types, as well as determine metal weathering rates in an effort to model discharge from the LLCF.

Static testing, using the Sobek ABA procedures (Sobek et al., 1978), involved the determination of paste pH, total-S, sulphide-S, and sulphate-S concentrations as well as AP, NP, and NPR (Norecol Dames and Moore, 1997), as explained in section 2.1.2.1. Values reported for the Panda kimberlite ore are:

ABA parameter	P_5	Mean	P_{95}
Paste pH	8.1	8.4	8.6
Total-S (wt. %)	0.20	0.47	0.90
Sulphate-S (wt. %)	0.01	0.04	0.09
Sulphide-S (wt. %)	0.12	0.43	1.03
AP (kg $CaCO_3$/t)	4	13	32
NP (kg $CaCO_3$/t)	99	240	465
NP/AP	7	18	75

Note that P_5 and P_{95} are the 5th and 95th percentile values (2σ) respectively. These data show a high NP and a relatively low AP, suggesting that the potential for acid generation in the Panda kimberlite is minimal. Also, simulated tailings were produced using Panda kimberlite. Values reported for ABA of the simulated Panda tailings are:

ABA Parameter	Value
Paste pH	8.4
Total-S (wt. %)	0.33
Sulphate-S (wt. %)	0.02
Sulphide-S (wt. %)	0.31
AP (kg $CaCO_3$/t)	9.7
NP (kg $CaCO_3$/t)	490.6
Inorganic-CO_2 (wt.	4.27
NP/AP	51

Kinetic testing was used to determine the rate of ion release during weathering of rock, and involves the use of both humidity cells and column tests (section 2.1.2.2). The test was run in one-week cycles for approximately 125 to 130 weeks. One litre of deionized water was used to leach the cell on the final day of the test cycle. Leachates were collected and analyzed for metals (As, Cu, Pb, Ni, and Zn) and general water quality parameters including pH, conductivity, sulphate, alkalinity, and acidity. No Panda kimberlite samples were included in humidity cell testing. However, results from other Ekati kimberlite samples, including the Misery and Fox kimberlite, indicate that low temperatures depress sulphide oxidation rates but do not significantly affect silicate weathering. Metal release rates are initially rapid but are speculated to decrease due to secondary mineral coatings on grains, and pH stabilizes between 7 and 8 for most materials.

A second series of kinetic tests were conducted using column testing. This technique is used to simulate the conditions that would exist along a flow path through the kimberlite storage facility. Testing was conducted on four simulated tailings samples, including Panda kimberlite. The test involved filling a plastic column with approximately 2 kg of sample and then re-circulating cold (~3°C), de-ionized water through the column at a rate of 2 L/week for several weeks. Approximately 100 mL of leachate was removed from the column every two weeks and analyzed for metals (Ag, Al, As, B, Ba, Be, Bi, Ca, Cd, Ce, Co, Cr, Cu, Fe, K, Li, Mg, Mn, Mo, Na, Ni, P, Pb, Sb, Se, Si, Sr, Ti, V, W, and Zn) sulphate, pH, and electrical conductivity. This sample volume was immediately replaced with de-ionized water. Results from these tests indicate that dissolution of Panda tailings produce constant pH's (between 7 and 8) and metal release rates that are initially rapid, but then are followed by erratic concentrations with no apparent increasing or decreasing trends.

Based on the tests conducted by Norecol, Dames and Moore (1997), it was concluded that the LLCF is expected to produce leachate metal concentrations below the guidelines stipulated in the Ekati Water Licence (Section 4.6). As well, the slow dissolution of silicate minerals is predicted to be the dominant weathering mechanism in kimberlite material. Therefore, significant seasonal effects are not expected to occur in the LLCF (Norecol Dames and Moore, 1997).

2.2.2 Clay Mineral Identification

In 1998 EBA Engineering Consultants Ltd. conducted a tailings characterization study that involved the investigation of geotechnical properties, clay mineralogy, settling rates, clarification, freeze-thaw effects, and thermal properties of processed kimberlite fines and process water being discharged to the LLCF (EBA Engineering Consultants Ltd., 1998). Determination of clay mineralogy of the Panda kimberlite was conducted by AGAT laboratories in Calgary, Alberta. X-ray diffraction analysis of clay minerals in the Panda kimberlite indicates the presence of illite and smectite minerals.

2.2.3 Other Work on LLCF Processed Fines

Other studies that have been conducted on the processed kimberlite fines at Ekati have included the determination of bulk geotechnical properties of the fines (EBA Engineering Consultants Ltd., 1998; EBA Engineering Consultants Ltd., 2002), adsorption of wastewater phosphorous by processed kimberlite fines (Graham, 2002), physical characteristics of the tailings particles including a determination of flocculant and coagulant doses required for processed fines (Howe, 1997), and the toxicity of processed kimberlite wastewater on freshwater zooplankton in the LLCF (Croquet de Rosemond, 2002).

2.3 Water-Rock Interactions in Serpentinized Ultramafic Rocks

Few studies have been conducted on the weathering of processed kimberlite and its effects on water quality. However, a number of authors have investigated the geochemistry of spring-waters issuing from ultramafic complexes composed predominantly of serpentine and olivine. Since kimberlite is predominantly composed of serpentine and olivine (Mitchell, 1986), the investigations of ultramafic spring-waters can be used as a natural analog to processed kimberlite weathering.

Spring waters issuing from serpentinized ultramafic rocks have been investigated by many authors and can be classified into two chemically distinct groups: Mg-HCO_3 type, and Ca-OH type (Barnes and LaMarche, 1969; Barnes et al., 1967; Barnes et al., 1978; Bruni et al., 2002; Pfeifer, 1977; Sato et al., 2002). The first type of water is characterized by neutral pH, high Mg and SiO_2, and low Ca concentrations with carbonate present. Table 2.1 contains representative analyses of this water type. These waters are typically found in near surface springs and depressions and are thought to represent the discharge of groundwater formed through the interaction of meteoric water with serpentine, olivine, and pyroxenes from the ultramafic complexes (Barnes and LaMarche, 1969; Barnes et al., 1967; Barnes et al., 1978; Bruni et al., 2002; Pfeifer, 1977).

	1	**2**	**3**	**4**
pH	8.3	8.71	11.86	11.77
Ca	9.5	3.4	47.4	53
Mg	51	101	0.020	0.3
Na	4.0	6.4	23.7	50
K	2.2	0.3	3.1	1.2
Cl	12	6.3	21.2	55
SO_4	2.6	20	0.14	0
CO_3	271	13.4	--	0
HCO_3	NA	489.6	1.26*	0
Fe_{total}	NA	0.03	NA	0
Mn	NA	0.02	NA	0.05
Al	0	NA	NA	0
SiO_2	31	4.6	1.44	0.3

1: Lake Roland, Maryland, U.S.A. Concentrations in mg/L (from Pfeifer, 1977)
2: Red Mountain, Stanislaus County, California (from Barnes et al., 1967)
3: Genova Province, Italy (from Bruni et al., 2002)
4: Sonoma County, California (from Barnes and O'Neil, 1969)
*concentration represents C_{total} reported as HCO_3

Table 2.1: Representative analyses of Mg-HCO_3 (1 and 2) and Ca-OH (3 and 4) waters found issuing from ultramafic complexes (NA = not analyzed).

The second type of water found issuing from springs associated with ultramafic bodies has a characteristically high pH and low carbonate and Mg concentrations, making Ca the only significant cation in solution. Representative analyses of this water type can be found in table 2.1. The origin of these waters has been explained as the interaction of meteoric water with ultramafic rock to produce serpentine under near surface conditions through the following reactions involving olivine and pyroxene (Barnes and LaMarche, 1969; Barnes et al., 1967; Barnes et al., 1978; Pfeifer, 1977):

$$2Mg_2SiO_{4(s)} + 2H^+ + H_2O_{(l)} \longrightarrow Mg_3Si_2O_5(OH)_{4(s)} + Mg^{2+}$$

$$MgSiO_{3(s)} + 2H^+ \longrightarrow H_2O_{(l)} + Mg^{2+} + SiO_{2(aq)}.$$

Any hydrolysis reaction, as shown above, leads to an increase in pH due to the reaction of acids, naturally present in the water, with minerals (Stumm and Morgan, 1996). However, Bruni et al. (2002) have suggested that the hydrolysis and serpentinization of pyroxene and forsterite alone are not sufficient to explain the unusually high pH's observed in the Ca-OH waters.

Ca-OH waters collected by Bruni et al. (2002) were found issuing from fracture zones and faults and were interpreted to have originated from deep aquifers composed predominantly of serpentinites and related rocks. Bruni et al. (2002) suggest that the high pHs of these waters are due to the extremely low P_{CO2} that results from the closed-system condition (with respect to CO_2) of the deep hydrologic circuits in which these waters are assumed to form. Through the use of reaction-path geochemical modeling, Bruni et al. (2002) demonstrated that the two types of waters could be genetically related in that the $Mg\text{-}HCO_3$ type water is formed due to the open system dissolution of serpentinites in meteoric waters, while the Ca-OH type water is formed by the closed system dissolution of serpentinites by Mg-HCO_3 type water.

Recent investigations of the water in contact with kimberlite material suggests that water-rock interactions within serpentinized ultramafic rocks are a relevant analog to help explain the evolution of waters in contact with processed kimberlite ore from diamond mining operations (Baker et al., 2003; Borisov et al., 1995; Sader et al., 2003). Baker et al. (2003) investigated the environmental geochemistry of kimberlite material from the Diavik Diamonds project, located immediately south of Ekati on Lac de Gras. Acid-base accounting and humidity cell tests were used to determine the behaviour of processed kimberlite waste when stored in a surficial impoundment. Their research indicates that the Diavik kimberlite is predominantly pyroclastic kimberlite composed of serpentine and olivine and that weathering of this material in a surface impoundment will produce an effluent with a pH near 8. Waters collected during humidity cell testing of this material were not analyzed for Mg or Si preventing a complete comparison of the ultramafic spring waters with the kimberlite humidity cell water chemistry. Borisov et al. (1995) investigated the water issuing from diamond quarries in East Siberia and noted pH values of approximately 8 as well as total dissolved solid concentrations approaching 4 to 8 g/L. The chemistry of these waters was dominated by SO_4, Cl, Mg, and Ca.

Sader et al. (2003) investigated the use of groundwater as a prospecting tool for the exploration of kimberlite. Groundwater samples were collected from exploration drill holes at depths up to 65 m below the surface. At these depths, it is likely that the waters sampled are from closed-system hydrologic circuits through the kimberlite. These deep samples had a maximum pH of 12.45 and Mg concentrations as low as <0.1 μg/L. Ca concentrations were not mentioned.

The objective of the three kimberlite investigations discussed above did not involve the determination of the controls on the chemistry of water in contact with kimberlite material. However, the similarity in mineralogy and effluent pH to that observed in ultramafic-water interactions suggests that the open and closed system interaction of kimberlite is analogous to the interactions of serpentinized ultramafics with water discussed by Bruni et al. (2002).

3 Sampling and Analytical Methods

3.1 Field Work

The purpose of the sampling program for this project was to collect specimens that would allow the determination of the mineralogical and chemical variations of the processed kimberlite fines and co-existing pore-water over time, as well as determine any changes that occur during processing of the ore and during storage in the containment facility. Therefore, solid and water samples were collected from three different areas: Panda open pit, discharge from the processing plant, and the Long Lake Containment Facility (LLCF). Four separate field seasons were conducted to collect samples necessary to accomplish the objective of this study: summer 2000, winter 2001, summer 2001, and summer 2002. The following is a discussion of the objectives and activities of each field season.

The initial field season, conducted from 20 June to 21 August 2000, was the first phase of the project. The objective of this field season was to become familiar with the LLCF, process plant, and mine operations, as well as to develop and conduct a sampling program to collect solids and pore-water from the unsaturated zone of the processed kimberlite. Kimberlite samples from the Panda pit, surficial water samples from the upstream side of Dyke B and Dyke C, and from the process plant discharge spigot were also collected during this first field season.

A drilling program was conducted during the second field season from 12 to 19 March 2001. The main objectives of this work were to obtain samples from below the frost table in the LLCF, since this zone was inaccessible during the summer 2000 sampling program, and to determine the vertical structure of the LLCF processed kimberlite fines. Figure 3.2 shows the location of drilling sites for this program.

The third field season was conducted during two separate site visits: 3 to 17 July 2001, and 23 to 27 August 2001. The objective of the July sampling was to collect both solid and water samples from the LLCF in order to observe the mineralogical and chemical evolution of the processed kimberlite-coexisting pore-water system within the LLCF. The second half of the summer 2001 field-work involved the collection of till samples and till pore-water samples in an effort to determine the effect of groundwater as an input to the pore-water of the processed kimberlite within the LLCF.

The final field season was again conducted over two trips. The first part of this work was carried out from 2 to 10 July 2002 while the second half was conducted from 15 to 22 August 2002. The objectives of this final field season was to collect data to further the characterization of pore-water chemistry and to establish better the temporal behaviour of the LLCF processed kimberlite fines pore-water in both an annual and seasonal time frame.

3.2 Sample Collection

This investigation is concerned with understanding the interaction of kimberlite and water. Therefore, both solid and water samples were collected. Water samples within the LLCF were collected from the unsaturated zone of the LLCF fines, the process plant discharge spigot, and from the upstream side of Dyke B and Dyke C. The suite of solid samples consists of processed kimberlite fines from the LLCF and unprocessed kimberlite from the Panda Pit. Figure 3.1 and 3.2 are maps showing the location of samples collected within the LLCF.

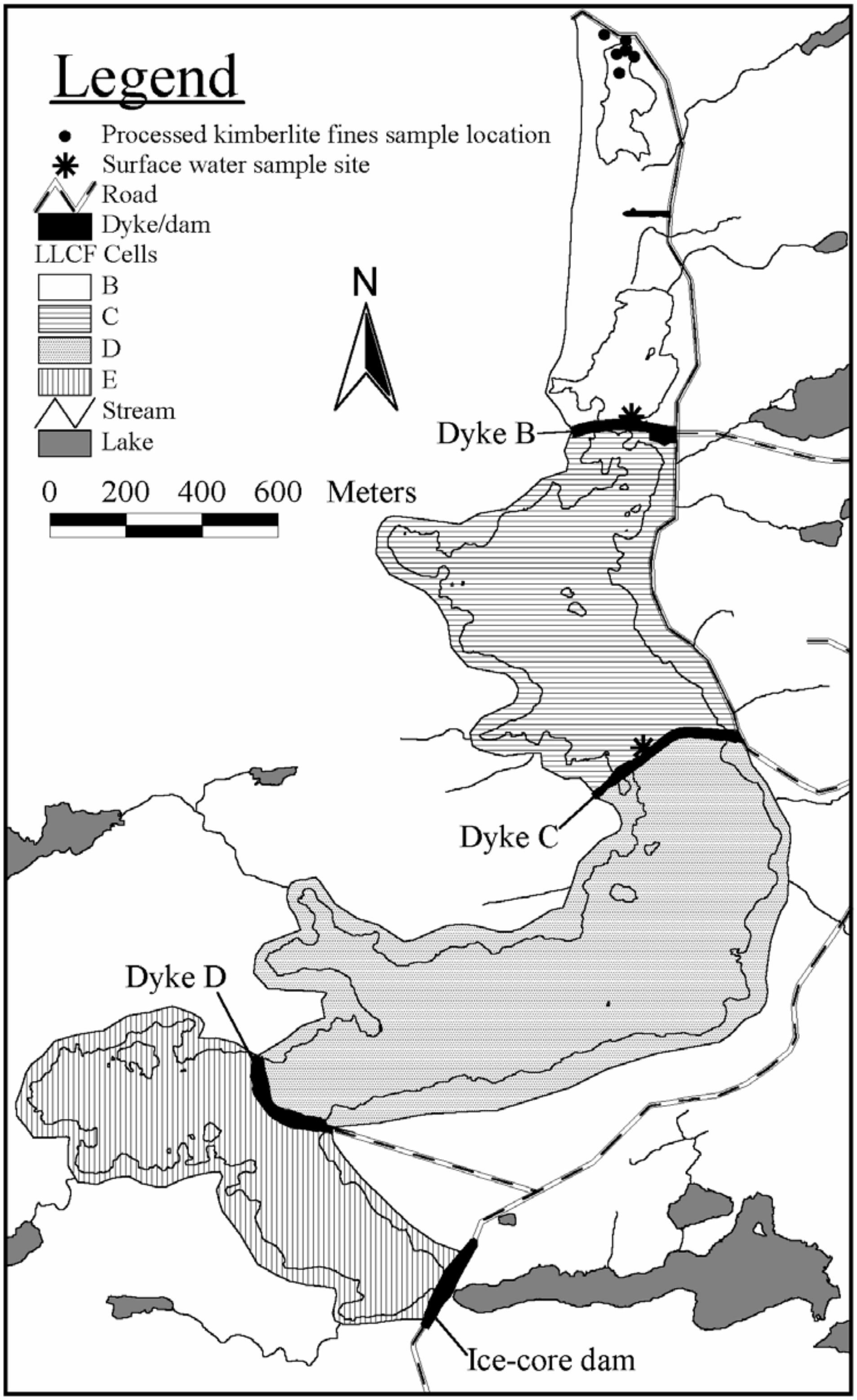

Figure 3.1: Map of the Long Lake Containment Facility showing cells, dykes, and sample locations.

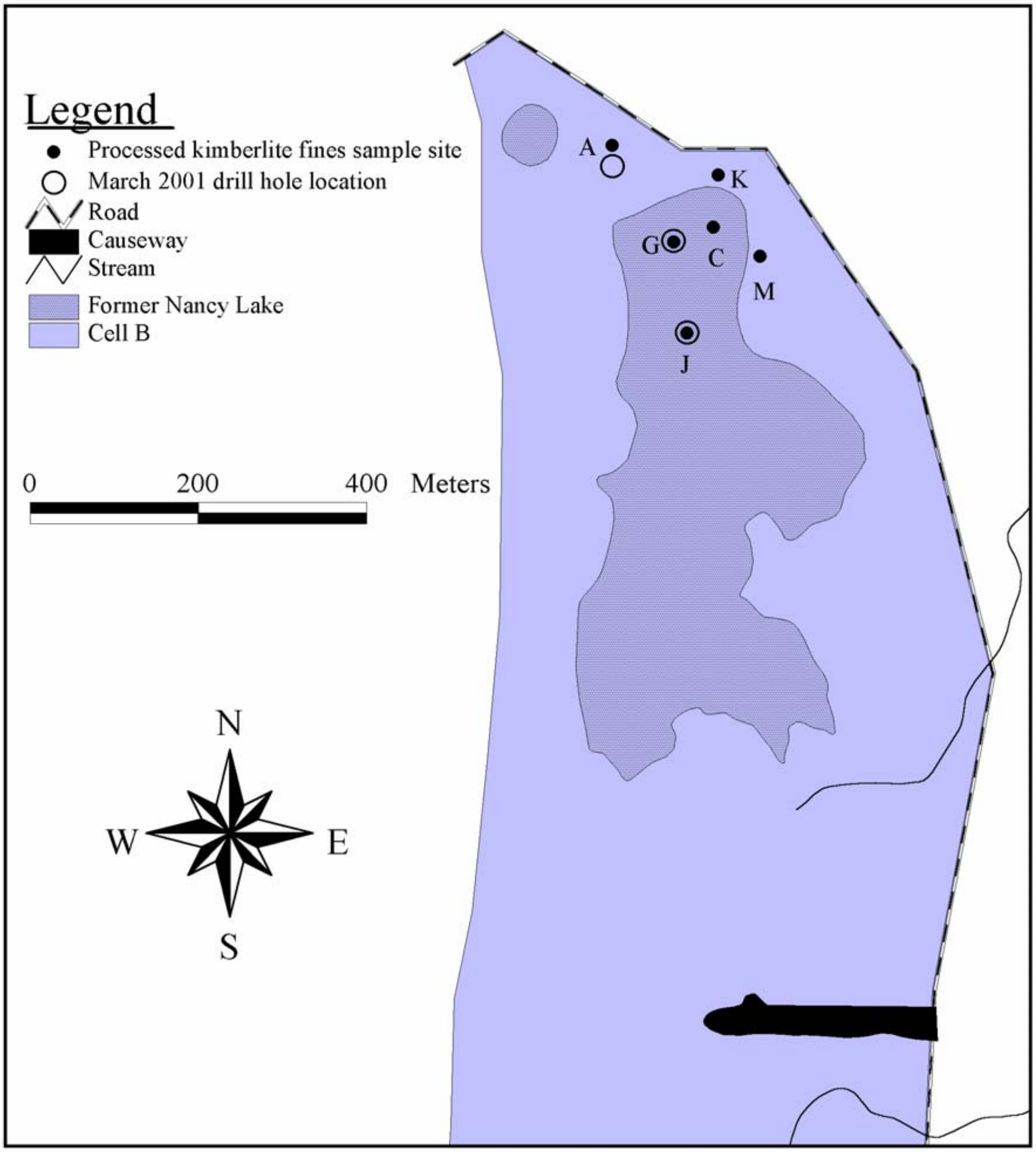

Figure 3.2: Map of the northern portion of Cell B showing the processed kimberlite fines sample sites and the March 2001 drilling locations.

Sample locations within the LLCF were chosen to obtain samples that would help define the LLCF mineral-water system, and to allow the safe collection of samples. The kimberlite fines deposited in the LLCF are very young (less than four years old at the start of this study) and the majority of fines had not had an adequate amount of time to de-water completely. As a result, all pore-water sample sites were located in the oldest and most de-watered reaches in the northern portion of Cell B (Figure 3.1 and Figure 3.2). Two surface water sample sites were also used in this study, which were positioned on the upstream side of Dyke B and Dyke C, respectively.

3.2.1 Water Samples

Three types of water samples were collected for this study: processed kimberlite fines pore-water, process plant water, and surface water. The following is a discussion of the three types of water samples collected and the collection methods used.

3.2.1.1 Kimberlite Fines Pore-water

Pore-water from the LLCF fines was collected using suction lysimeters and squeezing. The two methods of pore-water collection were employed to determine if there was a difference between the samples collected from each technique.

Soilmoisture Equipment Corporation model 1900 suction lysimeters were used in this study (Figure 3.3). Each lysimeter was composed of a 130 cm long polyvinyl chloride (PVC) tube that was terminated at one end by a rubber stopper fitted with a small length of rubber tubing and the other end by a porous ceramic cup (Figure 3.3). Using an auger, a hole was created in the kimberlite fines in order to install the lysimeter

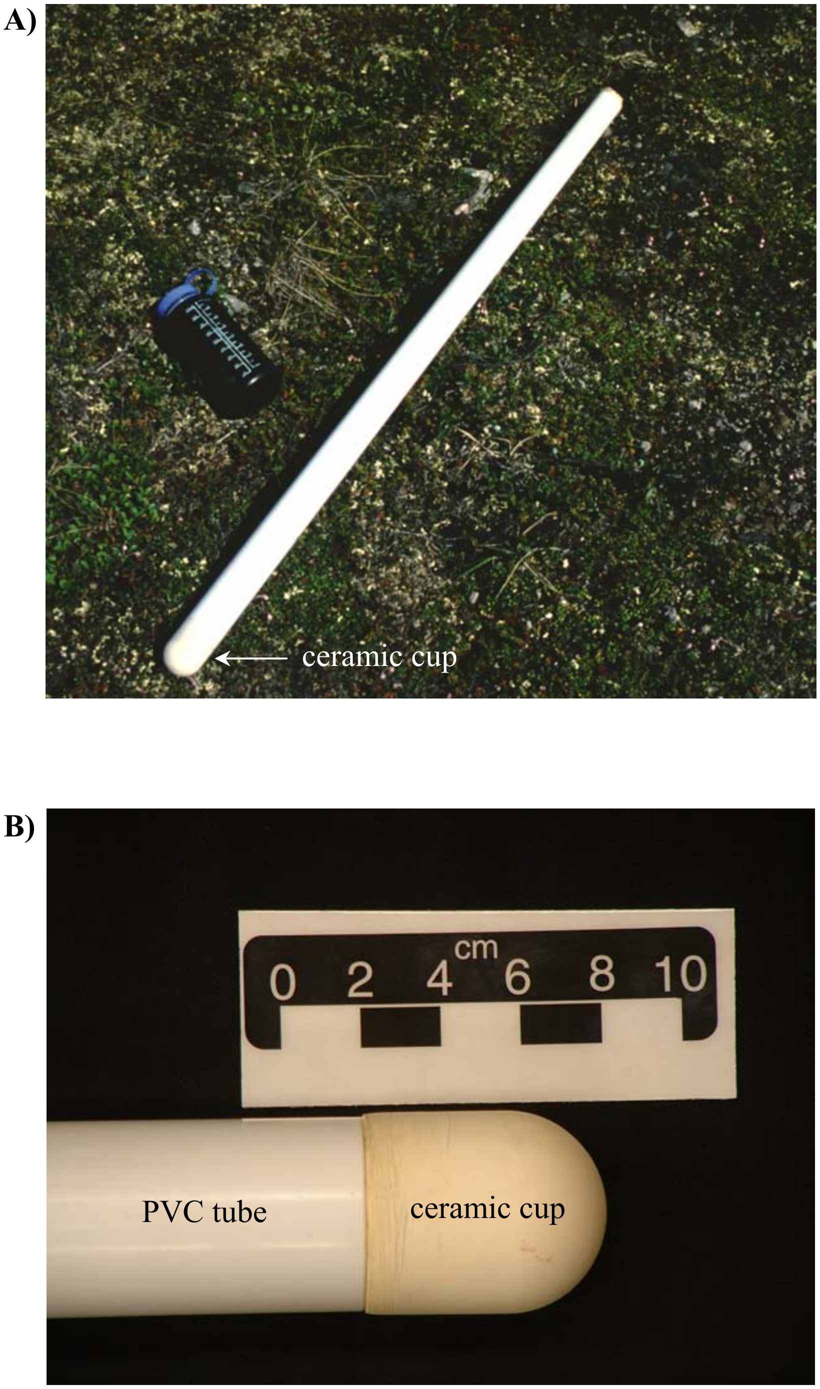

Figure 3.3: A) Suction lysimeter used in LLCF pore-water acquisition. The total length of the lysimeter is 130 cm (one litre bottle for scale). **B)** Close-up of the ceramic cup on the lysimeter. When the lysimeter is installed into the ground and evacuated, the micro-pores of the cup allow water to flow into the lysimeter.

to the desired depth of sample collection. After the lysimeter was placed in the hole, a slurry of distilled water and kimberlite fines was used to fill the hole. This step ensured that good contact was established between the lysimeter and the fines to allow water flow into the lysimeter. Once installed into the ground, a hand pump was used to create a vacuum inside the tube. The vacuum in the lysimeter created a pressure difference allowing pore-water water to flow from the unsaturated soil through the porous ceramic cup into the lysimeter.

Suction lysimeters were installed approximately 10 to 20 cm above the water table or the frost table, whichever was closer to the surface. Each lysimeter was purged three times prior to analytical sampling. Lysimeters were purged by allowing the lysimeter to fill with about 200 mL of water (approximately 1 day), and then removing all the water from the lysimeter. After the lysimeter was purged, the hand pump was used to create a vacuum again in order to collect more sample.

Water was removed from the lysimeters through the use of a suction system as seen in Figure 3.4. A plastic tube, approximately 200 cm long and 2 mm in diameter, was fed through the tubing in the top of the lysimeter until it reached the bottom of the ceramic cup. The other end of the thin plastic tube was fed through a rubber stopper which was placed in an Erlenmeyer flask. The vacuum pump was used to evacuate the flask, which allowed the water to be siphoned from the lysimeter. A small volume of sample was used to rinse the flask before analytical sample collection at each new station to help reduce contamination between sample sites. After the sample was collected, the tubing was removed and the lysimeter was evacuated to allow further sample collection.

Figure 3.4 – Picture of a sample site with a lysimeter. Lysimeters were placed in the ground about 10 – 20 cm above the ice layer and were purged three times before any analytical samples were taken. The flask and vacuum pump used to remove the water samples from the lysimeter can be seen on the left of the photo.

The second method used to extract pore-water from the kimberlite fines involved hand-coring with a 7.6 cm PVC pipe and then employing a core squeezing device, similar to those used in soil-water investigations (Böttcher et al., 1997; Patterson et al.). It has been found that soil-water samples collected using squeezing techniques display higher solute concentrations, and less scatter in the analytical data than pore-waters collected using suction lysimeters. Unlike suction lysimeters, squeezing techniques have the ability to provide high spatial resolution that allow water samples to be closely related to specific soil horizons (Heinrichs et al., 1997). Since one of the objectives of this study is to determine the major minerals and processes affecting pore-water chemistry in the processed kimberlite fines, suction lysimeters were chosen for sample collection because they collect pore-water from a volume of processed kimberlite, and therefore provide an average water chemistry for that location from which major processes can be determined. As well, due to the ease of sample collection using suction lysimeters, more samples could be obtained than had squeezing techniques been used alone.

However, there are few studies employing the use of suction lysimeters in the collection of mine waste pore-water. Squeezing samples were collected in this study as part of an on-going effort to compare the use of squeezing techniques with suction lysimeters in the collection of mine waste pore-water to determine if there are any significant differences between the two sampling techniques.

The squeezer was constructed with the assistance of the machinists at Ekati, using three 1.9 cm thick metal plates and four 1.3 cm diameter threaded rods each approximately 91 cm in length (Figure 3.5 and 3.6). The bottom and top plates were fixed while the middle plate moved up and down to facilitate squeezing. A two-ton

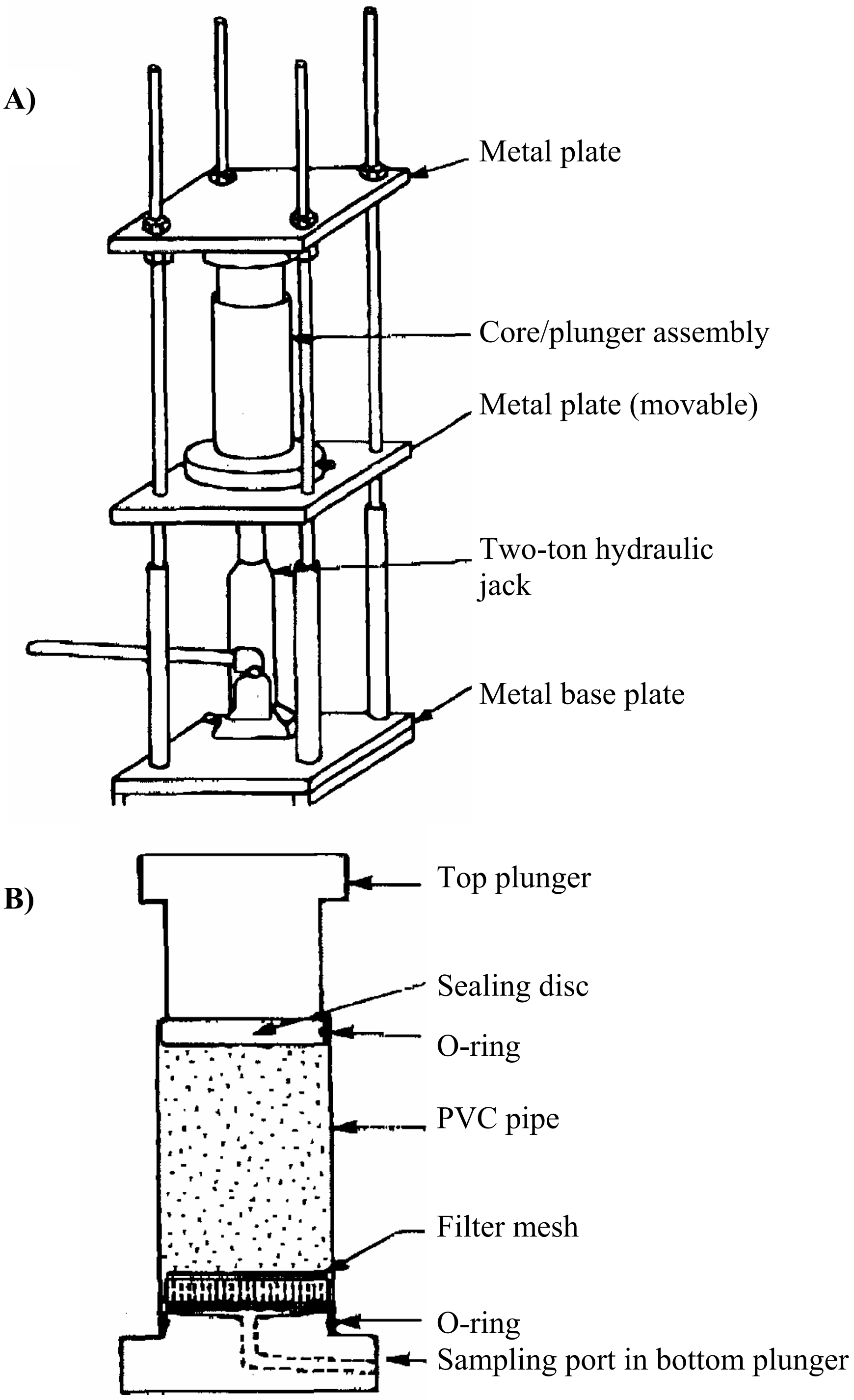

Figure 3.5: A) Diagram showing the main features of the apparatus used for squeezing samples. **B)** Diagram showing, in detail, the components of the core/plunger assembly. The plungers were machined from a solid piece of nylon.

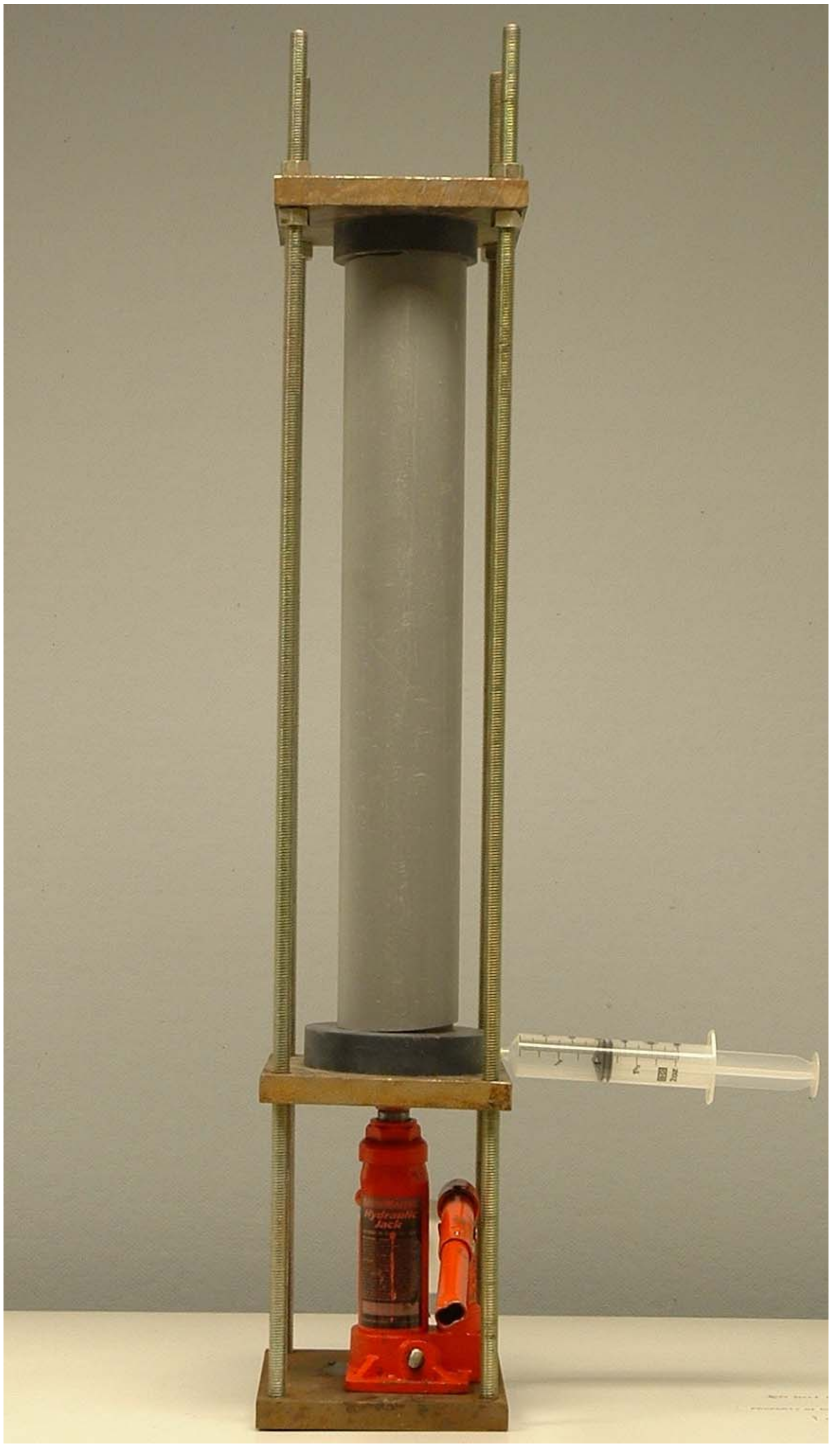

Figure 3.6: Image of assembled pore-water squeezer used in this investigation. The squeezer is approximately 91 cm tall. The syringe on the right hand side of the squeezer has a 60 mL capacity.

hydraulic jack was placed between the bottom and the middle plate and the core sample was placed between the middle and top plates. Nylon plungers were machined to fit exactly in the ends of the PVC pipe with the bottom plunger being fitted with a drain to allow collection of the water squeezed from the sample. The hydraulic jack was used to push the middle plate up and the plungers into the open ends of the core tube, extruding the water into a 60 mL syringe attached to the sampling port in the bottom plunger of the squeezer (Figure 3.6).

The squeezing core was collected by pushing, or hammering, a length of PVC pipe into the kimberlite fines to a depth of 30 to 50 cm (Figure 3.7). Once in the ground, a rubber stopper was inserted into the top of the pipe to create a partial vacuum as the pipe was pulled out of the fines. The core tube containing the sample was then sealed at both ends with laboratory film and duct tape. Core samples destined for squeezing were collected and transported back to the Ekati Environment Lab and squeezed within one hour of collection to ensure that no further reactions occurred as the sample re-equilibrated at the new temperature of the lab.

3.2.1.2 Process Plant Discharge Water

Process plant water was collected from the discharge spigot delivering fines and process water to the LLCF (Figure 3.8). These samples were collected by filling a plastic 10 gallon bucket with material immediately as it was discharged from the spigot into the LLCF. The bucket was then placed in the shade for 24 hours in order to allow the fine material to settle out of suspension to allow easier filtration during sample collection. The bucket was placed in the shade to prevent reactions from occurring due to the increase in temperature caused by the sun.

Figure 3.7: Picture showing how core samples of the LLCF kimberlite fines were collected. A PVC pipe was pushed or hammered into the ground and then a rubber stopper was fit into the top end of the pipe to create a partial vacuum. The pipe was then pulled out of the ground and sealed at both ends with laboratory film and duct tape.

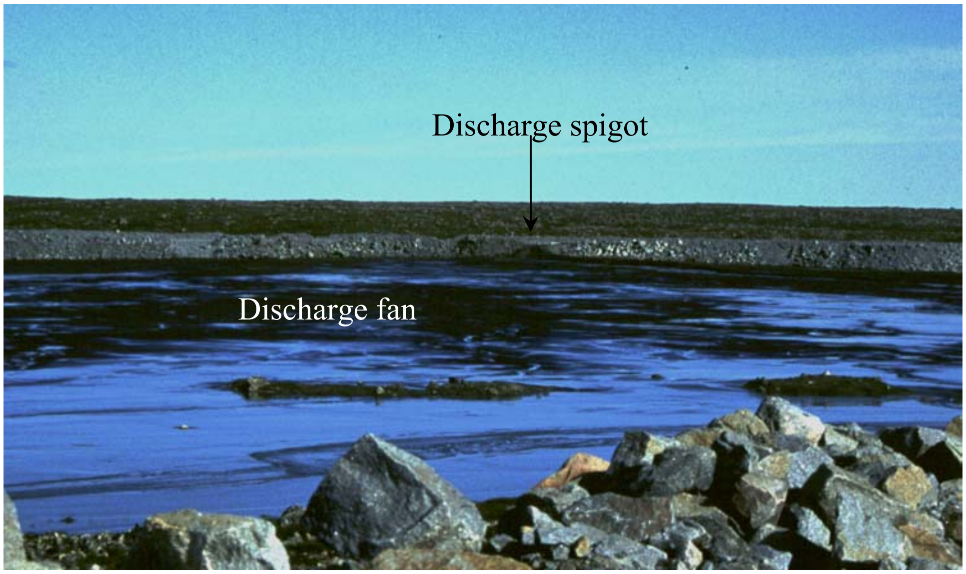

Figure 3.8: A) Spigot discharging process plant effluent into the LLCF. Samples of this material were collected by placing a plastic 10-gallon bucket into the discharge stream. **B)** View of Dyke C, looking north, and the low-angle fan created from the process plant discharge.

3.2.1.3 Surface Water

Surface water samples were collected from the upstream side of Dyke B and Dyke C respectively (Figure 3.1 and 3.9). Dyke C water samples were collected from the end of the water-reclaim barge that pumps water from the LLCF to the process plant to be used in the processing of kimberlite ore. A 500 mL plastic beaker was used to collect the sample from the top 30 cm of the water column adjacent to each respective dyke. Before a new sample was taken, the collection beaker was rinsed three times with a small volume of water from the new site in order to prevent contamination between sites.

3.2.2 Quality Assurance/Quality Control

The objective of quality assurance and quality control (QA/QC) in a water sampling program is to track the possible sources of sample contamination from collection to analysis as well as determine the imprecision of the analytical data. For this study, the QA/QC program involved the collection of field blanks, field duplicates, and laboratory splits.

The purpose of field blank samples is to monitor sample contamination that is introduced into the sample during collection. If field blanks are collected, transported, and stored with analytical samples then they provide an indication of the contamination that is introduced into the samples after collection in the field. A field blank is essentially a bottle of distilled de-ionized water of known composition, which is taken into the field during sample collection. During collection of the analytical sample, the lid is removed and the open field blank bottle is placed next to the location of sampling. Once the analytical sample is collected, the field blank sample is treated in exactly the same

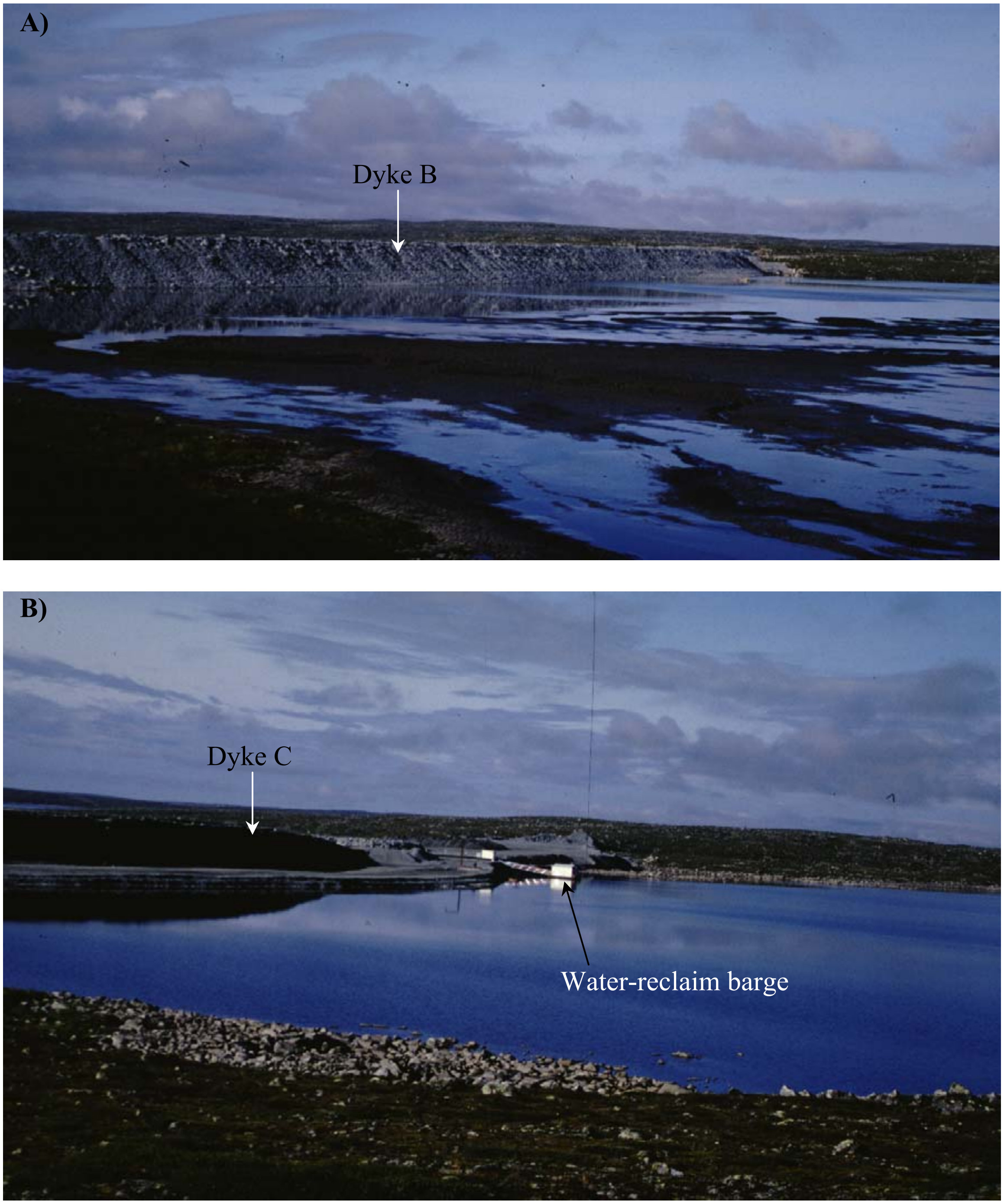

Figure 3.9: View, looking west, of the surface water sample sites on the upstream side of **A)** Dyke B and **B)** Dyke C. The surface water sample at Dyke C was collected from the process plant water-reclaim barge.

manner as the analytical sample, including preservation. A separate field blank sample is used for each aliquot collected (e.g. metals, anions, DOC). A total of 8 field blanks were collected for this study and a complete listing of field blank analyses can be found in Appendix A.

Field duplicate samples are collected in order to assess the imprecision of the analytical data provided by the laboratory as well as evaluate the variability of field samples. These samples are collected concurrently with the analytical sample at a specific site and treated in exactly the manner. A total of 13 pairs of duplicate samples were collected for this study and are listed in Appendix A.

Laboratory splits are made in the laboratory just before sample analysis by splitting one sample into two. Measurement of these samples is intended to determine the variation that occurs during analysis. The imprecision results obtained using lab splits are provided in a quality control report accompanying the data and are summarized in Appendix A.

The techniques used in the preparation of water samples are discussed in section 3.3.1.

3.2.3 Solid Samples

Two types of solid samples were collected for investigation: kimberlite ore from the Panda open pit, and processed kimberlite fines from the LLCF.

3.2.3.1 Kimberlite Ore

Panda kimberlite samples were collected in the open pit directly from recently blasted material in July 2000 as well as from drill core (D.D.H. PUC1-5) collected during an exploration drilling program conducted in 1995. Diamond drill hole PUC1-5 is a sub-horizontal section across the top portion of Panda, which was the first ore mined and processed at Ekati. Therefore, samples were obtained from this hole because it is representative of the kimberlite that was mined, processed, and deposited in the northern portion of Cell B in August 1998. Drill core samples were collected from the BHP Diamonds Exploration warehouse in Kelowna B.C. in August 2000. Samples were collected every 10 m depth, from a core approximately 200 m in length, in order to ensure that no one unit was preferentially sampled over another.

3.2.3.2 Processed Kimberlite Fines

Samples for mineralogical analysis were collected from the processed kimberlite fines using the same technique that was used in the collection of squeezer core, discussed in section 3.2.1.1. The only difference is that the mineralogy samples were collected using a 5.1 cm (inside diameter) PVC pipe instead of the 7.6 cm (inside diameter) PVC pipe used for the squeezer samples.

3.3 Sample Preparation

3.3.1 Water Samples

Although collection methods differed, all water samples were prepared in exactly the same manner. Three aliquots were collected for each water sample, which included one aliquot for cation analysis (30 mL high density polyethylene (HDPE) bottle), one for anion analysis (15 mL HDPE bottle), and one for dissolved organic carbon (DOC) analysis (10 mL amber glass vial). Amber glass was used to collect the DOC sample because dissolved organic carbon is light-sensitive.

All water samples were vacuum filtered with a 0.45 μm cellulose acetate bottle top filter and a hand pump. The water aliquot destined for cation analysis was preserved with approximately 240 μL mL of high purity 15.9 M nitric acid. The aliquot used for anion analysis was left unpreserved and filled to capacity in order to minimize headspace. The DOC aliquot was preserved with approximately 40 μL of 1:1 high purity concentrated sulphuric acid:deionized water. As well, pH, dissolved oxygen (DO), conductivity, temperature, and alkalinity were all measured in the field at the time of collection. Dissolved oxygen, conductivity, and temperature were measured first using one aliquot, then pH and alkalinity were measured using a fresh aliquot. Water samples were transported back to the lab in a cooler with ice packs and placed in a refrigerator at 4^{o}C until they could be analyzed.

3.3.2 Solid Samples

3.3.2.1 Processed Kimberlite Fines

Polished thin sections of kimberlite fines were prepared through a process of cutting the frozen core, partially thawing the frozen fines, sub-sampling the fines, drying the sub-samples, and stabilizing the sub-samples with cool-curing epoxy in order to allow the samples to be made into polished thin sections.

The first step in this process was to remove a core from the freezer and immediately cut it in half using a hand held power saw and a cutting jig constructed to fit the width of the core. These two halves were then allowed to partially thaw at 21^{o}C for about 30 to 40 minutes. This step was required in order to allow the core samples to be soft enough to sample easily, but not so soft that they fell apart during sampling. After this time, sub-samples were taken at pre-determined locations along the core using 3.8 cm diameter HDPE sample bottles from which the bottoms had been removed (Figure 3.10). The kimberlite fines sub-samples were then removed from the PVC core tube, the open bottom was covered with laboratory film and they were set aside to allow the sub-sampled kimberlite fines an opportunity to finish thawing and drying.

Finally, the kimberlite fines sub-samples were impregnated with a room-temperature curing epoxy (Epo-Tek 301 from Epoxy Technology Inc.). A room temperature curing epoxy was used to prevent the addition of excessive heat to the samples, which might have destroyed any secondary minerals that precipitated. This final step was used to ensure that the samples maintained their integrity while being shipped to Vancouver Petrographics for polished thin section preparation.

Once the kimberlite fines sub-samples were received at Vancouver Petrographics they were cut, set in epoxy, and polished without the use water to help prevent the destruction of the more delicate secondary minerals that might have formed after deposition in the containment facility.

3.3.2.2 Kimberlite Ore

Panda Pit kimberlite was prepared for thin section preparation by marking the approximate location of the section on the core sample. In order to ensure consistency in sample preparation, these sections were also prepared in the same manner as were the processed kimberlite fines samples.

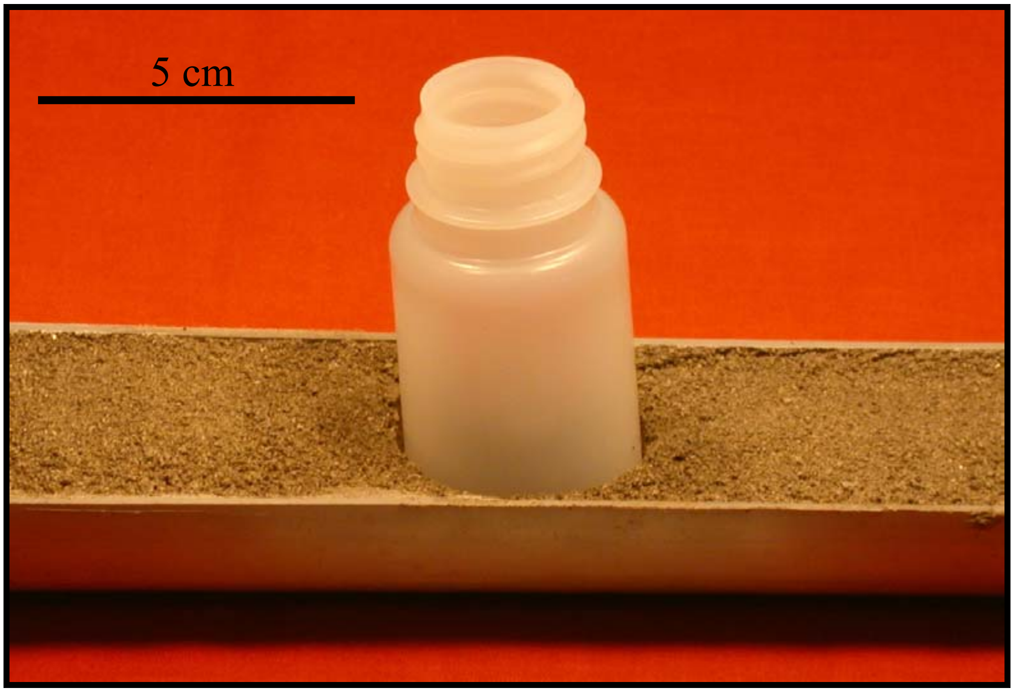

Figure 3.10: Image showing the technique used to sub-sample to processed kimberlite fines core samples for polished thin section preparation. A 3.8 cm diameter HDPE bottle, from which the bottom had been removed, was pushed into the partially thawed fines. The bottle containing the sample was then removed from the core casing, covered with laboratory film, and allowed to finish thawing and drying overnight.

3.4 Analytical Methods

3.4.1 Water Samples

All water samples were analyzed at Enviro-test Laboratories in Edmonton, Alberta. The list of analytes includes: Ag, Al, As, B, Ba, Be, Ca, Cd, Co, Cr, Cu, Fe_T, Hg, Mn, Mo, Na, Ni, Pb, Sb, Se, Sr, U, V, Zn, NH_3-N, Cl, dissolved organic carbon (DOC), dissolved inorganic carbon (DIC), F, NO_3-N, NO_2-N, PO_4-P, and SO_4. As mentioned above, each sample was composed of three aliquots, which were destined for cation, anion, and DOC analysis respectively. Table 3.1 is a list of analytes, analytical method used, and the reference for the method used.

3.4.2 Solid Samples

The objectives of the techniques used to analyze the solid samples were to identify the minerals present, to determine the chemical composition of the minerals present, and to determine the concentration of each mineral. To accomplish these objectives the solid samples were analyzed using the electron microprobe, the scanning electron microscope, and a combination of gravimetric and combustion techniques.

3.4.2.1 Electron Microprobe Analysis and Scanning Electron Microscopy

Electron microprobe analyses (EMPA) were conducted at Queen’s University on an ARL-SEMQ electron microprobe equipped with an energy dispersive spectrometer. The oxides in each analysis included SiO_2, TiO_2, Al_2O_3, Cr_2O_3, FeO, MnO, MgO, CaO, Na_2O, and K_2O.

Analyte	Analytical Method	Method Reference
Metals*	ICP-MS	APHA 3125
Si	ICP-OES	APHA 3120 B
Cl	Colorimetry	APHA 4500-Cl E
F	Ion selective electrode	APHA 4500-F C
SO_4	Ion Chromatography	APHA 4110 B
PO_4-P	Colorimetry	APHA 4500-P
NO_3-N	Colorimetry	APHA 4500-NO_3 H
NO_2-N	Colorimetry	APHA 4500-NO_2 B
NH_3-N	Colorimetry	APHA 4500-NH_3 F
DOC	Combustion-Infrared	APHA 5310 B
DIC	Combustion-Infrared	APHA 5310 B

* Metals include: Ag, Al, As, B, Ba, Be, Ca, Cd, Co, Cr, Cu, Fe, K, Hg, Mg, Mn, Mo, Na, Ni, Pb, Sb, Se, Sr, U, V, Zn

Table 3.1: List of analytical techniques used in the analysis of LLCF water samples.

Standard analytical conditions were used in the collection of data including an accelerating voltage of 15 kV, a take-off angle of 52.5°, an emission current of 100 mA, a beam current of approximately 40 nA, and a collection time of 200 seconds. The primary standard used in these analyses was NBS 470 and secondary standards were selected to be mineralogically and chemically similar to the minerals being analyzed in the samples. Uncorrected k-ratios were obtained by fitting the energy-dispersive spectroscopy (EDS) spectra with reference spectra using a least squares program, and oxide weight percents were then calculated using Bence-Albee correction factors (Albee and Ray, 1970).

Scanning electron microscopy was used together with qualitative EDS to help investigate the grain size, morphology, and identity of minerals present within the samples. The ARL-SEMQ electron microprobe was used in scanning electron microscope mode for this work.

3.4.2.2 Direct Combustion and $BaSO_4$ Gravimetry – Sulphur Concentration

Combustion and gravimetric techniques were employed to determine the concentration of S-bearing minerals in the kimberlite and processed kimberlite fines. ALS Chemex laboratories in Vancouver, British Columbia conducted these analyses.

The objective of the S analyses was to determine the sulphide and the sulphate concentration in the suite of samples. This determination involves direct combustion of the sample, and $BaSO_4$ gravimetry, which produces the total-S and sulphate-S concentrations respectively. Sulphide-S is then determined as the difference between the total-S and sulphate-S concentrations.

Direct combustion is used to determine the total S content in the sample. A small amount of sample (0.5 g to 0.6 g) is heated in a combustion furnace to a temperature of approximately 1370°C (Crock et al., 1999). At this temperature, any S in the sample is oxidized to SO_2 gas. The amount of infrared energy absorbed by the liberated SO_2 is measured by a solid-state infrared detector, which is converted to a total sulphur concentration.

The next step is to determine the amount of sulphate-S present in the samples using $BaSO_4$ gravimetry. Another 0.5 to 0.6 g sample is boiled for 30 minutes with an approximately 5 mass % Na_2CO_3 solution (Seal, 2003). Insoluble material is then removed by filtration and an approximately 10 mass % $BaCl_2$ solution is added to precipitate all the sulphate present in solution as insoluble $BaSO_4$. The precipitate is then filtered from solution, dried, and weighed. Samples with low sulphate content will produce a small amount of $BaSO_4$. Therefore, the precipitate produced by these samples may be analyzed by combustion furnace, as discussed for total sulphur, to determine sulphate-S content more accurately.

Sulphide-S concentration is then determined by subtracting the sulphate-S, determined by $BaSO_4$ gravimetry, from the total-S, determined by direct combustion.

3.4.2.3 Coulometric titration – Inorganic-C Concentration

Inorganic-C concentration in the suite of samples was determined by coulometric titration. In this technique approximately 0.01 g to 0.03 g of sample is acidified with 2N perchloric acid ($HClO_4$) and heated in a reaction vessel causing all the carbonate in the sample to be converted to $CO_{2(g)}$ (Crock et al., 1999). The gas liberated is carried through a reflux condenser and a scrubbing solution using CO_2–free air. Next, the liberated $CO_{2(g)}$ passes through a coulometer containing monoethanolamine and a pH indicator. Interaction of the $CO_{2(g)}$ with the monoethanolamine produces a titratable acid causing the colour of the solution to change (Crock et al., 1999). The acidic solution is then titrated back to the original pH. The amount of titrant used is then converted to the amount of $CO_{2(g)}$ generated and a weight percent inorganic-C (expressed as weight percent $CO_{2(g)}$) can be calculated from these results.

3.4.2.4 Sulphur Isotopes

Mud xenoclast and efflorescent mineral samples were analyzed for their sulphate-S isotopic composition. Sulphate minerals were first extracted from each sample to be analyzed (section 5.4). Sulphur was extracted from each sample on-line using continuous-flow technology. A Finnigan MAT 252 isotope-ratio mass spectrometer was then used to analyze the extracted sulphur for its $\delta^{34}S$ value, reported in permil (‰), as well as its S concentration, reported as weight percent sulphur (wt. % S). Standards used included NBS 123 and NBS 127.

4 LLCF Water Chemistry

The first objective of this project was to chemically define the components of the mineral-water system within the LLCF. To do this, 86 water samples were collected over three field seasons from 2000 to 2002. For a complete discussion of sample collection, preparation, and analysis refer to chapter 3. A complete listing of analytical data for all LLCF water samples can be found in Appendix A. Refer to figure 3.1 and 3.2 for maps showing the locations from which all water samples were taken.

4.1 Duplicate Samples and Analytical Imprecision

In an effort to quantify the imprecision of analytical results used in this investigation, ten pairs of duplicate water samples (20 total) were collected in the field, and submitted for analysis. Each pair of field duplicate samples was collected at the same time, and prepared and transported to the lab in exactly the same manner. Therefore, the difference between each pair of field duplicate analyses gives an idea of not only the reproducibility, or imprecision, of the data used for interpretations, but also the variation that exists within the field. As well, laboratory duplicate samples were analyzed by Envirotest laboratories. Unlike field duplicate samples, laboratory duplicate samples were created in the laboratory by dividing one sample into two immediately before analysis. Therefore, laboratory duplicate samples indicate the imprecision of the analytical technique used.

To calculate imprecision from field duplicates, the percent deviation from the mean for the concentrations of each element for all pairs of duplicate analyses was calculated using the following equation:

$$\% \ \ deviation \ \ from \ \ the \ \ mean = \left[\frac{analysis(1) - analysis(2)}{analysis(1) + analysis(2)} \right] x100\% .$$

The 95th percentile value, representing two standard deviations, of the percent deviation from the mean for each element was calculated. This value was then used as the imprecision for each element. A pair of duplicate analyses was used in calculations only if both concentrations were greater than five times the detection limit, a procedure followed by the lab used in this investigation, and both analyses had charge imbalances less than 15%, as calculated by PHREEQC. Charge imbalance is the percent difference between the total concentration of cations and the total concentration of anions in a water sample, and it gives an indication of the quality of the analytical data (section 6.1). Imprecision values calculated from LLCF duplicate water samples are listed in Appendix A.

The relative percent difference for each element calculated from laboratory duplicate analyses were provided in a quality control report accompanying the analytical reports provided by Envirotest Laboratories Inc. The average relative percent difference for each element is tabulated in Appendix A.

4.2 Description

4.2.1 Lysimeter Pore-Water

Elemental concentration ranges and average concentrations for the LLCF pore-water samples collected by suction lysimeter from 2000 to 2002 are listed in table 4.1 and table 4.2. On inspection of these tables, it can be seen that SO_4, Mg, and Ca dominate pore-water chemistry. As well, HCO_3 (reported as alkalinity), Na, and K are present in high to

	August 2000 (n=20)			July 2001 (n=17)		
	Min	Average	Max	Min	Average	Max
Temp. (^{o}C)	6.9	10.8	18.4	9.6	12.3	15.8
pH	8.10	8.46	9.00	7.32	7.89	8.37
Alk. (mg/L $CaCO_3$)	21.2	54.9	84.8	28.0	45.4	59.6
DO	2.4	4.2	8.8	2.7	5.1	6.5
Cond. (μS/cm)	342	2315	5210	577	2415	4414
Ag	⟵	bd	⟶	bd	0.0003	0.0003
Al	0.0059	0.0262	0.131	0.0017	0.0066	0.0192
As	0.00394	0.00638	0.0108	0.00386	0.00620	0.00955
B	0.005	0.011	0.020	0.012	0.023	0.033
Ba	0.0136	0.0412	0.0870	0.0183	0.0265	0.0410
Be	⟵	bd	⟶	⟵	bd	⟶
Ca	9.34	161	435	26.4	203	473
Cd	0.00034	0.00093	0.00166	0.00020	0.00121	0.00228
Co	bd	0.0013	0.0030	bd	0.0012	0.0031
Cr	bd	0.00192	0.00401	bd	0.00020	0.00067
Cu	bd	0.0039	0.0081	0.0006	0.0026	0.0056
Fe	bd	0.823	2.17	bd	0.746	1.33
Hg	bd	0.00008	0.00040	bd	0.00004	0.00005
K	5.71	22.0	40.5	13.8	31.6	57.9
Mg	13.4	278	719	49.1	345	867
Mn	0.0041	0.0531	0.119	0.0102	0.0804	0.221
Mo	0.248	0.638	1.24	0.396	0.760	1.25
Na	3.23	10.5	18	7.59	16.9	32.1
Ni	0.00816	0.115	0.288	0.0283	0.145	0.324
Pb	bd	0.00020	0.00063	bd	0.00008	0.00010
Sb	0.00232	0.0048	0.0068	0.00357	0.00497	0.00658
Se	bd	0.0046	0.0143	0.0004	0.0024	0.0080
Si	3.1	4.9	7.3	3.3	6.0	8.4
Sr	0.155	2.18	5.95	0.379	2.57	6.23
U	bd	0.00052	0.00149	0.00011	0.00040	0.00120
V	0.00361	0.0288	0.183	0.00266	0.00860	0.0231
Zn	0.0068	0.0258	0.0933	0.0015	0.0066	0.0150
NH_3-N	0.469	1.52	2.83	0.013	0.470	1.23
Cl	4	5	7	5	6	7
F	bd	0.11	0.35	bd	0.07	0.07
NO_3-N	bd	1.23	5.21	bd	1.1	13.4
NO_2-N	bd	0.161	0.627	bd	0.37	3.67
PO_4-P	0.003	0.016	0.027	bd	0.013	0.028
SO_4	69.1	1527	3960	171	1387	2930
DIC	3.9	12.2	18.8	6.5	10.2	13.2
DOC	2.7	5.7	9.4	4.3	6.4	16.2

Table 4.1: Lysimeter pore-water chemistry ranges for 2000 and 2001. All values are reported in mg/L unless specified otherwise (bd = below detection limit; NA = not analyzed). Major dissolved constituents are highlighted.

	July 2002 (n=9)			August 2002 (n=6)		
	Min	Average	Max	Min	Average	Max
Temp. (°C)	12.3	14.9	19.6	8.5	10.1	11.0
pH	6.66	7.24	7.54	5.80	7.20	7.65
Alk. (mg/L $CaCO_3$)	39.4	62.4	84.8	67.6	91.6	112.8
DO	6.4	9.1	17.0	8.5	9.5	11.0
Cond. (μS/cm)	1509	2893	5390	2278	3022	5510
Ag	bd	0.0011	0.0020	bd	0.0004	0.0004
Al	bd	0.0100	0.0100	bd	0.0850	0.1600
As	0.0034	0.0044	0.0056	0.0040	0.0047	0.0060
B	0.028	0.035	0.045	0.026	0.033	0.041
Ba	0.0250	0.0270	0.0307	0.0192	0.0248	0.0321
Be	←	bd	→	←	bd	→
Ca	90.1	225	438	79.3	207	420
Cd	0.0010	0.0021	0.0030	0.0009	0.0016	0.0027
Co	0.0004	0.0015	0.0030	0.0010	0.0020	0.0039
Cr	←	bd	→	←	bd	→
Cu	0.0032	0.0057	0.0154	0.0037	0.0051	0.0069
Fe	bd	0.014	0.029	bd	0.011	0.014
Hg	←	bd	→	←	NA	→
K	17.7	31.8	42.5	14.5	26.1	42.9
Mg	143	398	786	138	350	790
Mn	0.039	0.094	0.156	0.060	0.107	0.172
Mo	0.459	1.02	1.32	0.407	0.865	1.30
Na	9.7	14.3	19.9	4.5	11.9	19.1
Ni	0.0706	0.215	0.448	0.156	0.222	0.467
Pb	bd	0.0002	0.0004	bd	0.0001	0.0001
Sb	0.0038	0.0044	0.0053	0.0041	0.0044	0.0052
Se	bd	0.0040	0.0086	0.0043	0.0076	0.0224
Si	5.8	6.3	7.0	3.9	6.7	7.8
Sr	1.12	2.76	5.10	2.04	2.76	5.23
U	0.0005	0.0012	0.0017	0.0011	0.0020	0.0027
V	0.0040	0.0066	0.0099	0.0020	0.0025	0.0034
Zn	0.011	0.019	0.031	0.010	0.019	0.031
NH_3-N	0.013	0.268	0.515	bd	0.130	0.130
Cl	3	5	7	4	5	5
F	←	NA	→	←	NA	→
NO_3-N	0.952	19.3	84.2	10.5	23.4	80.5
NO_2-N	0.015	0.256	1.18	0.006	0.066	0.311
PO_4-P	0.005	0.019	0.033	0.003	0.011	0.022
SO_4	711	2112	4080	787	1648	3300
DIC	←	NA	→	15.0	19.8	23.7
DOC	13.0	17.7	21.4	10.7	13.5	18.1

Table 4.2: Lysimeter pore-water chemistry ranges for July and August 2002. All values are reported in mg/L unless specified otherwise (bd = below detection limit; NA = not analyzed). Major dissolved constituents are highlighted

moderate concentrations, pH ranges from 6.66 to 9.00, Fe concentrations have a maximum value of 2.17 mg/L, and average conductivity values exceed 2000 μS/cm with maximum conductivity values in excess of 4000 μS/cm. The high conductivity of these samples is correlated with an increase in the total dissolved solids concentration.

4.2.2 Squeezer Pore-Water

Results from analyses of pore-water samples collected by squeezing (section 3.2.1.1) are presented in table 4.3. Letters at the top of columns designate the sample location (Figure 3.2). For sample location G, two samples were collected in 2001 from the same core and are designated 2001-1 and 2001-2, respectively. The sample designated 2001-2 was collected after 2001-1 under higher pressures and is considered to represent the tightly bound micro pore-water.

Like pore-water samples collected using suction lysimeters, the squeezed pore-water data is enriched with SO_4, Mg, and Ca. Also similar to lysimeter samples, squeezed pore-waters have moderate to high concentrations of HCO_3, Na, and K, neutral to slightly basic pH, low Fe concentrations, and maximum conductivity values in excess of 4000 μS/cm. When compared to table 4.1 and table 4.2, it can be seen that all squeezed pore-water concentrations fall within the same ranges as the lysimeter samples. These data suggest that the squeezing technique produces results similar to the pore-water samples collected by suction lysimeter. It should also be noted that there is an increase in solute concentrations between the two samples collected from sample location G in 2001. Specifically Al, Ca, Mg, Mn, Sb, Sr, SO_4, and DIC are all significantly higher in 2001-2 relative to 2001-1. This effect was also noted by Böttcher et al. (1997), and is attributed

	A		G			K		M	
Sample	**2000**	**2001**	**2000**	**2001-1**	**2001-2**	**2000**	**2001**	**2000**	**2001**
Temp. (^{o}C)	18.80	19.53	16.93	20.43	21.47	18.57	19.53	19.93	19.40
pH	7.4	8.03	7.91	8.11	8.12	8.77	7.15	8.73	7.55
Alk. (mg/L CaCO$_3$)	36.4	32.8	52	36	40.4	62	66.4	60.8	52.8
DO	4.2	5.6	3.6	2.9	2.2	3.6	7.24	7.2	3.88
Cond. (μS/cm)	1599	4207	3533	1838	2225	283.9	1546	453.1	647
Ag	bd	0.0003	bd	0.0002	bd	bd	0.0003	bd	0.0003
Al	0.0166	0.0028	0.0228	0.0038	0.008	0.047	0.0026	0.0301	0.0099
As	0.00596	0.00735	0.0062	0.00297	0.0028	0.0105	0.00693	0.017	0.00951
B	0.023	0.03	0.023	0.037	0.037	0.026	0.047	0.023	0.032
Ba	0.0432	0.0403	0.0388	0.168	0.177	0.291	0.0395	0.477	0.489
Be	bd	bd	bd	bd	bd	bd	bd	bd	bd
Ca	170	467	318	185	243	23.5	240	35.5	31.5
Cd	0.00154	0.00201	0.00281	0.00118	0.00123	0.0009	0.00165	0.00125	0.00071
Co	0.0004	0.001	0.0033	0.0002	bd	bd	0.0016	0.0014	bd
Cr	0.00364	0.00017	0.00065	0.00008	0.00009	bd	0.00027	0.00063	0.00034
Cu	bd	bd	0.0142	bd	bd	bd	bd	0.0026	bd
Fe	bd	1.23	bd	0.54	0.528	0.14	0.563	0.009	0.05
Hg	0.00004	0.00004	bd	0.00007	bd	bd	0.00004	0.00004	0.00006
K	33	51.2	46.6	38.2	42.6	15.2	42.2	15.8	16
Mg	215	630	536	213	297	31.2	319	48	42.1
Mn	0.105	0.218	0.181	0.0978	0.124	0.0167	0.123	0.0188	0.0146
Mo	0.726	1.04	1.24	0.68	0.791	0.363	0.884	0.527	0.432
Na	18.2	31	19.4	22.1	23.4	7.45	20.2	9.05	9.09
Ni	0.0541	0.0852	0.396	0.0178	0.018	0.0192	0.215	0.0382	0.0171
Pb	0.0119	bd	0.00066	bd	bd	0.0004	bd	0.00051	bd
Sb	0.0079	0.00358	0.00655	0.0026	0.00316	0.012	0.00807	0.0156	0.00622
Se	0.0005	0.0003	0.0015	0.0002	0.0003	bd	0.0007	0.0011	bd
Si	3.1	3.9	6.7	4.6	5.1	NA	8.5	2.9	3.4
Sr	2.37	7.09	4.48	2.67	3.25	0.347	3.1	0.587	0.494
U	0.00012	bd	0.00117	bd	bd	bd	0.00044	0.00014	bd
V	0.00154	0.00136	0.00173	0.00035	0.00021	0.0022	0.00135	0.00233	0.0012
Zn	0.0083	0.0064	0.0443	0.0085	0.0092	0.076	0.0036	0.131	0.0021
NH_3-N	2.03	2.67	1.58	2.64	2.89	1.38	0.838	1.62	0.65
Cl	4	10	7	6	6	6	5	7	5
F	NA	bd	NA	0.06	bd	NA	bd	NA	0.06
NO_3-N	1.97	2.3	0.152	bd	0.098	0.136	0.242	3.61	0.293
NO_2-N	0.128	4.52	0.186	0.006	0.009	0.173	0.059	bd	0.004
PO_4-P	0.027	0.001	0.021	0.005	0.015	0.008	0.012	0.011	0.025
SO_4	1220	2850	2320	1060	1440	224	1490	338	168
DIC	6.8	8.4	6.6	5.2	7.3	8.2	14.4	12.7	4.8
DOC	4.7	7.4	9	6.8	7.2	12.3	15.4	7.4	12.4

Table 4.3: Squeezer pore-water chemistry for samples collected in 2000 and 2001. Note that each analysis represents one sample. All values are reported in mg/L unless specified otherwise (bd = below detection limit; NA = not analyzed). Major dissolved constituents are highlighted.

to the high solid:solution ratio of the micro-pore fluids sampled as the pressure of squeezing increases.

The main objective of collecting squeezed pore-water samples was to determine if different fractions of pore-water were sampled using each technique. In order to investigate the differences that exist between pore-water samples collected using suction lysimeter and squeezing techniques, it is necessary to compare analyses of each type of sample that were collected under the same conditions. Evaporation is indicated to be a process that is an important factor controlling the composition of pore-water. Therefore, it is important to compare both types of samples that were collected on the same day. Table 4.4 is a list comparing three different pairs of pore-water analyses collected using each technique. Highlighting indicates the sample that contains a significantly higher elemental concentration. If neither concentration is highlighted for a given element, then the data do not indicate a significant difference between the two collection methods. Analysis of table 4.4, using the calculated imprecision values (section 4.1), indicates that there does not appear to be a systematic difference between pore-water samples collected using suction lysimeter and squeezer techniques for most solutes. Mg, for example, appears to be concentrated in lysimeter samples from site A (2001) and K (2000). Conversely, Mg is concentrated in the squeezed pore-water sample at site K (2001). However, B, Ba, and NH_3-N concentrations appear to be consistently higher in squeezed pore-water samples while Cu appears to be consistently higher in lysimeter pore-water samples. The data in table 4.4 do not provide any conclusive evidence that LLCF pore-water samples collected using the suction lysimeter technique represent a different fraction of pore-water than do squeezing samples.

	Sample site A - 2001		Sample site K - 2000		Sample site K - 2001	
	Lysimeter	Squeezed	Lysimeter	Squeezed	Lysimeter	Squeezed
Temp. (^{o}C)	9.63	19.53	7.73	18.57	9.9	19.53
pH	7.97	8.03	8.89	8.77	8.13	7.15
Alk. (mg/L CaCO$_3$)	28	32.8	43.6	62	42.4	66.4
DO	5.9	5.6	2.8	3.6	2.65	7.24
Cond. (mS/cm)	4414	4207	569	283.9	1251	1546
Ag	0.0002	0.0003	bd	bd	bd	0.0003
Al	0.0017	0.0028	0.0411	0.047	0.0094	0.0026
As	0.00538	0.00735	0.0102	0.0105	0.00726	0.00693
B	0.012	0.03	0.014	0.026	0.02	0.047
Ba	0.0323	0.0403	0.0629	0.291	0.0193	0.0395
Be	bd	bd	bd	bd	bd	bd
Ca	473	467	26.2	23.5	74.8	240
Cd	0.00215	0.00201	0.00103	0.0009	0.0002	0.00165
Co	0.0019	0.001	0.0006	bd	0.0002	0.0016
Cr	0.00016	0.00017	0.00049	bd	0.00024	0.00027
Cu	0.0025	bd	0.0081	bd	0.0056	bd
Fe	1.02	1.23	0.234	0.14	bd	0.563
K	42.3	51.2	12.9	15.2	22.8	42.2
Hg	0.00004	0.00004	0.00003	bd	bd	0.00004
Mg	867	630	37.6	31.2	129	319
Mn	0.112	0.218	0.0172	0.0167	0.0211	0.123
Mo	1.18	1.04	0.405	0.363	0.634	0.884
Na	24.1	31	7.33	7.45	11.1	20.2
Ni	0.273	0.0852	0.0263	0.0192	0.0439	0.215
Pb	bd	bd	0.00041	0.0004	0.00007	bd
Sb	0.00459	0.00358	0.00575	0.012	0.00511	0.00807
Se	0.0013	0.0003	0.0004	bd	0.0005	0.0007
Si	6.6	3.9	NA	NA	5.7	8.5
Sr	6.23	7.09	0.374	0.347	0.959	3.1
U	0.00013	bd	0.00032	bd	0.00017	0.00044
V	0.00804	0.00136	0.00814	0.0022	0.00414	0.00135
Zn	0.0077	0.0064	0.0255	0.076	0.015	0.0036
NH$_3$-N	0.031	2.67	0.7	1.38	0.351	0.838
Cl	6	10	5	6	6	5
F	bd	bd	0.35	bd	0.06	bd
NO$_3$-N	0.059	2.3	0.052	0.136	0.081	0.242
NO$_2$-N	0.025	4.52	0.068	0.173	0.01	0.059
PO$_4$-P	bd	0.001	0.006	0.008	0.006	0.012
SO$_4$	2840	2850	165	224	534	1490
DOC	6.3	7.4	2.9	12.3	5.2	15.4
DIC	6.5	8.4	10.8	8.2	9.9	14.4

Table 4.4: Comparison of analyses of pore-water samples collected using suction lysimeter and squeezer techniques. Values are reported in mg/L unless specified otherwise. Values that are significantly higher in each pair of squeezer and lysimeter analyses are highlighted. The lack of a highlighted value indicates that there is no significant difference between techniques (bd = below detection; NA = not analyzed).

4.2.3 Process Plant Discharge Water

Table 4.5 is a summary of the average chemistry of process water discharging into the LLCF from 2000 to 2002. The most notable feature of the process plant water samples is that, as in the case of pore-water samples, SO_4 and HCO_3 are the dominant anions and Mg, Ca, Na, and K are the dominant cations. As well, pH values range from 7.7 to 9.0, the maximum dissolved Fe value is approximately 0.1 mg/L, which is lower than pore-water samples. Also, average electrical conductivity of discharge water samples over the three years ranges from 459 μS/cm to 1134 μS/cm, which indicates that discharge water samples are up to eight times more dilute than pore-water samples.

4.2.4 Surface Water

Surface water samples were collected from two locations within the LLCF. The first was located on the north side of Dyke B, and the second was located on the north side of Dyke C, with samples being collected from the water-reclaim barge that supplied water to the mineral processing plant. It should be noted that surface water samples are the most dilute water samples collected from the LLCF.

4.2.4.1 Dyke B

Table 4.6 lists the average surface water composition at Dyke B from 2000 to 2002. Alkalinity, SO_4, Mg, Ca, K, and Na dominate the chemistry of these waters with pH values between 8.11 and 8.83, dissolved Si concentrations between 1.0 mg/L and 2.4 mg/L, and dissolved Fe concentrations ranging from 0.005 mg/L to 0.135. As well, the average conductivity at Dyke B over all three years is approximately 400 μS/cm.

	2000	2001	2002
Number of samples	3	3	2
Temp. (°C)	10.1	15.8	20.2
pH	9.0	8.1	7.7
Alk. (mg/L $CaCO_3$)	66.6	64.9	59.6
DO	8.6	8.0	7.8
Cond. (μS/cm)	459	527	1134
Ag	bd	bd	0.0004
Al	0.0005	0.0020	bd
As	0.0133	0.0157	0.0070
B	0.026	0.073	0.062
Ba	0.442	0.333	0.101
Be	bd	bd	bd
Ca	20.7	11.8	54.1
Cd	0.00042	0.00058	0.0012
Co	0.0006	0.0003	0.0007
Cr	0.00641	0.00022	bd
Cu	0.0012	0.0023	0.0010
Fe	0.104	bd	0.020
Hg	0.00012	bd	bd
K	41.0	79.4	75.9
Mg	44.6	28.0	90.1
Mn	0.0111	0.0084	0.035
Mo	0.284	0.450	0.537
Na	11.2	14.6	22.5
Ni	0.0280	0.0934	0.0394
Pb	0.00012	0.00003	bd
Sb	0.0293	0.0346	0.0159
Se	0.0030	0.0015	0.0036
Si	NA	4.0	4.9
Sr	0.438	0.304	0.968
U	0.00015	0.00009	0.0005
V	0.00278	0.0057	0.0030
Zn	0.0014	0.0030	0.010
NH_3-N	1.19	0.785	1.53
Cl	16.3	29	55
F	0.08	bd	0.08
NO_3-N	7.26	4.51	3.3
NO_2-N	0.267	0.155	0.170
PO_4-P	0.045	0.010	0.017
SO_4	151	100	473
DIC	14.3	14.7	NA
DOC	3.1	3.6	14.7

Table 4.5: Average process plant discharge water analyses from 2000 to 2002. All values are reported in mg/L unless specified otherwise (bd = below detection limit; NA = not analyzed). Major dissolved constituents are highlighted.

	2000	2001	July 2002	Aug 2002
Number of samples	4	2	2	1
Temp. (°C)	10.5	12.1	15.67	11.87
pH	7.4	8.2	8.83	8.11
Alk. (mg/L $CaCO_3$)	73.0	23.4	10.46	61.6
DO	9.5	10.9	52.40	11.8
Cond. (μS/cm)	506	154	431	529
Ag	b.d.	bd	bd	bd
Al	0.0040	0.0086	0.0037	0.0036
As	0.00942	0.00234	0.00341	0.00387
B	0.022	0.017	0.030	0.033
Ba	0.134	0.093	0.104	0.112
Be	bd	bd	bd	bd
Ca	30.1	9.5	13.1	15.3
Cd	0.00069	bd	0.00027	0.00042
Co	0.0005	bd	0.0001	0.0003
Cr	0.00741	0.00021	0.00029	0.00055
Cu	0.0009	0.0042	0.0012	0.00390
Fe	0.144	0.005	0.006	0.0100
Hg	0.00010	bd	0.00003	0.00006
K	29.2	10.4	22.3	35.6
Mg	48.9	13.5	23.0	30.2
Mn	0.0171	0.0025	0.0009	0.0085
Mo	0.337	0.0675	0.154	0.220
Na	10.7	2.88	5.30	8.67
Ni	0.0298	0.0132	0.0102	0.0223
Pb	0.00020	bd	bd	0.00009
Sb	0.0162	0.0026	0.00464	0.00760
Se	0.0018	bd	0.0005	0.0006
Si	NA	1.0	1.80	2.4
Sr	0.473	0.148	0.235	0.307
U	0.00047	0.0001	0.00014	0.00013
V	0.00175	0.00091	0.00146	0.00133
Zn	0.0011	0.0019	0.0017	0.0054
NH_3-N	0.409	0.011	bd	bd
Cl	14	3	9	21
F	0.08	bd	NA	NA
NO_3-N	3.66	0.214	0.690	1.86
NO_2-N	0.725	0.060	0.098	0.203
PO_4-P	0.009	0.006	bd	bd
SO_4	181	49.4	103	124
DIC	17.6	7.8	NA	13.1
DOC	4.6	4.5	21.3	14.4

Table 4.6: Average dyke B surface water analyses from 2000 to 2002. All values are reported in mg/L unless specified otherwise (bd = below detection limit; NA = not analyzed). Major dissolved constituents are highlighted.

4.2.4.2 Dyke C

Table 4.7 lists the average surface water composition at Dyke C from 2000 to 2002. Similar to the chemistry of the surface water at Dyke B, the most significant components of Dyke C surface water analyses include alkalinity, SO_4, Mg, Ca, K, and Na. Also similar to Dyke B surface water, pH is approximately neutral (6.71 to 8.5), dissolved Si is low, ranging from 1.0 mg/L to 2.0 mg/L, and average dissolved Fe concentrations do not exceed 0.110 mg/L. Average conductivity of water samples collected from Dyke C is approximately 331 μS/cm.

4.3 Reduction-Oxidation Potential

4.3.1 Measurement of Reduction-Oxidation Potentials

Measurement of the reduction-oxidation potential of a solution is done using a meter that is essentially a high resistance voltmeter. The electrode of the meter is placed into the solution to measure the electrical potential of the water sample (measured in millivolts) (Snoeyink and Jenkins, 1980). Theoretically, redox potentials are well understood, but the practical measurement of these potentials in natural systems is plagued with problems that often inhibit meaningful application of Eh data. There are four main problems associated with the measurement and application of redox potential data: 1) A lack of internal equilibrium between different redox pairs (Lindberg and Runnels, 1984), 2) the development of mixed potentials (Stumm and Morgan, 1996), 3) the kinetics of electron transfer processes (Katakis and Gordon, 1987), and 4) the concentration of significant redox species in solution (Stumm and Morgan, 1996).

	2000	2001	Jul-02	Aug-02
Number of samples	3	2	2	2
Temp. (°C)	11.7	11.2	16.35	11.09
pH	8.5	7.6	8.08	6.71
Alk. (mg/L $CaCO_3$)	40.5	22.8	9.99	51.4
DO	9.3	10.2	43.6	10.8
Cond. (µS/cm)	222	215	324	565
Ag	bd	bd	bd	bd
Al	0.0053	0.0028	0.0042	0.0056
As	0.00409	0.0	0.00434	0.00307
B	0.012	0.0	0.031	0.031
Ba	0.149	0.2	0.148	0.129
Be	bd	bd	bd	bd
Ca	19.5	10.7	17.9	20.5
Cd	0.00041	0.00010	0.00062	0.00037
Co	0.0002	0.0001	0.0003	0.0002
Cr	0.00432	0.0	0.00090	0.00077
Cu	0.0012	0.0010	0.0035	0.00175
Fe	0.110	bd	0.006	0.0070
Hg	0.00006	bd	0.00005	0.00006
K	14.4	20.2	33.9	19.4
Mg	24.3	18.6	30.6	31.9
Mn	0.0085	0.0092	0.0041	0.0023
Mo	0.145	0.105	0.209	0.187
Na	6.6	6.26	12.4	13.5
Ni	0.0142	0.0157	0.0180	0.0160
Pb	0.00005	bd	0.00007	bd
Sb	0.0115	0.0071	0.00971	0.00775
Se	0.0014	0.0004	0.0009	0.0006
Si	NA	1.6	2.0	1.0
Sr	0.267	0.198	0.358	0.383
U	0.00028	0.0002	0.00028	0.00052
V	0.00083	0.00092	0.00137	0.00102
Zn	0.0016	0.0007	0.0038	0.0047
NH_3-N	0.165	0.167	0.403	0.150
Cl	12	12	43	49
F	0.08	bd	NA	NA
NO_3-N	4.10	3.35	4.37	3.15
NO_2-N	0.455	0.065	0.185	0.157
PO_4-P	0.006	0.006	bd	bd
SO_4	86	61.5	115	115
DIC	9.8	8.3	NA	12.9
DOC	3.4	3.1	17.4	10.4

Table 4.7: Average dyke C surface water analyses from 2000 to 2002. All values are reported in mg/L unless specified otherwise (bd = below detection limit; NA = not analyzed). Major dissolved constituents are highlighted.

The goal of measuring Eh of an aqueous system is to determine the potential at which all redox couples exist. If all redox-sensitive elements exist at the same potential, the water is said to be at internal redox equilibrium. Internal redox equilibrium requires that the values measured directly by a probe, or calculated indirectly using redox-couple concentrations are the same, but this is not always the case. Lindberg and Runnels (1984) looked at 700 groundwater analyses and found that very few samples had similar measured and calculated Eh values, indicating that internal equilibrium is not usually attained.

An additional problem with Eh measurements is the development of mixed potentials (Stumm and Morgan, 1996). Redox reactions involve the movement of electrons between redox pairs. The movement of electrons produces an electrical current, and the net current of the redox system is the sum of the currents from each half-reaction, called exchange currents. Redox potential is defined when the net current of the system is zero (i.e. exchange currents are equal). If the aqueous system being measured contains many different redox couples, there is the possibility that the exchange currents contributing to the net current will be from different couples. If this happens, the voltage measured will be a combination of two or more redox reactions and the potential will not be quantitatively meaningful.

Current flow is a dynamic process and therefore the kinetics of electron transfer reactions should also be considered when evaluating the validity of Eh data. A large number of redox reactions that occur in surface and ground waters involve the transfer of multiple electrons such as the reduction of $O_{2(g)}$ to H_2O:

$$1/2\,O_2 + 2H^+ + 2e^- \longrightarrow H_2O$$

Many of these multiple-electron transfer reactions involve structural re-organization, which cause them to be kinetically slow, or non-electroreactive (Katakis and Gordon, 1987). The slow rate of these reactions leads to very small currents, which may not be measurable, even with the most sophisticated field equipment, thereby providing meaningless potentials due to the apparent zero current at the electrode. Single electron reactions such as:

$$Fe^{3+} + e^{-} \longrightarrow Fe^{2+},$$

are very electroreactive. Therefore, waters that contain Fe as the significant redox species equilibrate quickly providing a quantitatively meaningful voltage (Kempton et al., 1990).

One final problem with the measurement of redox potentials is the concentration of the redox species in solution. Electrode current is used to measure the redox potential of a system and is proportional to the concentration of electrons involved in a reaction. If there is not an adequate number of moving electrons, then the current will be too low to be measured accurately. For example, in the case of the Fe^{2+}/Fe^{3+} system, it is difficult to obtain measurements of Eh if either Fe ion concentration is less than approximately 0.6 mg/L (Stumm and Morgan, 1996).

Due to the problems associated with Eh measurement of many surface and ground waters, Lindberg and Runnells (1984) suggest that the use of a measured master Eh for predicting the equilibrium chemistry of reactions in normal ground waters be abandoned. Instead, they suggest that a qualitative guide to the redox status of waters be obtained through the measurement of sensitive species such as dissolved oxygen. If Eh is used to model speciation of redox-sensitive pairs it is important to demonstrate the reversibility of the system and, therefore, the validity of the Eh measurement.

4.3.2 Reduction-Oxidation State of LLCF Waters

Eh was measured in the field for every water sample collected in this investigation. However, no sample produced a reading that was recordable. In every case, the Eh meter started at a value and then slowly decreased with no stabilization even after five minutes of measurement. The inability of the redox meter to produce stable potentials can most likely be attributed to the identity and concentrations of redox couples present in the waters.

The redox sensitive species present in the list of analytes for this study are: As, Co, Cr, Cu, Fe, Hg, Sb, Se, U, V, N, S, and dissolved oxygen. Thermodynamically meaningful Eh measurements may be possible in waters that contain significant amounts of dissolved Fe, Mn, and reduced S (Langmuir, 1996), but Tables 4.1 to 4.7 indicate that Fe and Mn are present at very low concentrations, and the water samples were not analyzed for reduced S. The low concentrations of Fe and Mn present in the LLCF waters would most likely not provide sufficient current to measure redox potential.

Analytical results of redox pairs were only obtained for NO_3-N, NO_2-N, and NH_3-N. As well, dissolved oxygen was measured in the field immediately upon sample collection. Therefore, theoretical Eh values for the H_2O/O_2, NH_3/NO_2, NH_3/NO_3, and NO_2/NO_3 redox pairs can be calculated on the basis of the Nernst Equation (Langmuir, 1996). These values have been calculated using the geochemical speciation and modeling program PHREEQC (section 6.1) and are tabulated in table 4.8. Note the inconsistency of the Eh values calculated from the analytical data, with the largest discrepancy existing between the nitrogen redox equilibria and the oxygen equilibrium, indicating that there is a lack of internal redox equilibrium in the LLCF water samples.

Dissolved organic carbon (DOC) concentrations greater than approximately 4 mg/L typically occur in anoxic waters found within lake bottom sediments, organic-rich waste ponds, water-logged soils, and deeper groundwater systems (Langmuir, 1996). The fact that LLCF water samples contain DOC concentrations that exceed 4 mg/L and high dissolved oxygen concentrations is another piece of evidence indicating the state of redox disequilibrium that exists within LLCF water samples (table 4.1 to 4.7).

Although the absolute values of Eh calculated are not necessarily quantitatively valid, they do provide a qualitative description of the redox status of the system. From the tabulated potentials calculated from the analytical data it can be seen that all the waters have very high Eh indicating that they are all oxidized. This is to be expected since all water samples taken in this investigation were in close contact with the atmosphere.

4.4 LLCF Water Types

When investigating the evolution of water chemistry, it is often useful to classify water samples based on the relative proportions of the dominant anions and cations in solution. Piper diagrams are useful in separating analytical data for the purpose of investigating sources of dissolved materials and geochemical reactions in natural waters (Piper, 1944). As well, these diagrams are useful to help classify a suite of water samples into types based on the dominant cations and anions present (Back, 1966).

Lysimeter	2000	2001	July 2002	August 2002
NH_3/NO_2	0.259	0.293	0.343	0.322
NH_3/NO_3	0.285	0.317	0.372	0.355
NO_2/NO_3	0.358	0.384	0.458	0.494
H_2O/O_2	0.744	0.768	0.805	0.816

Discharge	2000	2001	July 2002	August 2002
NH_3/NO_2	0.216	0.270	0.284	0.290
NH_3/NO_3	0.250	0.299	0.314	0.312
NO_2/NO_3	0.351	0.388	0.405	0.378
H_2O/O_2	0.713	0.752	0.768	0.757

Surface	2000	2001	July 2002	August 2002
NH_3/NO_2	0.271	0.305	0.264	0.394
NH_3/NO_3	0.298	0.329	0.292	0.414
NO_2/NO_3	0.381	0.404	0.366	0.446
H_2O/O_2	0.748	0.775	0.736	0.817

Table 4.8: Average Eh values (in volts) calculated from data for redox pairs analyzed in LLCF water samples.

Piper diagrams represent graphically the relative contribution of each of the major cations and anions to the overall water chemistry. They are constructed by first plotting the relative percent cation (Mg, Ca, and Na + K) and anion (HCO_3, SO_4, Cl) equivalents on two ternary diagrams. Next, these two points are transferred onto the quadrilateral portion of the diagram. Plotting data in the quadrilateral field causes some information to be lost through the combination of Mg and Ca, and SO_4 and Cl. However, projecting data to the quadrilateral is useful because it helps to graphically represent the combined effect of cations and anions (Drever, 1997). Figure 4.1 shows the plotting space for the Piper diagram with the dashed lines separating hydrochemical facies (Back, 1966).

Figure 4.2 is a Piper diagram for the LLCF water samples, with black dots representing pore-water analyses, open squares representing discharge water analyses, and open and closed triangles representing surface water samples from Dykes B and C, respectively. Inspection of this diagram indicates that each of the three types of samples have their own distinct chemical character.

Pore-water samples are characterized by high Mg and SO_4 percent, the lowest relative Na + K percent of any LLCF water samples, very low Cl percent, and an almost constant Ca percent.

Unlike pore-water samples, discharge waters have the highest Na + K, and the lowest Ca percent content of any LLCF water samples. As well, discharge water samples contain moderate Mg, and approximately10 to 20 equivalent percent more Cl than do pore-water samples.

Samples from both Dyke B and Dyke C plot in the same regions of figure 4.1 and are chemically similar to discharge water samples in their relative anion composition as well

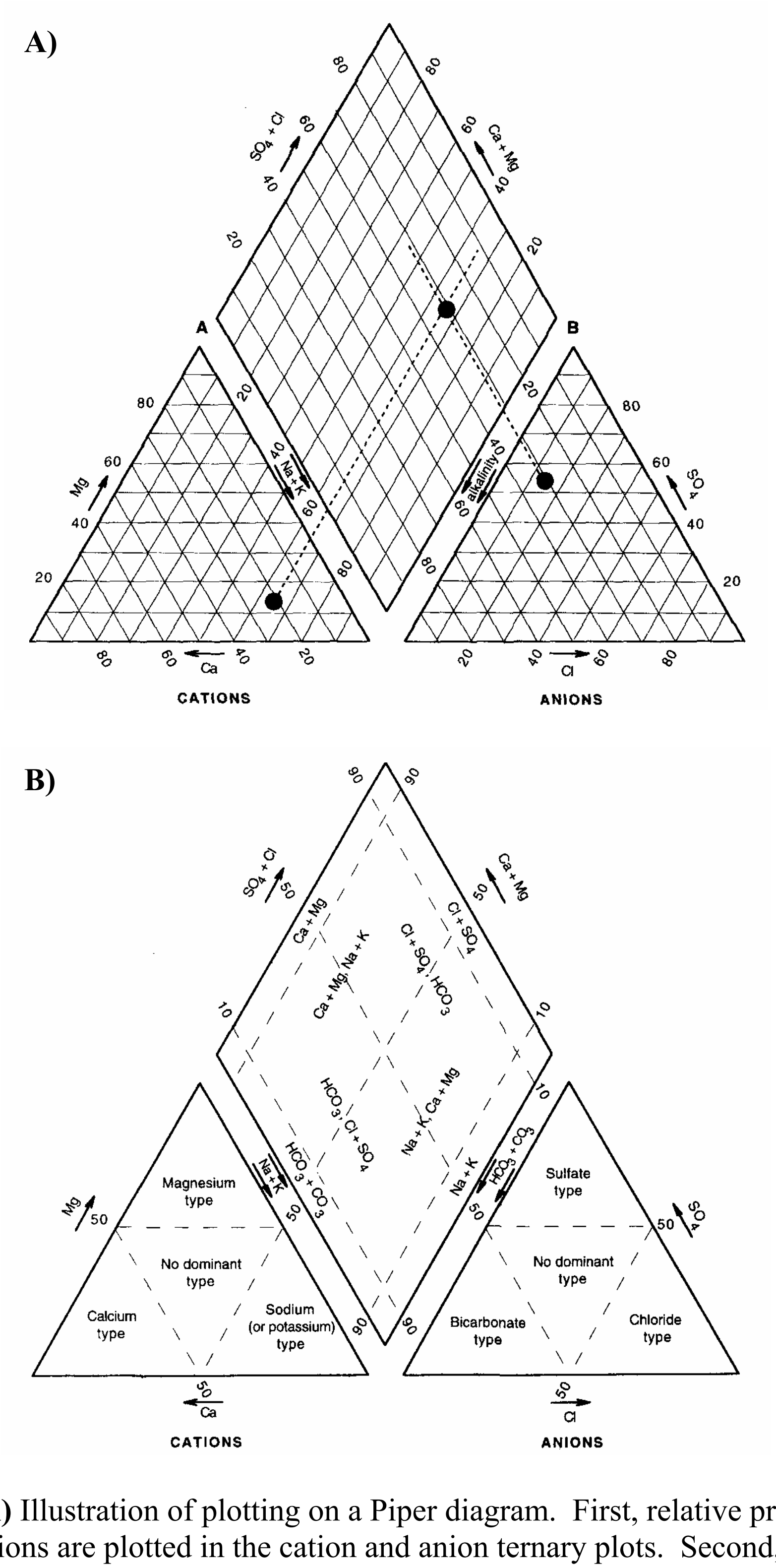

Figure 4.1: A) Illustration of plotting on a Piper diagram. First, relative proportions of cations and anions are plotted in the cation and anion ternary plots. Second, these points are transferred to the quadrilateral portion of the diagram as shown. **B)** Diagram showing the regions occupied by each of the water types on a Piper diagram (After Drever, 1997).

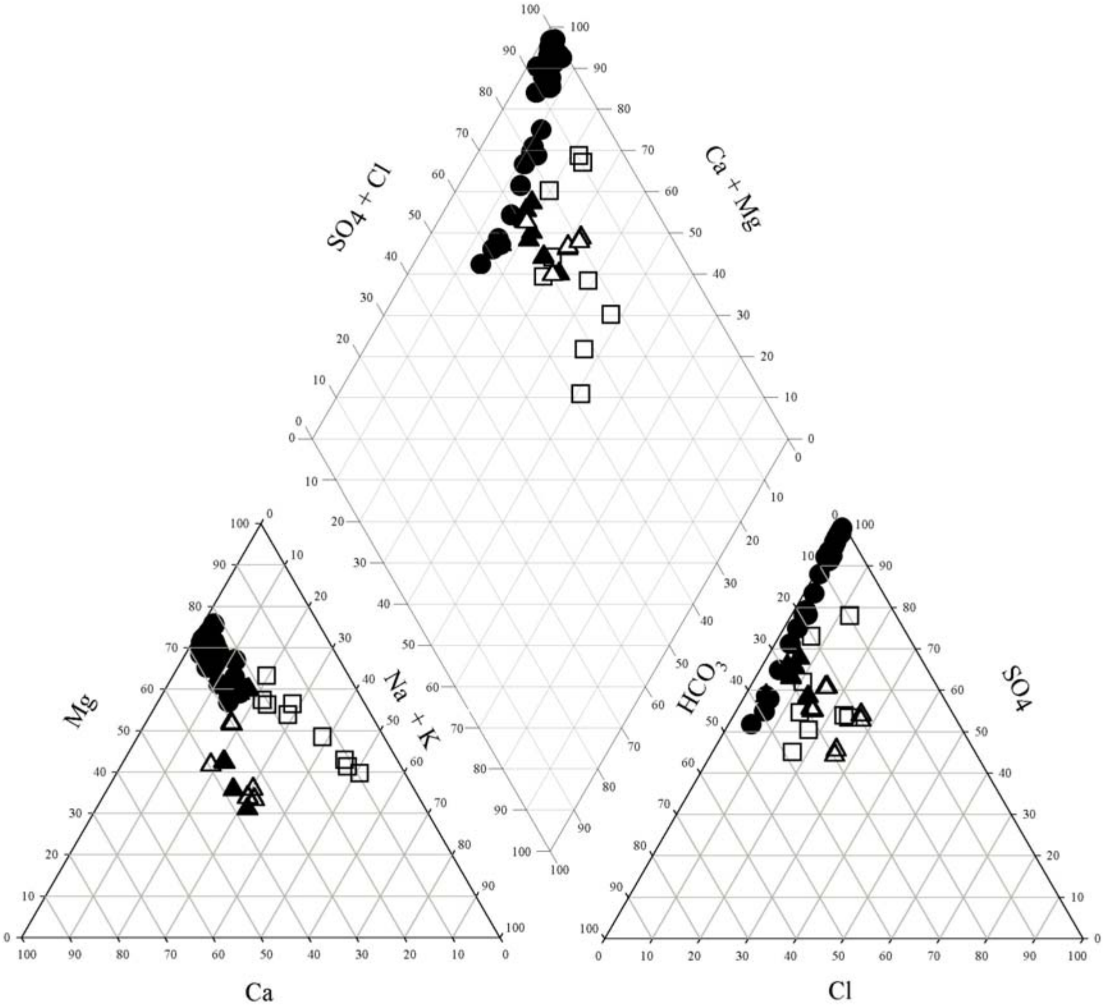

Figure 4.2: Piper diagram for LLCF water samples collected from 2000 to 2002. Solid black circles represent processed kimberlite fines pore-water, open squares represent process plant discharge water, and solid and open triangles represent surface water samples from Dyke B and Dyke C, respectively.

as relative Na + K content. The two characteristics of surface water samples that distinguish them from the pore-water and discharge water samples are that they contain the highest relative Ca content and lowest relative Mg content of all LLCF water samples.

All three types of water samples collected from the LLCF are SO_4-rich, plotting entirely within the SO_4 field of the anion ternary plot (Figure 4.2). While the pore-water analyses follow a linear trend along the HCO_3 axis towards the SO_4 apex, the discharge and surface water analyses all plot close to the lower central region of the SO_4 field, indicating that although SO_4 is the major anion, HCO_3 is also a major contributor to water chemistry. Besides distinguishing the pore-water analyses, the anion ternary plot does not allow the unique identification of the different water samples. However, the cation ternary is useful to distinguish the three types of water samples from each other.

The pore-water analyses are all clearly Mg-type waters (Back, 1966) while discharge water samples appear to straddle the boundary between the Mg field and the central cation field with no one dominant ion. However, the surface water samples all exist within the central field of the cation ternary, indicating that these waters are not dominated by any one cation.

4.5 Temporal Variations

One of the objectives of the sampling program developed for this investigation was to determine the temporal variation that exists within the LLCF mineral-water system over two time scales: seasonal and annual. The seasonal variation is the change that occurs in water chemistry from the beginning to the end of the summer while the annual variation is the change in water chemistry observed between years. In order to accomplish this objective, a suite of pore-water, discharge water, and surface water samples were collected over three field seasons, with two sample suites collected during the final field season; one at the beginning of the summer and one at the end of the summer.

4.5.1 Processed Kimberlite Fines Pore-Water

Temporal variations of elemental concentrations in pore-water analyses were investigated using box-and-whisker plots with concentration plotted along the horizontal axis and time along the vertical axis. These diagrams are constructed by calculating the 10th, 25th, 75th, and 90th percentile values for each element in all water sample suites. The 25th and 75th percentile form the left and right hand boundaries of the box, while the whiskers extend out to the 10th and 90th percentile values. The extent of box overlap between sample suites is used to determine whether there is an increase, decrease, or no change in elemental concentration ranges between sample suites.

The box-and-whisker plots for the complete list of pore-water analytes can be found in Appendix B. These plots show that there is little, if any, significant variation between the samples collected in July and August 2002, indicating little seasonal variation in the pore-water compositions. As well, when the concentration ranges between years are compared it can be seen that the majority of elements do not exhibit any strong increasing or decreasing trends.

However, there are a few exceptional elements that exhibit a concentration variation with time. Figure 4.3 contains the box-and-whisker diagrams for Fe, Cr, and NH_3-N.

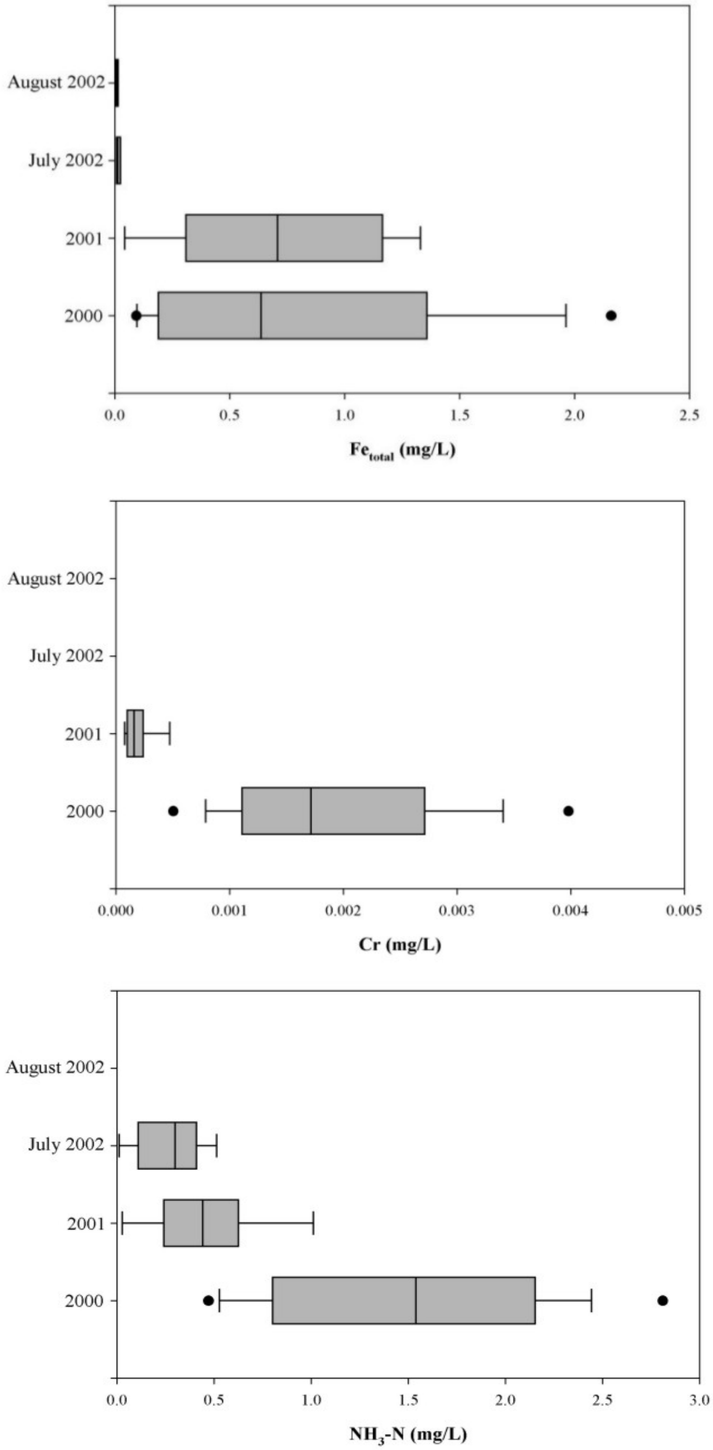

Figure 4.3: Lysimeter pore-water box-and-whisker plots for Fe, Cr, and NH_3-N. Note how the concentration of each element decreases with time. The absence of a box indicates that all analyses in that suite of samples contained concentrations below the detection limit.

These plots indicate that the concentration of these elements decreased in the LLCF processed kimberlite fines pore-water from 2000 to 2002. As well, the plots for pH and B (Figure 4.4) indicate that the concentration of H^+ and B increased in the LLCF pore-water samples during this investigation.

4.5.2 Surface Water

The temporal variation of surface water compositions has been investigated through the use of line plots with date of collection along the horizontal axis and concentration on the vertical axis. Elements with similar concentration ranges were plotted together, with the exception of the nitrogen containing species (NO_3, NO_2, NH_3), which have been plotted together to illustrate the relative abundance of the various forms of nitrogen. All temporal variation plots for surface water samples collected at Dyke B and Dyke C are compiled in Appendix B. Refer to figure 3.1 for a map indicating the location from which surface water samples were collected.

4.5.2.1 Dyke B

Figure 4.5A is a plot showing the temporal variation of the major dissolved components of the Dyke B water samples: SO_4, Ca, Mg, Na, K, and alkalinity. Inspection of figure 4.5A indicates that the major dissolved constituents experience a decrease in concentration from 2000 to 2001 and then an increase from 2001 to 2002. As well, pH appears to be relatively constant at a value of approximately 8 (Figure 4.5B).

Significant amounts of process plant effluent have not been discharged into Cell B since the latter part of 2000. Therefore, natural precipitation is currently the most significant input of water into Cell B. The dykes within the LLCF were constructed to

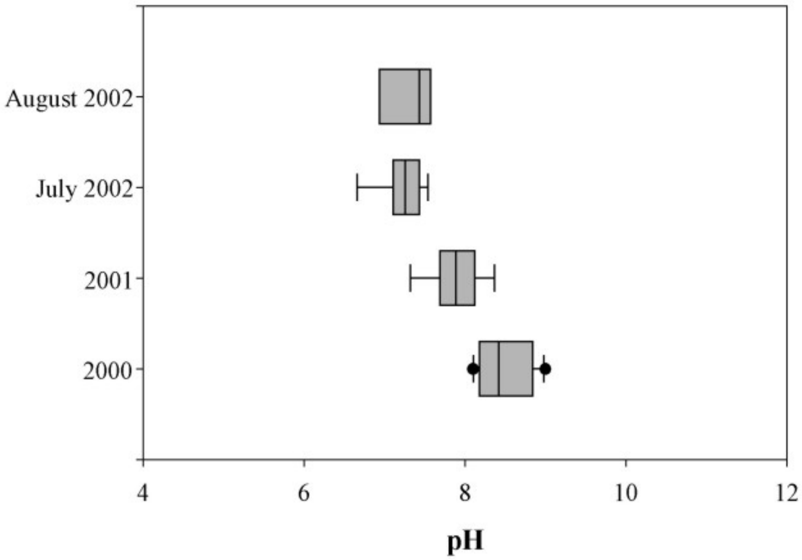

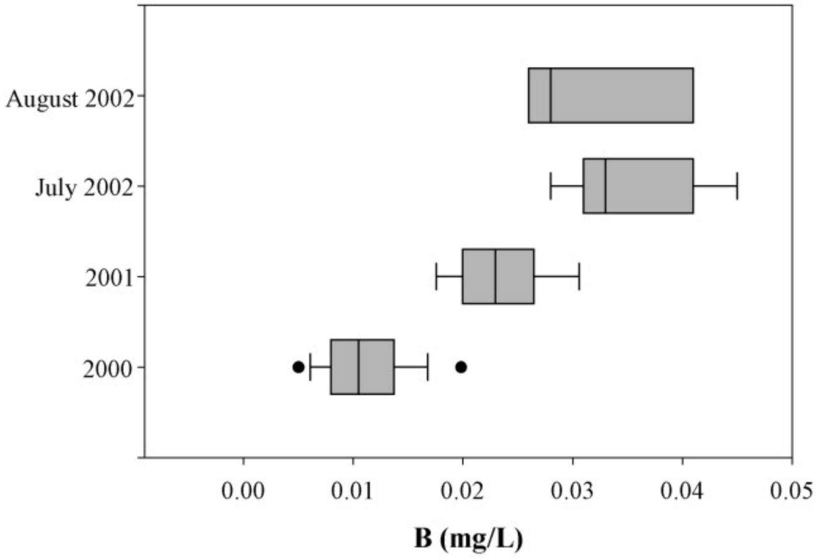

Figure 4.4: Lysimeter pore-water box-and-whisker plots for pH and B. Note how the concentration of each element increases with time. Note that pH = -log[H^+]. Therefore, as pH decreases the concentration of H^+ increases.

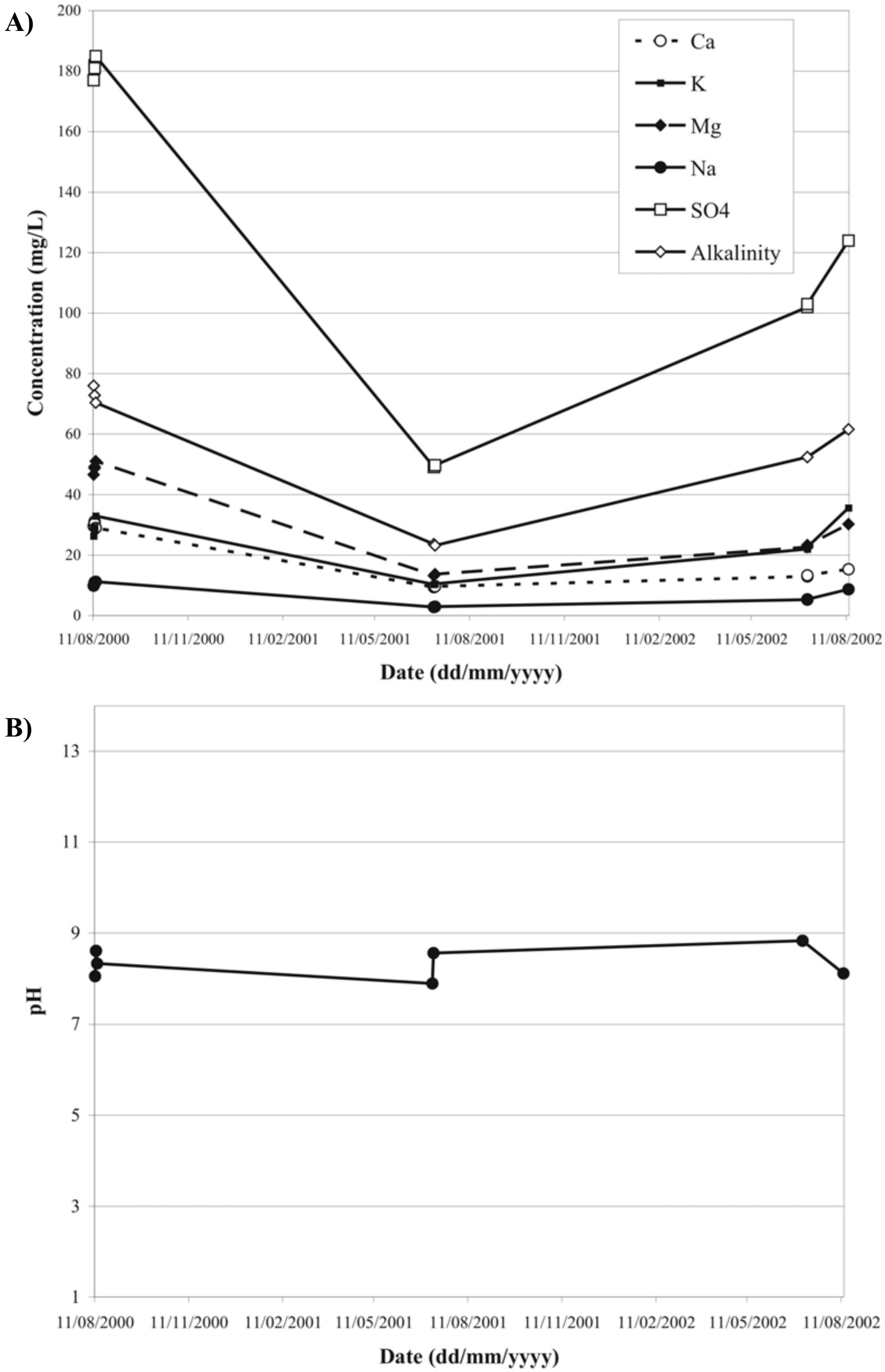

Figure 4.5: Temporal variation of the **A)** major dissolved constituents and **B)** pH of surface water collected from Dyke B. Samples are represented by dots.

help filter fine suspended material from the water column. High water levels have been observed in Dyke B, with the highest water levels noted in the summer of 2001 (Figure 4.6). However, no quantitative water level measurements were collected at Dyke B. The increase in water level at Dyke B is most likely due to the fact that the high turbidity of water in the southern end of Cell B has clogged the dyke, thus retarding the flow of water into Cell C. This has created a lake, the level of which is affected by the amount of spring runoff and the rate at which water can drain from Cell B. Variations in the amount of snow-melt water that fills the Cell B 'lake' during freshet, will lead to variations in the concentrations of dissolved constituents, as is the case for the majority of elements in the Dyke B surface waters.

Some analytes, including Fe, Cr, NH_3, Al, Cu, and PO_4, do not exhibit this pronounced decrease and increase in concentration as noted previously (Appendix B). Fe, Cr, and NH_3 experience a constant decrease in concentration from 2000 to 2002, which is similar to the behaviour of these elements in the processed kimberlite pore-water. However, the variation of Al, Cu, and PO_4 behaves opposite to the majority of elements in that they experience a maximum during the summer of 2001 rather than a minimum.

4.5.2.2 Dyke C

Unlike surface water collected at Dyke B, the majority of elements in Dyke C surface water samples indicate a moderate to strong increase in concentration with time. Figure 4.7 shows the temporal variation of both the major dissolved constituents and pH in Dyke C surface water samples. These plots show that the major dissolved elements experience an increase in concentration with time while the pH remains relatively constant at a value

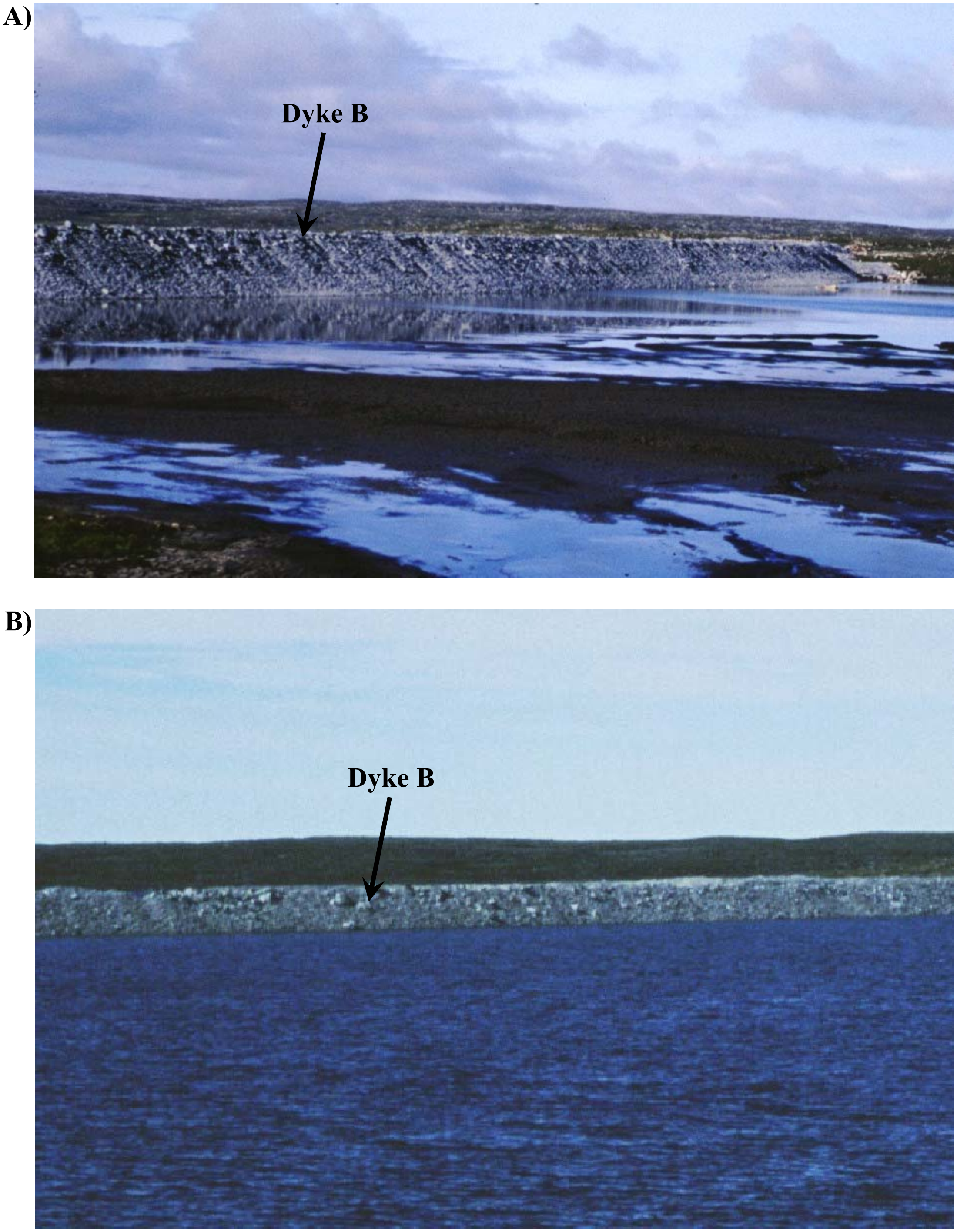

Figure 4.6: Images of the water level at Dyke B, in the south end of Cell B, in **A)** 2000, and **B)** 2001. Note how much higher the water level in the south end of Dyke B is in 2001 compared to 2000. Both of these images are looking southwest at the north side of Dyke B.

A)

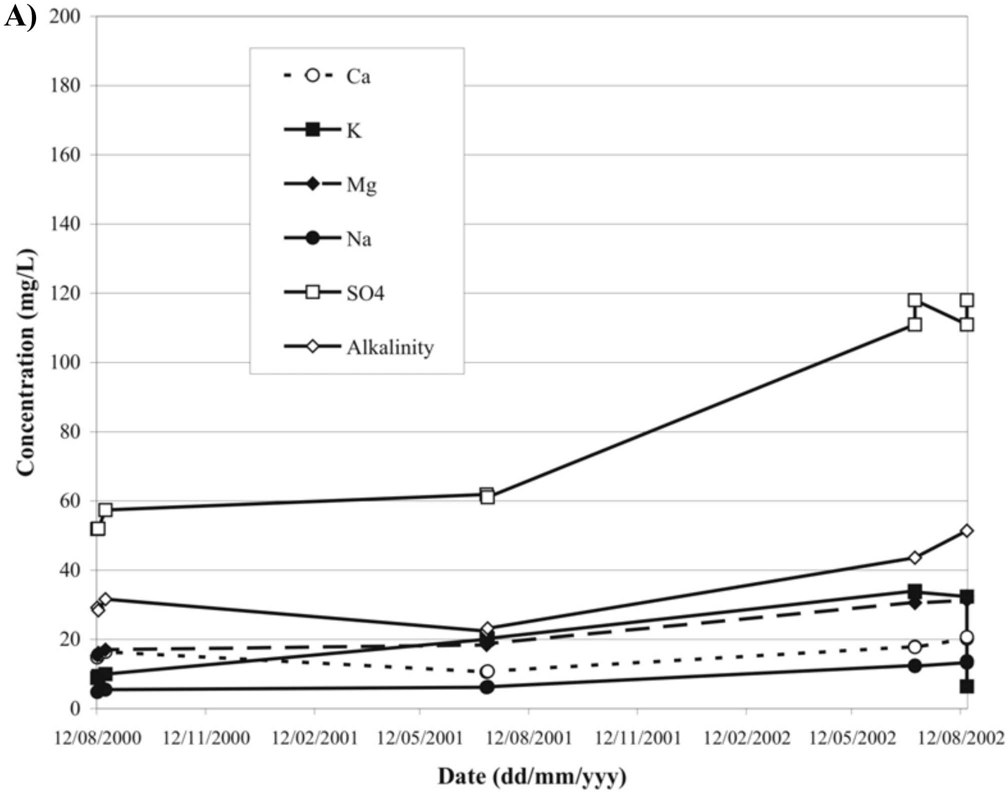

B)

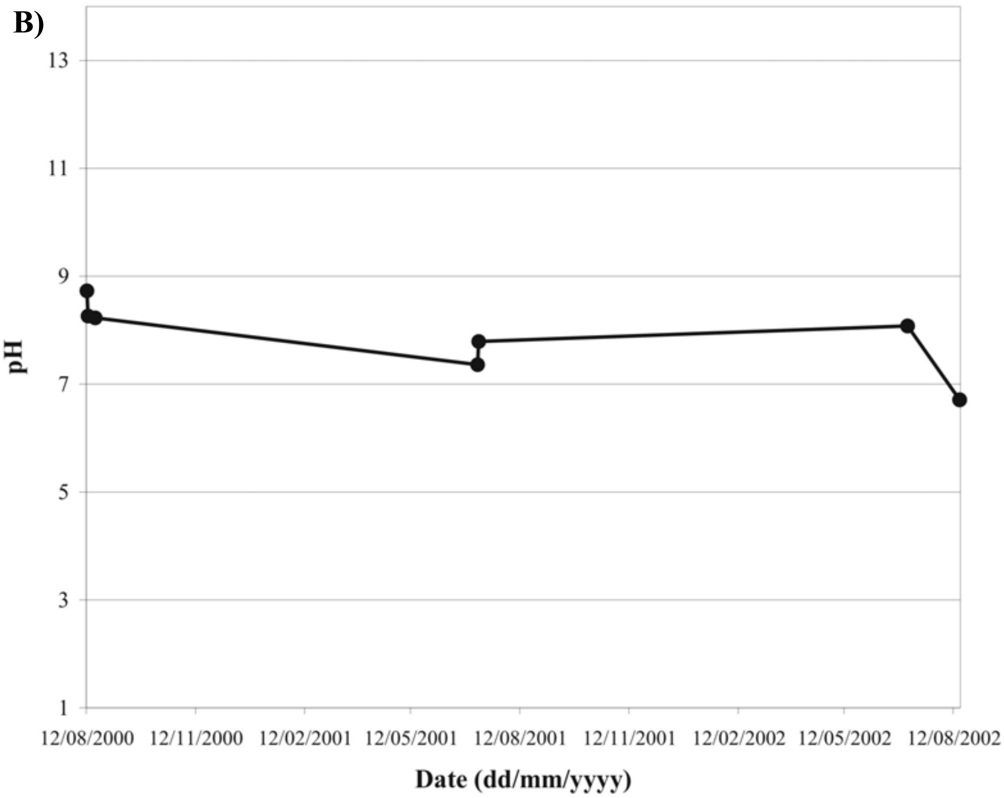

Figure 4.7: Temporal variation of the **A)** major dissolved constituents and **B)** pH of surface water collected from Dyke C. Samples collected are represented by dots.

of approximately 8. Process plant effluent has been continuously discharged into Cell C since late 2000, providing a significant volume of water to this cell. The dissolved material in the process plant discharge water is continuously being added to Cell C causing the water of this cell to become more concentrated with time. However, because process plant discharge water is the main source of dissolved solids in Cell C, the solute concentrations observed at Dyke C will increase only until they are equal to the concentration of process plant discharge water.

4.5.2.3 Ice-Core Dam

From August 1998 to September 2002, Ekati Environment personnel collected samples of water discharging from the LLCF, approximately once a week, for the purposes of in-house water quality monitoring. Figure 3.1 indicates the location from which this sample was collected. The data for major dissolved constituents and pH has been plotted in Figures 4.8 and 4.9, respectively. Inspection of these plots indicates that, similar to the surface water samples collected from the north side of Dyke C, the water discharging from the LLCF to the receiving environment is becoming more concentrated with time while pH remains relatively constant at approximately 7.0. As well, it should be noted that increases in the concentration of dissolved constituents was not experienced until approximately August of 1999. This lag time is most likely due to the rate at which the plume of process plant discharge water migrated south through the LLCF. As the discharge spigot moves further south, closer to the ice-core dam, not only will the concentrations of dissolved constituents discharging to the environment increase, but also variations in the chemistry of process plant effluent will be more immediately observed at the ice-core dam.

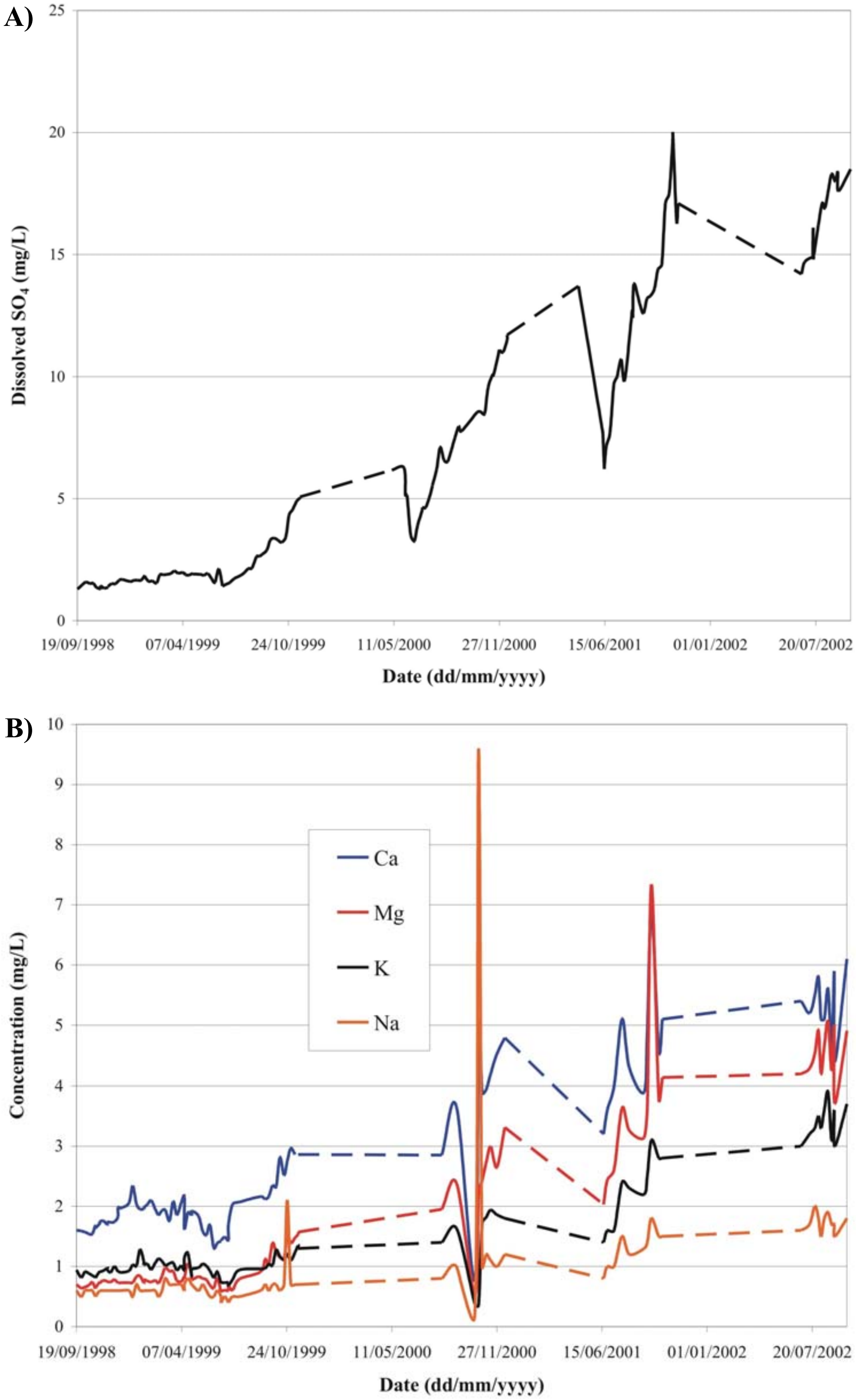

Figure 4.8: Temporal variation of the dissolved **A)** SO_4 and **B)** major cation concentrations in water samples collected of LLCF water discharging into the receiving environment. Dashed lines represent periods when no samples were collected.

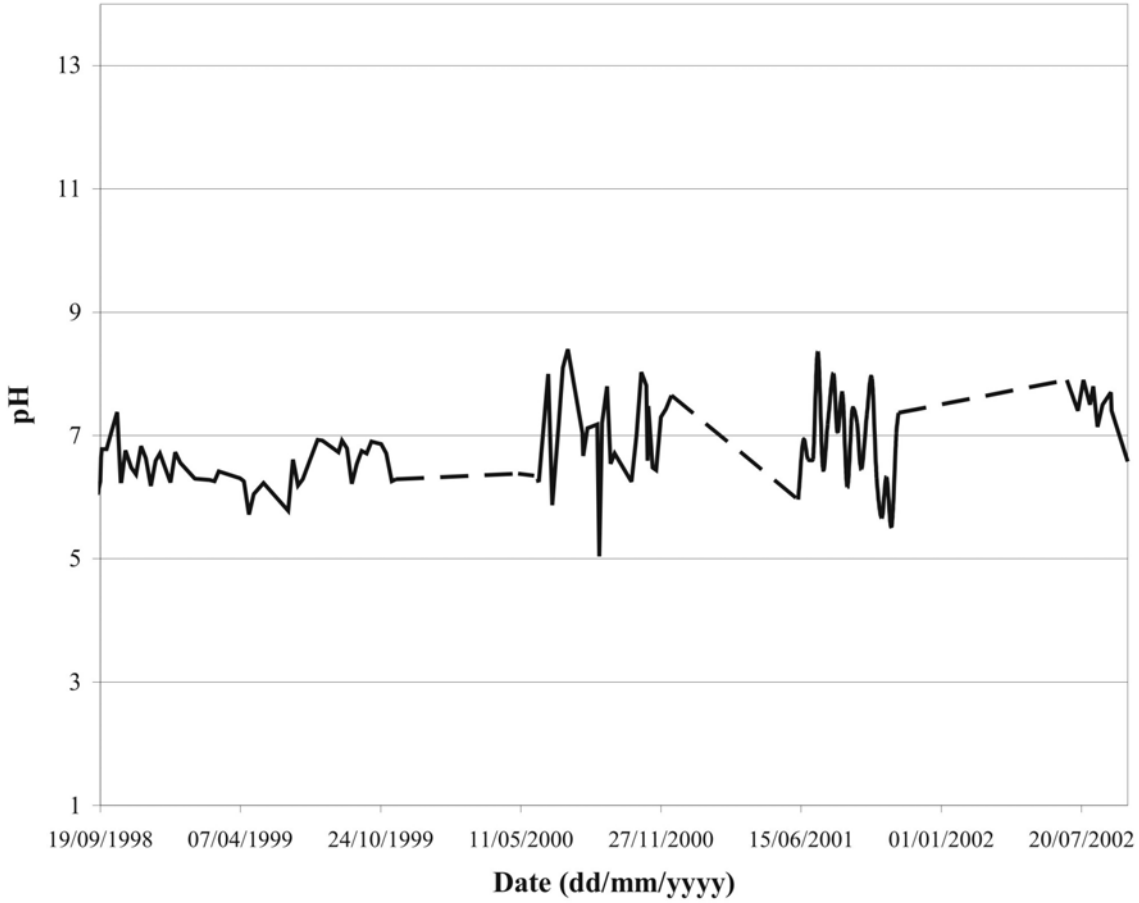

Figure 4.9: Temporal variation of the pH of water samples collected of LLCF water discharging into the receiving environment at the ice-core dam. Dashed lines represent periods when no samples were collected.

4.6 LLCF Water Quality

The water quality requirements of discharge from the LLCF are outlined in the Ekati Water License agreement, which is an agreement entered into by BHPBilliton Inc. and is in accordance with the Northwest Territories Waters Act and Regulations of the Northwest Territories Water Board (Northwest Territories Water Board, 1997). The specific effluent quality requirements listed in the Ekati Water License are:

	Maximum average concentration (mg/L)	**Maximum concentration of any grab sample (mg/L)**
Total NH_3	2.0	4.0
Total Al	1.0	2.0
Total As	0.50	1.0
Total Cu	0.10	0.20
Total Ni	0.15	0.30
Total suspended solids	25	50

The water license also stipulates that all discharge shall have a pH of between 6.0 and 9.0. It should be noted that the water quality requirements stipulated in the Ekati Water License pertain only to the concentration of LLCF effluent discharged to the environment at the ice-core dam (Figure 3.1). All cells within the LLCF will be used to store processed kimberlite fines, except for Cell E, which will never receive process plant effluent directly. Instead, Cell E is intended to act as a final clarifying cell to allow fine suspended particles to settle out of suspension before LLCF water is discharged to the environment. Since processed kimberlite fines have not completely filled Cell C, the solute concentrations at Dyke C can be used to estimate the concentrations that could be expected at the ice-core dam when the LLCF reaches full capacity. Therefore, process plant discharge and surface water samples collected within the LLCF represent maximum concentrations that can be used to predict the water quality that might be expected at the ice-core dam when the LLCF reaches its maximum storage capacity. On inspection of tables 4.5 to 4.7, the average water compositions for process plant discharge and surface waters, it can be seen that the concentration for all regulated parameters in process plant and all surface waters are below those stipulated by the Ekati Water License.

This list of regulated parameters in the Ekati Water License is not as extensive as water quality guidelines that have been recommended by other jurisdictions in Canada, including the National Guidelines and Standards Office (NGSO) and the British Columbia Ministry of Water, Land, and Air protection (BCMWLAP). It should be noted that Ekati is not required to follow these water quality guidelines, unlike the water quality regulations stipulated in the Ekati Water License Agreement. Comparison of LLCF water samples with NGSO and BCMWLAP guidelines is done here for predictive purposes in order to identify parameters that might be of concern in the future.

Tables 4.9 to 4.11 list the average process plant discharge water, Dyke B surface water, and Dyke C surface water, respectively, together with the NGSO and BCMWLAP water quality guidelines for the protection of freshwater aquatic life (British Columbia Ministry of Water Land and Air Protection, 2003; National Guidelines and Standards Office, 2002). Drinking water for the mine is not currently taken from a lake that is affected by LLCF discharge, and there is no agricultural activity around the region of the mine. Therefore, the guidelines for the protection of freshwater aquatic life have been used to evaluate the quality of LLCF water. It should also be noted that the LLCF waters used in this comparison are not being discharged to the environment. However, they can

	2000	2001	2002
pH	9.03	8.15	7.79
Temperature (°C)	10.1	15.8	20.4
Hardness (mg/L $CaCO_3$)	235.2	144.8	428.2
Al	0.0005	0.0020	bd
Al acute WQG[1,2]	0.1	0.1	0.1
Al chronic WQG[1,2]	0.05	0.05	0.05
As	0.0133	0.0157	0.0094
As acute WQG[1,2]	0.005	0.005	0.005
Cd	0.00042	0.00058	0.0014
Cd acute WQG[2]	0.000017	0.000017	0.000017
Cu	0.0012	0.0023	0.0015
Cu acute WQG[1]	0.0241	0.0156	0.0423
Cu chronic WQG[1]	0.0094	0.0058	0.0171
Mn	0.0111	0.0084	0.0303
Mn acute WQG[1]	3.13	2.14	5.26
Mn chronic WQG[1]	1.64	1.24	2.49
Ni	0.0280	0.0934	0.0394
Ni WQG[2]	0.025-0.150	0.025-0.150	0.025-0.150
Se	0.0030	0.0015	0.0039
Se chronic WQG[1]	0.002	0.002	0.002
Zn	0.0014	0.0030	0.0103
Zn acute WQG[1]	0.082	0.074	0.287
Zn chronic WQG[1]	0.0568	0.0486	0.2612
NH_3-N	1.19	0.785	1.35
NH_3-N acute WQG[1]	0.682	4.50	7.82
NH_3-N chronic WQG[1]	0.131	0.732	1.07
F	0.08	bd	0.07
F acute WQG[1]	0.3	0.3	0.3
NO_3-N	7.26	4.51	4.34
NO_3-N acute WQG[1]	200	200	200
NO_3-N chronic WQG[1]	40	40	40
NO_2-N	0.267	0.155	0.660
NO_2-N acute WQG[1,3]	0.060	0.060	0.060
NO_2-N chronic WQG[1]	0.020	0.020	0.020
SO_4	151	100	393
SO_4 acute WQG[1]	100	100	100
SO_4 alert level[1,4]	50	50	50

[1] BC Ministry of Water, Land, and Air Protection guideline

[2] National Guidelines and Standards Office guideline

[3] NGSO maximum guideline (taken from US EPA average criteria)

[4] alert level to monitor health of aquatic moss populations on an occasional basis

Table 4.9: Average process plant discharge water concentrations and corresponding water quality guidelines (highlighted rows) from the National Guidelines and Standards Office (NGSO) and the BC Ministry of Water, Land, and Air Protection (BCMWLAP). Acute guidelines are the maximum allowable concentrations at any given time and chronic guidelines are 30-day average concentrations. All values are reported in mg/L unless stated otherwise (bd = below detection limit, NA = not analyzed).

	2000	2001	2002
pH	7.4	8.2	8.47
Temperature (^oC)	10.5	12.1	13.8
Hardness (mg/L $CaCO_3$)	276.0	79.0	145.7
Al	0.0040	0.0086	0.0040
Al acute WQG[1,2]	0.1	0.1	0.1
Al chronic WQG[1,2]	0.05	0.05	0.05
As	0.00942	0.00234	0.00364
As acute WQG[1,2]	0.005	0.005	0.005
Cd	0.00069	bd	0.00035
Cd acute WQG[2]	0.000017	0.000017	0.000017
Cu	0.0009	0.0042	0.0026
Cu acute WQG[1]	0.0279	0.0094	0.0157
Cu chronic WQG[1]	0.0110	0.0032	0.0058
Mn	0.0171	0.0025	0.0048
Mn acute WQG[1]	3.58	1.41	2.15
Mn chronic WQG[1]	1.82	0.95	1.25
Ni	0.0298	0.0132	0.0163
Ni WQG[2]	0.025-0.150	0.025-0.150	0.025-0.150
Se	0.0018	bd	0.0006
Se chronic WQG[1]	0.002	0.002	0.002
Zn	0.0011	0.0019	0.0038
Zn acute WQG[1]	0.173	0.033	0.075
Zn chronic WQG[1]	0.1470	0.0075	0.0493
NH_3-N	0.409	0.011	0.006
NH_3-N acute WQG[1]	14.3	3.69	1.90
NH_3-N chronic WQG[1]	1.84	0.709	0.366
F	0.08	bd	NA
F acute WQG[1]	0.3	0.3	0.3
NO_3-N	3.66	0.214	1.278
NO_3-N acute WQG[1]	200	200	200
NO_3-N chronic WQG[1]	40	40	40
NO_2-N	0.725	0.060	0.150
NO_2-N acute WQG[1,3]	0.060	0.060	0.060
NO_2-N chronic WQG[1]	0.020	0.020	0.020
SO_4	181	49.4	114
SO_4 acute WQG[1]	100	100	100
SO_4 alert level[1,4]	50	50	50

[1] BC Ministry of Water, Land, and Air Protection guideline
[2] National Guidelines and Standards Office guideline
[3] NGSO maximum guideline (taken from US EPA average criteria)
[4] alert level to monitor health of aquatic moss populations on an occasional basis

Table 4.10: Average Dyke B surface water analyses and corresponding water quality guidelines (highlighted rows) from the National Guidelines and Standards Office (NGSO) and the BC Ministry of Water, Land, and Air Protection (BCMWLAP). Acute guidelines are the maximum allowable concentrations at any given time and chronic guidelines are 30-day average concentrations. All values are reported in mg/L unless stated otherwise. (bd = below detection limit, NA = not analyzed).

	2000	2001	2002
pH	8.41	7.58	7.395
Temperature (^{o}C)	12.3	11.2	13.7
Hardness (mg/L $CaCO_3$)	105.4	103.2	175.0
Al	0.0048	0.0028	0.0051
Al acute WQG^{1,2}	0.1	0.1	0.1
Al chronic WQG^{1,2}	0.05	0.05	0.05
As	0.00228	0.00392	0.00368
As acute WQG^{1,2}	0.005	0.005	0.005
Cd	0.00013	0.00010	0.00051
Cd acute WQG^{2}	0.000017	0.000017	0.000017
Cu	0.0011	0.0010	0.00305
Cu acute WQG^{1}	0.0119	0.0117	0.0185
Cu chronic WQG^{1}	0.0042	0.0041	0.0070
Mn	0.0068	0.0092	0.0032
Mn acute WQG^{1}	1.70	1.68	2.47
Mn chronic WQG^{1}	1.07	1.06	1.38
Ni	0.0142	0.0157	0.017
Ni WQG^{2}	0.025-0.150	0.025-0.150	0.025-0.150
Se	0.0013	0.0004	0.00075
Se chronic WQG^{1}	0.002	0.002	0.002
Zn	0.0011	0.0014	0.0048
Zn acute WQG^{1}	0.045	0.038	0.097
Zn chronic WQG^{1}	0.0191	0.0121	0.0713
NH_3-N	0.054	0.167	0.275
NH_3-N acute WQG^{1}	2.37	11.1	13.9
NH_3-N chronic WQG^{1}	0.456	1.84	1.79
F	0.08	bd	NA
F acute WQG^{1}	0.3	0.3	0.3
NO_3-N	4.35	3.35	4.45
NO_3-N acute WQG^{1}	200	200	200
NO_3-N chronic WQG^{1}	40	40	40
NO_2-N	0.287	0.065	0.158
NO_2-N acute WQG^{1,3}	0.060	0.060	0.060
NO_2-N chronic WQG^{1}	0.020	0.020	0.020
SO_4	53.8	61.5	111
SO_4 acute WQG^{1}	100	100	100
SO_4 alert level^{1,4}	50	50	50

[1] BC Ministry of Water, Land, and Air Protection guideline

[2] National Guidelines and Standards Office guidelines

[3] NGSO maximum guideline (taken from US EPA average criteria)

[4] alert level to monitor health of aquatic moss populations on an occasional basis

Table 4.11: Average Dyke C surface water analyses and corresponding water quality guidelines (highlighted rows) from the National Guidelines and Standards Office (NGSO) and the BC Ministry of Water, Land, and Air Protection (BCMWLAP). Acute guidelines are the maximum allowable concentrations at any given time and chronic guidelines are 30-day average concentrations. All values are reported in mg/L unless stated otherwise (bd = below detection limit, NA = not analyzed).

5 Petrography and Mineral Chemistry

As stated previously, the first objective of this research was to chemically and mineralogically define the components of the mineral-water system within the LLCF. Chapter 4 discusses the composition and trends observed in the water samples collected from the LLCF. This chapter will discuss the chemical and mineralogical variations of the kimberlite ore, and processed kimberlite fines. For a complete discussion of solid sample collection, preparation, and analytical techniques refer to chapter 3.

5.1 Kimberlite Ore

Panda kimberlite is composed predominantly of crater facies material, which consists of volcaniclastic and varying amounts of epiclastic material (Carlson et al., 1998). The mineralogy is relatively simple with serpentine and olivine composing approximately 60% to 70% of the rock. Petrographic examination of the Panda kimberlite was concerned with the identification of minerals present in the pipe, as well as an estimation of relative abundances of each mineral.

5.1.1 Serpentine – $Mg_3Si_2O_5(OH)_4$

Serpentine is the most abundant mineral found in Panda kimberlite comprising approximately 30% to 60% of the samples. Estimates of serpentine content are difficult due to the heterogeneous nature of Panda kimberlite as well as the similarity in appearance between the groundmass serpentine and mudstone xenoliths found throughout the suite of samples. Serpentine typically occurs as very fine-grained, brown, massive to acicular aggregates composing the majority of the fine-grained kimberlite matrix material (Figure 5.1). As well, serpentine is also present as pseudomorphs of olivine grains either completely or partially replacing olivine along fractures within the crystals or around grain margins (Figure 5.2). EDS spectra indicate that both groundmass and replacement serpentine are similar in composition and are composed mostly of Mg and Si with minor amounts of Al and Fe (Figure 5.3).

5.1.2 Olivine – $(Mg,Fe)_2SiO_4$

Olivine is the second most abundant mineral in the Panda kimberlite, with modal estimates ranging from 20% to 40%. Olivine occurs as highly fractured crystals varying in size from approximately 0.5 mm to 20 mm, and are typically found partially to completely altered to serpentine (Figure 5.2). Electron micro-probe analyses (EMPA) of olivine found within the kimberlite are listed in Appendix C. These analyses indicate that Panda olivine is forsteritic (Mg_2SiO_4), with compositions ranging from approximately Fo_{90} to Fo_{94} (Table 5.1).

5.1.3 Oxides

Oxide minerals within the Panda kimberlite are approximately 1 to 10 µm in diameter and are found mainly in the fine-grained matrix surrounding macrocrysts and xenoclasts. As well, oxide minerals typically contain varying amounts of Ca, Ti, Mg, Fe, Al, and Mg (Figure 5.4). These data indicate that perovskite, ilmenite, and various spinel group minerals constitute the oxide mineral assemblage in the suite of samples, which are common kimberlitic oxide minerals (Mitchell, 1986).

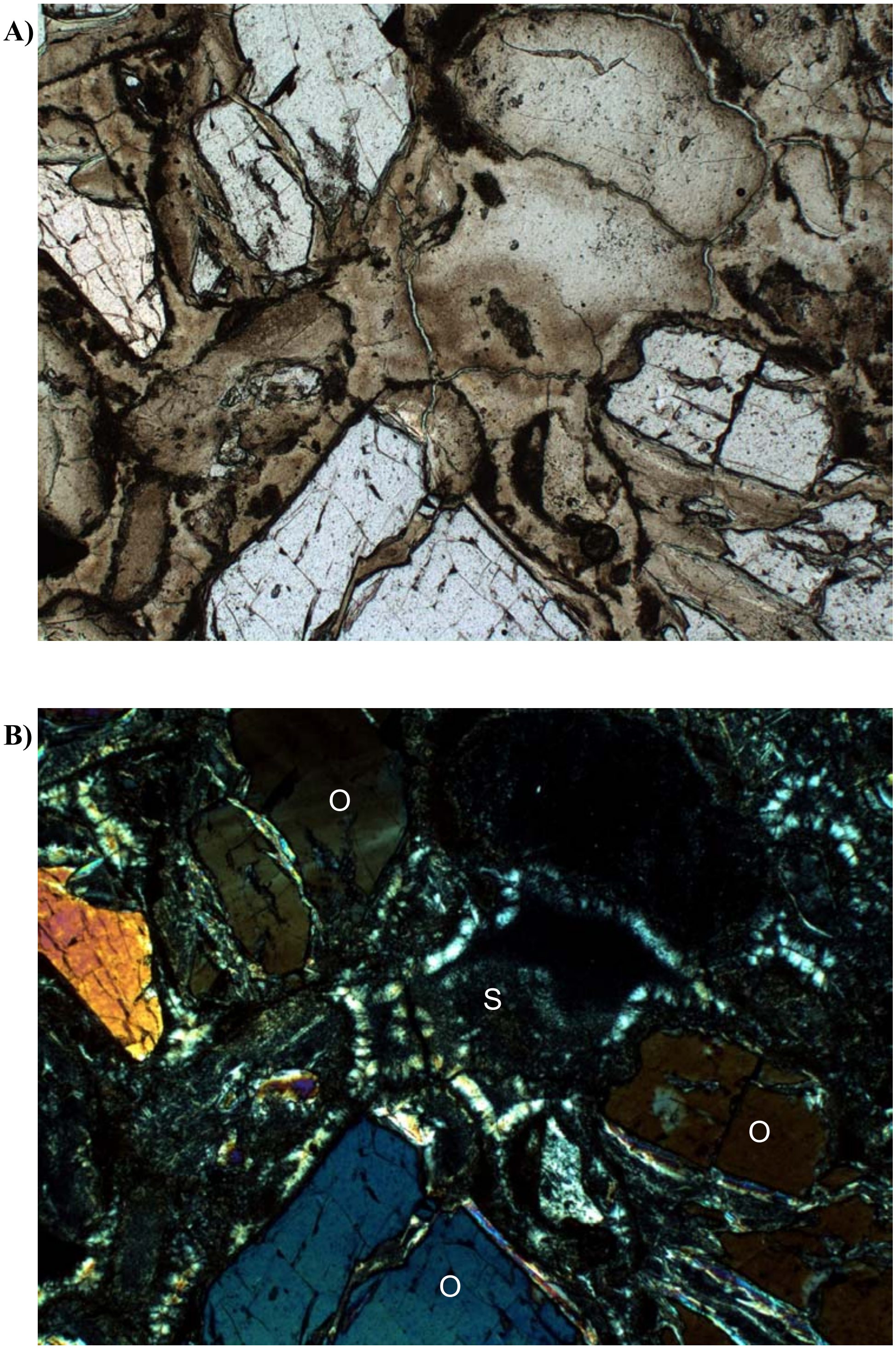

Figure 5.1: A) Fine-grained acicular groundmass serpentine and fine-grained massive groundmass serpentine as seen under plane polarized light. **B)** The same area as above viewed under crossed Nicols. (O = olivine; S = serpentine; field of view (FOV) = 2 mm x 1.34 mm).

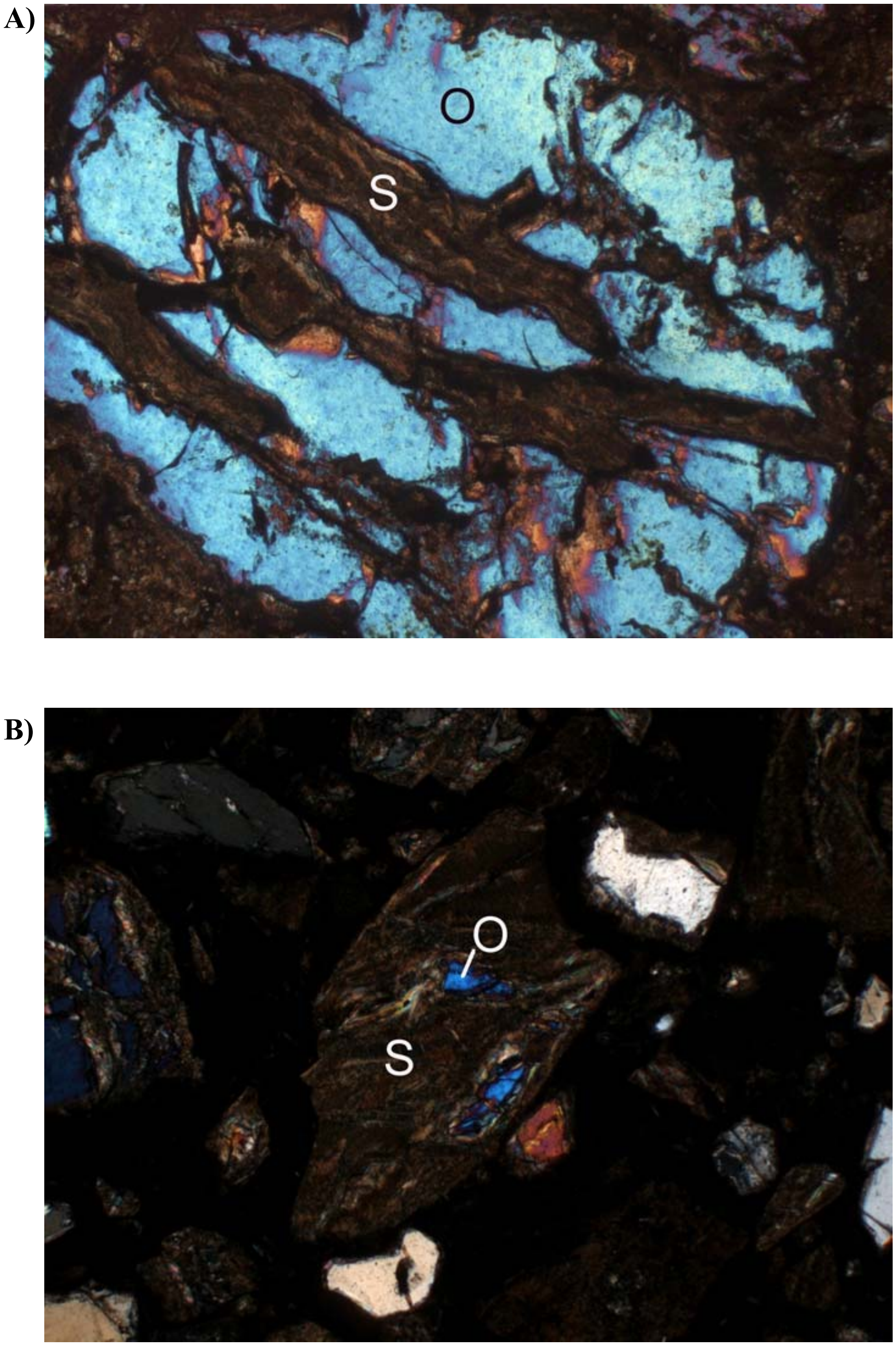

Figure 5.2: A) Highly fractured and serpentinized olivine macrocryst. **B)** Sub-angular olivine macrocryst that has been almost entirely replaced by serpentine (O = olivine, S = serpentine). Both A and B are under crossed Nicols (FOV = 2mm x 1.34 mm).

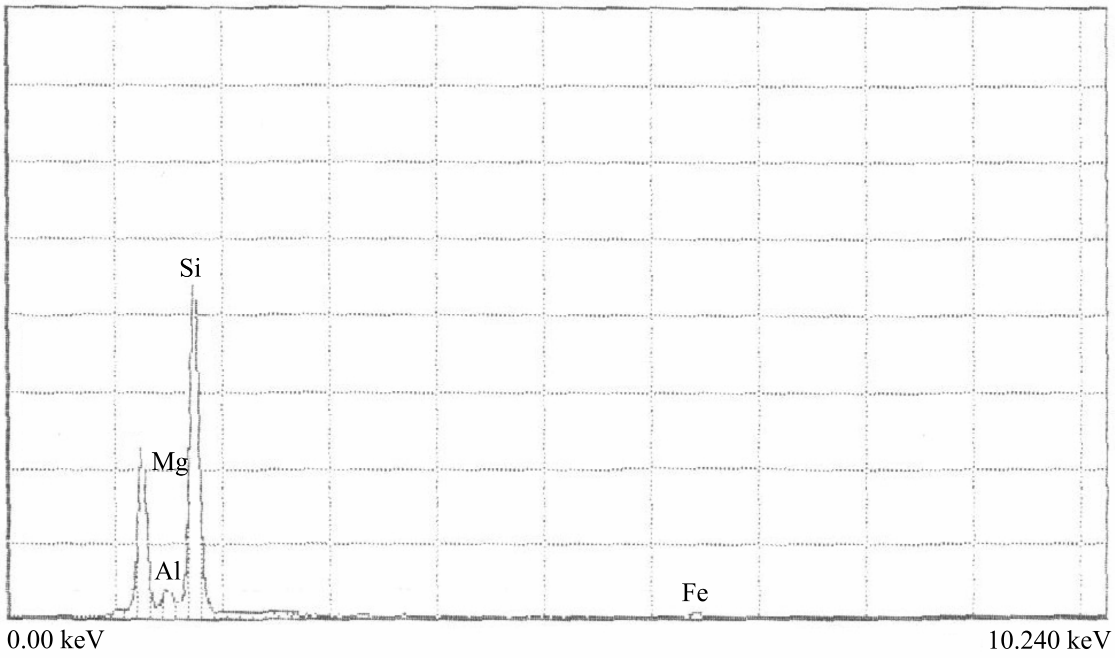

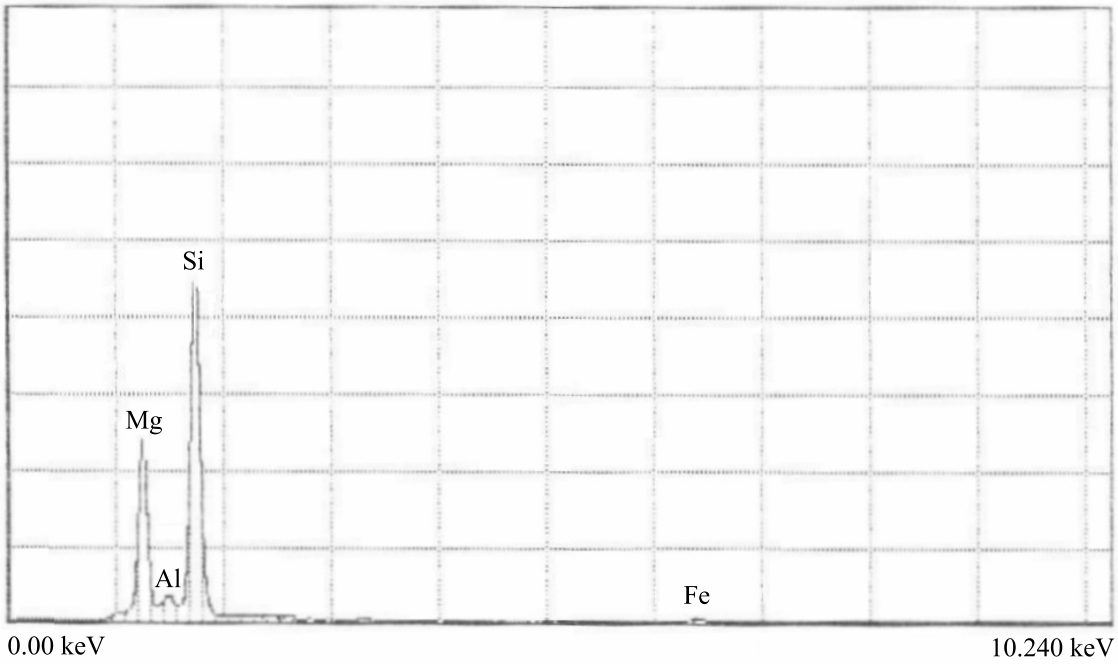

Figure 5.3: Representative EDS spectra for groundmass (top) and pseudomorph (bottom) serpentine from Panda kimberlite. Note the similarity in composition with predominantly Mg and Si, and minor amounts of Al and Fe.

	Formula	Minimum	Maximum
Olivine (n=14)			
Forsterite	Mg_2SiO_4	89.82	94.01
Fayalite	Fe_2SiO_4	5.99	10.18
Garnet (n=8)			
Grossular	$Ca_3Al_2Si_3O_{12}$	11.17	17.47
Pyrope	$Mg_3Al_2Si_3O_{12}$	49.61	66.23
Almandine	$Fe^{2+}{}_3Al_2Si_3O_{12}$	5.19	17.19
Spessartine	$Mn_3Al_2Si_3O_{12}$	0.33	1.49
Uvarovite	$Ca_3Cr_2Si_3O_{12}$	8.25	17.11
Andradite	$Ca_3(Fe^{3+},Ti)_2Si_3O_{12}$	3.25	5.61
Pyroxene (n=10)			
Enstatite	$Mg_2Si_2O_6$	40.18	92.45
Ferrosilite	$Fe_2Si_2O_6$	6.22	26.94
Wollastonite	$Ca_2Si_2O_6$	0.25	28.57
Acmite	$NaFe^{3+}Si_2O_6$	0	4.31

Table 5.1: End-member compositional ranges for solid solution minerals in the Panda kimberlite (n = number of grains analyzed).

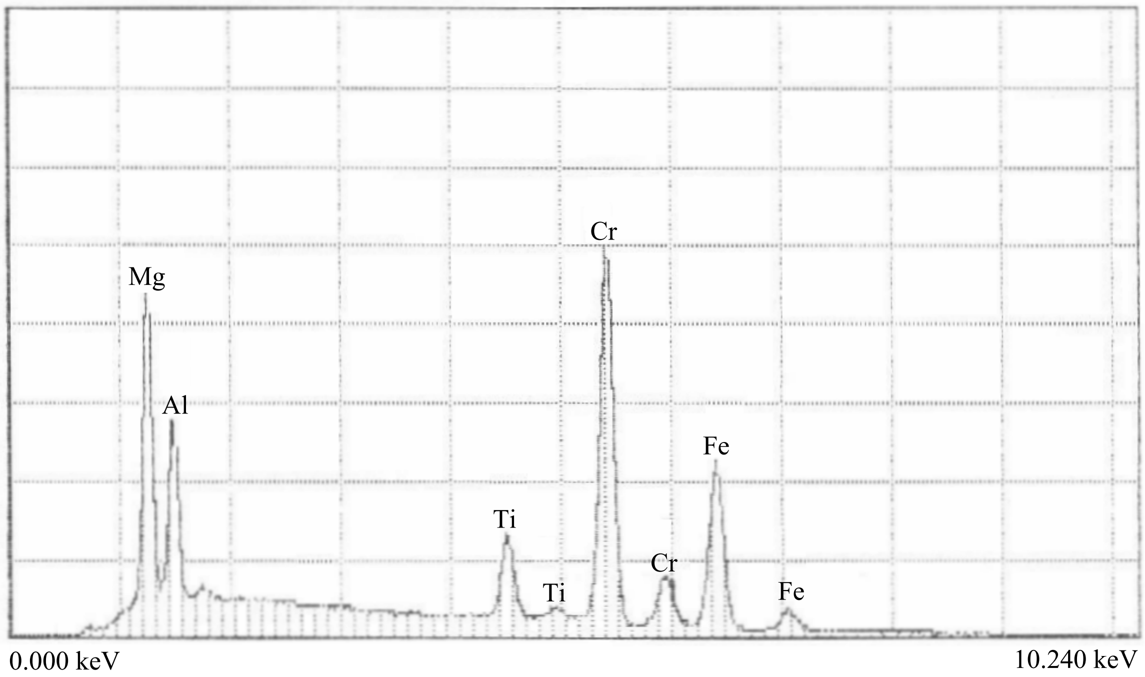

Figure 5.4: Representative EDS spectrum of oxide minerals found in the Panda kimberlite. All oxide minerals are varying proportions of the elements shown here.

5.1.4 Phlogopite – $K_2Mg_6Si_6Al_2O_{20}(OH)_4$

Phlogopite is present in the Panda kimberlite predominantly as long thin tabular crystals that are commonly kinked or bent, possibly reflecting deformation that occurred due to the explosive nature of kimberlite eruption and emplacement (Figure 5.5). Estimates of phlogopite modal concentrations range from approximately 5% to 10%.

5.1.5 Pyroxene – $(Mg,Ca,Fe)_2Si_2O_6$

Pyroxene is present in the Panda kimberlite as sub-rounded to sub-angular crystals (Figure 5.6). Table 5.1 lists maximum and minimum end-member compositions for pyroxenes in the suite of samples as determined by EMPA. A complete list of pyroxene analyses are found in Appendix C. Some grains have been altered to serpentine around grain margins and along interior fractures. However, serpentinization of pyroxene is not as pronounced and widespread as olivine. Modal estimates of pyroxene concentration are approximately 5%.

5.1.6 Garnet – $(Mg,Fe,Ca)_3(Al,Cr)_2Si_3O_{12}$

Garnet is present in the sample suite as irregularly shaped fragments to rounded, highly fractured grains, ranging in colour from red to colourless in plain polarized light (Figure 5.7). Most garnet is surrounded by kelyphitic alteration that is composed primarily of pyroxene, spinel, phlogopite, and serpentine (Mitchell, 1986). Kimberlite garnets are typically part of the solid solution series including pyrope ($Mg_2Al_2Si_3O_{12}$), almandine ($Fe_3Al_2Si_3O_{12}$), grossular ($Ca_3Al_2Si_3O_{12}$), uvarovite ($Ca_3Cr_2Si_3O_{12}$), and

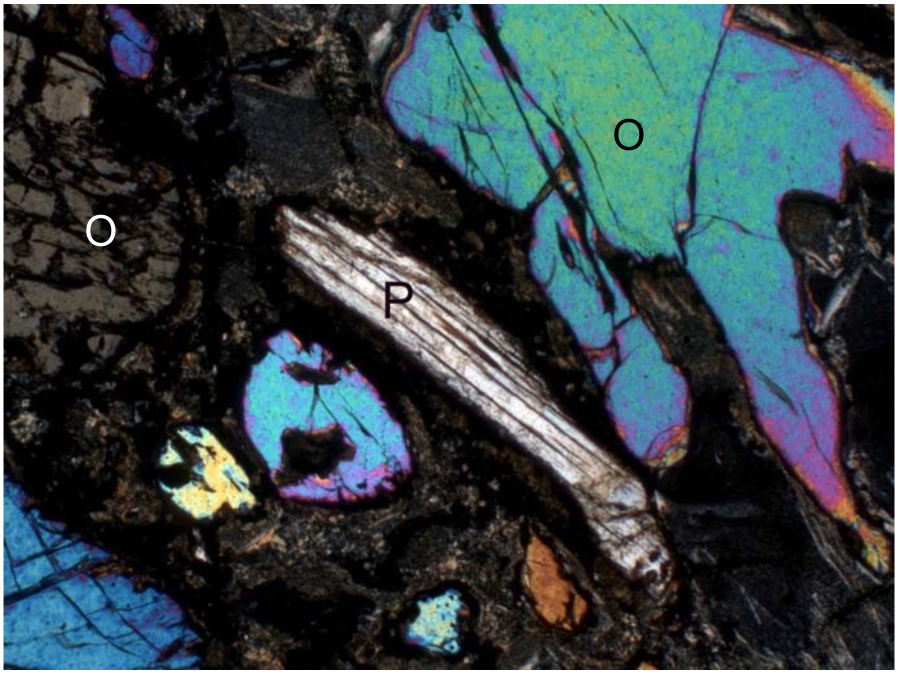

Figure 5.5: Long thin phlogopite crystal under crossed Nicols. The fine-grained groundmass is predominantly serpentine (P = phlogopite, O = olivine; FOV = 2mm x 1.34mm).

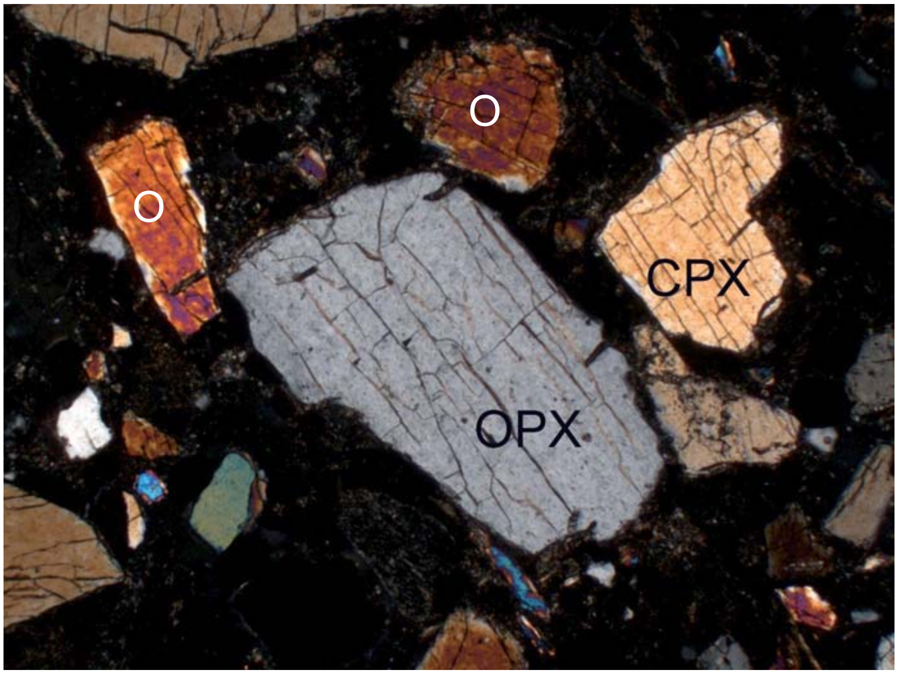

Figure 5.6: Tabular, sub-angular pyroxene macrocrysts viewed under crossed Nichols. This is a very common habit of pyroxene minerals Panda kimberlite (OPX = orthopyroxene, CPX = clinopyroxene, O = olivine; FOV = 2mm x 1.34 mm).

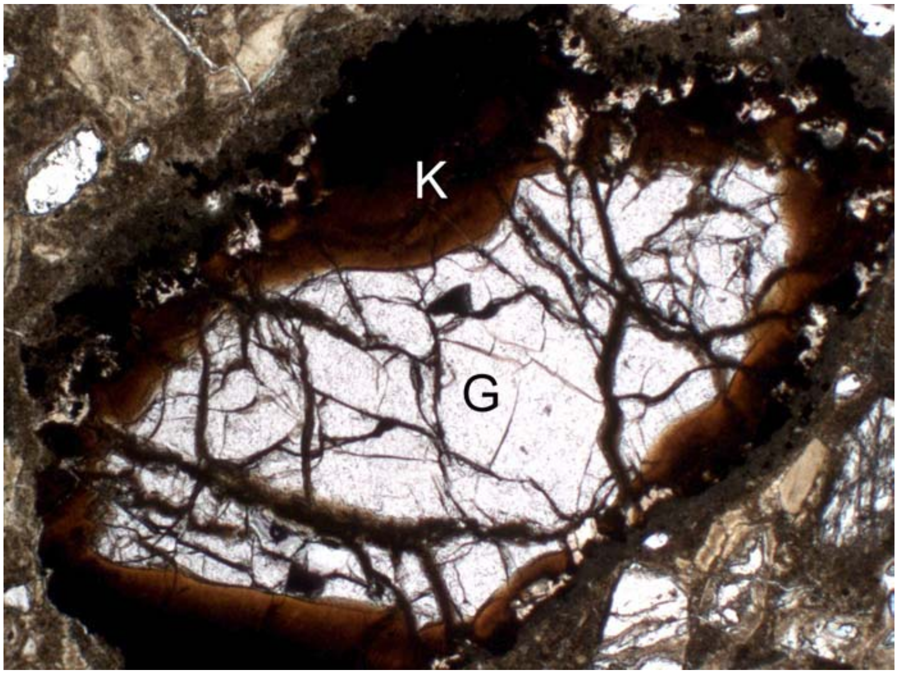

Figure 5.7: Highly fractured garnet macrocryst in plane polarized light. Note the well developed dark red-brown kelyphitic rim, common to many Panda garnets. (G = garnet, K = kelyphite; FOV = 2mm x 1.34mm).

knorringite ($Mg_3Cr_2Si_3O_{12}$) (Mitchell, 1986). Table 5.1 summarizes Panda garnet compositions in terms of these end-member compositions. A complete list of chemical analyses of garnet can be found in Appendix C. Garnet is a very minor component of the samples analyzed, with modal abundances not exceeding 5%.

5.1.7 Calcite – $CaCO_3$

Calcite typically forms the groundmass material of pelletal and juvenile lapilli found throughout the kimberlite (Figure 5.8). EDS spectra indicate that a small amount of Mg substitution occurs in calcite found in the Panda kimberlite (Figure 5.8). Coulometric titration (section 3.4.2.4) of kimberlite ore samples indicate that calcite concentrations range from approximately 2.5 wt % to 5 wt. %.

5.1.8 Wood

The Panda kimberlite also contains wood material, present as pieces up to one metre in length, dispersed throughout the pipe (Figure 5.9). The wood, which is similar to the redwoods *Sequoia* and *Metasequoia*, appears relatively fresh and unaltered with marginal amounts of permineralization (Nassichuk and Dyke, 1998; Nassichuk and McIntyre, 1995).

5.1.9 Mud Xenoclasts

Mud xenoclasts are found throughout the Panda kimberlite and range in size from millimeters to centimeters. In hand specimen they are uniformly fine-grained, dark grey to black in colour, and typically contain kimberlite minerals, most commonly olivine and

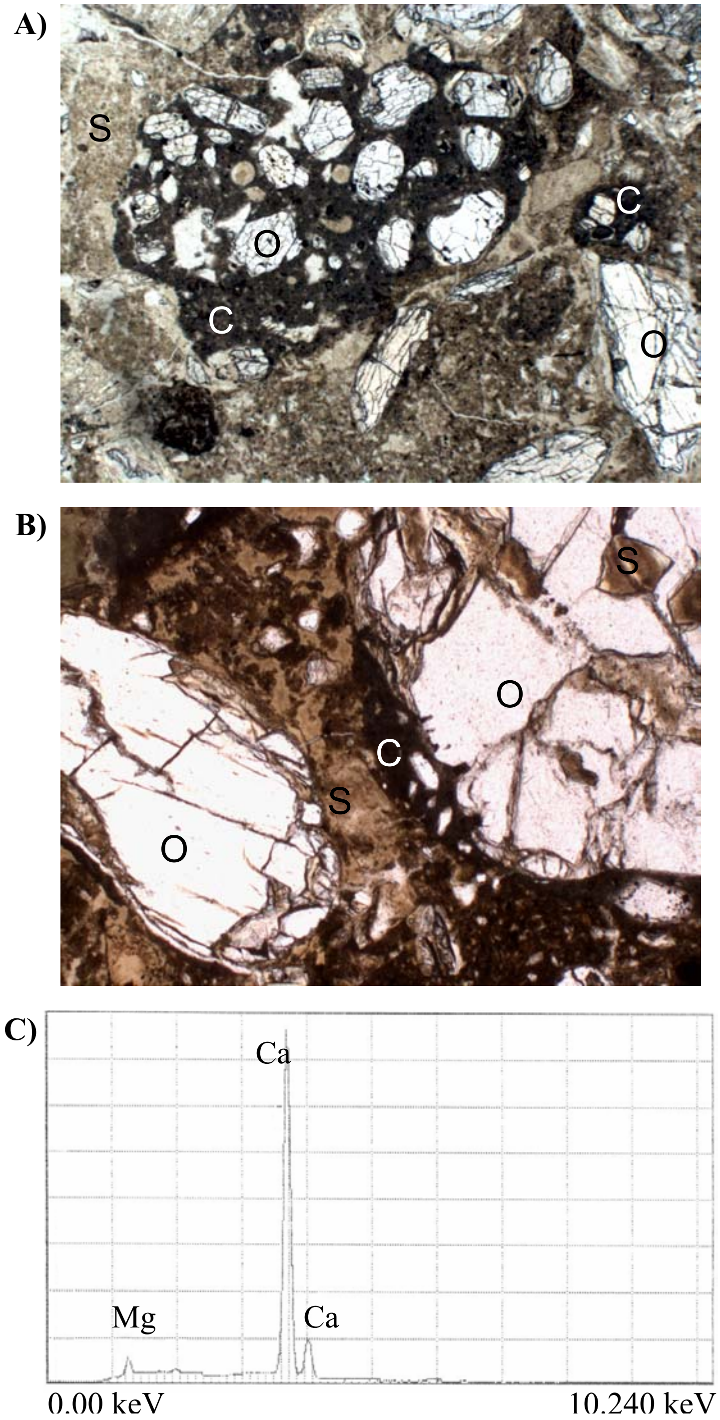

Figure 5.8: **A)** Juvenille lapilli composed of olivine, serpentine, and oxide crystals set in a calcite groundmass. **B)** Pelletal lapillus composed of a large central serpentinized olivine grain that is rimmed with microphenocrystal olivine and oxide crystals set in a calcite groundmass (O = olivine, S = serpentine, C = calcite; FOV = 2mm x 1.34 mm). **C)** Representative EDS spectra of calcite from lapilli within the Panda kimberlite.

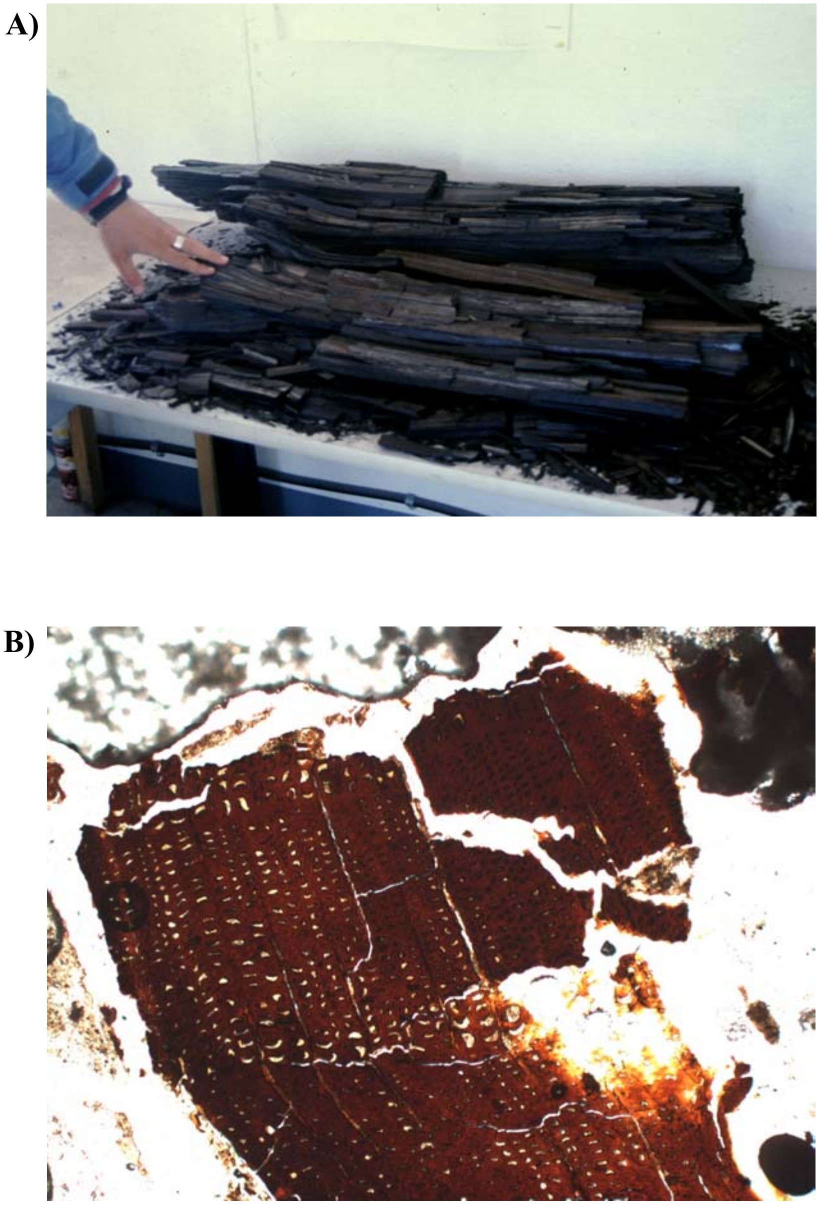

Figure 5.9: **A)** Wood fragments collected during mining operations from the Panda pit. **B)** Image of wood fragment from Panda kimberlite polished thin section under plane polarized light (FOV = 0.8mm x 0.54mm).

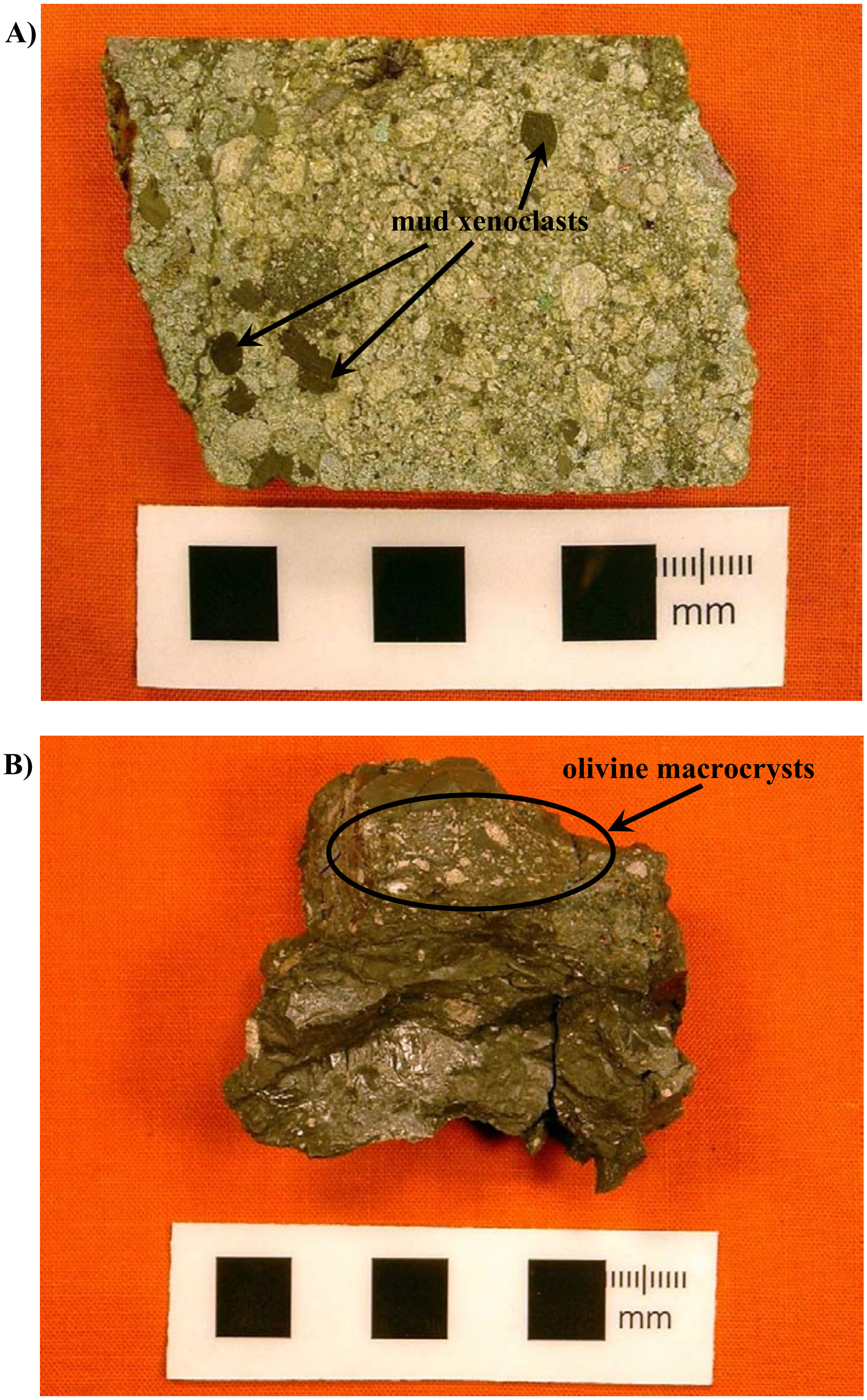

Figure 5.10: **A)** Image of Panda kimberlite core sample indicating mud xenoclasts. Note the variable shape and size of the mud within the kimberlite. **B)** Large piece of mud xenoclast material collected from freshly blasted material in the Panda open-pit. Note the olivine macrocrysts embedded in the margin of the mud. The black squares in each image are 1 cm wide.

serpentine, embedded in their margins (Figure 5.10). In thin section, the mudstone is very fine-grained, medium to dark brown and opaque (Figure 5.11). Mud xenoclasts are highly variable in shape and often appear to ooze through the kimberlite, suggesting pre-lithification incorporation into the kimberlite. Mud xenoclasts commonly exhibit deflection of planar fabric, as defined by black lineations within the mud, possibly an organic carbon phase incorporated into the mud material (Figure 5.11). These data also suggest that the mud was still soft during emplacement of the kimberlite. X-ray diffraction analysis of the mud xenoclast indicates that smectite, quartz, and pyrite are the main minerals present in this material.

Due to the similarity in appearance of the kimberlite groundmass material and the mud xenoclasts, it is difficult to discern how much (modal %) of the mudstone has been incorporated into the kimberlite. The similarity in appearance between the mud xenoclasts and the kimberlite groundmass material can be seen in Figure 5.11. Previous studies have also noted that much of the volcaniclastic kimberlite from the Lac de Gras area contains mud-rich inter-clast matrices, making it difficult to discern the two phases (Field and Scott-Smith, 1998; Graham et al., 1998).

5.1.10 Sulphide and Sulphate

Petrographic examination of kimberlite thin sections indicates that sulphide minerals are essentially restricted to the mud xenoclast phase in the Panda kimberlite. These sulphides, identified as pyrite by EDS, are present as very fine-grained framboidal grains, which range in size from approximately 0.5 μm to 10 μm in diameter, with the majority less than 5 μm in diameter (Figure 5.12).

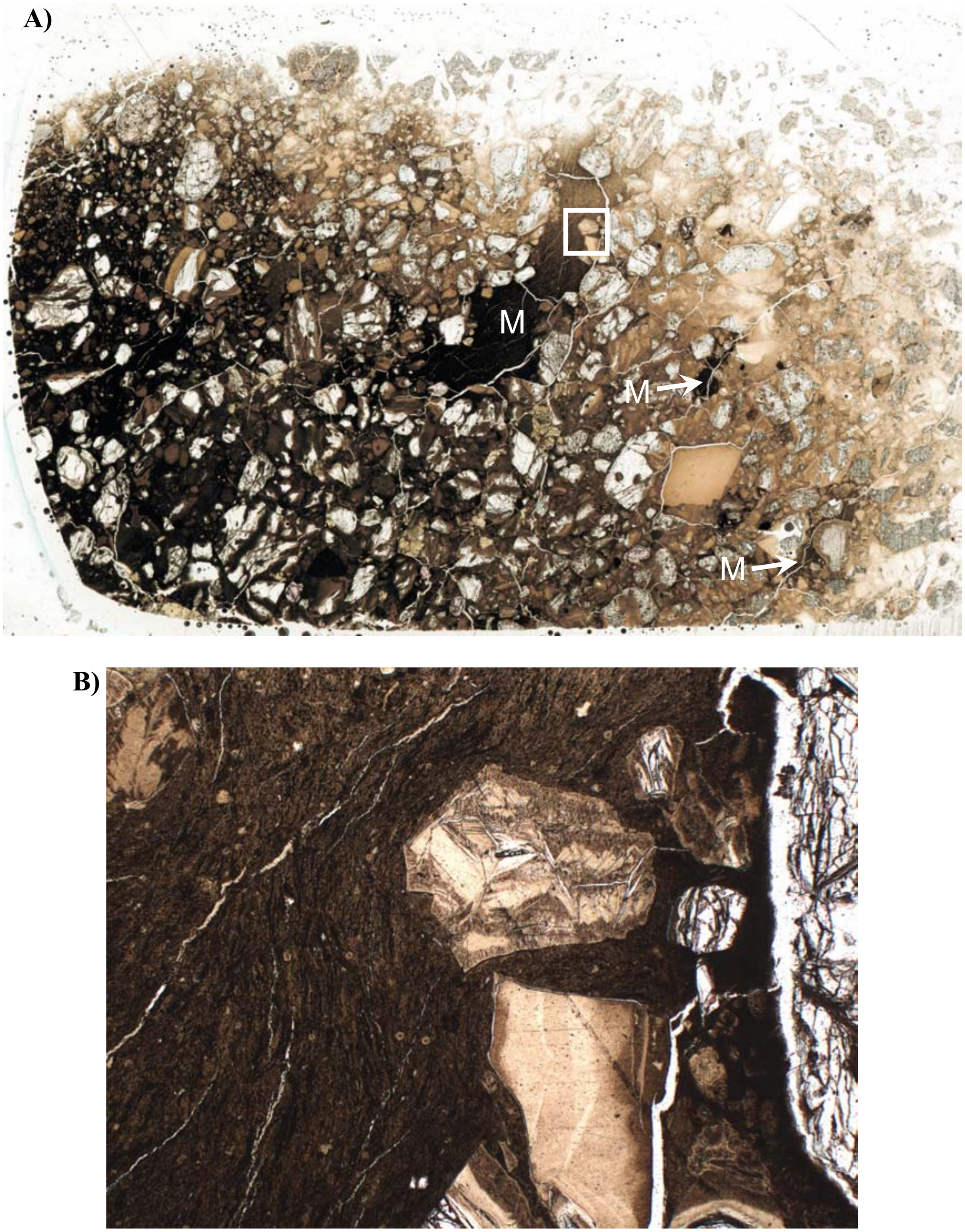

Figure 5.11: A) Panda kimberlite polished thin section indicating the location of mud xenoclasts (M). Note the variable size and shape, and fine-grained nature of these clasts and the similarity in appearance of the mud and kimberlite matrix on the left side of the image. Also note the olivine and serpentine grains embedded into the margins of mud xenoclasts. (FOV = 34 mm x 22 mm). **B)** Magnified view of area indicated by the white box in A. Note the deflection of the planar fabric of the mud xenoclasts around the embedded grains suggesting pre-lithification incorporation of the mud into the kimberlite (FOV = 2 mm x 1.34 mm).

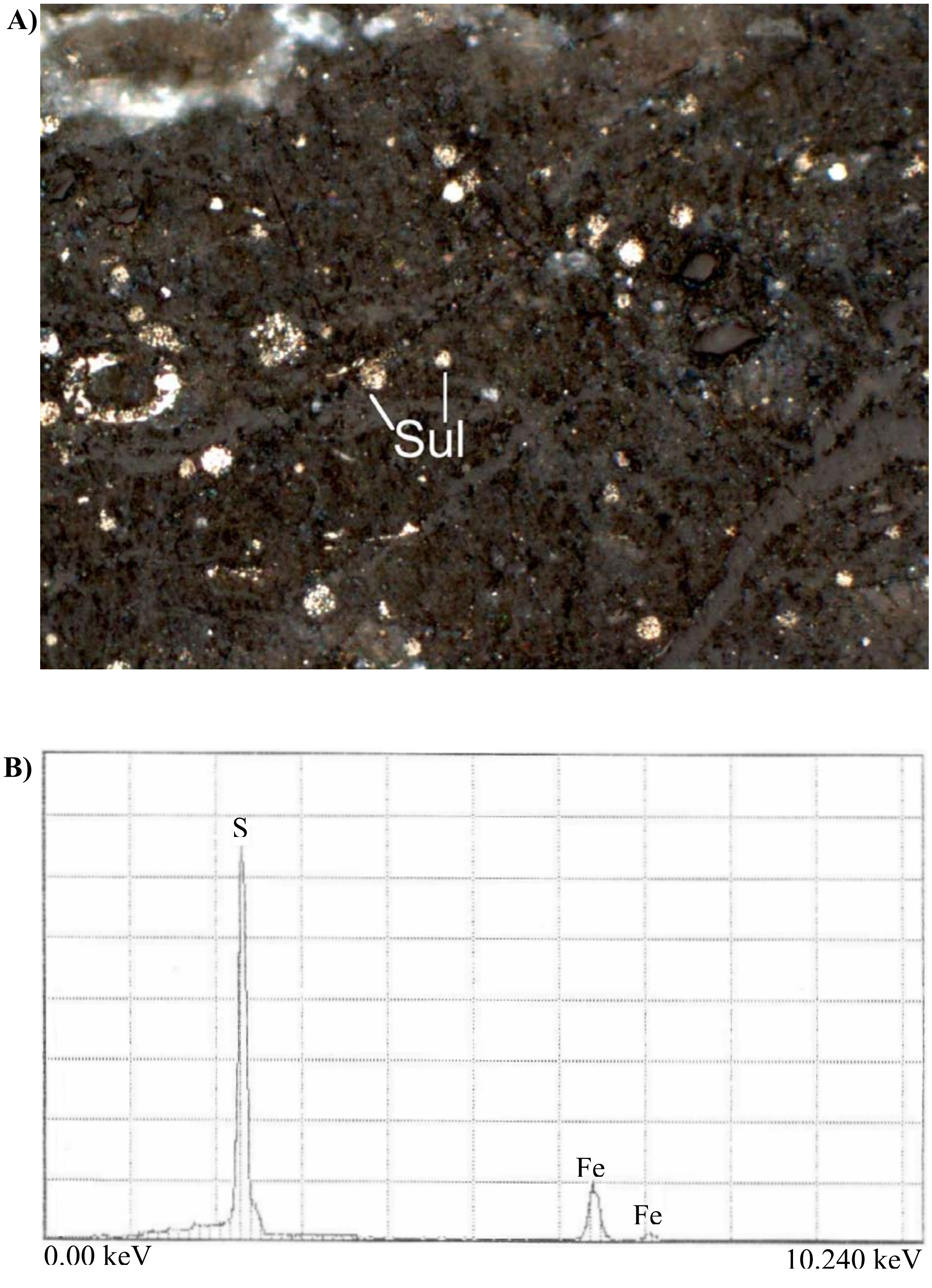

Figure 5.12: **A)** Representative reflected light image of a mud xenoclast showing the very-fine grained framboidal habit of the mudstone sulphides (FOV = 160 μm x 107 μm). **B)** Representative EDS spectrum of a typical mud xenoclast sulphide grain. This spectrum indicates that the mud sulphides are pyrite.

Sulphide and sulphate analyses (section 5.3) indicate that the mud xenoclasts contain both sulphide as well as sulphate minerals. However, sulphate minerals are not readily identifiable in thin section due to the fine-grained opaque nature of the mud clasts. In an effort to locate the source of sulphate minerals in the mud, X-ray element maps were collected for Fe, Ca, and S (Figure 5.13). Energy dispersive spectrometric analysis of the regions that contain both Ca and S, but no Fe, indicates that the main sulphate phase in the mud xenoclasts is a Ca-SO_4 mineral, most likely gypsum or anhydrite (Figure 5.14). These maps show that sulphate minerals are found as very fine-grained disseminations, as well as fracture filling precipitates within the clasts. It should be noted that no significant amounts of sulphate minerals were found within the kimberlite ore.

5.2 Processed Kimberlite Fines

The mineralogy of the processed kimberlite fines is essentially identical to the kimberlite ore described in the previous section, consisting primarily of serpentine and olivine with lesser amounts of phlogopite, calcite, oxides, pyroxene, and minor amounts of sulphide.

In hand sample the processed kimberlite fines are medium green-grey with no observable reaction fronts or iron oxide staining (Figure 5.15). The fines are composed of alternating fine- and coarse-grained layers (Figure 5.16). The coarse layers contain grains that are approximately 0.1 mm to 1 mm in diameter, and are dominated by olivine and serpentine with lesser amounts of phlogopite and mud, and accessory amounts of pyroxene and garnet. The fine-grained layers are typically 1 to 5 centimetres thick and contain serpentine, olivine, phlogopite, and mud grains surrounded by an

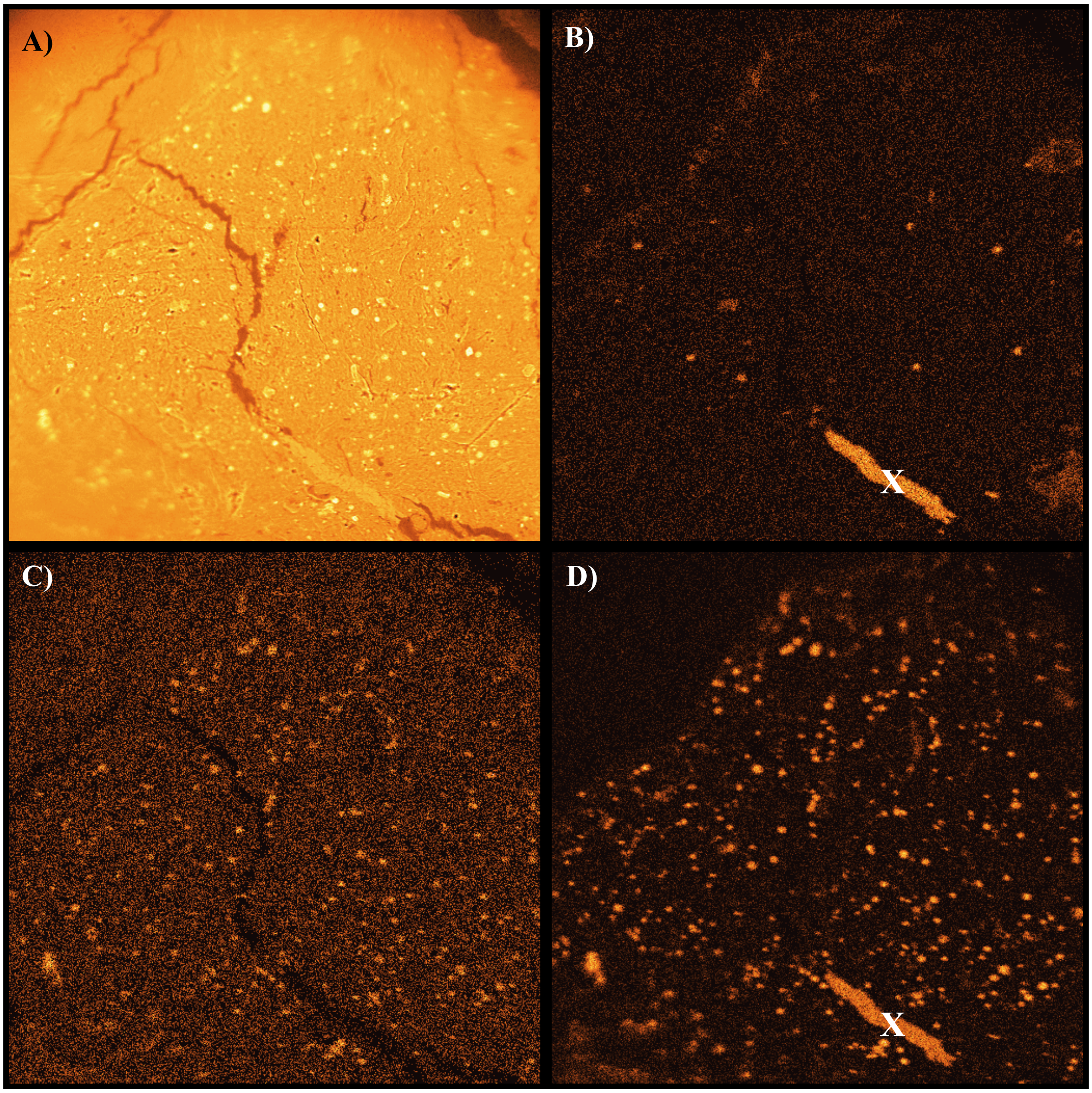

Figure 5.13: **A)** Backscattered electron image of mud xenoclasts. **B)** Ca X-ray element map. **C)** Fe X-ray element map. **D)** S X-ray element map. All images are of the same region. Operating conditions: 15 kV accelerating voltage, 125 nA beam current, 200 times magnification, 1000 passes. The 'X' in **B** and **D** marks the location at which the EDS spectrum in figure 5.13 was collected (FOV = 360 μm).

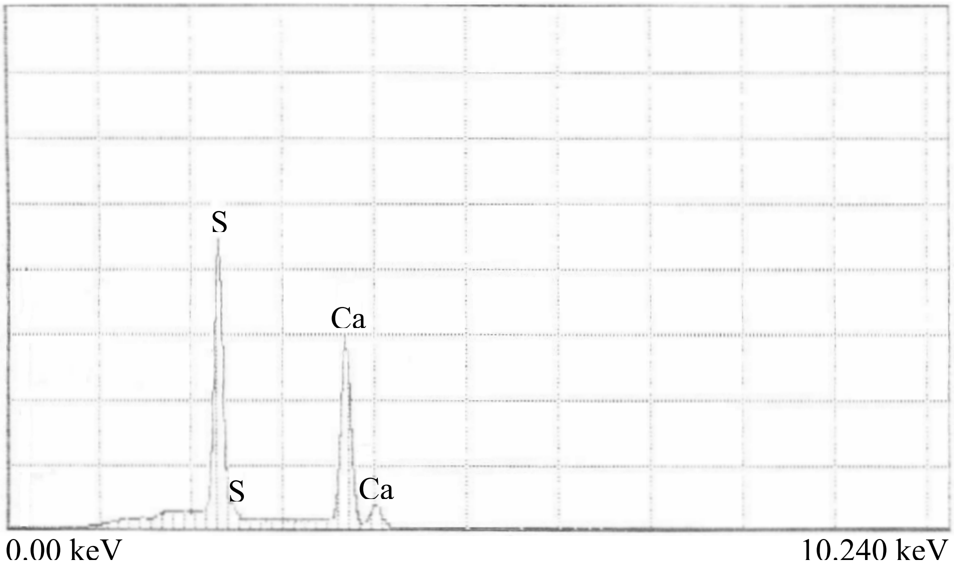

Figure 5.14: EDS spectrum collected from the spot marked X in Figure 5.13. Note that this material is composed of Ca and S only.

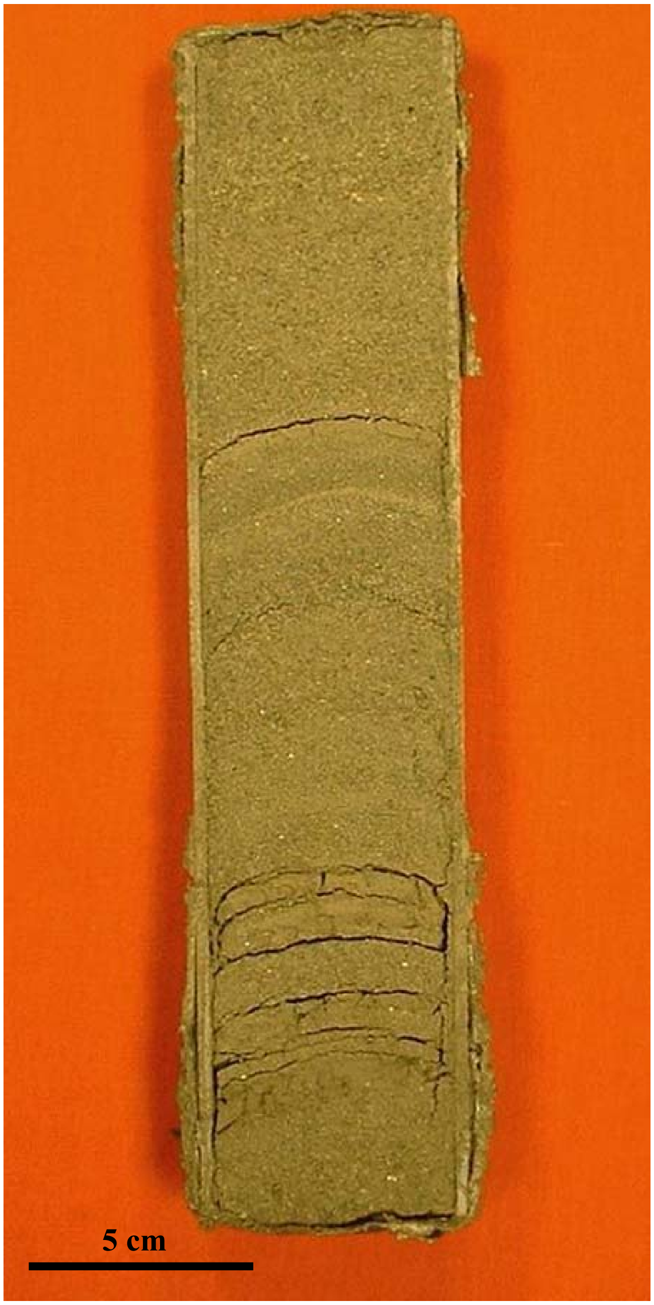

Figure 5.15: Image of processed kimberlite fines core sample. Note the lack of obvious reaction fronts and iron-oxide staining. This image is a very good representation of all processed fines core samples collected for this investigation. The coarse and fine layers evident in this image are caused by the differential settling of coarse and fine material depending on the distance from the process plant discharge spigot.

A)

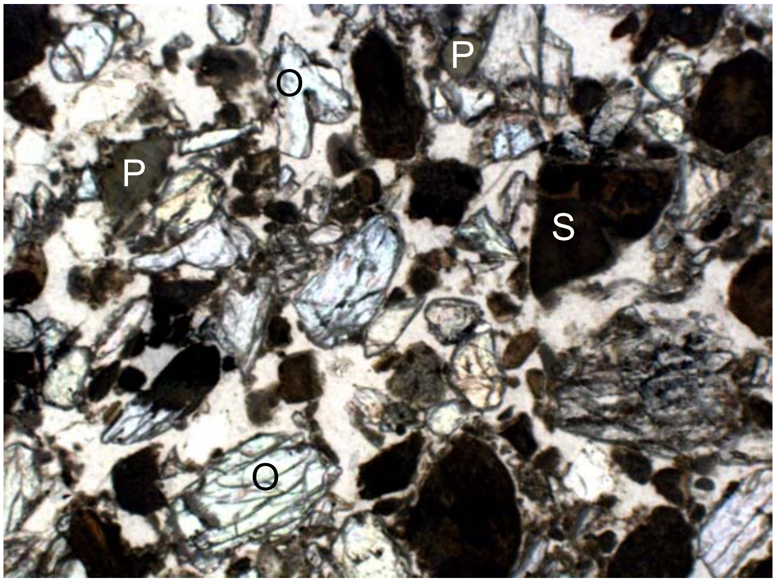

B)

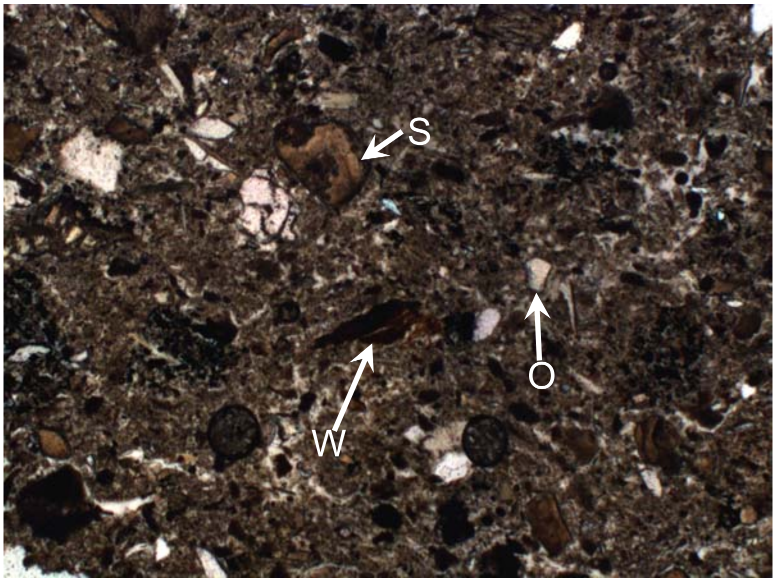

Figure 5.16: **A)** Representative image of coarse grained processed kimberlite fines layer in plane polarized light. The majority of grains are composed of serpentine and olivine with lesser amounts of phlogopite. Note the high porosity and lack of significant fine-grained material (O = olivine, S = serpentine, P = phlogopite; FOV = 2 mm x 1.34 mm). **B)** Representative image of fine-grained processed kimberlite fines layer in plane polarized light. Note how the fine-grained layers contain coarse clasts set in a very fine-grained matrix. The amount of coarse clasts is variable (O = olivine, S = serpentine, W = wood fragment; FOV = 6 mm x 5.2 mm).

abundance of very fine-grained material. Like the kimberlite ore, the majority of sulphides in the fines are located within mud grains and do not exhibit any evidence of oxidation such as oxidation rims, or iron-oxide staining around the grains (Figure 5.17).

5.2.1 Clay Mineralogy

X-ray diffraction analyses were conducted on the clay-sized fraction (<5 μm) of the LLCF processed kimberlite fines. The method used to separate the <5 μm size fraction is based on Stoke's Law for the settling rate of particles in a fluid. This size fraction was separated by washing the >0.6 mm size fraction of processed fines with distilled water while using an ultrasonic gun to dislodge fine-grained material from the surface of larger grains. This suspension was centrifuged for approximately 20 seconds at 1000 rpm. This step was used to cause all material that was >5 μm to settle out, leaving particles <5 μm in suspension. Next, the suspension was centrifuged again for 60 seconds at 6000 rpm, causing all material to settle out of suspension. The supernatant was poured off and the residue was poured onto a glass slide and allowed to dry subsequent to X-ray diffraction analysis. Three slides were prepared for each sample using this method.

In order to enable identification of clay minerals, each of the slides was treated differently. One slide was heated to 550°C for approximately 2 hours, one slide was glycolated in an ethylene glycol-filled desiccator, and one slide was analyzed as is. Observation of the behaviour of low angle peaks from each of these treatments helps to identify the clay minerals present in the sample (Brown and Brindley, 1980).

Figure 5.18 shows representative X-ray spectra for each of the three treatments discussed above. The 14.5 Å reflection in the untreated sample shifts up to

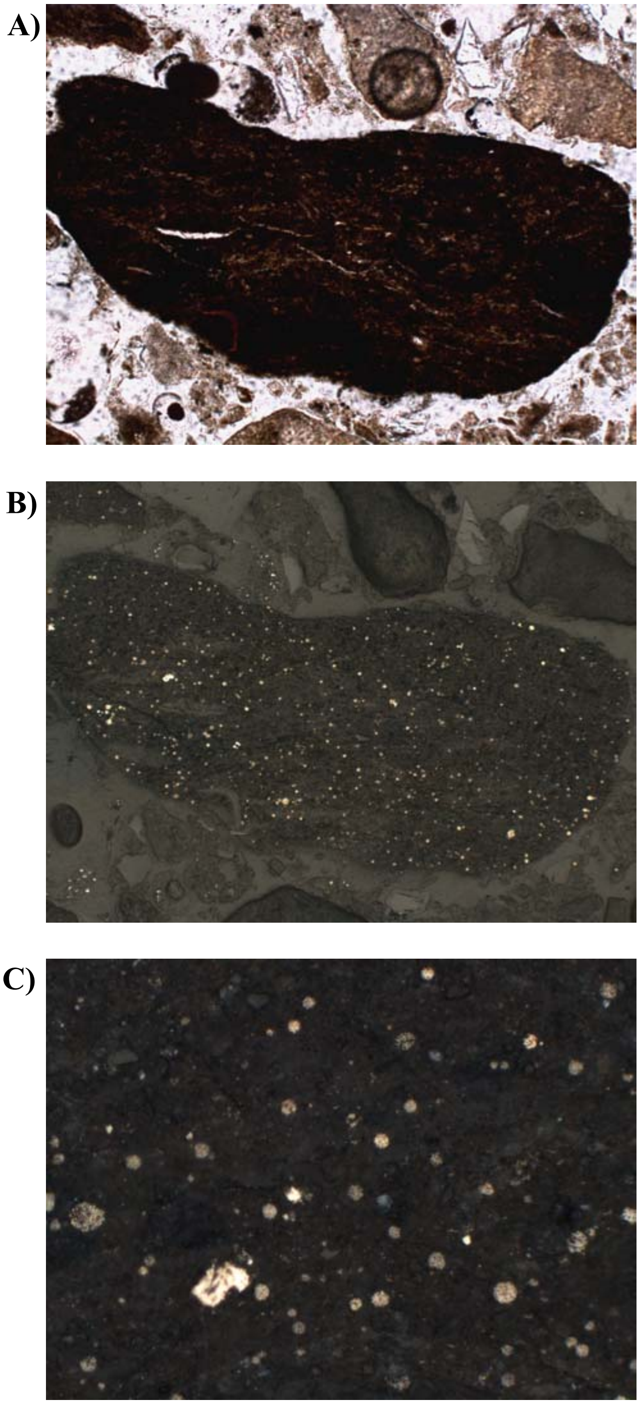

Figure 5.17: **A)** Image of mud grain from processed kimberlite fines as viewed under plane polarized light (FOV = 0.8mm x 0.54mm). **B)** The same mud grain as in A, but under reflected light. Notice the abundance of small framboidal pyrite grains that are characteristic of the mud xenoclasts found in the Panda kimberlite (FOV = 0.8mm x 0.54mm). **C)** High magnification of view of framboidal pyrite grains from B. Note the lack of oxide rims on any of the grains in the field of view (FOV = 160μm x 107μm).

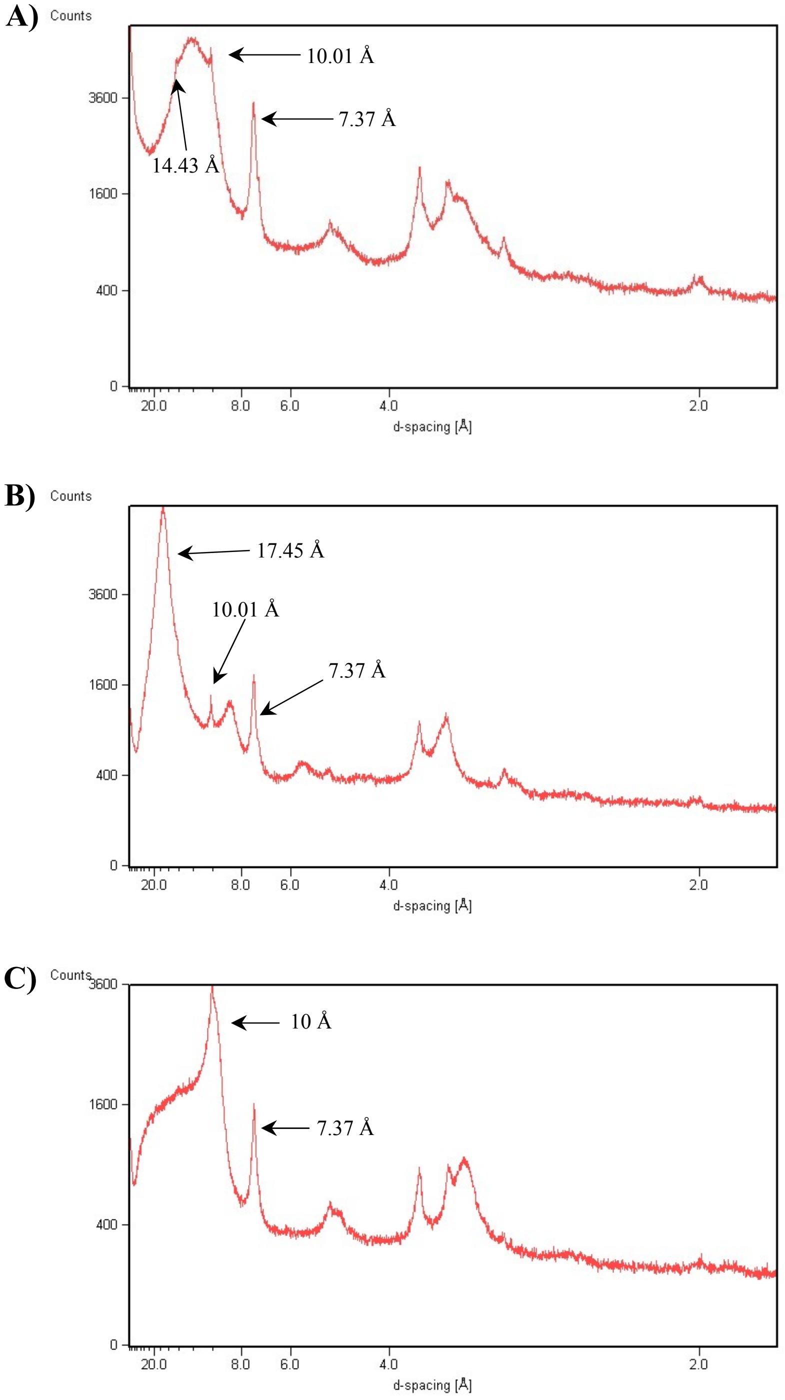

Figure 5.18: A) XRD spectrum for an untreated clay fraction sample. The peak at 14.43 Å corresponds to the 001 smectite reflection. **B)** XRD spectrum for ethylene glycol treated sample. Note how the 001 reflection has shifted up to 17.45 Å. Also note that the 10.01 Å and the 7.37 Å are unaffected. **C)** XRD spectrum for sample heated at 550°C. Note how the 001 reflection has collapsed to approximately 10 Å.

approximately 17 Å upon glycolation, and collapses to approximately 10 Å upon heating at 550°C. This behaviour is characteristic for the 001 reflection of smectite group minerals [$(\frac{1}{2}Ca, Na)_{0.7}(Al, Mg, Fe)_{4-6}(Si,Al)_8O_{20}(OH)_4 \cdot nH_2O$] (Brown and Brindley, 1980). However, these observations do not uniquely identify the specific smectite mineral present. The 060 reflection is a diagnostic feature that can be used to identify specific smectite group minerals, with the 060 reflection for saponite occurring at approximately 1.52 Å (Brindley, 1980). The reflection occurring at 1.53 Å in the LLCF fines samples indicates that saponite is the main smectite mineral present in the LLCF fines (Figure 5.19). Other clay fraction minerals identified, based on the most intense peak of their spectra, include phlogopite [$K_2Mg_3AlSi_3O_{10}(OH)_2$] (10 Å reflection) and chrysotile [$Mg_3Si_2O_5(OH)_4$] (7.36 Å reflection) (Bailey, 1980). No other serpentine minerals were indicated to be present by X-ray diffraction, suggesting that chrysotile is the main serpentine mineral present in the processed kimberlite fines.

5.2.2 Efflorescent Crust

During long periods of a week or more with no precipitation, a very fine-grained white efflorescent crust forms on the surface of the processed kimberlite fines (Figure 5.20). As soon as it rains, this efflorescent precipitate immediately dissolves. This material was observed and collected in both 2000 and 2002. X-ray diffraction analysis of this material indicates that it is almost entirely hexahydrite ($MgSO_4 \cdot 6H_2O$) (Figure 5.21). Some XRD data suggest that gypsum might be present as well, but hexahydrite is by far the dominant phase present.

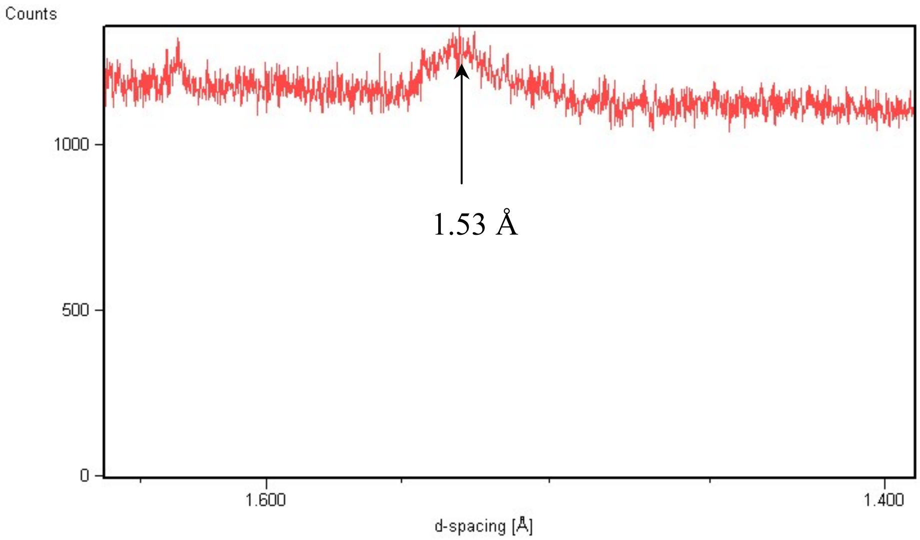

Figure 5.19: XRD spectrum of LLCF processed kimberlite fines showing the peak at 1.53 Å. This peak corresponds to the 060 reflection of saponite, which identifies it as the main smectite mineral present in the processed kimberlite fines.

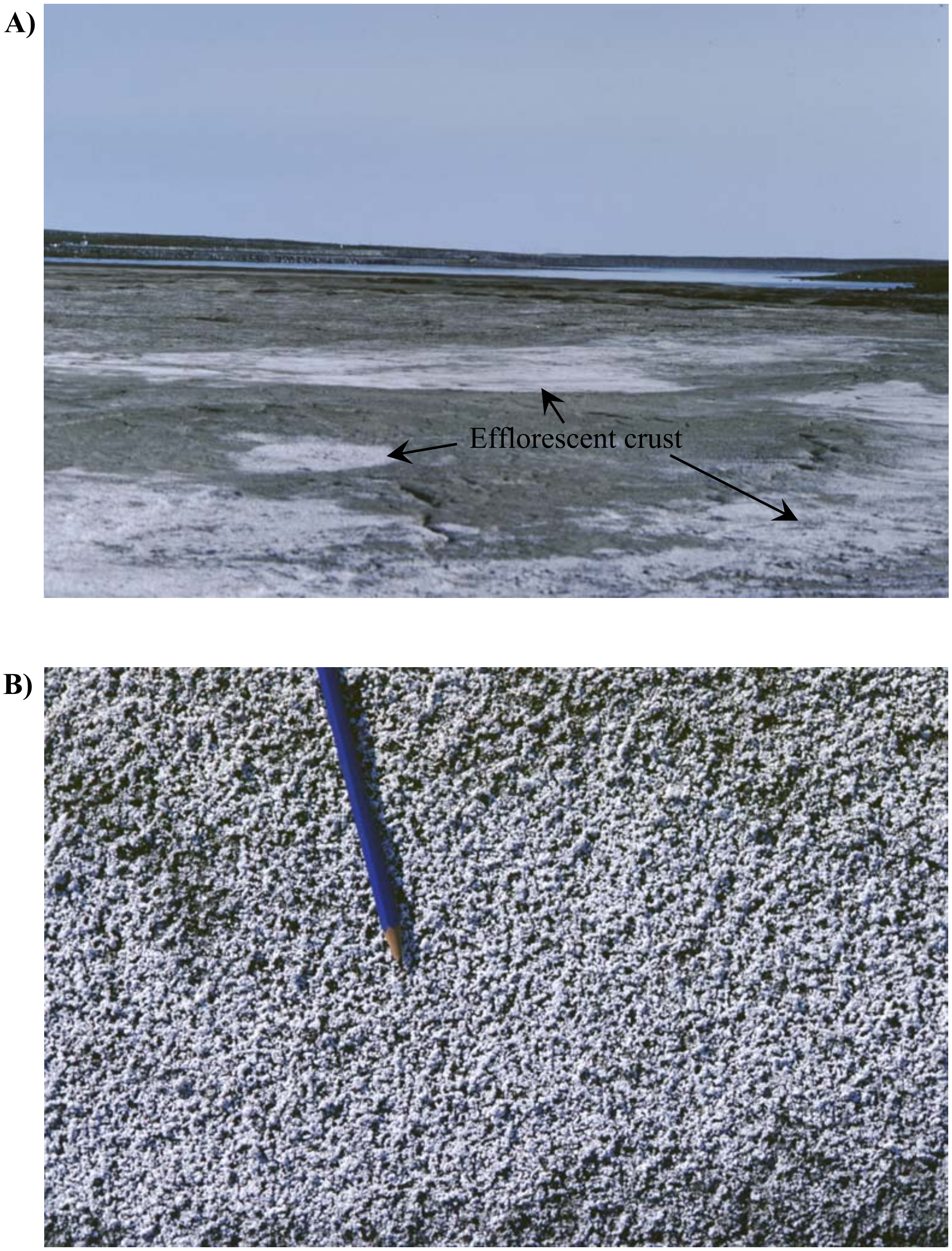

Figure 5.20: **A)** Picture of Cell B looking south at Dyke B. The white patches on the surface of the processed kimberlite fines are the efflorescent crust that forms during prolonged periods with no rain. **B)** Close-up of the precipitate seen in **A**.

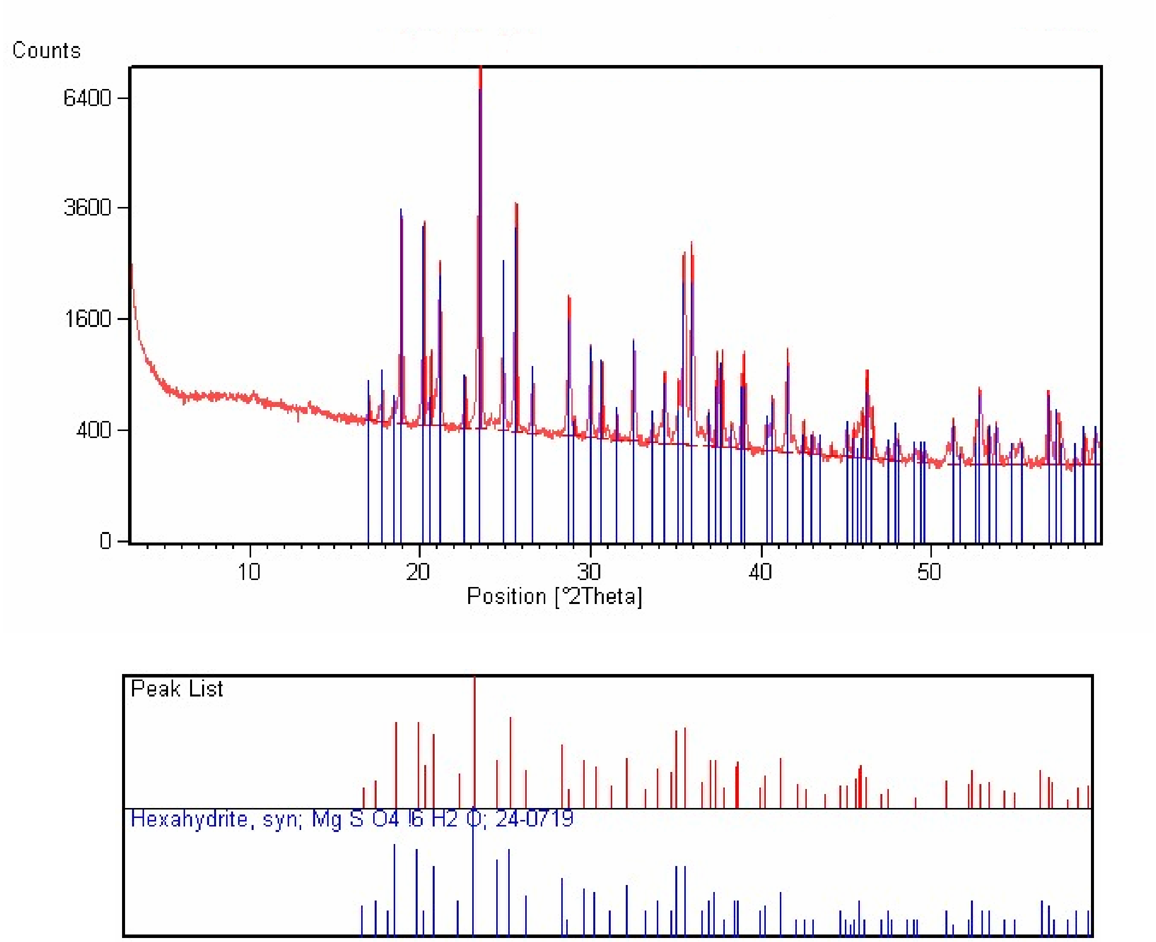

Figure 5.21: X-ray diffraction spectrum for the efflorescent precipitate that forms on the surface of the LLCF processed kimberlite fines. This patterns indicates that the crust is predominantly composed of hexahydrite ($MgSO_4 \cdot 6H_2O$).

5.3 Inorganic-C, Sulphate-S, and Sulphide-S

Analyses were conducted in order to determine the amount and location of inorganic-C (representing carbonate minerals), sulphate-S, and sulphide-S within the Panda kimberlite ore. To accomplish this objective, three types of solid samples were selected for analysis: mud xenoclasts from kimberlite ore, kimberlite ore, and processed kimberlite fines. It should be noted that kimberlite ore samples were selected so that they did not contain any obvious mud xenoclast material. However, due to the incorporation of an indeterminate amount of mud into the kimberlite matrix (section 5.1.9), there is most likely a small amount of mud contamination in these samples. All samples were analyzed for total-S, sulphate-S, and inorganic-C using the methods described in section 3.4.2.3 and 3.4.2.4. Imprecision of these analyses have been calculated using the method described in section 4.1. Total-S and sulphate-S are reported as weight percent S while inorganic-C is reported as weight percent CO_2. The results of these analyses are summarized in table 5.2, and the complete suite of analyses is listed in Appendix D.

Inorganic-C concentrations are lowest in the mud (average 0.50 wt. % CO_2) and highest in the processed kimberlite fines (average 2.38 wt. % CO_2), with inorganic carbon concentrations in mud samples up to three times lower than kimberlite ore (average 1.40 wt. % CO_2). These data indicate that carbonate minerals are found mostly in the kimberlite ore, rather than the mud xenoclasts. As well, concentrations of inorganic-C in processed kimberlite fines samples are approximately two to three times higher than pre-processed kimberlite ore. Approximately 10 weight percent to 20 weight percent of kimberlite processed at Ekati becomes coarse kimberlite reject material (section 1.1.7).

		Inorganic-CO_2 (wt %)			Sulphate-S (wt %)			Sulphide-S (wt %)		
Sample type	N	P_5	Mean	P_{95}	P_5	Mean	P_{95}	P_5	Mean	P_{95}
Mud xenoclast	6	0.40	0.50	0.68	0.18	0.27	0.38	1.82	2.54	3.19
Kimberlite ore	3	1.10	1.40	1.91	0.12	0.14	0.16	0.20	0.21	0.22
Kimberlite fines	17	1.38	2.38	3.04	0.01	0.04	0.09	0.17	0.25	0.35

Table 5.2: Inorganic-CO_2, sulphate-S, and sulphide-S analyses of mud xenoclasts, kimberlite ore, and processed kimberlite fines. P_5 and P_{95} represent the 5th and 95th percentile values calculated from the analytical data (Appendix D). N = number of samples analyzed.

Such a large increase in inorganic-C content can not be adequately explained as a relative increase due to the 10 to 20 weight percent of kimberlite removed from the fines as coarse reject material during mineral processing. Therefore, these data indicate that carbonate minerals most likely have precipitated in the processed kimberlite fines at some point after mining of the ore.

Trends in sulphate-S concentrations are exactly opposite to inorganic carbon with the highest concentrations in the mud xenoclasts (average 0.27 wt. %) and the lowest concentrations in the processed kimberlite fines (average 0.04 wt. %), indicating that mud xenoclasts are the main source of sulphate minerals in the kimberlite ore, and that sulphate is being removed from the processed kimberlite at some point after the ore is extracted from the open pit. Sulphate minerals were not found in kimberlite ore material through petrographic examination and X-ray element mapping (section 5.1.10). Therefore, the moderate amount of sulphate-S in the kimberlite ore samples is most likely a product of the incorporation of mud xenoclasts into the kimberlite during emplacement. This is consistent with previous work, indicating that many volcaniclastic kimberlites from the Lac de Gras area contain mud-rich inter-clast matrices (Field and Scott-Smith, 1998; Graham et al., 1998).

Similar to sulphate-S, sulphide-S is most concentrated in the mud xenoclasts with an average sulphide-S concentration of 2.54 wt. %. As well, table 5.2 indicates that there is a small increase in the concentration of sulphide-S in the processed kimberlite fines relative to the kimberlite ore, with average concentrations of 0.25 and 0.21 wt. % respectively. This small increase is not significant and is most likely a relative increase caused by the effective removal of 10 to 20 weight percent of kimberlite material from the processed kimberlite fines during the heavy mineral separating step of the kimberlite ore processing circuit (section 2.2.5).

5.4 Sulphur Isotopes

There are two possible sources of dissolved sulphate in the pore-water of the processed kimberlite fines: gypsum (or anhydrite) dissolution and pyrite oxidation. However, there does not appear to be any significant pyrite oxidation in the processed kimberlite fines at present (section 5.2). In an effort to determine if the dissolved sulphate is from the dissolution of gypsum found in the mud xenoclasts (section 5.3), stable sulphur isotopes from the dissolved SO_4 in the processed kimberlite pore-water, as well as from sulphate minerals present in the mud xenoclasts, were analyzed. If the isotopic composition of sulphate-S from the mud xenoclasts matches the pore-water SO_4 it can be tentatively concluded that gypsum present in the mud xenoclasts is most likely the main source of dissolved SO_4.

In order to obtain a measure of the composition of the pore-water, hexahydrite ($MgSO_4{\cdot}6H_2O$) from the surface of the fines was analyzed. This hexahydrite is found to precipitate on the surface of the processed kimberlite fines during the summer months as a result of pore-water evaporation (section 5.2.2). Fractionation of sulphur isotopes does not normally occur during precipitation of sulphate minerals and the solutions from aqueous solutions (Seal, 2003). Therefore, the hexahydrite forming on the surface of the fines is expected to have the same sulphur isotope composition as the dissolved SO_4 found in the pore-water. Samples of the hexahydrite were collected directly from the surface of the fines. Pieces of the efflorescent crust were collected and placed in a glass vial using tweezers. Before S-isotope analysis, the crust was ground and identified as hexahydrite using XRD.

The gypsum/anhydrite present in the kimberlite is essentially restricted to mud xenoclasts found throughout the ore (section 5.3). In order to analyze the isotopic composition of sulphate-S in mud, the sulphate minerals first had to be extracted. Two mud samples, containing the highest sulphate-S concentrations were chosen for the extraction (section 5.3). Mud material was ground to -200 mesh and boiled for 20 minutes in 50 mL of ultra-pure SO_4-free water (Hall et al., 1988). The mixture was centrifuged, and the solution was decanted and set aside. The residue was boiled with 50 mL of water twice more, producing approximately 150 mL of supernatant. The method described by Hall et al. (1988) was modified so that the dissolved SO_4 in the supernatant was precipitated by evaporating the solution to dryness in a drying oven at $65^{o}C$, instead of precipitating it as $BaSO_4$ with an excess of $BaCl_2$. The resulting precipitate was identified, by XRD, as syngenite ($K_2Ca(SO_4)_2{\cdot}H_2O$) in all extracted samples.

Table 5.3 lists the S concentration and $\delta^{34}S$ values obtained from gypsum/anhydrite in the mud xenoclasts and the hexahydrite. This table shows that 1) all sulphate-S $\delta^{34}S$ values are negative and 2) there is a significant difference between the hexahydrite and the gypsum/anhydrite values. The mud xenoclasts found in kimberlites throughout the Lac de Gras region are thought to be derived from sediments deposited in a marine setting, possibly the Western Interior Seaway, during the upper Cretaceous (Doyle et al., 1998; Field and Scott-Smith, 1998). Therefore, the sulphate minerals present in the mud xenoclasts most likely precipitated from seawater incorporated into the sediments during deposition. Sulphate minerals precipitating from seawater have $\delta^{34}S$ values that range

Sample	Type	S (wt. %)	$\delta^{34}S$
OA-1	Mud sulphate	12	-9.5
OA-2*	Mud sulphate	13	-9.6
OB-1	Mud sulphate	12	-8.8
21-1	Mud sulphate	5	-6.7
EFF-1	Pore-water SO_4	12	-18.6
EFF-2*	Pore-water SO_4	13	-18.6

* denotes duplicate of the sample immediately above

Table 5.3: Sulphur concentration and isotopic composition for mud xenoclast gypsum/anhydrite and hexahydrite from the surface of the fines.

from approximately +10 ‰ to +30 ‰ (Seal, 2003). However, the negative values for the kimberlite mud xenoclast suggest that there is another source of dissolved sulphate.

Pyrite is also present in the Panda mud xenoclasts and is a possible source for the dissolved sulphate. The pyrite has a framboidal texture (section 5.1.10) suggesting biogenic formation through the reduction of dissolved SO_4 originally present in the sediments. Sulphate-reducing bacteria, such as *Desulfovibrio desulfuricans*, selectively reduce $^{32}SO_4$ in solution thereby forming pyrite with a negative $\delta^{34}S$ (Faure, 1986). It has been shown that oxidation of pyrite produces negligible amounts of S-isotope fractionation (Seal, 2003). Therefore, the negative $\delta^{34}S$ values deduced for the processed kimberlite pore-water SO_4 (based on the hexahydrite analyses) could be from the oxidation of biogenic pyrite with a highly negative $\delta^{34}S$. However, this hypothesis is inconsistent with other data presented thus far (sections 5.2 and 5.3). If biogenic pyrite oxidation is the source of pore-water SO_4, then one would expect to observe the products of these reactions in the field or in hand sample. However, there is little evidence in the LLCF suggesting that pyrite oxidation is occurring significantly at present. Thus it is unclear what the negative $\delta^{34}S$ values mean.

The other feature noted in Table 5.3 is the difference between the pore-water sulphate $\delta^{34}S$ values and the mud xenoclast sulphate $\delta^{34}S$ values. This difference was unexpected because hexahydrite forming the efflorescent crust on the surface of the fines represents the last stages of evaporation when all of the sulphate is precipitated from the pore-water as it is transported to the surface. Therefore, the S-isotopic signature of this mineral was expected to approximate that of the pore-water. If the LLCF pore-water SO_4 is assumed to be from the dissolution of gypsum/anhydrite in the mud xenoclasts, then the hexahydrite and gypsum/anhydrite would be expected to have approximately the same $\delta^{34}S$ values, which is not the case. A possible explanation of the difference in $\delta^{34}S$ values between the mud sulphate and the pore-water is that the pore-water experienced S-isotope fractionation during extreme evaporation and precipitation of the hexahydrite. More work is needed to explain both features of the data noted in table 5.3.

The purpose of analyzing sulphate-S isotopes was to help determine the source of dissolved SO_4 in the kimberlite fines pore-water. However, these data do not provide conclusive evidence. The discussion above outlines only two possible explanations for the observed S-isotopic signatures. Further work could include analysis of the dissolved SO_4-S isotopic signature from process plant effluent in order to obtain the $\delta^{34}S$ value before any evaporation of pore-water occurs, as well as analysis of the S-isotopic signature of pyrite present in the mud xenoclasts.

6 Controls on LLCF Water Chemistry

The second objective of this investigation was to use major element chemistry of the LLCF water samples, together with the minerals observed, to identify the processes affecting the chemistry of water within the LLCF, including pore-water and process plant discharge water. This was accomplished using geochemical modeling software to perform calculations and construct diagrams to help deduce the minerals and processes affecting water chemistry. All calculations, including speciation, reaction path, and inverse modeling were conducted using the PHREEQC software code (Parkhurst and Appelo, 1999), with the LLNL thermodynamic database that is distributed with the PHREEQC software. The LLNL database, prepared at the Lawrence Livermore National Laboratory, was used for calculations because saponite, a Mg-rich trioctahedral smectite found in the processed kimberlite fines (section 5.2.1), is not found in the other database files distributed with PHREEQC. Note that all water analyses with an absolute charge imbalance greater than 15% were not used in modeling calculations.

Charge imbalance is a measure of the difference between the total sum of cations and anions in a water analysis. As well, charge imbalance can be used as an indication of the quality of the analytical data. Ideally, a solution should have a charge imbalance of zero. However, this is usually not the case. Therefore it is necessary to decide on a threshold charge imbalance above which an analysis will not be included in interpretations because the quality of the results is suspect.

6.1 Mineral Saturation

The first step in deducing the factors controlling the chemistry of the LLCF water samples is to determine the minerals that are at saturation in the LLCF water samples. The saturation index for each mineral is calculated using the following equation:

$$SI = \log\left(\frac{IAP}{K_{sp}}\right),$$

where SI is saturation index, IAP is the ion activity product, and K_{sp} is the solubility product (Nordstrom and Munoz, 1986). The IAP is calculated by multiplying the dissolved activities of the constituent ions, with each activity raised to the power of its coefficient in the dissociation reaction. For example, the dissolution reaction for chrysotile is:

$$Mg_3Si_2O_5(OH)_{4(s)} + 6H^+_{(aq)} \longrightarrow 2SiO_{2(aq)} + 3Mg^{2+}_{(aq)} + 5H_2O_{(l)},$$

and the IAP for this reaction is:

$$IAP_{chrysotile} = \frac{a^2_{SiO_2} \cdot a^3_{Mg^{2+}}}{a^6_{H^+}}.$$

The IAP is numerically equivalent to the K_{sp} value listed in thermodynamic databases only when the system is at equilibrium with respect to a specific phase, making the saturation index equal to zero. The logarithm of the ratio of the IAP to the K_{sp} gives an indication of the degree that a solution is undersaturated or supersaturated with respect to a given mineral phase (Nordstrom and Munoz, 1986). If the SI for a mineral is less than 0 (IAP is less than K_{sp}), the mineral will be unstable in solution and will tend to dissolve. If the SI for a mineral is greater than zero (IAP greater than K_{sp}), the mineral will be stable in the solution and, if possible, will tend to precipitate. However, a positive saturation index does not necessarily mean that a mineral will precipitate from solution because the kinetic requirements for crystallization from solution might be too great to overcome (Drever, 1997). An SI of approximately 0 indicates that the mineral is at equilibrium with the solution and will not tend to dissolve or precipitate (Nordstrom and Munoz, 1986).

6.1.1 Mineral Saturation in LLCF Waters

The saturation indices for minerals found within the Panda kimberlite and those expected to be possible candidates for secondary precipitation have been calculated using PHREEQC and the LLNL database. It should be noted that complexation of metals with dissolved organic material was not considered in these calculations. Since the stability constants for complexes of Ca and Mg, the two most abundant cations in LLCF waters (section 4.2), with organic complexes are at least an order of magnitude smaller than those for trace metal complexes (Schnitzer, 1978), the omission of metal-organic complexes from speciation calculations is not expected to significantly affect speciation calculation results.

The average, minimum, and maximum SI values for each mineral in pore, discharge, and surface water samples have been listed in tables 6.1 and 6.2 respectively. Minimum and maximum values have been included in these tables to provide information on the spread of saturation indices. Mean SI values for LLCF water samples have been included in table 6.1 and 6.2 because they provide an indication of the skewness of the values for each mineral. If only the minimum and maximum values were reported, there would be no indication of whether the majority of samples were closer to the minimum or

Mineral	Formula	Pore-water			Discharge		
		Min	Mean	Max	Min	Mean	Max
Aragonite	$CaCO_3$	-1.98	**-0.31**	0.45	-0.83	**-0.20**	0.45
Artinite	$Mg_2CO_3(OH)_2{:}3H_2O$	-10.67	**-5.17**	-3.11	-5.59	**-4.19**	-2.20
Barite	$BaSO_4$	0.40	**0.81**	1.15	0.91	**1.24**	1.64
Brucite	$Mg(OH)_2$	-7.86	**-3.94**	-2.60	-4.00	**-3.18**	-1.83
Calcite	$CaCO_3$	-1.83	**-0.17**	0.60	-0.68	**-0.05**	0.60
$CO_{2(g)}$	CO_2	-4.34	**-3.30**	-2.13	-4.55	**-3.59**	-2.84
Chrysotile	$Mg_3Si_2O_5(OH)_4$	-11.71	**-1.42**	2.48	-1.01	**-0.57**	0.98
Diopside	$CaMgSi_2O_6$	-10.74	**-3.93**	-1.22	-3.95	**-3.59**	-2.70
Dolomite	$CaMg(CO_3)_2$	-2.09	**1.18**	2.72	0.31	**1.54**	2.79
Enstatite	$MgSiO_3$	-6.14	**-2.72**	-1.40	-2.59	**-2.46**	-1.99
Epsomite	$MgSO_4 \cdot 7H_2O$	-4.58	**-2.91**	-2.19	-4.46	**-3.97**	-3.45
Forsterite	Mg_2SiO_4	-14.35	**-7.31**	-4.87	-6.91	**-6.50**	-5.56
Goethite	$FeOOH$	3.88	**5.38**	6.73	4.62	**4.90**	5.21
Gypsum	$CaSO_4 \cdot 2H_2O$	-2.37	**-0.78**	-0.05	-2.53	**-1.94**	-1.30
Hexahydrite	$MgSO_4 \cdot 7H_2O$	-4.82	**-3.15**	-2.43	-4.69	**-4.20**	-3.69
Magnesite	$MgCO_3$	-1.99	**-0.35**	0.46	-0.72	**-0.10**	0.48
Monticellite	$CaMgSiO_4$	-16.45	**-9.38**	-6.92	-9.12	**-8.69**	-7.84
Montmorillonite-Ca	$Ca_{0.165}Mg_{0.33}Al_{1.67}Si_4O_{10}(OH)_2$	3.58	**5.09**	7.03	2.10	**2.61**	3.12
Montmorillonite-K	$K_{0.33}Mg_{0.33}Al_{1.67}Si_4O_{10}(OH)_2$	3.45	**4.94**	6.87	2.25	**2.77**	3.28
Montmorillonite-Mg	$Mg_{0.495}Al_{1.67}Si_4O_{10}(OH)_2$	3.75	**5.25**	7.19	2.30	**2.80**	3.31
Montmorillonite-Na	$Na_{0.33}Mg_{0.33}Al_{1.67}Si_4O_{10}(OH)_2$	3.05	**4.53**	6.44	1.71	**2.22**	2.74
Saponite-Ca	$Ca_{0.165}Mg_3Al_{0.33}Si_{3.67}O_{10}(OH)_2$	-4.67	**4.02**	7.29	2.79	**3.56**	4.34
Saponite-K	$K_{0.33}Mg_3Al_{0.33}Si_{3.67}O_{10}(OH)_2$	-4.97	**3.79**	7.05	2.87	**3.64**	4.42
Saponite-Mg	$Mg_{3.165}Al_{0.33}Si_{3.67}O_{10}(OH)_2$	-4.59	**4.11**	7.37	2.90	**3.68**	4.46
Saponite-Na	$Na_{0.33}Mg_3Al_{0.33}Si_{3.67}O_{10}(OH)_2$	-5.32	**3.38**	6.62	2.34	**3.11**	3.87
Sepiolite	$Mg_4Si_6O_{15}(OH)_2{:}6H_2O$	-15.00	**-1.98**	3.88	-2.79	**-1.77**	0.26
Amorph. SiO_2	SiO_2	-1.07	**-0.79**	-0.60	-1.13	**-1.00**	-0.91
Quartz	SiO_2	0.32	**0.60**	0.80	0.19	**0.35**	0.48
α-Cristobalite	SiO_2	-0.26	**0.02**	0.21	-0.37	**-0.22**	-0.10
β-Cristobalite	SiO_2	-0.74	**-0.46**	-0.27	-0.82	**-0.69**	-0.58
Tridymite	SiO_2	0.13	**0.41**	0.60	0.00	**0.15**	0.29

Table 6.1: Saturation indices calculated from LLCF pore and discharge water samples. Average saturation indices appear in bold.

		Dyke B Surface			**Dyke C Surface**		
Mineral	**Formula**	**Min**	**Mean**	**Max**	**Min**	**Mean**	**Max**
Antigorite	$Mg_{48}Si_{34}O_{85}(OH)_{62}$	-58.91	**9.77**	56.40	-175.88	**-82.61**	-6.80
Aragonite	$CaCO_3$	-1.40	**-0.33**	0.15	-1.99	**-1.17**	-0.32
Artinite	$Mg_2CO_3(OH)_2{:}3H_2O$	-7.14	**-4.65**	-3.34	-9.81	**-6.91**	-4.49
Barite	$BaSO_4$	0.53	**0.87**	1.10	0.71	**0.84**	0.94
Brucite	$Mg(OH)_2$	-4.78	**-3.42**	-2.45	-6.90	**-4.78**	-3.08
Calcite	$CaCO_3$	-1.25	**-0.19**	0.29	-1.85	**-1.02**	-0.17
$CO_{2(g)}$	CO_2	-4.20	**-3.73**	-3.19	-4.29	**-3.23**	-2.00
Chrysotile	$Mg_3Si_2O_5(OH)_4$	-4.49	**-0.21**	2.70	-11.74	**-5.99**	-1.25
Diopside	$CaMgSi_2O_6$	-6.42	**-3.53**	-1.59	-11.63	**-7.41**	-4.17
Dolomite	$CaMg(CO_3)_2$	-1.04	**1.16**	2.09	-2.19	**-0.56**	0.99
Enstatite	$MgSiO_3$	-4.00	**-2.51**	-1.50	-6.59	**-4.45**	-2.79
Epsomite	$MgSO_4{\cdot}7H_2O$	-4.85	**-4.27**	-3.90	-4.79	**-4.51**	-4.22
Forsterite	Mg_2SiO_4	-9.11	**-6.26**	-4.25	-13.81	**-10.12**	-6.89
Goethite	$FeOOH$	4.00	**4.70**	5.32	2.61	**4.38**	5.21
Gypsum	$CaSO_4{:}2H_2O$	-2.66	**-2.14**	-1.79	-2.55	**-2.32**	-2.07
Hexahydrite	$MgSO_4{\cdot}6H_2O$	-5.09	**-4.50**	-4.14	-5.02	**-4.75**	-4.46
Magnesite	$MgCO_3$	-1.49	**-0.36**	0.08	-2.06	**-1.25**	-0.54
Magnetite	Fe_3O_4	-1.92	**2.32**	7.48	-2.22	**0.70**	4.52
Monticellite	$CaMgSiO_4$	-11.12	**-8.34**	-6.38	-15.86	**-12.20**	-9.01
Montmorillonite-Ca	$Ca_{0.165}Mg_{0.33}Al_{1.67}Si_4O_{10}(OH)_2$	0.86	**1.47**	2.57	-0.53	**1.58**	2.45
Montmorillonite-K	$K_{0.33}Mg_{0.33}Al_{1.67}Si_4O_{10}(OH)_2$	0.80	**1.41**	2.60	-0.76	**1.53**	2.45
Montmorillonite-Mg	$Mg_{0.495}Al_{1.67}Si_4O_{10}(OH)_2$	1.03	**1.64**	2.75	-0.37	**1.75**	2.61
Montmorillonite-Na	$Na_{0.33}Mg_{0.33}Al_{1.67}Si_4O_{10}(OH)_2$	0.30	**0.91**	2.10	-0.96	**1.12**	2.02
Saponite-Ca	$Ca_{0.165}Mg_3Al_{0.33}Si_{3.67}O_{10}(OH)_2$	-1.69	**2.74**	5.65	-9.95	**-3.16**	1.82
Saponite-K	$K_{0.33}Mg_3Al_{0.33}Si_{3.67}O_{10}(OH)_2$	-1.88	**2.60**	5.52	-10.26	**-3.29**	1.72
Saponite-Mg	$Mg_{3.165}Al_{0.33}Si_{3.67}O_{10}(OH)_2$	-1.60	**2.83**	5.75	-9.87	**-3.07**	1.92
Saponite-Na	$Na_{0.33}Mg_3Al_{0.33}Si_{3.67}O_{10}(OH)_2$	-2.37	**2.11**	5.03	-10.46	**-3.69**	1.29
Sepiolite	$Mg_4Si_6O_{15}(OH)_2{:}6H_2O$	-8.58	**-2.44**	1.48	-19.88	**-10.22**	-3.63
Amorph. SiO_2	SiO_2	-1.56	**-1.39**	-1.15	-2.04	**-1.43**	-1.29
Quartz	SiO_2	-0.17	**-0.01**	0.24	-0.64	**-0.04**	0.11
Cristobalite(alpha)	SiO_2	-0.75	**-0.59**	-0.34	-1.22	**-0.62**	-0.47
Cristobalite(beta)	SiO_2	-1.23	**-1.07**	-0.82	-1.71	**-1.10**	-0.95
Tridymite	SiO_2	-0.36	**-0.21**	0.04	-0.84	**-0.24**	-0.08

Table 6.2: Saturation indices calculated from LLCF surface water samples. Average saturation indices appear in bold.

maximum reported value. This point is especially significant if the SI for a mineral has a negative minimum and a positive maximum, yet the majority of samples exist at or very near saturation. For example, calcite SI values in pore-water samples range from -1.83 to 0.60, yet the average value of -0.17 suggests that the mean SI of samples are very close to saturation.

On inspection of tables 6.1 and 6.2 it can be seen that chrysotile, forsterite, enstatite, and diopside are undersaturated in all LLCF water samples, indicating that they are all unstable and will tend to dissolve. As well, the Ca, Mg, Na, and K forms of the smectite clays montmorillonite and saponite are stable in all water samples collected from the LLCF. The stability of these clay minerals is consistent with the fact that smectite minerals form early in the weathering of unstable Fe-, Mg, and Ca- rich minerals, such as the serpentine, olivine, and pyroxene found in the Panda kimberlite (Langmuir, 1996).

The mean calcite saturation indices listed in tables 6.1 and 6.2 are –0.17, -0.05, -0.19, and –1.02 for pore, discharge, Dyke B, and Dyke C water samples, respectively. These data suggest that calcite is at or very near saturation in the discharge, pore, and Dyke B waters, and undersaturated in the Dyke C surface waters collected from the process plant water-reclaim barge. Aragonite saturation indices are also at or near saturation in all except Dyke C water samples. The mean partial pressures of CO_2 calculated to be in equilibrium with LLCF water samples fall within the range of pressures defined by atmospheric CO_2 and soil CO_2, with values of $10^{-3.5}$ and 10^{-2} atm, respectively (Langmuir, 1996).

Saturation indices listed in Tables 6.1 and 6.2 indicate that gypsum is undersaturated in all water samples. The maximum average gypsum saturation index reported for any water sample collected is from processed kimberlite pore-water, at a value of –0.78. This indicates that gypsum is not likely precipitating anywhere in the containment facility and, if present, will dissolve.

Finally, the saturation indices for five forms of SiO_2 that have been included in the listings of tables 6.1 and 6.2, including quartz, amorphous silica, α-cristobalite, β-cristobalite, and tridymite. α-Cristobalite, β-cristobalite, and tridymite are high temperature silica polymorphs and quartz is the stable form of SiO_2 below 500°C and 1 bar pressure (Deer et al., 1992). However, experimental studies indicate that the precipitation of quartz is extremely slow at low temperatures and is therefore unlikely in the LLCF (Langmuir, 1996). High dissolved silica concentrations from the weathering of mafic minerals in volcanic rocks, especially in the unsaturated zone, may lead to the precipitation of cristobalite, tridymite, and/or opal (Langmuir, 1996). For this reason, cristobalite and tridymite have also been included in the saturation indices tabulated in table 6.1 and 6.2. In pore and discharge water samples, the saturation indices for quartz, α-cristobalite and tridymite are approximately 0 suggesting that some form of variably crystalline silica mineral is saturated in these waters. The silica minerals become undersaturated in the surface water samples collected from Dyke B and Dyke C.

The minerals identified in the analysis of the saturation indices are the most probable mineralogical influences on the LLCF water chemistry. The next step in determining which of these minerals are actually helping to control water chemistry is to look at pore-, discharge, and surface water samples with these minerals in mind.

6.2 Processed Kimberlite Fines Pore-Water

Fines and co-existing pore-water samples collected from the LLCF were taken from the active layer, which develops every summer in the top 80 to 150 cm of the processed kimberlite. This layer is predominantly unsaturated with localized perched water tables developing only after heavy rainfall, especially during mid to late August. As a result, the processed kimberlite fines experience a significant amount of evaporation during the summer months. If periods without rain persist for a week or more, an efflorescent crust, composed predominantly of the Mg-sulphate mineral hexahydrite ($MgSO_4 \cdot 6H_2O$), begins to accumulate on the surface of the processed kimberlite (section 5.2.2).

6.2.1 Evaporation

In order to evaluate the effect of evaporation on pore-water chemistry it is necessary to first identify an element that is neither added nor removed from solution during evaporation (Eugster and Jones, 1979). As noted in the discussion of mineral saturation indices, gypsum never reaches saturation within the pore-water samples. Also it should be noted that barite is indicated to be supersaturated in all LLCF water samples (Tables 6.1 and 6.2). However, there is no significant amount of Ba-bearing minerals in the processed kimberlite fines to dissolve and act as a source of Ba for barite precipitation. Therefore, barite is most likely not a significant sink for sulphate in the LLCF. As well, analyses of the processed kimberlite fines indicate that the mean sulphate-S content of the processed kimberlite fines is 0.04 weight percent (section 5.3), which is most likely due to the precipitation of sulphate as the core-samples are dried in the laboratory. As the core are air-dried in the laboratory, a small amount of a fine white precipitate forms on the exposed core surface. These data suggest that all the gypsum has been dissolved from the processed kimberlite in the mineral processing plant, and that sulphate salts are not precipitating until very high salinities are reached, as is evidenced by the efflorescent crust forming on the fines in the lab and the field (section 5.2.2).

Chloride is usually chosen as the tracer when investigating the effects of evaporation on water chemistry (Eugster and Jones, 1979). However, Cl concentrations in LLCF pore-water samples are too low to ensure meaningful calculations due to the fact that small changes in a small concentration have large relative effects compared to small changes in a large concentration. Therefore, sulphate is being used as a tracer of evaporation in the LLCF processed kimberlite fines since it appears to be conservative in solution during evaporation until the very last stage, and it is present in relatively large concentrations.

Since the conservative element remains in solution during evaporation, it represents the degree of concentration of the water. A plot of any element versus the tracer ion will demonstrate whether an element remains in solution or is removed from solution during evaporation. The comparison is done by calculating a reaction path representing the compositions that would result if an element remained in solution during the incremental evaporation of the most dilute pore-water samples. For an element to remain in solution during evaporation, no solids containing it can precipitate during the process. Therefore, evaporation calculations were carried out for the LLCF pore-water samples allowing no solids to precipitate.

The concentrations calculated from the evaporation simulations are plotted as a line on a graph of the conservative element versus the element of interest. The actual water data can then be plotted on the same diagram for comparison. The pattern of the data on this type of diagram suggests that certain mechanisms are operating. The generalization can be made that data plotting above the calculated evaporation line suggests that there is a source supplying the element to solution while data plotting below the evaporation line suggests that the ion is being removed from solution, possibly through the processes of mineral precipitation and co-precipitation, sorption, cation exchange, or biological action (Drever, 1997; Eugster and Jones, 1979).

6.2.2 Evaporation of Processed Kimberlite Fines Pore-Water

Figures 6.1 to 6.4 are plots demonstrating the behaviour of major solute concentrations as evaporation increases. The two parallel lines in these diagrams represent the evaporation of two of the most dilute samples and they are intended to bracket the range of concentrations that would be expected from the evaporation of pore-water.

The behaviour of Ca and Mg during evaporation is shown in Figure 6.1. From this diagram it can be seen that the data for both of these elements plot within the evaporation field in the diagram. This indicates that Ca and Mg remain in solution throughout the evaporation process (Eugster and Jones, 1979). Therefore, it can be concluded that no Ca or Mg minerals are precipitating from the LLCF pore-water samples collected. However, it should be noted that the conservation of Ca and Mg in the LLCF pore-water samples collected for this investigation does not preclude these elements from being precipitated as efflorescent salts on the surface of the tailings, which has been shown with the formation of hexahydrite on the surface of the processed kimberlite fines (section 5.2.2).

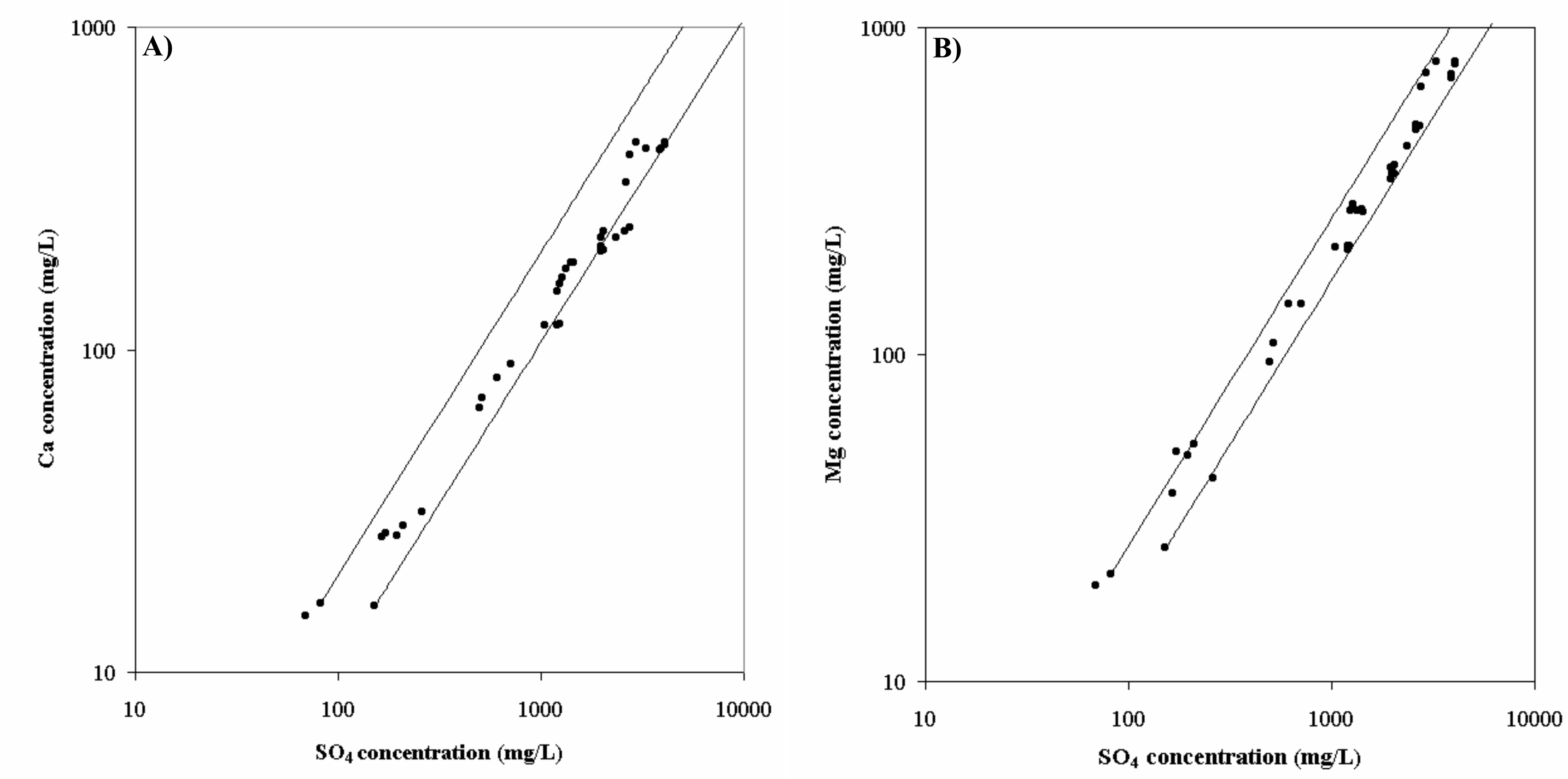

Figure 6.1: Plots showing the behaviour of **A)** Ca and **B)** Mg during evaporation of the LLCF processed kimberlite pore-water. The two solid lines bracket the range of concentrations that can be expected through the evapoconcentration of the most dilute samples.

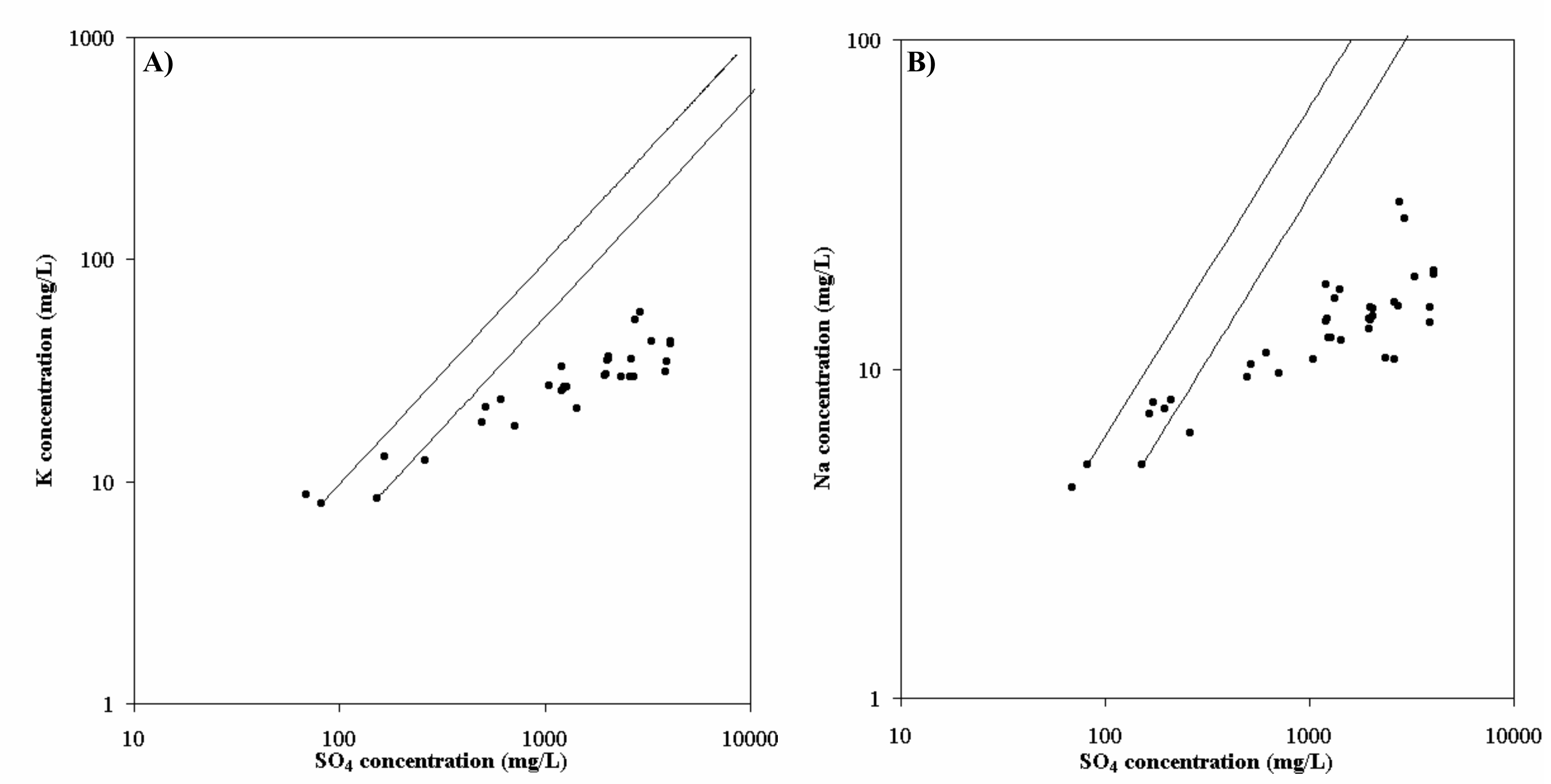

Figure 6.2: Plots showing the behaviour of **A)** K and **B)** Na during evaporation of the LLCF processed kimberlite pore-water. The two solid lines bracket the range of concentrations that can be expected through evapoconcentration of the most dilute samples.

Figure 6.2 shows the evaporation plots for Na and K and suggests that these elements behave similarly in the processed kimberlite pore-water. All except the most dilute samples plot in a linear trend below the calculated evaporation field suggesting that Na and K are progressively removed from solution during evaporation. The mechanism removing Na and K from solution could be a combination of mechanisms including clay mineral precipitation, ion exchange, surface adsorption, and biogenic action (Eugster and Jones, 1979).

The Si and alkalinity (representing $HCO_3^- + CO_3^{2-}$) evaporation diagrams are shown in Figure 6.3. These graphs demonstrate that both Si and alkalinity reach a relatively constant value and remain virtually unchanged as the sulphate concentration increases. The lack of correlation of the Si and alkalinity concentration with evaporation suggests that there is a phase controlling the concentration of these constituents (Eugster and Jones, 1979). Aqueous stability diagrams (section 6.2.3.4) and calculated P_{CO_2} values (section 6.1.1) suggest that a form of amorphous silica and ambient CO_2 partial pressures are controlling the concentrations of Si and alkalinity, respectively.

Like Si and alkalinity, Cl concentrations appear to remain constant as evapoconcentration increases (Figure 6.4). No Cl-bearing mineral has been found to be in equilibrium with LLCF pore-waters and there are no documented cases where Cl exhibits this behaviour with evaporation. If mineral surfaces have a net positive charge then negatively charged anions can adsorb onto the positive surface (Langmuir, 1996). The ability of a sorbent phase to adsorb negative anions is known as anion exchange capacity. The anion exchange capacity of Panda kimberlite was not measured. However, it has been noted that kimberlite readily adsorbs PO_4 and As (Graham, 2002), both of

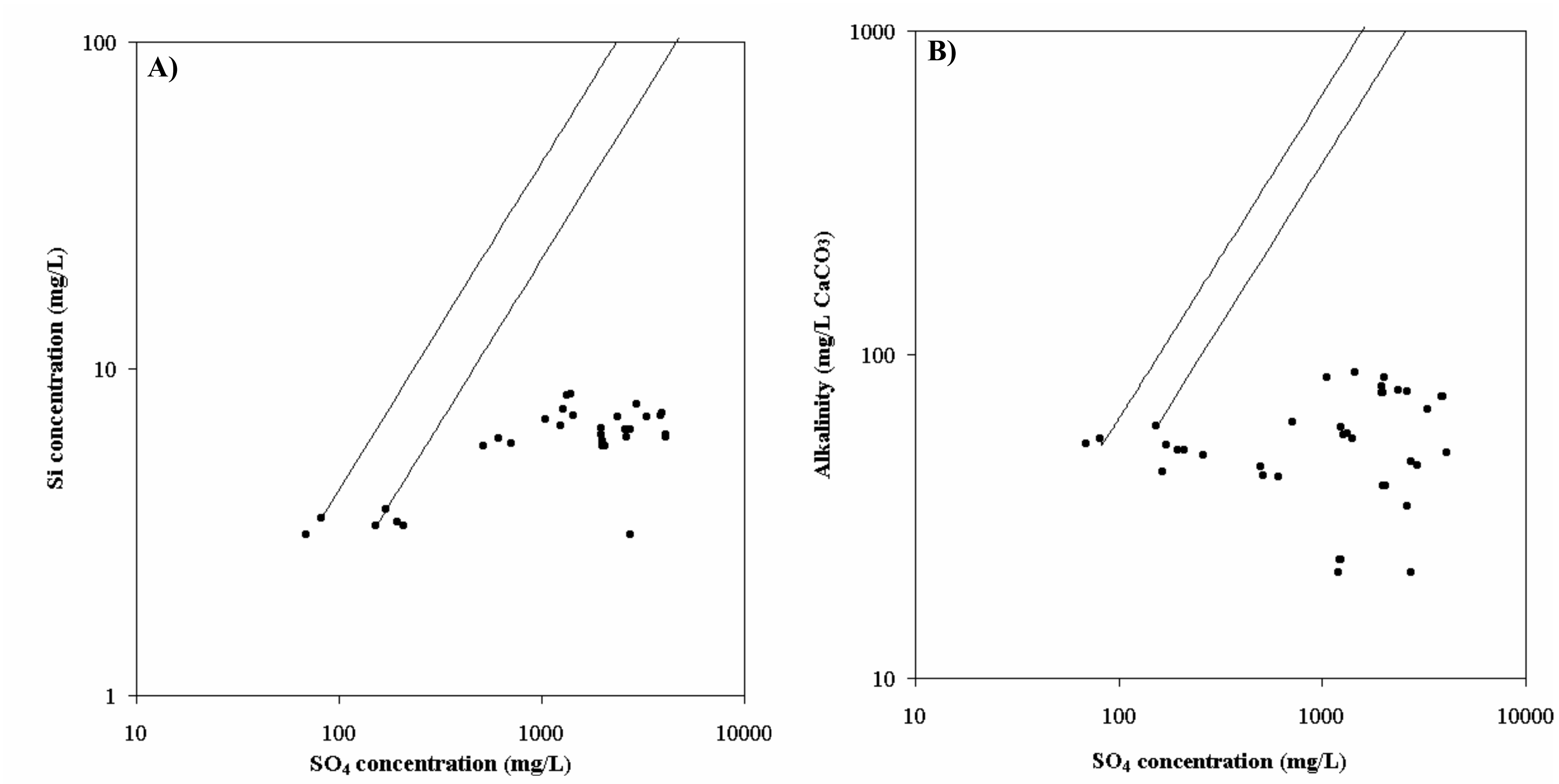

Figure 6.3: Plots showing the behaviour of **A)** Si and **B)** alkalinity during evaporation of the LLCF processed kimberlite pore-water. The two solid lines bracket the range of concentrations that can be expected through evapoconcentration of the most dilute samples.

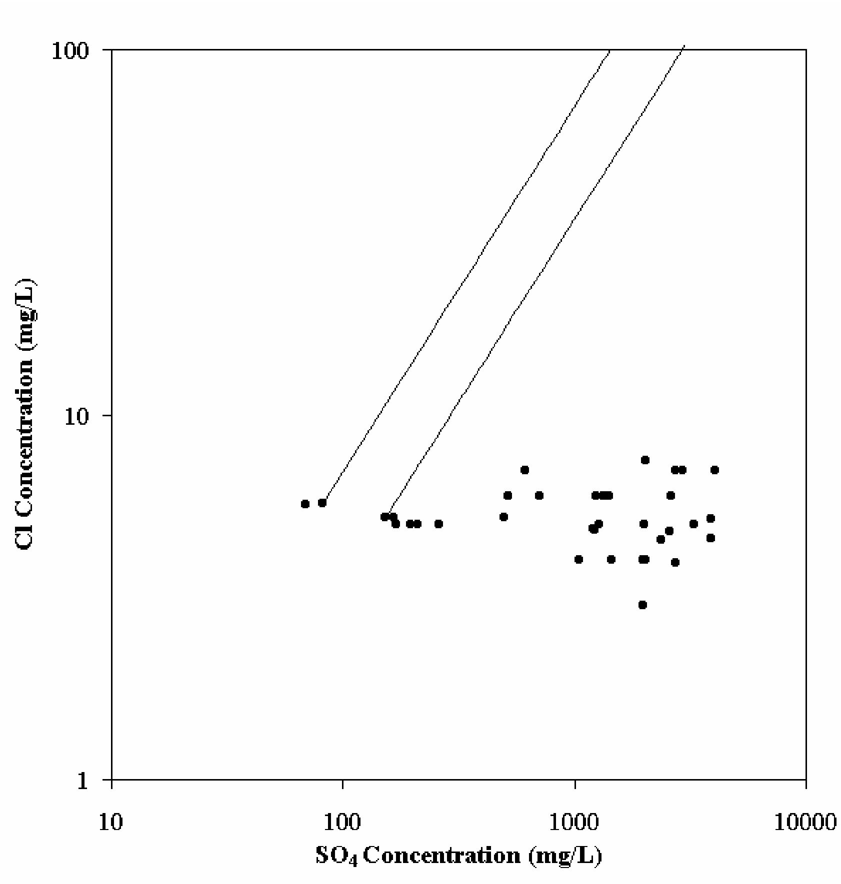

Figure 6.4: Plots showing the behaviour of Cl during evaporation of the LLCF processed kimberlite pore-water. The two solid lines bracket the range of concentrations that can be expected through the evapoconcentration of the most dilute samples.

which form negative ions in solution. The adsorptive ability of kimberlite material could help to explain the constant Cl concentrations observed within the fines pore-water, but further work is required to more fully explain this phenomenon.

The technique of plotting elements versus conservative evaporation tracers is useful in identifying whether element concentrations may be controlled by evaporation, or whether there is an addition or removal of ions from solution as evaporation increases. However, the source of the addition or removal of ions from solution is not identified through the use of these diagrams. In order to identify the phases responsible for the addition or removal of ions, it is necessary to plot the water compositions on mineral stability diagrams.

6.2.3 Mineralogical Controls on Pore-Water Chemistry

Aqueous mineral stability diagrams are used to determine the minerals and reactions that might be controlling the chemistry of a given solution (Nordstrom and Munoz, 1986). Water is assumed to be present and stable over the entire diagram. Reactions represented can include dissolution-precipitation of a mineral from solution, as well as reactions between two minerals and ions in solution. The lines on mineral stability diagrams represent the locus of points along which the reaction of interest is at equilibrium.

The first step in the construction of these diagrams is to define the chemical system of interest. A list of mineral phases present in the designated chemical system is used to derive the chemical reactions to be plotted. For illustration purposes, consider the dissolution of gypsum from solution. The equation for this reaction is:

$$CaSO_4 \cdot 2H_2O_{(s)} \longrightarrow Ca^{2+}_{(aq)} + SO^{2-}_{4(aq)} + 2H_2O_{(l)}.$$

The mass action expression for gypsum dissociation is (Parkhurst and Appelo, 1999):

$$K_{sp} = a_{Ca^{2+}} \cdot a_{SO_4^{2-}} = 10^{-4.4823}, \text{ at } 25^{o}\text{C (assuming } a_{H_2O} = 1).$$

Mineral stability diagrams involve linear relationships between the activities of dissolved constituents. Therefore, the logarithm of the mass action expression is taken in order to obtain a linear relationship of the above product. The result is:

$$\log K_{sp} = \log a_{Ca^{2+}} + \log a_{SO_4^{2-}} = -4.4823.$$

Rearranging the above expression to solve for Ca^{2+} yields,

$$\log a_{Ca^{2+}} = -4.4823 - \log a_{SO_4^{2-}},$$

which can then be plotted on a graph with the axes $\log a_{Ca^{2+}}$ and $\log a_{SO_4^{2-}}$, as shown in Figure 6.5. The solid line in this diagram represents the locus of points where the saturation index for gypsum is 0. If a water analysis plots below this line it is undersaturated and, if present, gypsum will tend to dissolve. In contrast, if a water plots above this line it is supersaturated and, if kinetically possible, gypsum will tend to precipitate. If a series of analyses from the same water plot along the gypsum equilibrium line in Figure 6.5, then it can be concluded that gypsum is likely controlling the Ca^{2+} and SO_4^{2-} concentrations in solution.

Mineral stability diagrams were constructed for five chemical systems including a) CaO-CO_2-H_2O, b) MgO-CO_2-H_2O, c) CaO-SO_4-H_2O, d) MgO-SiO_2-H_2O, and e) MgO-SiO_2-Al_2O_3-H_2O. The chemical reactions and thermodynamic data used to construct these diagrams were taken from the LLNL database distributed with the PHREEQC software. Table 6.3 is a summary of the dissociation reactions used in the construction of

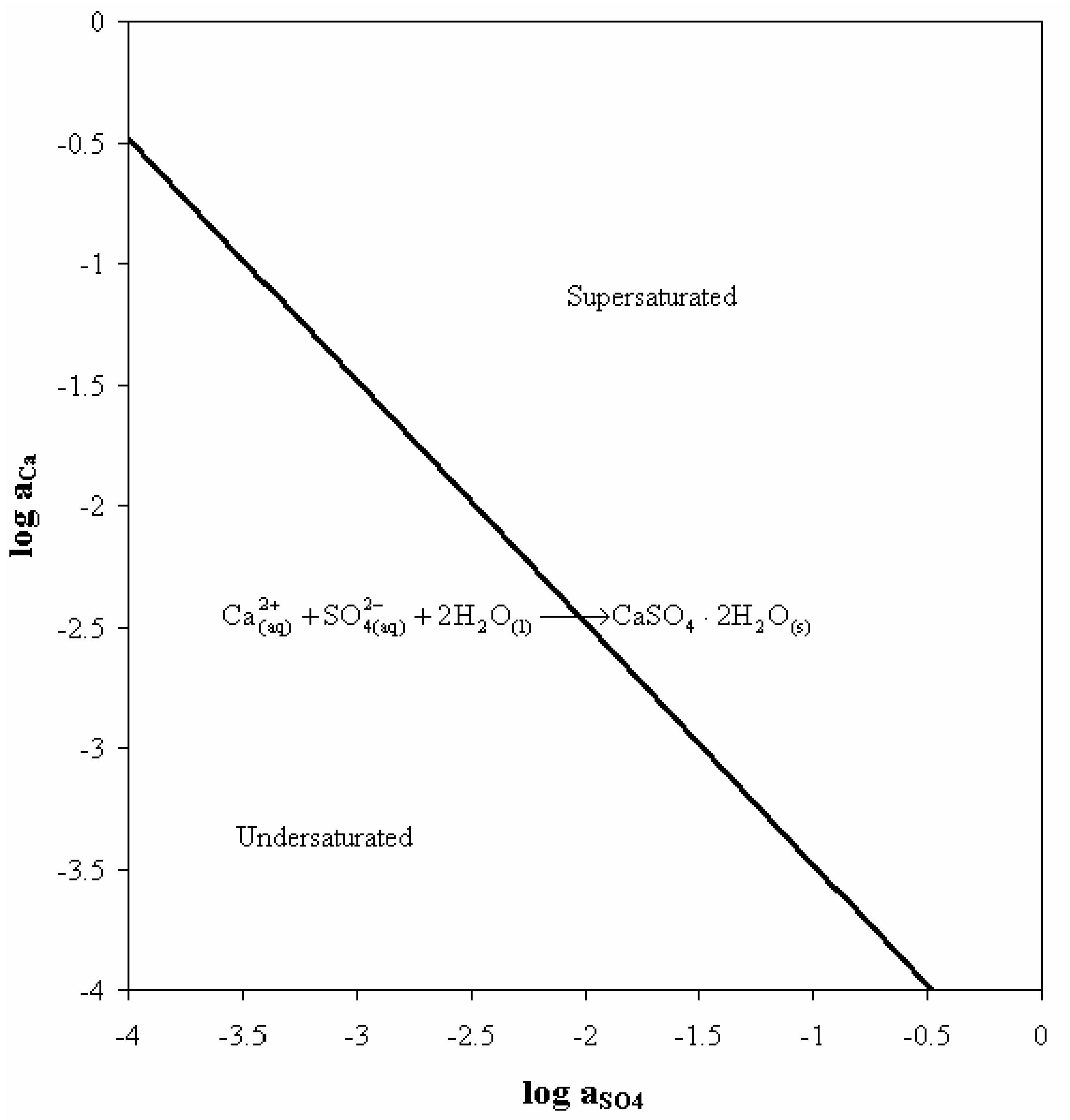

Figure 6.5: Gypsum aqueous stability diagram constructed at 25°C. The solid line represents the equilibrium dissolution-precipitation of gypsum. Points that plot above the line are supersaturated and gypsum will likely precipitate from the solution. However, if points plot below the line, the water is undersaturated with respect to gypsum and it will tend to dissolve.

Mineral	**Dissolution Reaction**	**log K_{25}**
Gypsum	$CaSO_4{\cdot}2H_2O \longrightarrow Ca^{2+} + SO_4^{2-} + 2H_2O$	-4.4823
Calcite	$CaCO_3 + H^+ \longrightarrow Ca^{2+} + HCO_3^-$	1.8487
Chrysotile	$Mg_3Si_2O_5(OH)_4 + 6H^+ \longrightarrow 3Mg^{2+} + 2SiO_{2(aq)} + 5H_2O$	31.1254
Sepiolite	$Mg_4Si_6O_{15}(OH)_2{\cdot}6H_2O + 8H^+ \longrightarrow 4Mg^{2+} + 6SiO_2 + 11H_2O$	30.4439
Brucite	$Mg(OH)_2 + 2H^+ \longrightarrow Mg^{2+} + 2H_2O$	16.2980
14A-Clinochlore	$Mg_5Al_2Si_3O_{10}(OH)_8 + 16H^+ \longrightarrow 5Mg^{2+} + 2Al^{3+} + 3SiO_{2(aq)} + 12H_2O$	67.2391
Mg-saponite	$Mg_{3.165}Al_{0.33}Si_{3.67}O_{10}(OH)_2 + 7.32H^+ \longrightarrow 3.165Mg^{2+} + 0.33Al^{3+} + 3.67SiO_{2(aq)} + 4.66H_2O$	26.2523
Kaolinite	$Al_2SiO_5(OH)_4 + 6H^+ \longrightarrow 2Al^{3+} + 2SiO_{2(aq)} + 5H_2O$	6.8101
Mg-montmorillonite	$Mg_{0.495}Al_{1.67}Si_4O_{10}(OH)_2 + 6H^+ \longrightarrow 0.495Mg^{2+} + 1.67Al^{3+} + 4SiO_{2(aq)} + 4H_2O$	2.3879
Magnesite	$MgCO_3 + H^+ \longrightarrow Mg^{2+} + HCO_3^-$	2.2936

Table 6.3: List of the dissolution reactions used in the construction of aqueous mineral stability diagrams. Log K values quoted in the table are for 25°C as in the LLNL thermodynamic database distributed with the PHREEQC software.

these diagrams. All log K values are quoted for 25°C as listed in the LLNL thermodynamic database. Note that all stability diagrams have been constructed at 12°C.

6.2.3.1 CaO-CO_2-H_2O

Figure 6.6 shows the stability diagram for the CaO-CO_2-H_2O system. The solid line represents the equilibrium line for calcite ($CaCO_3$). Figure 6.6A shows the plotting space of all LLCF water samples and it can be seen that pore-, discharge, and surface water samples all plot in the same region of the diagram. Note how the data straddle the calcite equilibrium line and are apparently not influenced by the precipitation or dissolution of this mineral.

Figure 6.6B contains only pore-water data points showing the difference between samples collected in each successive year (2000 to 2002). The 2000 suite of samples all plot highest along the $\log\left(a_{Ca^{2+}}/a_{H^+}\right)$ axis, the suite of 2002 samples plots the lowest, while the 2001 samples plot in between the 2000 and 2002 samples. The displacement of the data points closer to the calcite equilibrium line suggests that precipitation of calcite is causing the Ca^{2+} to decrease. However, the Ca evaporation plot (Figure 6.1A) does not indicate significant removal of Ca from solution, which suggests that calcite is not yet precipitating as a result of evaporation. In fact, it was shown in section 4.4.1 that pore-water Ca remains fairly constant and that pH of the pore-water samples decreased steadily from 2000 to 2002. It is this increase in H^+ concentration that is responsible for the movement of data points in figure 6.6. From these data, it seems that the Ca concentration in the processed kimberlite pore-water is not currently controlled by calcite precipitation. It is known that Mg^{2+} inhibits the precipitation of calcite while aragonite ($CaCO_3$) precipitation is unaffected by the presence of Mg^{2+} (Alkattan et al., 2002;

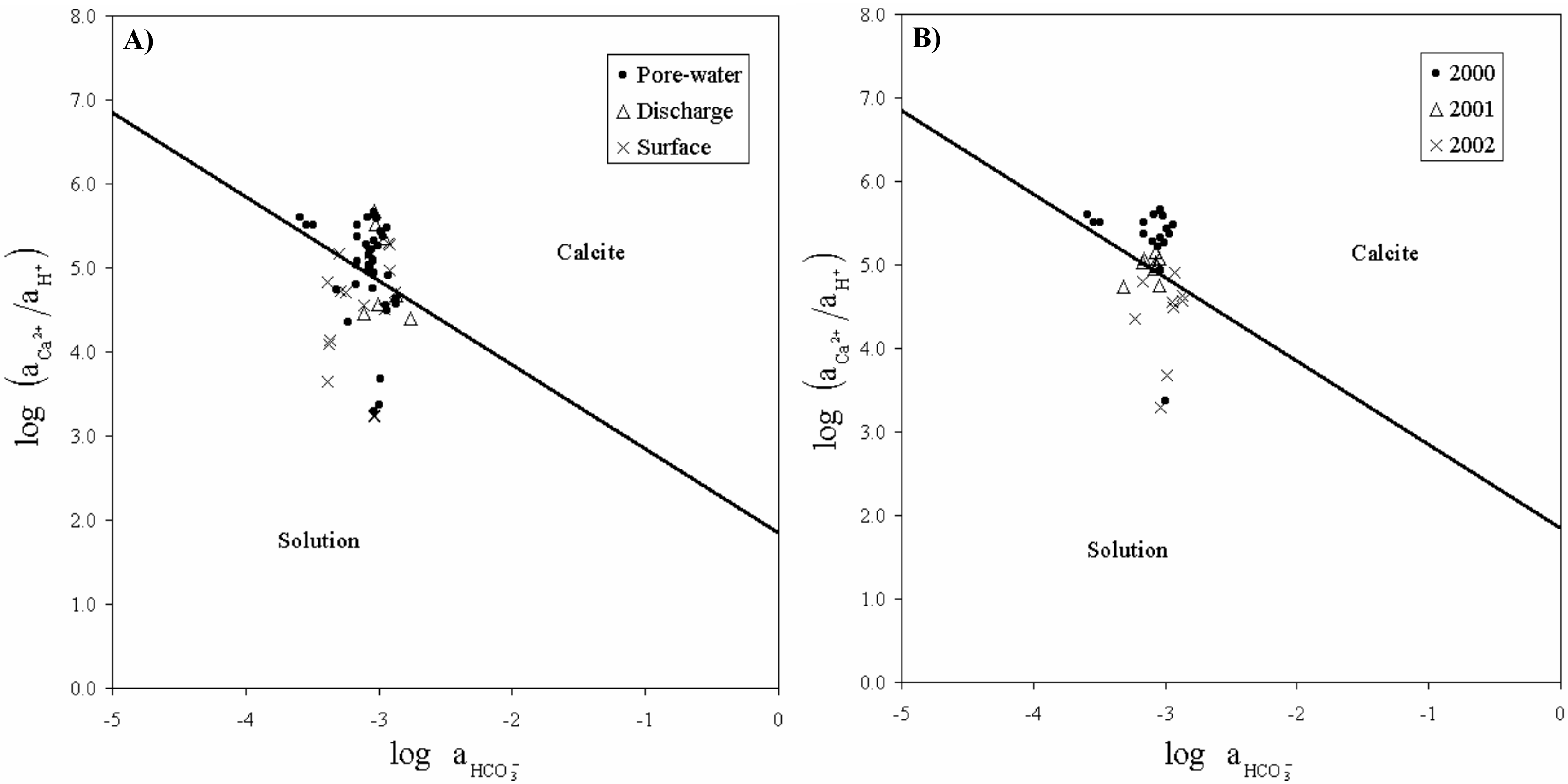

Figure 6.6: Mineral stability diagrams for the CaO-CO_2-H_2O system constructed at 12°C. **A)** Stability diagram for all types of water samples. **B)** Stability diagram separating the suite of 2000, 2001, and 2002 pore-water samples. The solid line in each diagram represents calcite solubility.

Berner, 1975). Therefore, aragonite is usually formed before calcite when the Mg^{2+}/Ca^{2+} ratio is greater than 1. LLCF pore-water Mg^{2+}/Ca^{2+} ratios are approximately 1.5 to 1.8. The high Mg concentration of the LLCF pore-water could be inhibiting the growth of calcite and be the reason for the lack of calcite precipitation. Any $CaCO_3$ that does precipitate from solution will most likely be aragonite. As well, the lack of calcite precipitation, calculated CO_2 partial pressures (section 6.1.1), and the narrow range of the HCO_3 activities in Figure 6.6 indicate that alkalinity is currently being controlled by ambient atmospheric and soil CO_2.

6.2.3.2 MgO-CO_2-H_2O

The stability diagram for the MgO-CO_2-H_2O system is shown in figure 6.7 with the solid line representing magnesite ($MgCO_3$) equilibrium. Similar to the calcite stability diagram, it can be seen that all LLCF water samples plot in approximately the same space in Figure 6.7A. As well, when the annual sample suites are separated from one another, as in figure 6.7B, it can be seen that the temporal behaviour is similar to that noted in the calcite diagram with the 2000 data plotting the highest along the $\log\left(a_{Mg^{2+}}/a_{H^+}\right)$ axis, 2002 data plotting the lowest, and the 2001 data plotting in between these two. It was shown, in section 4.4.1, that pore-water Mg concentration remained fairly constant from 2000 to 2002 while pH decreased steadily. It is this increase in H^+ concentration that is causing the movement of data points observed in figure 6.7B. Similar to Ca, the Mg evaporation diagram of figure 6.1B does not indicate removal of Mg from solution. Therefore, it is unlikely that magnesite precipitation is currently affecting Mg concentrations of the pore-water samples collected.

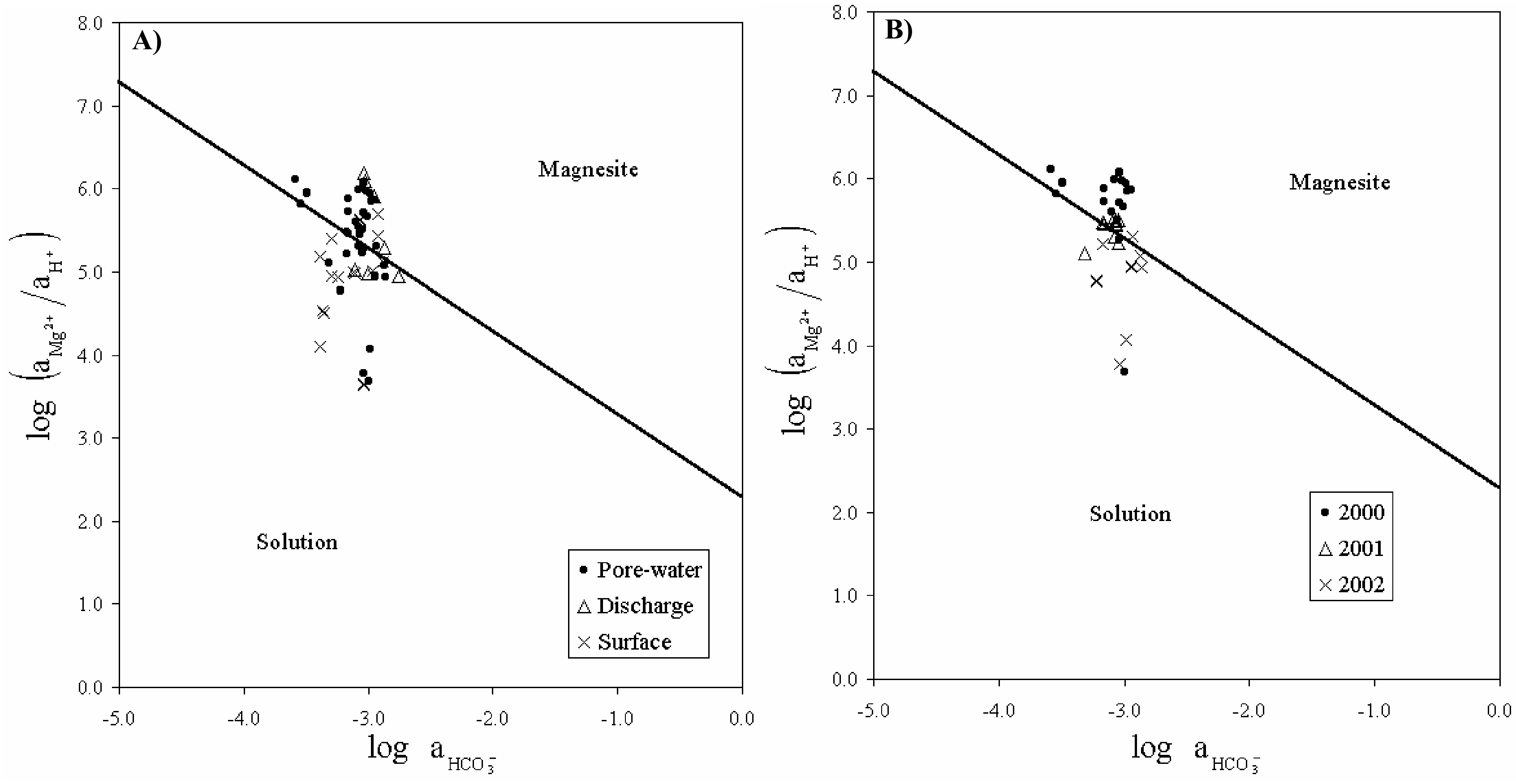

Figure 6.7: Mineral stability diagrams for the MgO-CO_2-H_2O system constructed at 12°C. **A)** Stability diagram for all types of water samples. **B)** Stability diagram separating the suite of 2000, 2001, and 2002 pore-water samples. The solid line in each diagram represents calcite solubility.

6.2.3.3 CaO-SO_4-H_2O

The stability diagram for the CaO-SO_4-H_2O system is presented in figure 6.8 with the solid line indicating gypsum equilibrium. This diagram shows that the most-dilute pore-, discharge, and surface water samples plot in the lower left portion of the diagram while the most concentrated pore-water samples plot in the upper right portion of the stability diagram. Note the linear trend that does not reach gypsum solubility, indicating that Ca^{2+} and $SO_4^{2-}$are not being removed from the suite of water samples collected in this study, and are most likely controlled by evapoconcentration.

6.2.3.4 MgO-SiO_2-H_2O

Figure 6.9 shows the stability diagram for the MgO-SiO_2-H_2O system. The most notable feature of this diagram is that the pore-water silica activities appear to be bound at high a_{SiO_2} by the dashed line, most likely representing the solubility of some form of amorphous silica. This suggests that some form of variably crystalline silica is precipitating from the pore-waters collected. These data help to explain the constant Si concentration observed in figure 6.3A.

The annual pore-water sample suites have been plotted in figure 6.9B. Note the separation of each of the sample suites and the downward movement of the data points to sepiolite saturation. Much like the calcite and magnesite stability diagrams, the change in $\log\left(a_{Mg^{s+}} / a_{H^+}^2\right)$ at approximately constant $\log a_{SiO_2}$ is most likely caused by the decrease in pore-water pH from 2000 to 2002, rather than from the precipitation from pore-waters sampled in this investigation.

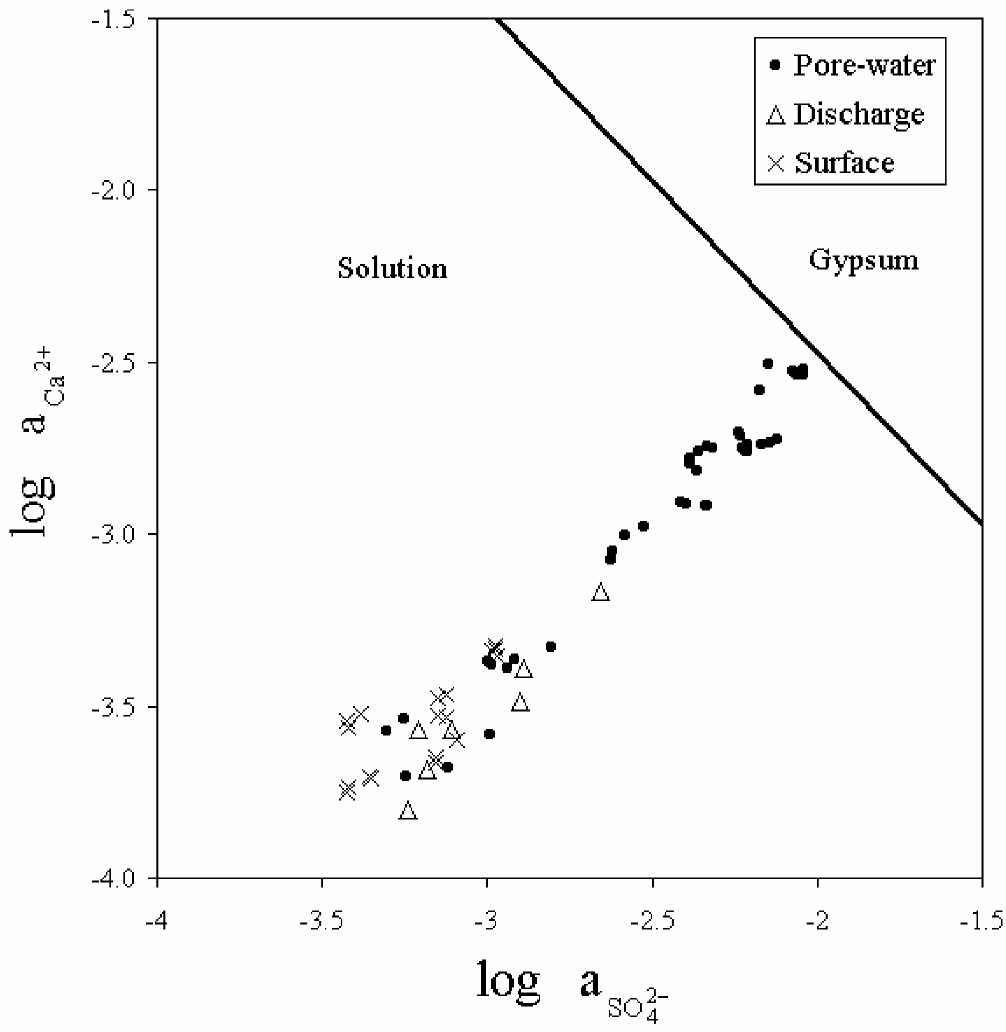

Figure 6.8: Mineral stability diagrams for the CaO-SO$_4$-H$_2$O system constructed at 12°C. The solid line represents gypsum solubility. Note how no water samples reach gypsum saturation.

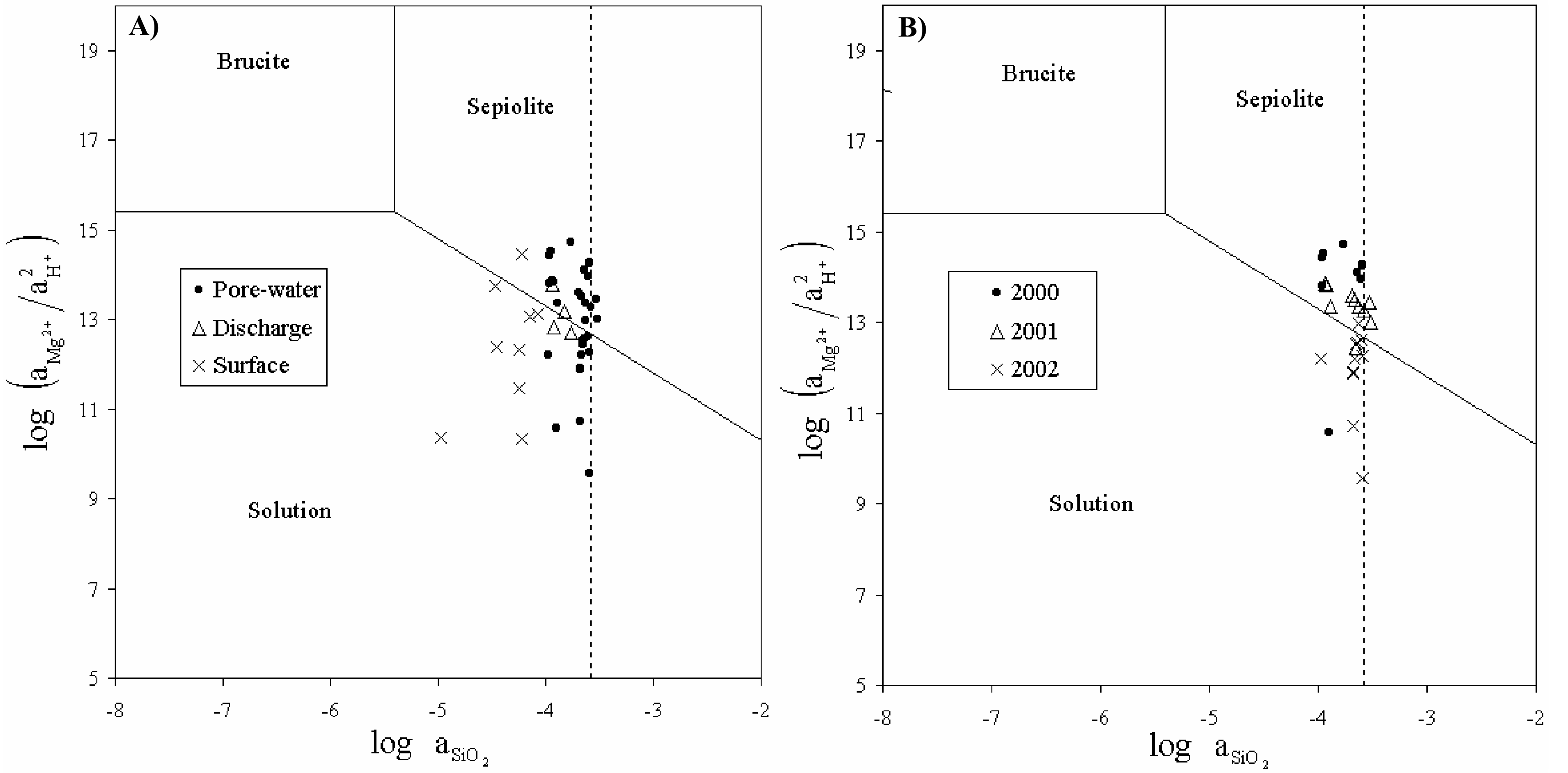

Figure 6.9: Mineral stability diagrams for the MgO-SiO_2-H_2O system constructed at 12°C. **A)** Stability diagram for all types of water samples. **B)** Stability diagram separating the suite of 2000, 2001, and 2002 pore-water samples. The vertical dashed line in each diagram represents silica solubility.

6.2.3.5 $MgO-SiO_2-Al_2O_3-H_2O$

Due to the complicated behaviour of Al in solution, a three-dimensional diagram is required to represent the solubilities of aluminosilicate minerals (Drever, 1997). The axes of these diagrams are Al concentration, silica activity, and pH. However, because dissolved Al concentrations are often very low, it can be assumed that Al remains in the solid phase (Drever, 1997). Therefore, reactions can be written and balanced with Al being conserved in minerals, and the solubilities of aluminosilicates can then be plotted on a two-dimensional diagram. The $MgO-SiO_2-Al_2O_3-H_2O$ phase diagram, representing the solubilities of Mg-aluminosilicate minerals present in the processed kimberlite fines, is shown in figure 6.10. Amorphous silica is the only mineral indicated to be at equilibrium with the solution plotted in these diagrams. However, it should be noted that saponite and kaolinite are indicated to be stable, but not necessarily precipitating, in LLCF water samples.

6.2.3.6 Na and K

Figure 6.2 indicates that Na and K are being removed from the pore-water solution, possibly by a combination of mechanisms including mineral precipitation, cation exchange or sorption (Eugster and Jones, 1979). Smectite clay minerals have been identified in both the kimberlite ore as well as the processed kimberlite fines. Therefore, it is probable that Na and K are being removed from pore-water solution through exchange with these clay minerals.

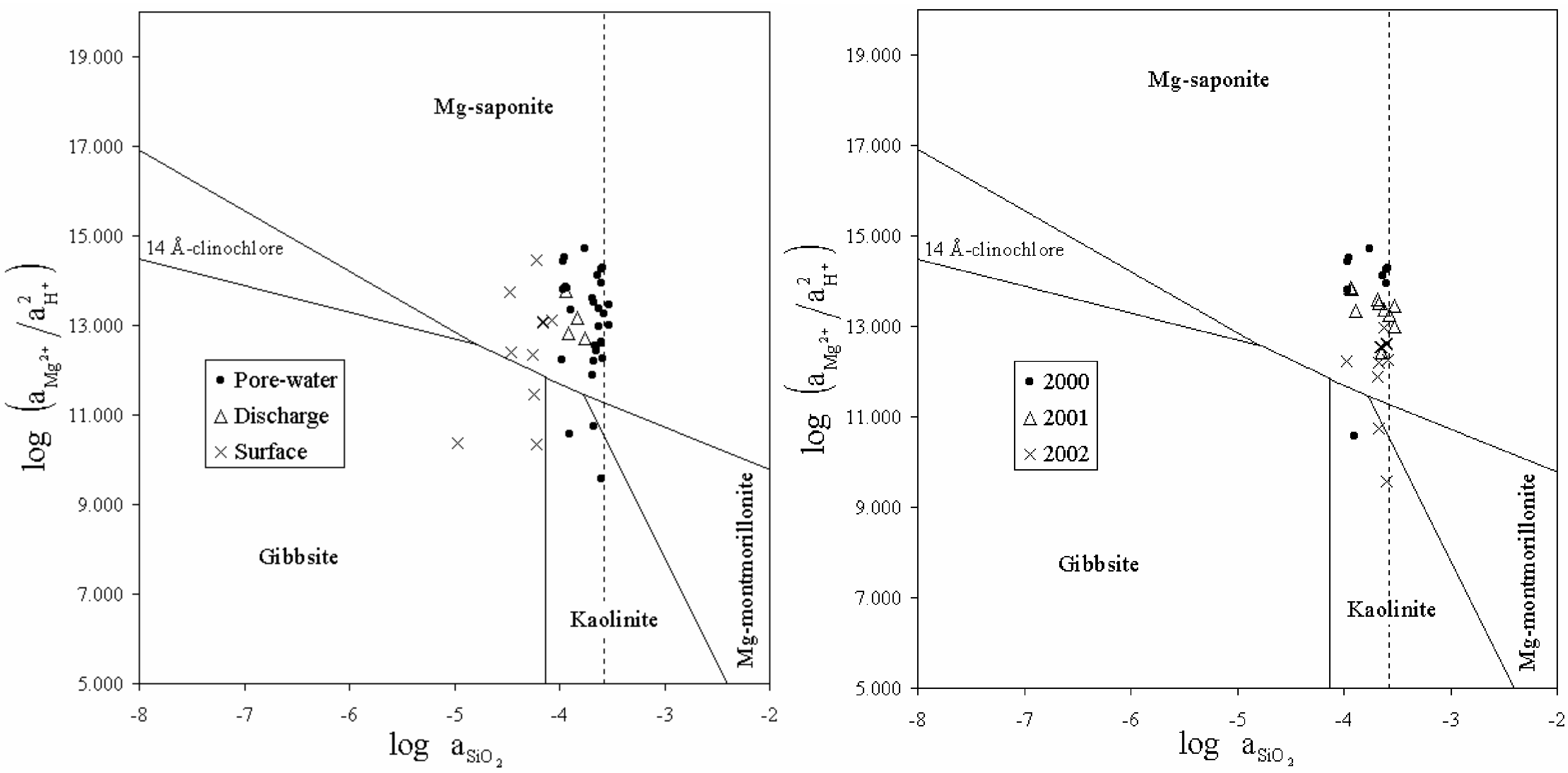

Figure 6.10: Mineral stability diagrams for the MgO-SiO_2-Al_2O_3-H_2O system constructed at 12°C. Note that Al is assumed to be conservative in the solid phase in these diagrams. **A)** Stability diagram for all types of water samples. **B)** Stability diagram separating the suite of 2000, 2001, and 2002 pore-water samples. The vertical dashed line in each diagram represents silica solubility.

6.2.3.7 pH

It has been noted that pH of the LLCF pore-water is dropping with time from an average 2000 value of 8.46 to an average 2002 value of 7.22 (section 4.5.1). There are three possible hypotheses to explain this decrease in pH: (1) Pyrite is oxidizing causing acid to be generated and the pH to decrease, (2) calcite, magnesite, or sepiolite could be precipitating from the pore-water, which produces protons, thereby decreasing pH, and (3) NH_4^+ is oxidizing to form NO_3^-, which generates protons leading to a decrease in pH.

Although the oxidation of pyrite is one of the most common causes of decreasing pH in mine waste, this possibility seems to contradict the current lack of significant evidence of pyrite oxidation in the LLCF (Chapter 5). It is possible that a very small amount of pyrite oxidation is occurring in the processed kimberlite fines and the acid produced is enough to lower the average pore-water pH approximately 1.2 units. If pyrite oxidation is the source of the decrease in pH, iron-oxide staining and increased dissolved Fe concentrations would be expected. However, these two phenomena are not observed in the processed kimberlite fines.

Pore-water data were shown to approach the calcite, magnesite, and sepiolite equilibrium dissolution lines in sections 6.2.3.1, 6.2.3.2, and 6.2.3.4, respectively. The precipitation of these minerals results in the production of protons, as shown by the reverse reactions listed in Table 6.3. This hypothesis appears to contradict the observations of the behaviour of pore-water solutes with evaporation (section 6.2.2). It was shown that Mg and Ca are conservative in solution as evaporation progresses, suggesting that no Ca and Mg minerals are precipitating from solution. However, much like the pyrite oxidation argument, this contradiction could be explained by the fact that only a small amount of precipitation of each of these minerals may be required to cause the observed decrease in pH. The amount of precipitation of each mineral required to decrease the pH 1.2 units from 2000 to 2002 might remove so little Ca and Mg from solution that it is virtually imperceptible in the evapoconcentration plots of section 6.2.2.

Ammonium (NH_4^+) is oxidized to NO_3^- following the half-reaction:

$$NH_4^+ + 3H_2O \longrightarrow 8e^- + 10H^+ + NO_3^- .$$

This reaction shows that as NH_4^+ is oxidized to NO_3^-, 10 protons are generated. Calculated Eh values from LLCF pore-water indicate oxidizing conditions (section 4.3.2) and NH_3-N concentrations are decreasing with time (section 4.5.1), suggesting that NH_4^+ in the pore-water could be oxidizing to $NO_3^-$and producing the acid causing the decrease in pore-water pH. However, if NH_4^+ is oxidizing to NO_3^- one would expect to see a rise in the concentration of NO_3^-, which is not observed in the processed kimberlite pore-water. A possible explanation for the lack of increasing NO_3^- could be that bacteria and algae, that are ubiquitous in mine waste settings, could be consuming the NO_3^- produced from NH_4^+ oxidation.

It should be noted that the processed kimberlite fines in the northern-most end of Cell B were a maximum of 4 years old during this investigation. As a result of this young age, significant amounts of secondary minerals are not yet observed in the processed kimberlite fines because there has not been adequate time for their accumulation. Since two of the three hypotheses presented above involve the precipitation of minerals from solution, it is not possible to validate these hypotheses with field observations at this time. Therefore, further sample collection is required to help explain the decrease in pH observed in the processed kimberlite fines pore-water.

6.2.4 Evolution of Pore-Water Chemistry

Hardie and Eugster (1970) developed a model to interpret the chemistry of natural waters undergoing evapoconcentration that is based on a series of chemical divides encountered as the solution becomes more concentrated. The chemical divides effectively fractionate the solution, with the evolutionary path being significantly affected by the initial concentration of solutes (Hardie and Eugster, 1970). Figure 6.11 is a schematic diagram representing some possible paths the Hardie-Eugster model predicts for the evaporation of natural waters. As can be seen, calcite is the first mineral to precipitate in all paths. The composition of the resulting solution of this first chemical divide will depend on whether the concentration of Ca^{2+} is greater than or less than one half of the alkalinity ($HCO_3^- + CO_3^{2-}$) (Hardie and Eugster, 1970).

If a water is in equilibrium with calcite and atmospheric CO_2, the charge balance equation for the solution is:

$$2m_{Ca^{2+}} + m_{H^+} = m_{HCO_3^-} + 2m_{CO_3^{2-}} + m_{OH^-},$$

where m is the concentration of the solute in moles per kilogram of solution. If $m_{H^+} = m_{OH^-}$, which is legitimate for natural waters at an approximately neutral pH, then the charge balance equation becomes:

$$2m_{Ca^{2+}} = m_{HCO_3^-} + 2m_{CO_3^{2-}}.$$

The evaporation of a solution satisfying the above equation will result in the precipitation of calcite without the increase of Ca^{2+} relative to alkalinity ($HCO_3^- + CO_3^{2-}$) or alkalinity relative to Ca^{2+}. If $2m_{Ca^{2+}} > m_{HCO_3^-} + m_{CO_3^{2-}}$, the resulting solution will experience an increase in Ca^{2+} concentration relative to alkalinity in order to satisfy the

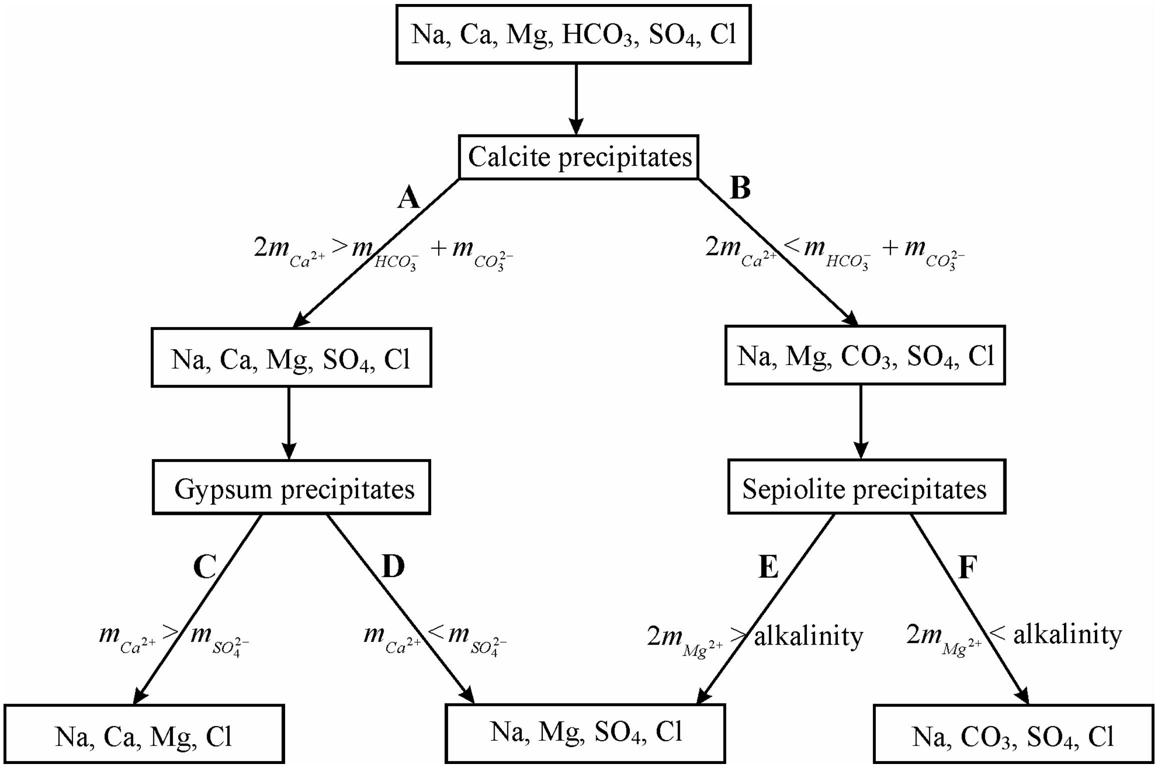

Figure 6.11: Schematic diagram representing the fractionation experienced through the development of chemical divides in evaporating natural waters (modified from Drever, 1997). Note that this diagram does not represent all possible evolutionary paths.

calcite equilibrium expression. This solution will follow the path labeled A in figure 6.11.

However, if $2m_{Ca^{2+}} < m_{HCO_3^-} + m_{CO_3^{2-}}$ the resulting solution will become depleted of Ca^{2+} as calcite precipitates and will follow path B in figure 6.11. As evaporation proceeds and the solubility of each salt is reached, it will begin to precipitate with its constituent elements following a chemical divide similar to the one described for calcite.

The only mineral that is indicated to be currently precipitating from the LLCF pore-water samples is amorphous silica. However, the data presented here are not representative of pore-water from the entire thickness of the processed kimberlite active layer. Specifically, there is a lack of very near-surface (10 to 20 cm) pore-water samples. Therefore, these data do not represent a complete evolutionary suite of samples. However, data on the mineralogy of the efflorescent crust reflects the final composition of the water from which it precipitated.

The first chemical divide predicted by the Hardie-Eugster evaporation model is calcite precipitation. Figure 6.12A is a plot of Ca^{2+} versus alkalinity (HCO_3^- + CO_3^{2-}) for LLCF pore-water showing the equation $2m_{Ca^{2+}} = m_{HCO_3^-} + 2m_{CO_3^{2-}}$ as a solid line. This graph indicates that almost all pore-water samples have Ca^{2+} concentration greater than one half of the alkalinity. Therefore, as the LLCF pore-water migrates towards the surface of the fines, through capillary action, it will follow path A, shown in figure 6.11, and calcite or aragonite will precipitate.

The next chemical divide that is encountered in the Hardie-Eugster model is gypsum precipitation. The evolution of the resulting solution depends on whether the SO_4^{2-} concentration is greater than or less than the Ca^{2+}. Figure 6.12B is a plot of Ca^{2+} versus

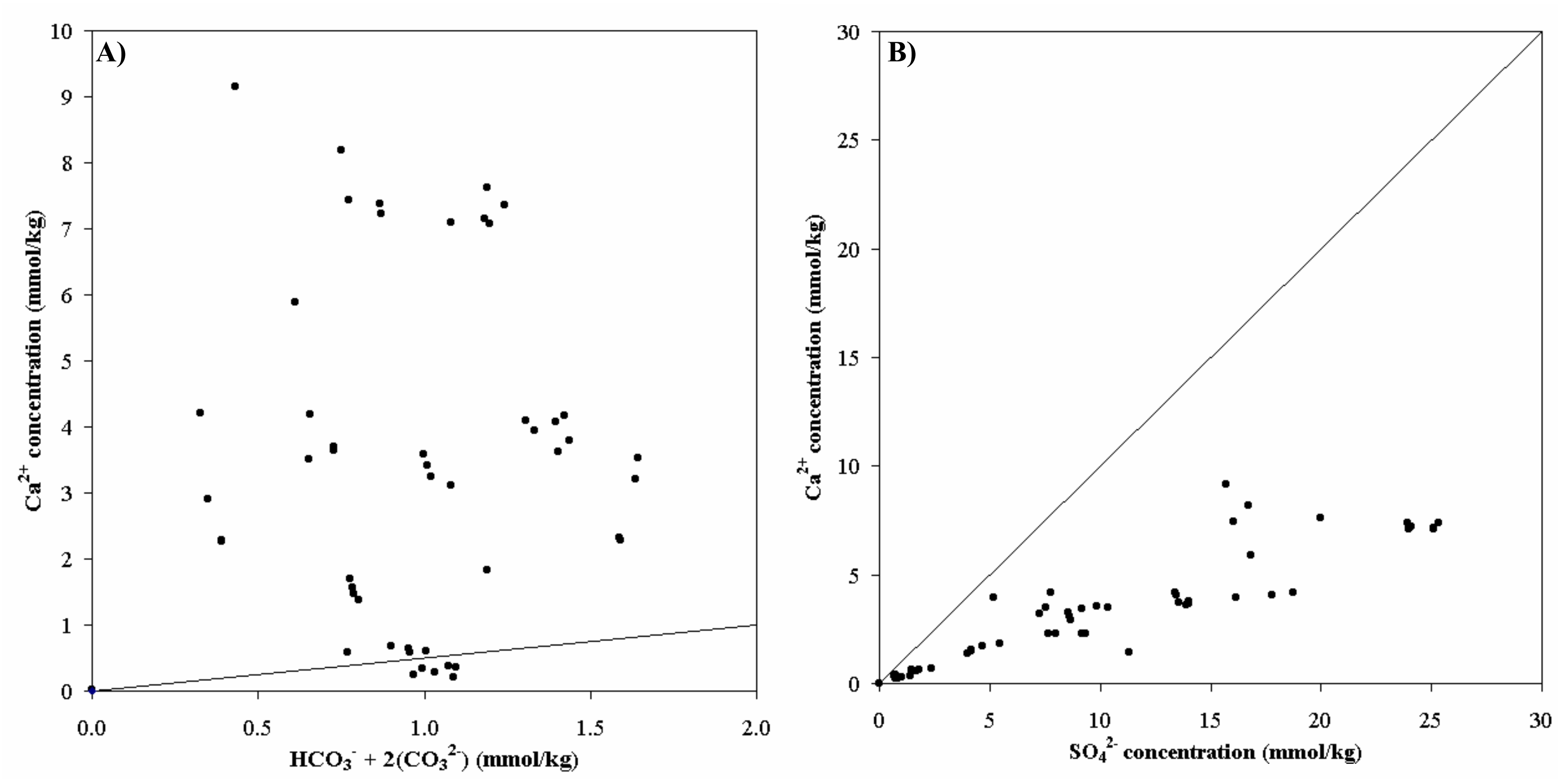

Figure 6.12: A) Plot of Ca^{2+} concentration versus alkalinity for the LLCF pore-water samples with the solid line representing the equation $2m_{Ca^{2+}} = m_{HCO_3^-} + 2m_{CO_3^{2-}}$. **B)** Plot of Ca^{2+} versus SO_4^{2-} for the LLCF pore-water samples with the equation $m_{Ca^{2+}} = m_{SO_4^{2-}}$ represented by the solid line.

SO_4^{2-} indicating that all pore-water samples have SO_4^{2-} concentration greater than Ca^{2+}. Therefore, the resulting solution should follow the path labeled D in figure 6.11, become depleted of Ca and contain mostly Mg, SO_4, Na, K, and Cl. The main phase forming the efflorescent crust on the surface of the fines has been identified as hexahydrite ($MgSO_4 \cdot 6H_2O$) (section 5.2.2), which is consistent with the Hardie-Eugster model.

Based on the evolutionary path described above, it is probable that calcite and gypsum reach saturation and precipitate near the surface of the LLCF fines, possibly forming a caliche layer. Due to the young age of the processed kimberlite fines in the northern end of Cell B, no significant amounts of secondary mineral precipitation has been observed below the surface of the fines, but a near-surface caliche layer could develop in the future. The more soluble Mg, Na, and K sulphate salts are transported to and precipitated on the surface of the fines. When rain falls on the fines, the soluble efflorescent salts will readily dissolve and wash into the fines, whereas the sparingly soluble calcite and gypsum will dissolve more slowly. Therefore, the resulting pore-water chemistry will be controlled not only by the solubility of the phases that precipitate as a result of evaporation, but also by the kinetics of dissolution of these same phases (Drever, 1997). With time, as more sparingly soluble salts precipitate, the pore-water will become dominated by solutes derived from high solubility salts. Therefore, it can be hypothesized that through time, the LLCF pore-water chemistry will become predominantly Mg and SO_4.

6.3 Process Plant Discharge Water – Inverse Modeling

The second objective of this investigation was to use major element chemistry of water samples, together with kimberlite mineralogy, to evaluate the processes affecting water quality in the LLCF. All water that enters the LLCF, besides natural precipitation, has been used in the process plant to wash and size the crushed and ground ore. The intimate contact of water with crushed ore provides the opportunity for minerals to dissolve and precipitate from solution. Therefore, the composition of water within the LLCF is directly affected by the reactions that occur during mineral processing. It is not possible to determine the phase transfers that occur during mineral processing based on the composition of discharge water chemistry alone. Inverse modeling uses a mass-balance approach to determine a set of phase transfers responsible for the change in chemistry between two water samples along the same flow path (Drever, 1997; Parkhurst and Appelo, 1999). Therefore, PHREEQC has been used to conduct inverse modeling using initial and final process plant water chemistry, together with the kimberlite mineralogy, to help deduce the phase transfers that have resulted in the water chemistry observed in the process plant discharge effluent.

Water used for mineral processing is taken from a water-reclaim barge, which was located on the north side of Dyke C during sampling for this study (section 3.2.1.3). The water is pumped to the process plant where it is used to wash the crushed kimberlite ore. Processed kimberlite is hydraulically pumped to the LLCF, using process water, at a solids content of approximately 45 volume percent. The amount of water used to pump the processed fines to the containment facility accounts for approximately 10 percent of the volume of water in the circuit per day, which is replaced with water pumped from

Dyke C making the approximate residence time for water in the mineral processing circuit 10 days (Mike Rylatt pers. comm.). Therefore, Dyke C and process plant discharge water samples exist along the same flow path through the process plant.

Inverse modeling calculations use an initial and final solution, together with minerals that are known to exist along the flow path, to calculate the amount of dissolution or precipitation of each phase that is required to obtain the changes in water chemistry observed. Detailed knowledge of the geology and geochemistry of the system helps to determine the most probable solutions from the models generated by the software. Since the water from Dyke C and the water discharging from the process plant exist along the same flow path they can be used as initial and final solution inputs for inverse modeling calculations designed to investigate the processes affecting the change in water quality through the process plant.

The compositions of the initial and final solutions used in the inverse calculations are listed in table 6.4A. Only the major elements (Ca, Mg, K, Na, Si, SO_4, and HCO_3) were used for this modeling because they compose more than 90% of the water analyses, on an equivalent basis. Chloride was also included since its concentration increases noticeably through the mineral processing circuit. Phases that were included in the mass-balance calculations were chosen based on the mineralogical work discussed in chapter 6 and are listed in table 6.4B. Although no significant concentrations of Cl-bearing minerals were found in the kimberlite ore, halite was added to the list of phases to represent a Cl-bearing phase. It should be noted that the abbreviated list of analytes used for inverse modeling calculations does not significantly affect the charge imbalances of the solutions used in the calculations.

A)	**Dyke C (AR-02-UD45)**	**Discharge (AR-02-DD145)**
Sample Date	04-Jul-02	09-Jul-02
Temperature (^oC)	16.35	20.25
pH	8.08	7.74
DO	9.99	7.84
Alkalinity (mg/L $CaCO_3$)	43.6	59.6
Ca	17.8	54.1
Fe	0.005	0.018
K	33.7	81.2
Mg	30.5	90.2
Na	12.3	22.5
Si	2.00	4.9
Cl	43	55
SO_4	118	472

B)

Mineral	**Formula**
Calcite	$CaCO_3$
Chrysotile	$Mg_3Si_2O_5(OH)_4$
CO_2(g)	CO_2
Forsterite	Mg_2SiO_4
Gypsum	$CaSO_4 \cdot 2H_2O$
Halite	NaCl
Magnesite	$MgCO_3$
Saponite-Ca	$Ca_{0.165}Mg_3Al_{0.33}Si_{3.67}O_{10}(OH)_2$
Saponite-K	$K_{0.33}Mg_3Al_{0.33}Si_{3.67}O_{10}(OH)_2$
Saponite-Mg	$Mg_{3.165}Al_{0.33}Si_{3.67}O_{10}(OH)_2$
Saponite-Na	$Na_{0.33}Mg_3Al_{0.33}Si_{3.67}O_{10}(OH)_2$
Am. silica	SiO_2
Fayalite	Fe_2SiO_4
Pyrite	FeS_2
Ferrihydrite	$Fe(OH)_3$

Table 6.4: A) Dyke C and process plant discharge water analyses used in inverse modeling calculations. All concentrations are reported as mg/L unless specified otherwise. **B)** Phases used in inverse modeling calculations.

6.3.1 Inverse Modeling – Scenarios

Eight different scenarios (designated 1, 2, 3, 4, 5, 6, 7, and 8) were designed for inverse modeling calculations, using slightly differing input parameters. Scenario 1 was designed to represent the end-member case where the increase in SO_4 concentration was assumed to be due solely to the dissolution of gypsum in the mud xenoclasts found in the ore. As well, scenario 1 calculations assumed that the increase in dissolved Fe through the process plant is negligible. Therefore, Fe was omitted from the solution chemistry used in these calculations. Models calculated from scenario 1 included all the phases listed in table 6.4B without pyrite, fayalite (as a component of olivine), or ferrihydrite.

Scenario 2 was similar to scenario 1, except that fayalite was included in the calculations as the only source of Fe. The purpose of this was to determine the amount of fayalite required to dissolve in order to produce the change in dissolved Fe concentrations observed.

It has been noted, in chapters 4 and 5, that dissolved Fe concentrations in LLCF waters are low, Fe-oxide staining is not observed in the processed fines, and processed kimberlite pyrite does not have noticeable oxidation rims. These data suggest that pyrite oxidation is not occurring significantly at present. However, the possibility that pyrite oxidation is occurring, even in low quantities, cannot be ruled out. Therefore, a scenario was designed to test whether pyrite oxidation could account for the observed changes in water chemistry through the process plant. Like scenarios 1 and 2, the third scenario assumes that gypsum is a source of dissolved SO_4. However, pyrite is also included to determine the amount required to account for the increase in dissolved Fe.

Scenarios 4, 5, and 6 were designed to be identical to scenarios 1, 2, and 3, respectively, except that magnesite was included as the carbonate mineral instead of calcite.

Finally scenario 7 was designed to represent the end-member situation in which all the dissolved SO_4 is due to pyrite oxidation. All phases from table 6.4B, except gypsum and fayalite, were included in modeling calculations for scenario 7. Ferrihydrite was also included as a sink for the excess Fe produced by pyrite oxidation. Scenario 8 was designed to be identical to scenario 7 except that magnesite was included as the carbonate mineral, instead of calcite. These last two scenarios were designed to determine the amount of pyrite required to oxidize, and the amount of ferrihydrite required to precipitate, in order to account for the changes in water chemistry through the process plant.

6.3.2 Inverse Modeling Results

Although the models calculated for each scenario are mathematically possible, they are not necessarily geochemically possible. Detailed knowledge of the mineralogy and geochemistry of kimberlite and kimberlite fines is required to accept or reject each model as a possible explanation for the change in chemistry through the process plant. The following discussion is an evaluation of the models calculated using the scenarios discussed above.

6.3.2.1 Scenarios 1, 2, and 3

Scenarios 1, 2 and 3 represent variations on the same main theme: gypsum is the main source of dissolved SO_4. The most significant difference between these three sets of calculations is the inclusion of fayalite or pyrite. Twelve different mass transfer models were derived for each set of inverse-modeling calculations for scenarios 1 to 3.

The calculated models can be classified into two groups. The first group involves the precipitation of forsterite while the second group does not involve forsterite mass transfer at all. It is unlikely that forsterite will precipitate from solution due to the high degree of undersaturation of the discharge waters with respect to forsterite (table 6.1), as well as the kinetic barriers to forsterite precipitation. Therefore, the models suggesting forsterite precipitation have been ignored, leaving only two solutions remaining in each of the three sets of inverse calculations (designated a and b respectively). The six remaining models are listed in table 6.5. Note the similarity of the phase transfers calculated in each of the three modeling runs.

All six models indicate that between 17.63 and 17.88 moles of $CaCO_3$ precipitate from solution. This is consistent with the increase in inorganic-CO_2 content of the processed kimberlite fines relative to the kimberlite ore discussed in section 5.3. The processed kimberlite inorganic-CO_2 content is higher than the kimberlite ore, yet calcite it not currently precipitating in significant amounts from the processed kimberlite pore-water (section 6.2.3.1). Therefore, carbonate should be precipitating in the mineral processing circuit, according to models 1 to 3.

Table 6.5 suggests that between 4.147 and 4.170 millimoles of gypsum dissolve per kilogram of solution according to all 6 models. Discharge water is undersaturated with respect to gypsum indicating that if present, gypsum will tend to dissolve (section 6.1.1). The kimberlite ore contains an average sulphate-S concentration of 0.14 weight percent while the processed kimberlite fines contain little to no sulphate-S. The small amount of

Mineral	**Formula**	**1a**	**1b**	**2a**	**2b**	**3a**	**3b**
Calcite	$CaCO_3$	-17.88	-17.88	-17.86	-17.86	-17.63	-17.63
Chrysotile	$Mg_3Si_2O_5(OH)_4$	5.959	5.959	5.954	5.954	5.875	5.875
CO_2(g)	CO_2	17.88	17.88	17.86	17.86	17.63	17.63
Forsterite	Mg_2SiO_4	--	--	--	--	--	--
Gypsum	$CaSO_4 \cdot 2H_2O$	0.004151	0.00417	0.004151	0.004169	0.004147	0.0004164
Halite	$NaCl$	0.000596	0.000559	0.0005957	0.0005952	0.0005922	0.0005577
Saponite-Ca	$Ca_{0.165}Mg_3Al_{0.33}Si_{3.67}O_{10}(OH)_2$	108.3	108.3	108.2	108.2	106.8	106.8
Saponite-K	$K_{0.33}Mg_3Al_{0.33}Si_{3.67}O_{10}(OH)_2$	0.004247	0.004247	0.004247	0.004247	0.004239	0.004239
Saponite-Mg	$Mg_{3.165}Al_{0.33}Si_{3.67}O_{10}(OH)_2$	-108.3	-108.3	-108.2	-108.2	-106.8	-106.8
Saponite-Na	$Na_{0.33}Mg_3Al_{0.33}Si_{3.67}O_{10}(OH)_2$	-0.00011	--	-0.0001106	--	-0.0001048	--
Am. Silica	SiO_2	-11.92	-11.92	-11.91	-11.91	-11.75	-11.75
Fayalite	Fe_2SiO_4	NI	NI	0.0000001261	0.0000001261	NI	NI
Pyrite	FeS_2	NI	NI	NI	NI	0.000000252	0.000000252

Table 6.5: Mass transfer models calculated using PHREEQC. The three sets of inverse calculations are designated 1, 2, and 3 respectively while the models calculated from each set are labelled a and b. All mole transfers are reported in terms of moles of phase transferred per kilogram of solution. Positive mole transfers indicate dissolution and negative mole transfers indicate precipitation. Note that dashes indicate that the phase was not indicated to dissolve or precipitate by the model and NI indicates that the phase was not included in modeling calculations.

sulphate-S in the processed fines is most likely from the precipitation of pore-water solutes as the core samples dried in the laboratory, rather than from sulphate minerals in the processed kimberlite (section 5.3). This suggests that the sulphate minerals in the kimberlite ore completely dissolve during mineral processing. Therefore, the small amount of gypsum that is indicated to dissolve in table 6.5 is consistent with the complete removal of the small amount of gypsum from the kimberlite ore during mineral processing. If any more sulphate minerals were present in the processed ore, they would dissolve causing discharge water SO_4 concentrations to be higher.

Table 6.5 suggests that the net mole transfer of saponite is essentially zero. In each model the same amount of Ca-saponite that is suggested to dissolve is the same as the amount of Mg-saponite that is suggested to precipitate. The mineral stability diagram for the MgO-SiO_2-Al_2O_3 chemical system (section 6.2.3.5) indicates that LLCF waters are in equilibrium with saponite. Therefore, the mass-transfer of the various saponite minerals to and from solution could be thought of in terms of sorption and cation exchange reactions between clay minerals in the kimberlite ore.

The solutions calculated for inverse models 1 to 3 indicate that 11.75 to 11.92 moles of SiO_2 precipitate per kilogram of solution during processing of the ore. Some form of variably crystalline silica mineral at or near supersaturation in process plant effluent discharging into the LLCF (section 6.1) is indicated to be controlling SiO_2 concentrations in the processed kimberlite pore-water (section 6.2.3.4). These data suggest that silica precipitates in the process plant before deposition in the LLCF, which is suggested by all six solutions listed in table 6.5.

Iron was included in the second and third set of inverse modeling calculations with fayalite and pyrite specified as the Fe-bearing minerals. These calculations were conducted in order to determine the amount of each Fe-bearing phase that would be required to cause the changes in dissolved Fe through the process plant (table 6.4A). Table 6.5 suggests that when Fe is included in the calculations 1.261×10^{-7} moles of fayalite or 2.520×10^{-7} moles of pyrite are required to dissolve. As well, it should be noted that inclusion of these Fe phases in models 2 and 3 does not significantly change the mole transfers calculated from model 1.

6.3.2.2 Scenarios 4, 5, and 6

Inverse modeling carried out using scenarios 4, 5, and 6 resulted in the calculation of eight models each. Similar to the models calculated for scenarios 1, 2, and 3, calculations using scenarios 4, 5, and 6 produced two main groups of models. For each scenario, six of the calculated models involved the precipitation of forsterite while two did not involve the transfer of any forsterite at all. Since forsterite precipitation is unlikely, due to kinetic and thermodynamic constraints (section 6.3.2.1), the six models involving the precipitation of forsterite are most likely not geochemically possible. The remaining two models from each scenario (six in total) are listed in table 6.6. When compared to table 6.5, the most notable feature of this table is that chrysotile, $CO_{2(g)}$, halite, amorphous silica, fayalite, and pyrite phase transfers are exactly the same in scenarios 4, 5, and 6 as they are in scenarios 1, 2, and 3, respectively. As well, it should be noted that the carbonate mineral phase transfers are numerically identical for each corresponding scenario (i.e. 1 and 4, 2 and 5, 3 and 6) even though scenarios 4, 5, and 6 involved magnesite rather than calcite. The most significant difference between the six calcite-

Mineral	**Formula**	**4a**	**4b**	**5a**	**5b**	**6a**	**6b**
Magnesite	$MgCO_3$	-17.88	-17.88	-17.86	-17.86	-17.63	-17.63
Chrysotile	$Mg_3Si_2O_5(OH)_4$	5.959	5.959	5.954	5.954	5.875	5.875
CO_2(g)	CO_2	17.88	17.88	17.86	17.86	17.63	17.63
Forsterite	Mg_2SiO_4	--	--	--	--	--	--
Gypsum	$CaSO_4 \cdot 2H_2O$	0.003954	0.003954	0.004151	0.004169	0.004147	0.0004164
Halite	$NaCl$	0.0006	0.0005593	0.0005957	0.0005592	0.0005922	0.0005577
Saponite-Ca	$Ca_{0.165}Mg_3Al_{0.33}Si_{3.67}O_{10}(OH)_2$	-0.01789	-0.01789	-0.01908	-0.01920	-0.01907	-0.01917
Saponite-K	$K_{0.33}Mg_3Al_{0.33}Si_{3.67}O_{10}(OH)_2$	0.003012	0.002829	0.004247	0.004247	0.004239	0.004239
Saponite-Mg	$Mg_{3.165}Al_{0.33}Si_{3.67}O_{10}(OH)_2$	0.01500	0.01500	0.01495	0.01495	0.01493	0.01493
Saponite-Na	$Na_{0.33}Mg_3Al_{0.33}Si_{3.67}O_{10}(OH)_2$	-0.0001234	--	-0.0001106	--	-0.0001048	--
Am. Silica	SiO_2	-11.92	-11.92	-11.91	-11.91	-11.75	-11.75
Fayalite	Fe_2SiO_4	NI	NI	0.0000001261	0.0000001261	NI	NI
Pyrite	FeS_2	NI	NI	NI	NI	0.000000252	0.000000252

Table 6.6: Mass transfer models calculated using PHREEQC. The three sets of inverse calculations are designated 4, 5, and 6 respectively while the models calculated from each set are labelled a and b. All mole transfers are reported in terms of moles of phase transferred per kilogram of solution. Positive mole transfers indicate dissolution and negative mole transfers indicate precipitation. Note that dashes indicate that the phase was not indicated to dissolve or precipitate by the model and NI indicates that the phase was not included in modeling calculations.

bearing models (1, 2, and 3) and the six magnesite–bearing models (4, 5, and 6) is the clay mineral phase transfers. Calculations using scenarios 1, 2, and 3 produced models that involved a large amount of Ca-saponite to dissolve and Mg-saponite to precipitate. However, saponite mineral transfers in the models calculated using scenarios 4, 5, and 6 are much smaller.

The twelve models calculated using scenarios 1 to 6 are essentially identical with only small variations in the calculated phase transfers. All of the models are consistent with the observations of kimberlite ore, processed kimberlite fines, pore-, discharge, and surface water samples. Therefore it seems likely that the actual mass transfers during processing of the kimberlite ore can be thought of as a combination of mole transfers suggested in tables 6.5 and 6.6.

One final notable feature of the inverse models summarized in tables 6.5 and 6.6 is that all of the main phase transfers happen in exactly the same ratios. When the moles of calcite (or magnesite), $CO_{2(g)}$, and amorphous silica transferred are compared to the moles of chrysotile transferred in each model, it can be seen that the resulting ratios are 3:1, 3:1, and 2:1, respectively. These data suggest that possibly the most significant net reaction occurring during the processing of kimberlite ore is:

$$Mg_3Si_2O_5(OH)_{4(s)} + 3CO_{2(g)} \longrightarrow 3MgCO_{3(s)} + 2SiO_{2(s)} + 2H_2O_{(l)}\,.$$

6.3.2.3 Scenarios 7 and 8

Scenarios 7 and 8 were designed to test whether pyrite oxidation alone could account for the increase in dissolved SO_4 through the process plant. Due to mass-balance constraints, all models calculated using these two scenarios resulted in a significant amount of chrysotile precipitation. However, chrysotile is undersaturated in the majority of discharge water samples collected (section 6.1.1). As well, chrysotile is slow to precipitate and does not form readily at low temperatures, such as atmospheric conditions (Drever, 1997). Therefore, it is unlikely that any of the models calculated using scenarios 7 and 8 are geochemically feasible.

7 Conclusions

This project is one of the first field-based investigations of the waste produced by diamond mining in the Canadian Arctic. Therefore, the objectives of this research were to provide an initial definition and characterization of the mineral-water system that exists within the processed kimberlite containment facility, as well as to determine the main processes that are controlling the chemistry of this water. Three field seasons produced a suite of both water and solid samples that were examined and analyzed in order to address each of the objectives of this research.

Three types of waters were identified within the LLCF: 1) Processed kimberlite pore-water, 2) Process plant discharge water, and 3) Surface water. While all of the water samples have pH values ranging from 7 to 9 and low dissolved Fe concentrations, each water type has its own characteristic chemical signature. Pore-water samples, representing the most concentrated waters, are characterized by high SO_4, Mg, and Ca , and the lowest Na, K, and Cl equivalent percent of all samples collected. Discharge water samples, which are less concentrated than pore-water samples, are characterized by the highest Na and K, and the lowest Ca percent of all LLCF waters. Finally, the two characteristic features of the LLCF surface waters, representing the most dilute LLCF waters, are that they contain the highest Ca and lowest Mg equivalent percent of all samples collected.

Kimberlite ore, collected from the Panda kimberlite, and processed kimberlite fines, collected from the north end of Cell B, have almost identical mineralogy composed predominantly of serpentine and forsteritic olivine with lesser to minor amounts of phlogopite, pyroxene, spinel, calcite, garnet, pyrite, and gypsum. Fine-grained black mud xenoclasts are also ubiquitous in both kimberlite ore and processed kimberlite fines, occurring in clasts that range in size from millimeters to centimeters. Petrographic and X-ray diffraction examination as well as inorganic-C, sulphate-S, and sulphide-S analyses of the suite of solid samples indicate that pyrite and gypsum are found to be essentially restricted to the mud material, while carbonate minerals are restricted to the kimberlite ore. These analyses also indicate that carbonate mineral content is increased in the processed kimberlite fines relative to the kimberlite ore, while sulphate minerals are essentially absent from the processed kimberlite fines. As well, there appears to be no change in pyrite content from kimberlite ore to processed kimberlite fines. Core samples of the processed kimberlite fines do not exhibit any obvious reaction fronts, or Fe-oxide staining. These data, together with water data, suggest that pyrite oxidation is not currently a significant contributor to LLCF water chemistry.

During prolonged periods without rainfall an efflorescent crust composed of hexahydrite forms on the surface of the processed kimberlite fines indicating that evaporation is affecting the pore-water of the fines. Analysis of data from the suite of pore-water samples collected for this study indicates that SO_4, Ca, and Mg, the most abundant solutes, remain in solution as evaporation progresses. This suggests that no minerals containing these elements are precipitating from the pore-waters collected for this study. However, the progressive removal of Na and K from solution as evaporation progresses, is most likely due to the sorption and cation-exchange of these ions with cryptocrystalline mineral surfaces and clay minerals present in the fines. Finally, Si and HCO_3 concentrations are constant at all degrees of evaporation. Aqueous mineral stability diagrams and mineral saturation calculations suggest that amorphous silica and atmospheric CO_2 are respectively controlling the concentration of these constituents.

The majority of water that enters the LLCF has been used in the processing of kimberlite ore. Therefore, the reactions that occur during the mineral processing circuit directly affect the water chemistry observed within the LLCF since process plant discharge water is the starting point from which all other waters evolve. Inverse modeling has been used, together with representative water analyses and kimberlite mineralogy, to calculate phase transfers that could be responsible for the water chemistry being discharged from the process plant. Dissolved SO_4 is one of the most significant components of all LLCF water samples. Typically, in mine waste environments, dissolved SO_4 is derived from the oxidation of sulphide minerals and is often used as an indication of this process. Pyrite oxidation is not currently indicated to be occurring in significant amounts within the LLCF. However, it can not be ruled out completely and must be considered when conducting the inverse modeling calculations.

Since SO_4 is one of the most significant components of LLCF water chemistry, and both gypsum and pyrite are present in the kimberlite ore as sources of dissolved SO_4, a number of scenarios were used for inverse calculations in order to represent end-member situations where gypsum and pyrite were respectively the main sources of SO_4. All models calculated using scenarios in which pyrite was the only source of dissolved SO_4 were found to be geochemically unreasonable. However, when pyrite and gypsum were both included in inverse model calculations, the vast majority of dissolved SO_4 was calculated to be from gypsum dissolution and only a very small amount of pyrite was indicated to oxidize. These inverse calculations suggest that the gypsum present in the mud xenoclasts, although volumetrically minor, is one of the most significant contributors to LLCF water chemistry. Other phase transfers that are calculated to contribute to the chemistry of process plant effluent are the dissolution of serpentine and atmospheric CO_2, cation-exchange with clay minerals present in the kimberlite ore, and the precipitation of carbonate and silica.

7.1 Recommendations

This research has provided initial information concerning the identity and composition of components within the processed kimberlite containment facility at one of Canada's first operating diamond mines. Gypsum, one of the most significant contributors to LLCF water chemistry, and pyrite, one of the main sources of acid generation in mine waste, are both essentially restricted to the mud xenoclasts found throughout the Panda kimberlite ore. Although pyrite oxidation is probably not currently occurring within the fines, it has the potential to develop in the near future. This mud material has been noted in many Lac de Gras kimberlites and is thought to have been deposited over the entire Lac de Gras region at the bottom of the Western Interior Seaway during the upper Cretaceous (Baker et al., 2003; Carlson et al., 1995; Carlson et al., 1998; Doyle et al., 1998). Therefore, the modal estimation and detailed mineralogical investigation of mud material present in Lac de Gras kimberlites is one of the most important methods to help predict the effect processed kimberlite from diamond mining operations will have on water quality.

7.2 Future Work

The focus of this research has been on the processed kimberlite fines within the active layer of the LLCF, which is in contact with the atmosphere. Research on springs issuing from serpentinized ultramafic bodies, which are mineralogically similar to kimberlite, suggests that the closed system interaction of these rocks with water results in water chemistry that is very different from that observed in the open system water-rock interactions (Bruni et al., 2002). The LLCF has become segregated into three layers, with the lowermost unit composed of unfrozen, saturated kimberlite fines. This unfrozen layer is separated from the atmosphere by a frozen layer approximately 4 metres thick and contains a large amount of water that could potentially flow into and affect the chemistry of the LLCF. Therefore, future work on the processed kimberlite fines in the LLCF should include the investigation and characterization of the processed kimberlite fines and co-existing pore-water, as well as determination of the hydrogeologic flow regime that exists within this lower unit. This information will help to further evaluate the effect processed kimberlite fines will have on downstream water quality after LLCF closure, as well as to determine the effectiveness of this method of processed kimberlite fines storage.

Increasing atmospheric CO_2 levels, due to increased fossil fuel use, has become a concern of many global policy makers. Recent agreements, including the Kyoto Protocol, have been designed to put forward guidelines and targets to help reduce the effects of anthropogenic emissions contributing to global warming, including atmospheric CO_2. Mineral carbonization has recently received much attention as a method to permanently store industrially produced CO_2 (Hansen et al., 2003). Power is generated at Ekati by a diesel-burning generation plant, which releases a large amount of CO_2 into the atmosphere every year.

Investigations of tailings from serpentine asbestos mining operations in southern Quebec have identified the formation of hydromagnesite [$Mg_5(CO_3)_4(OH)_2(H_2O)_4$] on the surface of the piles, indicating that CO_2 sequestration occurs spontaneously in this material (Huot et al., 2003). As well, Bruni et al. (2002) found that spring waters issuing from serpentinized ultramafic complexes in Italy form calcite ($CaCO_3$) as they emerge from the rock masses.

The net reaction for the carbonation of serpentine has been identified as (Lackner, 2002; Zevenhoven and Kohlmann, 2001):

$$Mg_3Si_2O_5(OH)_{4(s)} + 3CO_{2(g)} \longrightarrow 3MgCO_{3(s)} + 2SiO_{2(s)} + 2H_2O_{(l)}.$$

The reaction listed above is exactly the reaction that is suggested to be occurring naturally during the processing of kimberlite ore at Ekati (section 6.3.2.2). Since the majority of minerals composing kimberlite are serpentine and olivine, the the potential exists to use the processing of kimberlite ore and the waste produced from diamond mining to help reduce CO_2 generated as a result of mine operations. Further work could include investigation of the feasibility of using processed kimberlite fines to sequester CO_2 produced at the mine.

The final closure plan for the LLCF involves the revegetation of the surface of the fines. The decomposition of organic matter that accumulates in the humus layer of a soil generates organic acids, which decrease the pH of the soil (Drever, 1997). This decreased pH can lead to increased dissolution of soil minerals and leaching of potentially toxic elements such as Pb, Zn, Ni, Cr, Co, and As. Serpentine soils contain increased levels of Ni, Cr, and Co, which is thought to help explain the relative infertility of serpentine soils (Proctor and Woodell, 1975). Since the processed kimberlite fines are essentially composed of serpentine and olivine, it can be speculated that revegetation within the LLCF has the potential to increase the Ni, Cr, and Co concentrations in the pore-water as the decrease in pH leads to increased mineral dissolution. Nickel concentrations already exceed the National Guidelines and Standards Office guidelines in some LLCF water samples (section 4.6) and it can be speculated that increased mineral dissolution will increase the concentration of this potentially toxic element further. After fines are no longer actively deposited in the LLCF, the water will most likely be controlled predominantly by the interaction of water with the processed kimberlite fines, rather than by the composition of effluent discharging from the process plant. Therefore, further work should include a study to investigate the behaviour of the processed kimberlite fines with decreasing pH in an effort to determine the concentrations of potentially toxic elements within the processed kimberlite fines as well as to develop a model to help predict the long-term release rate of these elements.

The study of the environmental effects of mine waste is relatively new, having only developed significantly over the past two decades (Price, 2003). Most mining sectors, including base-metal and gold, have origins that date back long before this time. Therefore, a significant amount of waste has been generated and deposited from these operations that have led to large amounts of pollution. The diamond mining industry in Canada began in August 1998, decades after the initial mine waste studies were conducted. Therefore, an opportunity exists to investigate, predict, and mitigate any problems posed by diamond mining before they have the chance to develop into larger scale issues. This will help both the economics of these operations, by helping to reduce post-mining costs, as well as the environment, by identifying potential problems early in the life of the industry and providing information to help deal with the issues unique to the waste produced from diamond mining in the Canadian north.

8 References

Albee, A.L. and Ray, L., 1970. Correction Factors for Electron Probe Microanalysis of Silicates, Oxides, Carbonates, Phosphates, and Sulfates. Analytical Chemistry, 42(12): 1408-1414.

Alkattan, M., Oelkers, E.H., Dandurand, J.L. and Schott, J., 2002. An Experimental Study of Calcite Dissolution Rates at Acidic Conditions and 25°C in the Presence of $NaPO_3$ and $MgCl_2$. Chemical Geology, 190: 291-302.

Back, W., 1966. Hydrochemical Facies and Ground-Water Flow Patterns in Northern Part of Atlantic Coastal Plain. Submitted to United States Geological Survey Professional Paper 498-A, Washington. 42 pp.

Bailey, S.W., 1980. Structures of Layer Silicates. In: G.W. Brindley and G.Brown (Editors), Crystal Structures of Clay Minerals and their X-Ray Identification. Spottiswoode Ballantyne Ltd., London, pp. 123.

Baker, M.J., Blowes, D.W., Logsdon, M.J. and Jambor, J.L., 2003. Environmental Geochemistry of Kimberlite Materials: Diavik Diamonds Project, Lac de Gras, Northwest Territories, Canada. Exploration and Mining Geology, 10(3): 155-163.

Barnes, I. and LaMarche, V.C.J., 1969. The Relationship Between Fluids in Some Fresh Alpine-Type Ultramafics and Possible Modern Serpentinization, Western United States. Geological Society of America Bulletin, 80: 1947-1960.

Barnes, I., LaMarche, V.C.J. and Himmelberg, G., 1967. Geochemical Evidence of Present-Day Serpentinization. Science, 156: 830-832.

Barnes, I., O'Neil, J.R. and Trescases, J.J., 1978. Present Day Serpentinization in New Caledonia, Oman, and Yugoslavia. Geochimica et Cosmochimica Acta, 42: 144-145.

Berg, G.W. and Carlson, J.A., 1998. The Leslie Kimberlite Pipe of Lac de Gras, Northwest Territories, Canada: Evidence for Near Surface Hypabyssal Emplacement, Seventh International Kimberlite Conference Extended Abstracts, pp. 81-83.

Berner, R.A., 1975. The role of Magnesium in the Crystal Growth of Calcite and Aragonite from Sea Water. Geochimica et Cosmochimica Acta, 39: 489 - 504.

Borisov, V.N., Alexeev, S.V. and Pleshevenkova, V.A., 1995. The Diamond Mining Quarries of East Siberia as a Factor Affecting Surficial Water Quality. In: Y.K. Kharaka et al. (Editors), Eighth International Symposium on Water Rock Interaction. A.A. Balkema, Vladivostock, Russia, pp. 863-866.

Böttcher, G., Brumsack, H.J., Heinrichs, H. and Pohlmann, M., 1997. A New High-Pressure Squeezing Technique for Pore Fluid Extraction from Terrestrial Soils. Water, Air, and Soil Pollution, 94: 289-296.

Brindley, G.W., 1980. Order-Disorder in Clay Mineral Structures. In: G.W. Brindley and G. Brown (Editors), Crystal structures of clay minerals and their X-ray identification. Spottiswoode Ballantyne Ltd., London, pp. 125-195.

British Columbia Ministry of Water Land and Air Protection, 2003. Water Quality Guidelines Reports. Retrieved June 16, 2003, from http://wlapwww.gov.bc.ca/wat/wq/wqhome.html.

Brown, G. and Brindley, G.W., 1980. X-ray Diffraction Procedures for Clay Mineral Identification. In: G.W. Brindley and G.Brown (Editors), Crystal structures of clay minerals and their X-ray identification. Spottiswoode Ballantyne Ltd., London, pp. 305 - 359.

Bruni, J., Canepa, M., Giovanni, C., Cioni, R., Cipolli, F., Longinelli, A., Marini, L., Ottonello, G. and Zuccolini, M.V., 2002. Irreversible Water-Rock Mass Transfer Accompanying the Generation of the Neutral, Mg-HCO_3 and High-pH, Ca-OH Spring Waters of the Genova Province, Italy. Applied Geochemistry, 17: 455-474.

Carlson, J.A., Kirkley, M.B., Ashley, R.M., Moore, R.O. and Kolebaba, M.R., 1995. Geology and Exploration of Kimberlites on the BHP/Dia Met claims, Lac de Gras Region, Northwest Territories, Canada, Sixth International Kimberlite Conference (Novosibirsk) Extended Abstracts, pp. 98-100.

Carlson, J.A., Kirkley, M.B., Thomas, E.M. and Hillier, W.D., 1998. Recent Canadian Kimberlite Discoveries. In: J.J. Gurney, J.L. Gurney, M.D. Pascoe and S.H. Richardson (Editors), Seventh International Kimberlite Conference. Red Roof Design, University of Cape Town, South Africa, pp. 81-89.

Crock, J.G., Arbogast, B.F. and Lamothe, P.J., 1999. Laboratory Methods for the Analysis of Environmental Samples. In: G.S. Plumlee and M.J. Logsdon (Editors), The environmental geochemistry of mineral deposits. Part A: Processes, Techniques, and Health Issues. Society of Economic Geologists, pp. 265-287.

Croquet de Rosemond, S.J., 2002. The effects of Processed Kimberlite Effluent on Freshwater Zooplankton. Masters Thesis, Department of Toxicology, University of Saskatchewan, Saskatoon, 151 pp.

Deer, W.A., Howie, R.A. and Zussmann, J., 1992. An Introduction to the Rock-Forming Minerals; 2nd Edition. Addison Wesley Longmann Limited, Essex, England, 696 pp.

Doyle, B.J., Kivi, K. and Scott-Smith, B.H., 1998. The Tli Kwi Cho (DO27 and DO18) Diamondiferous Kimberlite Complex, Northwest Territories, Canada. In: J.J. Gurney, J.L. Gurney, M.D. Pascoe and S.H. Richardson (Editors), Seventh International Kimberlite Conference. Red Roof Designs, University of Cape Town, pp. 194-204.

Drever, J.I., 1997. The Chemistry of Natural Waters: Surface and Groundwater Environments. Prentice-Hall Inc., 436 pp.

EBA Engineering Consultants Ltd., 1995. Tailings Dam Preliminary Design, December 1995. Submitted to Ekati Environment Department. 108 pp.

EBA Engineering Consultants Ltd., 1998. Tailings Characterization Study. Submitted to Ekati Environment Department. 69 pp.

EBA Engineering Consultants Ltd., 2002. Ekati Diamond Mine Processed Kimberlite Deposition Investigation. Submitted to Ekati Environment Department, Edmonton. 13 pp.

Elberling, B., Schippers, A. and Sand, W., 2000. Bacterial and Chemical Oxidation of Pyritic Mine Tailings at Low Temperatures. Journal of Contaminant Hydrology, 41: 225-238.

Eugster, H.P. and Jones, B.F., 1979. Behaviour of Major Solutes During Closed-Basin Brine Evolution. American Journal of Science, 279: 609-631.

Evangelou, V.P. and Zhang, Y.L., 1995. A Review: Pyrite Oxidation Mechanisms and Acid Mine Drainage Prevention. Critical Reviews in Environmental Science and Technology, 25(2): 141-199.

Faure, G., 1986. Principles of Isotope Geology. John Wiley and Sons, New York, 589 pp.

Field, M. and Scott-Smith, B.H., 1998. Contrasting Geology and Near-Surface Emplacement of Kimberlite Pipes in Southern Africa and Canada. In: J.J. Gurney, J.L. Gurney, M.D. Pascoe and S.H. Richardson (Editors), Seventh International Kimberlite Conference. Red Roof Design, University of Cape Town, pp. 214-237.

Graham, I., Burgess, J.L., Bryan, D., Ravenscroft, P.J., Thomas, E., Doyle, B.J., Hopkins, R. and Armstrong, K.A., 1998. Exploration History and Geology of the Diavik Kimberlites, Lac de Gras, Northwest Territories, Canada. In: J.J. Gurney, J.L. Gurney, M.D. Pascoe and S.H. Richardson (Editors), Seventh International Kimberlite Conference. Red Roof Design, University of Cape Town, pp. 262-279.

Graham, K.P., 2002. Investigation of the Fate of Wastewater Phosphorous Within the Processed Kimberlite Containment Area at BHP's Ekati Diamond Mine, Department of Civil and Environmental Engineering, University of Alberta, Edmonton, 136 pp.

Hall, G.E.M., Pelchat, J.-C. and Loop, J., 1988. Separation and Recovery of Various Sulphur Species in Sedimentary Rocks for Stable Sulphur Isotopic Determination. Chemical Geology, 67: 35-45.

Hansen, L., Dipple, G.M. and Gordon, T., 2003, Carbonate-Altered Serpentinites, Atlin, BC: a Natural Analog to CO_2 Sequestration. GAC-MAC-SEG Vancouver 2003 Annual General Meeting (Abstracts), Vancouver, B.C., 28: No. 494.

Hardie, L.A. and Eugster, H.P., 1970. The evolution of Closed-Basin Brines. Mineralogical Society of America Special Papers, 3: 273-290.

Heinrichs, H., Böttcher, G., Brumsack, H.J. and Pohlmann, M., 1997. Squeezed Soil-Pore Solutes - A comparison to Lysimeter Samples and Percolation Experiments. Water, Air, and Soil Pollution, 89: 189-204.

Hoffman, P.F., 1989. Precambrian Geology and Tectonic History of North America. In: A.W. Bally and A.R. Palmer (Editors), The Geology of North America. Geological Society of North America, Boulder, CO, pp. 447-512.

Howe, D.J., 1997. The Physical and Chemical Characteristics of Kimberlite Fines. Masters Thesis, Department of Mining and Mineral Process Engineering, University of British Columbia, Vancouver, 217 pp.

Huot, F., Beaudoin, G. and Dipple, G.M., 2003, Evaluation of Southern Quebec Asbestos Residues for CO_2 Sequestration by Mineral Carbonation; Preliminary Result. GAC-MAC-SEG Vancouver 2003 Annual General Meeting (Abstracts), Vancouver, B.C., 28: No. 353.

Isachsen, P.F. and Bowring, S.A., 1994. Evolution of the Slave Craton. Geology, 22: 917-920.

Jambor, J.L., Dutrizac, J.E., Groat, L.A. and Raudsepp, M., 2002. Static Tests of Neutralization Potentials of Silicate and Aluminosilicate Minerals. Environmental Geology, 43: 1-17.

Katakis, D. and Gordon, G., 1987. Mechanisms of Inorganic Reactions. John Wiley and Sons, Inc., New York, 384 pp.

Kempton, J.H., Lindberg, R.D. and Runnels, D.D., 1990. Numerical Modelling of Platinum Eh Measurements by Using Heterogeneous Electron Transfer Kinetics. In: D.C. Melchior and R.L. Bassett (Editors), Chemical Modelling of Aqueous Systems II. American Chemical Society, Washington, D.C., pp. 339-349.

Kjarsgaard, B.A., Wilkinson, L. and Armstrong, J.A., 2002. Geology, Lac de Gras Kimberlite Field, Central Slave Province, Northwest Territories-Nunavut; Geological Survey of Canada, Open File 3238, 1:250 000.

Kusky, T.M., 1989. Accretion of the Archean Slave Province. Geology, 17: 63 - 67.

Lackner, K.S., 2002. Carbonate Chemistry for Sequestering Fossil Carbon. Annual Reviews of Energy and the Environment, 27: 193-232.

Langmuir, D.L., 1996. Aqueous Environmental Geochemistry. Prentice-Hall Inc., New Jersey, 600 pp.

Lapakko, K.A., 2003. Developments in Humidity-Cell Tests and Their Application. In: J.L. Jambor, D.W. Blowes and A.I.M. Ritchie (Editors), Environmental Aspects of Mine Wastes. Mineralogical Association of Canada, Vancouver, pp. 147-164.

Lindberg, R.D. and Runnels, D.D., 1984. Groundwater Redox Reactions: An analysis of Equilibrium State Applied to Eh Measurements and Geochemical Modelling. Nature, 225: 925-927.

Meldrum, J.L., Jamieson, H.E. and Dyke, L.D., 2001. Oxidation of Mine Tailings from Rankin Inlet, Nunavut, at Subzero Temperatures. Canadian Geotechnical Journal, 38: 957-966.

Mine Environment Neutral Drainage (MEND) Project, 1991. Acid Rock Drainage Prediction Manual - MEND Project 1.16.1b. Submitted to CANMET, North Vancouver.

Mine Environment Neutral Drainage (MEND) Project, 2000. MEND Manual Volume 3 - Prediction. Submitted to CANMET.

Mitchell, R.H., 1986. Kimberlites: Mineralogy, Geochemistry, and Petrology. Plenum Press, New York, 442 pp.

Nassichuk, W.W. and Dyke, D.R., 1998. Fossils Recovered from Kimberlite Pipes in the Lac de Gras Field, Slave Province, Northwest Canada; Geological Implications, Seventh International Kimberlite Conference Extended Abstracts, Cape Town, pp. 612-614.

Nassichuk, W.W. and McIntyre, D.J., 1995. Cretaceous and Tertiary Fossils Discovered in Kimberlites at Lac de Gras in the Slave Province, Northwest Territories. Geological Survey of Canada - Current Research, 1995-B: 109-114.

National Guidelines and Standards Office, 2002. Canadian Environmental Quality Guidelines. Retrieved June 16, 2003, from http://www.ec.gc.ca/ceqg-rcqe/English/ceqg/water/default.cfm.

Nicholson, R.V., 1994. Iron-Sulfide Oxidation Mechanisms: Laboratory Studies. In: J.L. Jambor and D.W. Blowes (Editors), The Environmental Geochemistry of Sulfide Mine wastes: Short Course Handbook. Mineralogical Asociation of Canada, Waterloo, Ontario, pp. 163-183.

Nordstrom, D.K., Alpers, C.N., Ptacek, C.J. and Blowes, D.W., 2000. Negative pH and Extremely Acidic Mine Waters from Iron Mountain, California. Environmental Science and Technology, 34(2): 254-258.

Nordstrom, D.K. and Munoz, J.L., 1986. Geochemical Thermodynamics. Blackwell Scientific Publications, 477 pp.

Norecol Dames and Moore, 1997. Acid/Alkaline (ARD) and Geochemical Characterization Program. Submitted to Ekati Environment Department. 36 pp.

Northwest Territories Water Board, 1997. Class "A" Water License N7L2-1616 (Ekati Diamond Mine). Retrieved June 16, 2003, from http://www.monitoringagency.net/website/key%20documents/BHP's%20Class%20A%20Water%20Licence%20N7L2%20-%201616.pdf.

Parkhurst, D.L. and Appelo, C.A.J., 1999. User's guide to PHREEQC (Version 2) - A Computer Program for Speciation, Batch-Reaction, One Dimensional Transport, and Inverse Geochemical Calculations. U.S. Geological Survey, Denver, Colorado, pp. 312.

Patterson, R.J., Frappe, S.K., Dykes, L.S. and Mcleod, R.A., 1978. A Coring and Squeezing Technique for the Detailed Study of Subsurface Water Chemistry. Canadian Journal of Earth Sciences, 15(1): 162-169.

Pell, J.A., 1997a. Kimberlites in the Slave craton, Northwest Territories, Canada: A preliminary review. Russian Geology and Geophysics, 38(1): 5-16.

Pell, J.A., 1997b. Kimberlites in the Slave Craton, Northwest Territories, Canada. Geoscience Canada, 24(2): 77-90.

Pfeifer, H.R., 1977. A Model for Fluids in Metamorphosed Ultramafic Rocks: Observations at Surface and Subsurface Conditions (High pH Spring Waters). Schweizerische Mineralogische und Petrographische Mitteilungen, 57: 361-396.

Piper, A.M., 1944. A Graphic Procedure in the Geochemical Interpretation of Water-Analyses. Transactions, American Geophysical Union, 25: 914-923.

Price, W.A., 2003. Challenges Posed by Metal Leaching and Acid Rock Drainage, and Approaches Used to Address Them. In: J.L. Jambor, D.W. Blowes and A.I.M. Ritchie (Editors), Environmental Aspects of Mine Wastes. Short Course Series. Mineralogical Association of Canada, Vancouver, pp. 1-10.

Proctor, J. and Woodell, S.R.J., 1975. The Ecology of Serpentine Soils. Advances in Ecological Research, 9: 255-366.

Rescan Environmental Services Inc., 1996a. NWT Diamonds Project - Environmental Impact Statement (Volume I). Submitted to Ekati Environment Department. 538 pp.

Rescan Environmental Services Inc., 1996b. NWT Diamonds Project - Environmental Impact Statement (Volume II). Submitted to Ekati Environment Department. 698 pp.

Sader, J., Leybourne, M.I., McClenaghan, M.B., Hamilton, S.M. and Robertson, K., 2003. Field Procedures and Results of Groundwater Sampling in Kimberlite from Drillholes in the Kirland Lake and Lake Timiskaming areas, Northeastern Ontario. Geological Survey of Canada - Current Research, 2003-C11: 1-9.

Sato, T., Akita, N. and Arai, S., 2002. Geochemical Modelling of Hyperalkaline Spring Water and Precipitates at the Oman Ophiolite. Geochimica et Cosmochimica Acta, 66(15A): A669.

Schnitzer, M., 1978. Humic Substances: Chemistry and Reactions. In: M. Schnitzer and S.U. Khan (Editors), Soil Organic Matter. Elsevier, Amsterdam, pp. 1-64.

Seal, R.R., 2003. Stable-Isotope Geochemistry of Mine Waters and Related Solids. In: J.L. Jambor, D.W. Blowes and A.I.M. Ritchie (Editors), Environmental Aspects of Mine Wastes. Short Course Series. Mineralogical Association of Canada, Vancouver, pp. 303-334.

Singer, P.C. and Stumm, W., 1970. Acidic Mine Drainage: The Rate Determining Step. Science, 167: 1121-1123.

Snoeyink, V.L. and Jenkins, D., 1980. Water Chemistry. John Wiley and Sons, New York, 463 pp.

Sobek, A., Schuller, W.A., Freeman, J.R. and Smith, R.M., 1978. Field and Laboratory Methods Applicable to Overburdens and Minesoils. Submitted to U.S. Environmental Protection Agency - Report EPA-600/2-78-054.

Steffen Robertson and Kirsten Inc., 1989. Draft Acid Rock Drainage Technical Guide: Volume 1. Submitted to British Columbia Acid Mine Drainage Task Force, Vancouver, B.C. pp.

Stumm, W. and Morgan, J.J., 1996. Aquatic Chemistry: Chemical Equilibria and Rates in Natural Waters, 3rd Edition. John Wiley and Sons, Inc., New York, 1022 pp.

Wright, K.J., 1999. Possible Structural Controls of Kimberlites in the Lac de Gras Region, Central Slave Province, Northwest Territories, Canada. Masters Thesis, Department of Geological Sciences and Geological Engineering, Queen's University, Kingston, Ontario, 150 pp.

Zevenhoven, R. and Kohlmann, J., 2001. CO_2 Sequestration by Magnesium Silicate Mineral Carbonation in Finland. In: A. Lyngfelt, F. Johnsson and C. Azar (Editors), Second Nordic Minisymposium on Carbon Dioxide Capture and Storage, Goteborg, Sweden, pp. 13-18.

Appendix A: LLCF Water Analyses

This appendix contains **A)** analytical imprecision, **B)** LLCF water analyses from the 2000, 2001, and 2002 field seasons, and **C)** field blank analyses (d.l. = detection limit; NA = not analyzed).

Solution Number	Year	Sample Type
1-3	2000	Process plant discharge water
4-23	2000	Suction lysimeter pore-water
24-30	2000	Surface water
31-34	2000	Squeezer pore-water
35-37	2001	Process plant discharge water
38-54	2001	Suction lysimeter pore-water
55-58	2001	Surface water
59-63	2001	Squeezer pore-water
64-65	July 2002	Process plant discharge water
66-73	July 2002	Suction lysimeter pore-water
74-76	July 2002	Surface water
77	August 2002	Process plant discharge
78-83	August 2002	Suction lysimeter pore-water
84-86	August 2002	Surface water
87-94	2000-2002	Field Blanks

Sample numbers

All water samples are numbered with the year of collection, followed by sample type and location, and finally a sample number. Following are some examples of sample numbers and their meanings.

Discharge: *00-DW1* (00 = year; DW = discharge water; 1 = sample 1 of 2000)

Lysimeter pore-water: *00-LLAW1* (00 = year; LLAW = lysimeter pore-water sample from site A in the north end of the LLCF; 1 = sample 1 of 2000 field season)

Surface water: *00-UBW1* (00 = year; UBW = water sample from upstream side of dyke B; 1 = sample 1 of 2000 field season)

Squeezer pore-water: *00-LLAS1* (00 = year; LLAS = squeezed pore-water sample from site A in the north end of the LLCF, 1 = sample 1 of 2000 field season)

Field Blanks: 00-FB1 (00 = year; FB = field blank; 1 = sample 1 of 2000)

Note that imprecision increases significantly in reported values that are less than five times the detection limit.

A) LLCF Water Sample Imprecision

Analytical imprecision of LLCF water samples as determined from field and laboratory duplicate analyses (bd = all samples below detection limit; na = not available due to the fact the one or both analyses of all pairs of duplicates are less than 5 times the detection limit).

Solute	Field Duplicates	Laboratory Duplicates
Ag	na	1
Al	62	4
As	4	1
B	12	2
Ba	7	1
Be	bd	bd
Ca	5	1
Cd	27	9
Co	9	2
Cr	10	6
Cu	18	1
Fe	10	2
Hg	5	na
K	40	2
Mg	7	1
Mn	10	2
Mo	8	1
Na	5	3
Ni	5	3
Pb	na	1
Sb	9	2
Se	49	7
Si	46	3
Sr	3	1
U	7	2
V	6	2
Zn	53	4
NH_3-N	29	4
Cl	4	0
F	na	5
NO_3-N	73	3
NO_2-N	63	2
PO_4-P	84	2
SO_4	3	0
DOC	16	2

B) LLCF Water Analyses

2000 LLCF Water Analyses

Solution # Sample	units	d.l.	1 **00-DW1**	2 **00-DW2**	3 **00-DW3**	4 **00-LLAW1**	5 **00-LLAW2**
Sample date			12-Aug-00	13-Aug-00	19-Aug-00	12-Aug-00	14-Aug-00
Temp	°C		10.3	9.1	10.9	15.9	9.1
pH			8.74	9.09	9.25	8.32	8.42
Alkalinity	mg/L $CaCO_3$		70.2	63.6	66	21.2	23.2
DO	mg/L		7.6	9.7	8.6	3.7	3.2
Conductivity	µS/cm		543	380	454	1550	2099
Ag	mg/L	0.0001	<0.0001	<0.0001	<0.0001	<0.0001	<0.0001
Al	mg/L	0.0003	0.0006	0.0004	0.0004	0.023	0.0131
As	mg/L	0.00003	0.0111	0.014	0.0149	0.00622	0.00542
B	mg/L	0.001	0.023	0.029	0.027	0.012	0.008
Ba	mg/L	0.00005	0.148	0.385	0.792	0.0396	0.0358
Be	mg/L	0.0002	<0.0002	<0.0002	<0.0002	<0.0002	<0.0002
Ca	mg/L	0.004	28	17.2	17	152	119
Cd	mg/L	0.00005	0.00051	0.00039	0.00037	0.0012	0.00103
Co	mg/L	0.0001	0.0006	0.0006	0.0006	0.0012	0.0009
Cr	mg/L	0.00006	0.00665	0.00633	0.00624	0.00223	0.00128
Cu	mg/L	0.0006	0.0015	0.0009	0.0012	0.0033	0.0019
Fe	mg/L	0.005	0.13	0.094	0.088	0.687	0.626
Hg	mg/L	0.00002	0.00013	0.00013	0.00009	0.0004	0.00003
K	mg/L	0.005	42.7	44.4	36	33	25.7
Mg	mg/L	0.004	62.8	39.0	32.0	210	214
Mn	mg/L	0.0001	0.0142	0.0111	0.008	0.066	0.0514
Mo	mg/L	0.00006	0.333	0.262	0.256	0.858	0.771
Na	mg/L	0.005	11.7	10.9	11.1	18	14
Ni	mg/L	0.00006	0.0396	0.0171	0.0274	0.114	0.0947
Pb	mg/L	0.00005	<0.00005	0.00035	<0.00005	0.00016	0.0001
Sb	mg/L	0.00003	0.0284	0.0329	0.0266	0.00684	0.00616
Se	mg/L	0.0001	0.0039	0.0028	0.0022	0.0016	0.0014
Si	mg/L	0.1	NA	NA	NA	NA	NA
Sr	mg/L	0.0001	0.566	0.401	0.347	1.96	1.8
U	mg/L	0.00005	0.00016	0.00009	0.00021	0.00017	0.00012
V	mg/L	0.00005	0.00166	0.00264	0.00403	0.0234	0.0118
Zn	mg/L	0.0008	0.0012	0.0009	0.0022	0.0549	0.0194
NH_3-N	mg/L	0.005	1.61	1.24	0.713	2.3	2.29
Cl	mg/L	0.05	15.8	15.7	17.5	4.86	4.88
F	mg/L	0.05	0.08	0.07	0.08	0.15	0.08
NO_3-N	mg/L	0.002	10.1	6.19	5.5	0.359	0.244
NO_2-N	mg/L	0.002	0.391	0.27	0.141	0.077	0.078
PO_4-P	mg/L	0.001	0.02	0.031	0.085	0.006	0.009
SO_4	mg/L	0.05	231	125	95.5	1200	1210
DIC	mg/L	0.5	15	14	13.8	4.8	4.7
DOC	mg/L	0.5	2.9	3	3.5	4.8	4.6

2000 LLCF Water Analyses (cont'd)

Solution #	6	7	8	9	10	11
Sample	**00-LLDW2** (dup. of LLAW2)	**00-LLAW3**	**00-LLCW1A**	**00-LLCW2A**	**00-LLCW3A**	**00-LLCW1B**
Sample date	14-Aug-00	18-Aug-00	12-Aug-00	14-Aug-00	18-Aug-00	12-Aug-00
Temp	9.1	8.2	15.5	6.9	8.4	17.9
pH	8.42	8.32	n/a	8.92	8.52	8.18
Alkalinity	23.2	21.2	55.2	52.4	52.8	84.8
DO	3.2	2.4	5.2	6.3	4.2	5.2
Conductivity	2099	4078	351	627	349	2635
Ag	<0.0001	<0.0001	<0.0001	<0.0001	<0.0001	<0.0001
Al	0.0156	0.0106	0.131	0.0098	0.0601	0.0111
As	0.00551	0.00409	0.0108	0.00874	0.0102	0.00394
B	0.008	0.005	0.015	0.007	0.014	0.02
Ba	0.0361	0.0285	0.0583	0.0589	0.0854	0.0287
Be	<0.0002	<0.0002	<0.0002	<0.0002	<0.0002	<0.0002
Ca	120	239	16.4	11.0	14.9	232
Cd	0.00102	0.00085	0.00078	0.00034	0.00084	0.00166
Co	0.0009	0.0016	0.0003	<0.0001	0.0004	0.0016
Cr	0.00107	0.00079	0.0008	0.00123	0.00096	0.00309
Cu	0.0039	0.0025	0.0045	0.0029	0.0044	0.0061
Fe	0.647	1.37	0.145	0.093	0.178	0.978
Hg	0.00003	<0.00002	0.00005	0.00006	0.00004	0.00009
K	25.8	29.7	7.98	5.76	8.74	36.7
Mg	214	499	21.3	13.4	19.7	380
Mn	0.0515	0.0891	0.0125	0.005	0.0113	0.0897
Mo	0.775	0.611	0.2950	0.248	0.2930	1.24
Na	14.2	15.5	5.1000	3.23	4.3700	15.2
Ni	0.0958	0.158	0.0149	0.00816	0.0167	0.166
Pb	0.00063	<0.00005	0.00047	0.00007	0.00031	0.00008
Sb	0.00617	0.00409	0.00638	0.00511	0.00545	0.00442
Se	0.0013	0.0007	0.0004	0.0004	0.0004	0.0133
Si	NA	3.10	3.50	NA	3.10	NA
Sr	1.80	3.39	0.233	0.173	0.210	2.86
U	0.00012	0.00008	0.00032	0.00021	0.00030	0.00149
V	0.0118	0.00361	0.0266	0.0131	0.0116	0.183
Zn	0.0933	0.0103	0.0500	0.0136	0.0222	0.0174
NH_3-N	2.46	2.83	0.469	1.63	0.528	1.36
Cl	4.83	3.93	5.72	5.31	5.65	7.49
F	0.08	0.11	0.12	0.14	0.12	0.11
NO_3-N	0.127	<0.006	0.035	0.052	0.039	0.6
NO_2-N	0.079	0.009	0.061	<0.002	0.073	0.45
PO_4-P	0.003	0.012	0.018	0.005	0.025	0.019
SO_4	1230	2730	81.5	75.3	69.1	2030
DIC	4.6	3.9	12.3	12	12.1	18.8
DOC	5.5	5.6	2.7	5.1	2.8	8

2000 LLCF Water Analyses (cont'd)

Solution #	12	13	14	15	16	17
Sample	**00-LLCW2B**	**00-LLCW3B**	**00-LLGW1**	**00-LLGW2**	**00-LLGW3**	**00-LLDW3** (dup. of LLGW3)
Sample date	17-Aug-00	18-Aug-00	12-Aug-00	14-Aug-00	18-Aug-00	18-Aug-00
Temp	11.4	8.8	18.4	10.2	9.1	9.1
pH	8.11	8.16	8.14	8.1	8.19	8.19
Alkalinity	77.6	76.8	68.4	76.4	74.4	74.4
DO	4.2	4.3	4.8	8.8	3.9	3.9
Conductivity	3661	3798	4730	5090	5210	5210
Ag	<0.0001	<0.0001	<0.0001	<0.0001	<0.0001	<0.0001
Al	0.0125	0.0068	0.0099	0.0226	0.0059	0.0427
As	0.00409	0.00404	0.0049	0.00472	0.00434	0.00482
B	0.01	0.009	0.013	0.012	0.008	0.011
Ba	0.0192	0.0173	0.0173	0.0181	0.0136	0.0167
Be	<0.0002	<0.0002	<0.0002	<0.0002	<0.0002	<0.0002
Ca	222	232	425	435	417	420
Cd	0.00132	0.00134	0.00121	0.00113	0.00107	0.00118
Co	0.0018	0.0020	0.0028	0.0028	0.0024	0.003
Cr	0.00217	0.0025	0.00401	0.00191	0.00226	0.00279
Cu	0.0040	0.0038	0.0027	0.0066	0.0026	0.0053
Fe	1.15	1.32	1.89	1.87	1.97	2.17
Hg	<0.00002	<0.00002	0.00002	<0.00002	<0.00002	<0.00002
K	29.7	29.6	40.5	35.3	31.3	34.7
Mg	434	487	715	702	700	719
Mn	0.0829	0.0855	0.119	0.112	0.0936	0.114
Mo	0.994	1.00	0.907	0.867	0.798	0.866
Na	10.8	10.7	17.5	15.4	13.8	15.4
Ni	0.202	0.217	0.288	0.267	0.247	0.277
Pb	0.00007	0.00008	0.00008	0.00019	0.00008	0.00017
Sb	0.00326	0.00318	0.00284	0.00266	0.00232	0.0025
Se	0.0111	0.0105	0.0143	0.0124	0.0098	0.0108
Si	7.1	6.5	NA	NA	7.2	7.3
Sr	3.02	3.18	5.95	5.75	5.51	5.6
U	0.00085	0.00077	0.00118	0.00112	0.0009	0.00106
V	0.0111	0.00507	0.0290	0.0124	0.00423	0.00499
Zn	0.0087	0.0108	0.0264	0.0248	0.0169	0.0345
NH_3-N	1.81	1.95	2.18	2.08	1.63	1.45
Cl	4.55	4.8	5.46	5.14	4.58	5.18
F	0.07	0.07	0.06	0.09	<0.05	0.06
NO_3-N	1.45	2.31	3.57	3.98	5.15	5.21
NO_2-N	0.373	0.293	0.627	0.346	0.085	0.083
PO_4-P	0.02	0.019	0.012	0.019	0.023	0.024
SO_4	2360	2600	3960	3940	3880	3910
DIC	16.8	16.9	16.9	16.7	16.1	16
DOC	6.3	7.2	9.4	8.2	6.8	6.5

2000 LLCF Water Analyses (cont'd)

Solution #	18	19	20	21	22	23	24
Sample	**00-LLKW1**	**00-LLKW2**	**00-LLKW3**	**00-LLMW1**	**00-LLMW2**	**00-LLMW3**	**00-UBW1**
Sample date	12-Aug-00	14-Aug-00	18-Aug-00	17-Aug-00	18-Aug-00	19-Aug-00	11-Aug-00
Temp	13.6	7.9	7.7	8.1	8.8	10.9	11.8
pH	8.44	8.61	8.89	8.84	9	8.98	8.05
Alkalinity	45.2	48.8	43.6	60	58.4	60	76
DO	2.5	4.2	2.8	3.4	3.1	2.8	9.3
Conductivity	770	691	569	499	400	342	600
Ag	<0.0001	<0.0001	<0.0001	<0.0001	<0.0001	<0.0001	<0.0001
Al	0.0084	0.0221	0.0411	0.0078	0.0619	0.0087	0.0046
As	0.00732	0.00725	0.0102	0.00772	0.00723	0.00598	0.00905
B	0.017	0.011	0.014	0.008	0.007	0.006	0.021
Ba	0.087	0.023	0.0629	0.0545	0.0666	0.0556	0.138
Be	<0.0002	<0.0002	<0.0002	<0.0002	<0.0002	<0.0002	<0.0002
Ca	66.2	31.5	26.2	16.1	12.4	9.34	29.6
Cd	0.00078	0.00056	0.00103	0.00047	0.00044	0.00036	0.00052
Co	0.0003	0.0003	0.0006	0.0001	0.0005	<0.0001	0.0005
Cr	0.00344	0.00149	0.00049	0.00148	0.00279	0.00152	0.00767
Cu	0.0031	0.0027	0.0081	0.0034	0.0038	0.003	<0.0006
Fe	0.395	0.223	0.234	0.121	0.294	0.094	0.128
Hg	0.00011	0.00006	0.00003	0.00006	0.00005	0.00005	0.00009
K	18.4	12.4	12.9	8.38	6.93	5.71	26.3
Mg	95.1	41.7	37.6	25.6	18.4	13.4	46.6
Mn	0.0241	0.0122	0.0172	0.0073	0.0127	0.0041	0.0259
Mo	0.513	0.407	0.4050	0.345	0.298	0.259	0.323
Na	9.44	6.38	7.3300	5.14	4.37	3.55	9.88
Ni	0.0401	0.0223	0.0263	0.0157	0.0189	0.0103	0.0314
Pb	0.0001	0.00027	0.00041	<0.00005	0.00012	0.00017	<0.00005
Sb	0.00531	0.00532	0.00575	0.00671	0.00558	0.00501	0.0142
Se	0.001	0.0006	0.0004	0.0007	0.0005	0.0005	0.0016
Si	NA	NA	NA	3.30	5.20	3.10	NA
Sr	0.806	0.444	0.374	0.259	0.206	0.155	0.452
U	0.0005	0.00032	0.00032	0.00022	0.00025	0.00017	0.00051
V	0.131	0.0557	0.0081	0.0148	0.00895	0.00636	0.00156
Zn	0.013	0.0345	0.0255	0.0068	0.0082	0.0241	<0.0008
NH_3-N	0.529	0.683	0.7	1.21	1.2	1.11	0.287
Cl	5.21	4.99	5.21	5.23	5.06	4.96	13.5
F	0.12	0.11	0.35	0.13	0.11	0.1	0.08
NO_3-N	0.068	0.056	0.052	0.067	0.017	0.012	3.53
NO_2-N	0.205	0.058	0.068	0.049	0.026	0.013	0.912
PO_4-P	0.008	0.012	0.006	0.023	0.025	0.027	0.015
SO_4	496	260	165	152	107	85.4	177
DIC	10.7	10.6	10.8	13.2	13.2	13.3	18.5
DOC	5.2	5.5	2.9	6.4	5.1	4.4	5.3

2000 LLCF Water Analyses (cont'd)

Solution #	25	26	27	28	29	30
Sample	**00-UBW2**	**00-DBW2** (dup. of UBW2)	**00-UBW3**	**00-UCW1**	**00-UCW2**	**00-UCW3**
Sample date	12-Aug-00	12-Aug-00	13-Aug-00	12-Aug-00	13-Aug-00	19-Aug-00
Temp	9.9	9.9	10.3	11.6	13.6	11.6
pH	8.61	8.61	8.33	8.73	8.26	8.23
Alkalinity	72.8	72.8	70.4	29.2	28.4	31.6
DO	9	9	10.3	9.1	9.8	8.9
Conductivity	455	455	462	198	204	264
Ag	<0.0001	<0.0001	<0.0001	<0.0001	<0.0001	<0.0001
Al	0.0036	0.0067	0.001	0.0065	0.0036	0.0042
As	0.00922	0.00951	0.00989	0.0022	0.0023	0.00233
B	0.023	0.02	0.022	0.009	0.008	0.009
Ba	0.134	0.133	0.131	0.153	0.155	0.156
Be	<0.0002	<0.0002	<0.0002	<0.0002	<0.0002	<0.0002
Ca	30.5	31.1	29.0	14.8	15.6	16.4
Cd	0.00053	0.00125	0.00047	0.00013	0.00013	0.00013
Co	0.0005	0.0004	0.0004	0.0001	<0.0001	0.0001
Cr	0.00784	0.00721	0.00691	0.00328	0.00329	0.00349
Cu	0.0014	0.0013	0.0008	0.0009	0.0014	0.0011
Fe	0.137	0.17	0.141	0.086	0.089	0.096
Hg	0.00009	0.0001	0.00011	<0.00002	0.00002	<0.00002
K	28.1	29.3	32.9	8.85	9.42	9.99
Mg	49.2	48.7	51.0	15.4	16.1	17.0
Mn	0.0165	0.0135	0.0123	0.0017	0.0025	0.0162
Mo	0.337	0.344	0.343	0.076	0.0785	0.0816
Na	10.6	11	11.2	4.79	5.14	5.47000
Ni	0.029	0.0314	0.0273	0.00804	0.00834	0.00883
Pb	0.00024	0.00016	<0.00005	0.00005	<0.00005	<0.00005
Sb	0.0191	0.0144	0.0172	0.00584	0.00523	0.0204
Se	0.0018	0.0017	0.0021	0.0012	0.0013	0.0014
Si	NA	NA	NA	NA	NA	
Sr	0.473	0.485	0.482	0.184	0.195	0.204
U	0.00055	0.00051	0.00029	0.00019	0.0002	0.0003
V	0.00181	0.0018	0.00184	0.00053	0.00051	0.00049
Zn	0.0013	0.0029	<0.0008	0.0012	0.0012	0.0009
NH_3-N	0.197	0.496	0.656	0.032	0.043	0.088
Cl	13.8	14.2	14.3	10.6	11.2	12.2
F	0.08	0.07	0.09	0.07	0.12	0.060
NO_3-N	3.53	3.34	4.24	4.26	4.1	4.68
NO_2-N	0.975	0.957	0.055	0.057	0.063	0.742
PO_4-P	0.011	0.008	<0.001	0.002	<0.001	0.015
SO_4	181	182	185	51.9	52	57.4
DIC	18	15.7	7.1	6.8	6.9	18.2
DOC	5	3.6	4.6	3.2	3.4	3.3

2000 LLCF Water Analyses (cont'd)

Solution # **Sample**	31 **00-LLAS1**	32 **00-LLGS1**	33 **00-LLKS1**	34 **00-LLMS1**
Sample date	17-Aug-00	19-Aug-00	18-Aug-00	12-Aug-00
Temp	18.8	16.9	18.6	19.9
pH	7.4	7.91	8.77	8.73
Alkalinity	36.4	52	62	60.8
DO	4.2	3.6	3.6	7.2
Conductivity	1599	3533	284	453
Ag	<0.0001	<0.0001	<0.0005	<0.0001
Al	0.0166	0.0228	0.047	0.0301
As	0.00596	0.0062	0.0105	0.017
B	0.023	0.023	0.026	0.023
Ba	0.0432	0.0388	0.291	0.477
Be	<0.0002	<0.0002	<0.001	<0.0002
Ca	170	318	23.5	35.5
Cd	0.00154	0.00281	0.0009	0.00125
Co	0.0004	0.0033	<0.0005	0.0014
Cr	0.00364	0.00065	<0.0003	0.00063
Cu	<0.0006	0.0142	<0.003	0.0026
Fe	<0.005	<0.005	0.14	0.009
Hg	0.00004	<0.00002	<0.0001	0.00004
K	33.0	46.6	15.2	15.8
Mg	215	536	31.2	48.0
Mn	0.1050	0.1810	0.0167	0.0188
Mo	0.7260	1.2400	0.3630	0.5270
Na	18.2000	19.4000	7.4500	9.0500
Ni	0.0541	0.396	0.0192	0.0382
Pb	0.0119	0.00066	0.0004	0.00051
Sb	0.0079	0.00655	0.012	0.0156
Se	0.0005	0.0015	<0.0005	0.0011
Si	3.1	6.7	NA	2.9
Sr	2.37	4.48	0.347	0.587
U	0.00012	0.00117	<0.0003	0.00014
V	0.0015	0.0017	0.0022	0.0023
Zn	0.0083	0.0443	0.0760	0.1310
NH_3-N	2.03	1.58	1.38	1.62
Cl	4.02	6.58	5.89	6.86
F	NA	NA	NA	NA
NO_3-N	1.97	0.152	0.136	3.610
NO_2-N	0.128	0.186	0.173	<0.02
PO_4-P	0.027	0.021	0.008	0.011
SO_4	12.2	2320	224	338
DIC	4.7	9	12.3	7.4
DOC	6.8	6.6	8.2	12.7

2001 LLCF Water analyses

Solution # Sample	units	d.l.	35 **01-DW1**	36 **01-DW2**	37 **01-DW3**	38 **01-LLAW1**	39 **01-LLDW3** (dup. of LLAW1)
Sample Date			08-Jul-01	09-Jul-01	13-Jul-01	13-Jul-01	13-Jul-01
Temp	°C		12.0	14.0	21.5	13.4	13.4
pH			8.15	8.48	7.81	7.32	7.32
Alkalinity	mg/L $CaCO_3$		43.6	78.4	72.8	34.0	34.0
DO	mg/L		8.40	9.30	6.40	5.80	5.80
Conductivity	μS/cm		429	525	626	4339	4339
Ag	mg/L	0.0001	<0.0001	<0.0001	<0.0001	0.0002	<0.0001
Al	mg/L	0.0003	0.0022	0.0020	0.0018	0.0046	0.0022
As	mg/L	0.00003	0.0132	0.0191	0.0148	0.00521	0.00426
B	mg/L	0.001	0.075	0.078	0.067	0.021	0.019
Ba	mg/L	0.000	0.365	0.411	0.224	0.041	0.032
Be	mg/L	0.0002	<0.0002	<0.0002	<0.0002	<0.0002	<0.0002
Ca	mg/L	0.0	12.4	9.5	13.5	416.0	329.0
Cd	mg/L	0.00005	0.00050	0.00056	0.00068	0.00200	0.00141
Co	mg/L	0.0001	0.0004	0.0002	0.0003	0.0017	0.0011
Cr	mg/L	0.00006	0.00019	0.00023	0.00023	0.00007	<0.00006
Cu	mg/L	0.0006	0.0020	0.0013	0.0037	0.0031	0.0028
Fe	mg/L	0.005	<0.005	<0.005	<0.005	1.080	<0.005
Hg	mg/L	0.00002	<0.00002	0.00002	<0.00002	0.00004	<0.00002
K	mg/L	0.0	76.5	76.6	85.1	43.2	35.4
Mg	mg/L	0.00	27.8	24.2	32.1	798	506
Mn	mg/L	0.0001	0.0075	0.0076	0.0100	0.1170	0.0872
Mo	mg/L	0.00006	0.412	0.432	0.505	1.16	0.833
Na	mg/L	0.01	15.40	13.40	15.10	25.30	16.00
Ni	mg/L	0.00006	0.017	0.235	0.0282	0.278	0.224
Pb	mg/L	0.00005	<0.00005	0.00008	<0.00005	<0.00005	<0.00005
Sb	mg/L	0.00003	0.03190	0.03870	0.03310	0.00460	0.00357
Se	mg/L	0.0001	0.0014	0.0015	0.0017	0.0024	0.0020
Si	mg/L	0.1	4.2	3.3	4.5	6.1	6.2
Sr	mg/L	0.0001	0.304	0.267	0.342	5.54	3.68
U	mg/L	0.00005	0.00006	0.00013	0.00007	0.00038	0.00033
V	mg/L	0.00005	0.00438	0.00837	0.00430	0.01440	0.01080
Zn	mg/L	0.0008	0.0023	0.0032	0.0034	0.0075	0.0072
NH_3-N	mg/L	0.005	0.716	1.140	0.500	0.256	0.626
Cl	mg/L	1	34	24	29	6	6
F	mg/L	0.05	<0.05	<0.05	<0.05	<0.05	<0.05
NO_3-N	mg/L	0.006	5.800	7.400	0.315	<0.006	13.400
NO_2-N	mg/L	0.002	0.240	0.170	0.056	<0.002	3.670
PO_4-P	mg/L	0.001	0.001	0.029	0.001	0.004	0.014
SO_4	mg/L	0.05	101	87.2	113	2620	2620
DIC	mg/L	0.5	14.2	14.7	15.1	6.7	7.7
DOC	mg/L	0.5	3.4	3.7	3.8	6.3	6.4

2001 LLCF Water analyses (cont'd)

Solution #	40	41	42	43	44	45	46
Sample	**01-LLAW2**	**01-LLCW1**	**01-LLCW2**	**01-LLGW1**	**01-LLGW2**	**01-LLJW1**	**01-LLJW2**
Sample Date	14-Jul-01	10-Jul-01	13-Jul-01	10-Jul-01	13-Jul-01	10-Jul-01	13-Jul-01
Temp	9.6	13.1	15.8	13.1	14.3	11.7	13.9
pH	7.97	7.87	7.81	7.79	7.69	7.89	7.69
Alkalinity	28.0	59.6	56.4	46.8	45.6	37.6	36.4
DO	5.90	4.76	6.20	4.65	5.10	5.37	6.10
Conductivity	4414	2231	2398	4274	4372	2190	2022
Ag	0.0002	<0.0001	<0.0001	0.0003	0.0003	0.0002	0.0002
Al	0.0017	0.0043	0.0050	0.0093	0.0049	0.0051	0.0057
As	0.00538	0.00386	0.00415	0.00451	0.00457	0.00502	0.00484
B	0.012	0.023	0.023	0.030	0.026	0.033	0.028
Ba	0.032	0.023	0.021	0.029	0.025	0.039	0.033
Be	<0.0002	<0.0002	<0.0002	<0.0002	<0.0002	<0.0002	<0.0002
Ca	473	160	167	401	441	207	175
Cd	0.00215	0.00084	0.00078	0.00228	0.00213	0.00103	0.00099
Co	0.0019	0.0006	0.0007	0.0031	0.0030	0.0011	0.0011
Cr	0.00016	0.00014	0.00017	0.00025	0.00010	0.00012	0.00010
Cu	0.0025	0.0030	0.0026	0.0046	0.0019	0.0015	0.0031
Fe	1.020	<0.005	<0.005	1.250	1.330	0.260	0.360
Hg	0.00004	<0.00002	<0.00002	0.00004	0.00004	0.00003	0.00004
K	42.3	26.8	26.7	53.4	57.9	34.4	30.9
Mg	867	276	287	660	723	354	301
Mn	0.1120	0.0642	0.0693	0.2210	0.2150	0.1170	0.0986
Mo	1.18	0.616	0.549	1.25	1.14	0.654	0.588
Na	24.10	12.40	12.40	32.10	28.50	24.90	21.00
Ni	0.27300	0.10200	0.11000	0.32400	0.31800	0.18000	0.16700
Pb	<0.00005	<0.00005	<0.00005	<0.00005	<0.00005	0.00006	0.00010
Sb	0.00459	0.00395	0.00378	0.00502	0.00455	0.00545	0.00554
Se	0.0013	0.0030	0.0029	0.0034	0.0027	0.0015	0.0008
Si	6.6	6.7	7.5	6.5	7.8	4.7	5.6
Sr	6.2300	1.9900	2.1000	5.1800	5.5800	2.3200	2.0100
U	0.00013	0.00050	0.00045	0.00072	0.00075	0.00031	0.00027
V	0.00804	0.01130	0.00733	0.01550	0.00945	0.02310	0.01310
Zn	0.0077	0.0059	0.0047	0.0110	0.0056	0.0065	0.0106
NH_3-N	0.031	0.487	0.283	0.958	1.230	0.944	0.625
Cl	6	6	5	7	7	6	5
F	<0.05	<0.05	<0.05	<0.05	<0.05	0.07	0.06
NO_3-N	0.059	0.334	0.400	0.200	0.100	0.300	0.200
NO_2-N	0.025	0.039	<0.05	0.150	0.100	0.150	<0.05
PO_4-P	<0.001	0.012	0.007	0.010	0.007	0.009	0.006
SO_4	2840	1240	1270	2750	2930	1210	1140
DIC	6.5	13.2	12.7	10.5	11.0	8.3	8.4
DOC	6.3	5.0	16.2	8.1	5.7	5.2	8.2

2001 LLCF Water analyses (cont'd)

Solution #	47	48	49	50	51	52
Sample	**01-LLKW1**	**01-LLKW2**	**01-LLDW2** (dup. of LLKW2)	**01-LLMBW1**	**01-LLMBW2**	**01-LLMW1**
Sample Date	10-Jul-01	11-Jul-01	11-Jul-01	14-Jul-01	14-Jul-01	10-Jul-01
Temp	11.9	9.9	9.9	11.5	14.4	11.0
pH	8.04	8.13	8.13	7.69	7.92	8.37
Alkalinity	42.0	42.4	42.4	55.2	56.8	50.8
DO	4.63	2.65	2.65	6.10	6.50	4.66
Conductivity	1365.0	1251.0	1251.0	2420.0	2350.0	633.0
Ag	<0.0001	<0.0001	<0.0001	0.0003	0.0003	<0.0001
Al	0.0027	0.0094	0.0050	0.0071	0.0126	0.0071
As	0.00670	0.00726	0.00688	0.00802	0.00778	0.00873
B	0.019	0.020	0.021	0.024	0.027	0.020
Ba	0.018	0.019	0.019	0.023	0.021	0.026
Be	<0.0002	<0.0002	<0.0002	<0.0002	<0.0002	<0.0002
Ca	82.1	74.8	70.6	187.0	178.0	28.5
Cd	0.00080	0.00020	0.00082	0.00175	0.00166	0.00060
Co	0.0002	0.0002	0.0002	0.0012	0.0012	<0.0001
Cr	0.00008	0.00024	0.00019	0.00022	0.00034	<0.00006
Cu	0.0018	0.0056	0.0038	0.0023	0.0020	0.0006
Fe	<0.005	<0.005	<0.005	0.669	0.707	<0.005
Hg	<0.00002	<0.00002	<0.00002	0.00005	0.00004	<0.00002
K	23.3	22.8	21.6	39.6	37.4	14.3
Mg	143	129	108	279	276	53.1
Mn	0.0223	0.0211	0.0203	0.0852	0.0817	0.0108
Mo	0.632	0.634	0.536	0.939	0.894	0.468
Na	11.20	11.10	10.30	17.40	16.40	8.06
Ni	0.0469	0.0439	0.0425	0.136	0.128	0.029
Pb	<0.00005	0.00007	<0.00005	<0.00005	<0.00005	<0.00005
Sb	0.00497	0.00511	0.00498	0.00481	0.00480	0.00658
Se	0.0005	0.0005	0.0004	0.0047	0.0049	0.0009
Si	6.1	5.7	5.8	8.4	8.3	3.3
Sr	1.05	0.959	0.922	2.49	2.42	0.405
U	0.00017	0.00017	0.00018	0.00046	0.00048	0.00011
V	0.00467	0.00414	0.00393	0.00287	0.00266	0.00494
Zn	0.0033	0.0150	0.0071	0.0056	0.0072	0.0015
NH_3-N	0.109	0.351	0.355	0.013	0.229	0.557
Cl	7	6	6	6	6	5
F	<0.05	0.06	<0.05	<0.05	<0.05	0.07
NO_3-N	0.112	0.081	0.075	0.473	<0.006	0.197
NO_2-N	<0.002	0.010	0.010	0.026	<0.002	0.094
PO_4-P	0.010	0.006	0.028	0.020	0.015	0.018
SO_4	612	534	516	1400	1330	209
DIC	9.6	9.9	9.6	12.8	13.0	11.4
DOC	4.4	5.2	5.3	6.1	4.9	4.3

2001 LLCF Water analyses (cont'd)

Solution # **Sample**	53 **01-LLDW1** (dup. of LLMW1)	54 **01-LLMW2**	55 **01-UBW1**	56 **01-UBW2**	57 **01-UCW1**	58 **01-UCW2**
Sample Date	10-Jul-01	11-Jul-01	07-Jul-01	08-Jul-01	07-Jul-01	08-Jul-01
Temp	11.0	10.6	12.0	12.3	11.3	11.0
pH	8.37	8.12	7.89	8.56	7.36	7.79
Alkalinity	50.8	52.6	23.6	23.2	22.4	23.2
DO	4.66	5.24	10.41	11.30	9.59	10.76
Conductivity	633.0	577.0	156.0	152.0	216.0	214.4
Ag	<0.0001	<0.0001	<0.0001	<0.0001	<0.0001	<0.0001
Al	0.0060	0.0192	0.0091	0.0080	0.0030	0.0025
As	0.00861	0.00955	0.00234	0.00234	0.00389	0.00394
B	0.023	0.021	0.016	0.017	0.023	0.020
Ba	0.025	0.026	0.092	0.093	0.169	0.169
Be	<0.0002	<0.0002	<0.0002	<0.0002	<0.0002	<0.0002
Ca	26.4	27.0	9.3	9.7	10.6	10.8
Cd	0.00061	0.00057	<0.00005	<0.00005	0.00010	0.00010
Co	<0.0001	0.0001	<0.0001	<0.0001	0.0001	0.0001
Cr	0.00012	0.00067	0.00021	0.00020	0.00016	0.00015
Cu	0.0010	0.0014	0.0062	0.0022	0.0011	0.0009
Fe	<0.005	0.042	0.010	<0.005	<0.005	<0.005
Hg	<0.00002	<0.00002	<0.00002	<0.00002	<0.00002	<0.00002
K	13.8	13.9	10.3	10.5	20.0	20.3
Mg	49.1	50.5	13.2	13.7	18.4	18.8
Mn	0.0102	0.0144	0.0027	0.0022	0.0098	0.0085
Mo	0.396	0.455	0.0674	0.0676	0.105	0.106
Na	7.59	7.92	2.84	2.92	6.20	6.32
Ni	0.0283	0.0288	0.0133	0.0130	0.0157	0.0157
Pb	<0.00005	<0.00005	<0.00005	<0.00005	<0.00005	<0.00005
Sb	0.00647	0.00580	0.00264	0.00262	0.00720	0.00708
Se	0.0080	0.0008	<0.0001	<0.0001	0.0004	0.0004
Si	3.4	3.7	1.0	1.0	1.6	1.6
Sr	0.3790	0.3860	0.1470	0.1490	0.1960	0.2000
U	0.00120	0.00012	0.00010	0.00010	0.00020	0.00021
V	0.00482	0.00509	0.00090	0.00092	0.00092	0.00092
Zn	0.0021	0.0039	0.0025	0.0012	0.0014	<0.0008
NH_3-N	0.443	0.492	0.015	0.007	0.179	0.155
Cl	5	5	3	3	12	12
F	0.07	0.06	<0.05	<0.05	<0.05	<0.05
NO_3-N	0.193	0.211	0.232	0.195	3.400	3.300
NO_2-N	0.093	0.070	0.062	0.057	0.060	0.070
PO_4-P	0.018	0.019	0.006	0.006	0.006	0.006
SO_4	195	171	49.1	49.7	61.9	61.1
DIC	11.2	11.7	7.8	7.7	8.3	8.3
DOC	6.0	5.3	4.4	4.5	3.0	3.1

2001 LLCF Water analyses (cont'd)

Solution #	59	60	61	62	63
Sample	**01-LLAS1**	**01-LLGS1-01**	**01-LLGS1-02**	**01-LLKS1**	**01-LLMS1**
Sample Date	14-Jul-01	14-Jul-01	14-Jul-01	11-Jul-01	09-Jul-01
Temp	19.5	20.4	21.5	19.5	19.4
pH	8.03	8.11	8.12	7.15	7.55
Alkalinity	32.8	36.0	40.4	66.4	52.8
DO	5.60	2.90	2.20	7.24	3.88
Conductivity	4207	1838	2225	1546	647
Ag	0.0003	0.0002	<0.0001	0.0003	0.0003
Al	0.0028	0.0038	0.0080	0.0026	0.0099
As	0.00735	0.00297	0.00280	0.00693	0.00951
B	0.030	0.037	0.037	0.047	0.032
Ba	0.040	0.168	0.177	0.040	0.489
Be	<0.0002	<0.0002	<0.0002	<0.0002	<0.0002
Ca	467	185	243	240	31.5
Cd	0.00201	0.00118	0.00123	0.00165	0.00071
Co	0.0010	0.0002	<0.0001	0.0016	<0.0001
Cr	0.00017	0.00008	0.00009	0.00027	0.00034
Cu	<0.0006	<0.0006	<0.0006	<0.0006	<0.0006
Fe	1.23	0.540	0.528	0.563	0.050
Hg	0.00004	0.00007	<0.00002	0.00004	0.00006
K	51.2	38.2	42.6	42.2	16.0
Mg	630	213	297	319	42.1
Mn	0.2180	0.0978	0.1240	0.1230	0.0146
Mo	1.04000	0.68000	0.79100	0.88400	0.43200
Na	31.00	22.10	23.40	20.20	9.09
Ni	0.0852	0.0178	0.0180	0.215	0.0171
Pb	<0.00005	<0.00005	<0.00005	<0.00005	<0.00005
Sb	0.00358	0.00260	0.00316	0.00807	0.00622
Se	0.0003	0.0002	0.0003	0.0007	<0.0001
Si	3.9	4.6	5.1	8.5	3.4
Sr	7.09	2.67	3.25	3.10	0.494
U	<0.00005	<0.00005	<0.00005	0.00044	<0.00005
V	0.00136	0.00035	0.00021	0.00135	0.00120
Zn	0.0064	0.0085	0.0092	0.0036	0.0021
NH_3-N	2.67	2.64	2.89	0.838	0.650
Cl	10	6	6	5	5
F	<0.05	0.06	<0.05	<0.05	0.06
NO_3-N	2.30	<0.006	0.098	0.242	0.293
NO_2-N	4.52	0.006	0.009	0.059	0.004
PO_4-P	0.001	0.005	0.015	0.012	0.025
SO_4	2850	1060	1440	1490	168
DIC	7.4	6.8	7.2	15.4	12.4
DOC	8.4	5.2	7.3	14.4	4.8

July 2002 LLCF Water Samples

Solution #			64	65	66	67	68
Sample			**02-DW1**	**02-DD1**	**02-LLAW1**	**02-LLEW1**	**02-LLCW1**
	units	**d.l**		(dup. of DW145)		(dup. of LLA145)	
Sample Date			09-Jul-02	09-Jul-02	08-Jul-02	08-Jul-02	08-Jul-02
Temperature	°C		20.25	20.25	19.57	19.57	14.07
pH			7.74	7.74	7.33	7.33	6.66
Alkalinity	mg/L CaCO$_3$		59.6	59.6	49.6	49.6	62
DO	mg/L		7.84	7.84	17.04	17.04	7.85
Conductivity	µS/cm		1134	1134	5390	5390	1822
Ag	mg/L	0.002	0.0003	0.0004	<0.002	<0.002	<0.002
Al	mg/L	0.01	<0.01	<0.01	<0.01	<0.01	<0.01
As	mg/L	0.0004	0.0069	0.0071	0.0044	0.0042	0.0041
B	mg/L	0.002	0.061	0.062	0.031	0.032	0.037
Ba	mg/L	0.0001	0.101	0.101	0.0254	0.0258	0.027
Be	mg/L	0.0005	<0.0005	<0.0005	<0.0005	<0.0005	<0.0005
Ca	mg/L	0.5	54.0	54.1	431	438	90.1
Cd	mg/L	0.0001	0.0012	0.0011	0.0026	0.0026	0.0013
Co	mg/L	0.0001	0.0007	0.0007	0.003	0.0029	0.0004
Cr	mg/L	0.0004	<0.0004	<0.0004	<0.0004	<0.0004	<0.0004
Cu	mg/L	0.0006	0.0009	0.001	0.0042	0.0051	0.0154
Fe	mg/L	0.005	0.022	0.018	0.012	0.013	0.007
Hg	mg/L	0.0001	<0.0001	<0.0001	<0.0001	<0.0001	<0.0001
K	mg/L	0.1	70.6	81.2	41.8	42.5	17.7
Mg	mg/L	0.01	89.9	90.2	774	786	143
Mn	mg/L	0.001	0.035	0.035	0.153	0.156	0.039
Mo	mg/L	0.0001	0.53	0.544	1.32	1.31	0.637
Na	mg/L	0.5	22.4	22.5	19.4	19.9	9.7
Ni	mg/L	0.0001	0.0393	0.0394	0.448	0.431	0.0706
Pb	mg/L	0.0001	<0.0001	<0.0001	<0.0001	0.0003	0.0004
Sb	mg/L	0.0004	0.0158	0.016	0.0038	0.0038	0.0053
Se	mg/L	0.0004	0.0034	0.0037	0.0086	0.0078	0.0014
Si	mg/L	0.1	4.9	4.9	6.2	6.3	5.9
Sr	mg/L	0.0001	0.971	0.964	5.1	5.04	1.12
U	mg/L	0.0001	0.0004	0.0005	0.0014	0.0014	0.001
V	mg/L	0.0001	0.003	0.0029	0.0047	0.0045	0.0068
Zn	mg/L	0.002	0.011	0.009	0.023	0.026	0.031
NH$_3$-N	mg/L	0.005	1.51	1.54	0.3	0.329	0.336
Cl	mg/L	1	55	55	7	7	6
F	mg/L	0.05	0.07	0.08	NA	NA	NA
NO$_3$-N	mg/L	0.006	0.052	6.53	71.1	84.2	2.89
NO$_2$-N	mg/L	0.002	0.004	0.335	0.9	1.18	0.042
PO$_4$-P	mg/L	0.001	0.001	0.032	0.024	0.028	0.006
SO$_4$	mg/L	0.05	474	472	4080	4080	711
DIC	mg/L	0.5	NA	NA	NA	NA	NA
DOC	mg/L	0.5	15.7	13.6	18.8	18.9	21.4

July 2002 LLCF Water Samples (cont'd)

Solution # **Sample**	70 **02-LLGW1**	71 **02-LLKW1**	72 **02-LLMW1**	73 **02-LLDW1** (dup. of LLM145)	74 **02-UBW1**	75 **02-UDW1** (dup. of UC145)	76 **02-UCW1**
Sample Date	07-Jul-02	08-Jul-02	07-Jul-02	07-Jul-02	04-Jul-02	04-Jul-02	04-Jul-02
Temperature	13.17	15.07	12.27	12.27	15.67	16.35	16.35
pH	7.54	7.11	7.26	7.26	8.83	8.08	8.08
Alkalinity	84.8	39.4	76	76	52.4	43.6	43.6
DO	6.36	6.67	7.08	7.08	10.46	9.99	9.99
Conductivity	1509	2997	2214	2214	431	324	324
Ag	0.0005	<0.002	<0.002	0.0008	<0.0001	<0.0001	<0.0001
Al	<0.01	0.01	<0.01	<0.01	0.0043	0.0034	0.005
As	0.0044	0.0034	0.0056	0.0055	0.00342	0.00433	0.00435
B	0.045	0.033	0.028	0.031	0.029	0.031	0.03
Ba	0.0307	0.0267	0.0252	0.025	0.105	0.147	0.148
Be	<0.0005	<0.0005	<0.0005	<0.0005	<0.0002	<0.0002	<0.0002
Ca	119	203	223	201	13.3	17.8	17.9
Cd	0.001	0.0025	0.003	0.0026	0.00028	0.00057	0.00066
Co	0.0012	0.0014	0.0009	0.0009	0.0001	0.0003	0.0003
Cr	<0.0004	<0.0004	<0.0004	<0.0004	0.00032	0.00082	0.00097
Cu	0.0032	0.0047	0.0041	0.0037	0.0012	0.0024	0.0046
Fe	<0.005	0.029	0.012	0.005	0.006	0.005	0.006
Hg	<0.0001	<0.0001	<0.0001	<0.0001	0.00003	0.00005	0.00005
K	26.9	35.6	30	30.3	22.6	33.7	34
Mg	213	358	373	355	23.3	30.5	30.7
Mn	0.091	0.097	0.065	0.06	0.0011	0.0041	0.004
Mo	0.459	1.28	1.25	1.21	0.154	0.21	0.208
Na	10.7	14.4	14.2	15.4	5.37	12.3	12.5
Ni	0.118	0.208	0.17	0.164	0.0102	0.018	0.018
Pb	0.0001	0.0001	<0.0001	<0.0001	0.00006	0.00006	0.00008
Sb	0.0044	0.0042	0.0048	0.0048	0.00465	0.00979	0.00963
Se	0.0023	<0.0004	0.0024	0.0023	0.0005	0.0008	0.0009
Si	7	5.8	6.3	6	1.80	2.00	2.00
Sr	1.54	2.62	2.64	2.7	0.235	0.357	0.359
U	0.0017	0.0005	0.0011	0.0011	0.00014	0.00028	0.00028
V	0.004	0.0099	0.0079	0.0073	0.00149	0.00135	0.00138
Zn	0.011	0.02	0.012	0.012	0.0021	0.0025	0.0051
NH_3-N	0.071	0.013	0.515	0.484	0.006	0.405	0.4
Cl	4	4	3	3	9	43	42
F	NA	NA	NA	NA	NA	NA	NA
NO_3-N	5.15	0.977	1.47	1.45	0.696	4.33	4.41
NO_2-N	0.036	0.015	0.038	0.025	0.097	0.183	0.186
PO_4-P	0.02	0.009	0.032	0.033	0.001	<0.001	<0.001
SO_4	1050	2040	1970	1990	103	118	111
DIC	NA	NA	NA	NA	NA	NA	NA
DOC	13	16.9	15.6	18.6	19.2	16.8	17.9

August 2002 LLCF Water Analyses

Solution #			77	78	79	80	81
Sample			**02-DW2**	**02-LLAW2**	**02-LLCW2**	**02-LLDW2**	**02-LLGW2**
	units	**d.l**				(dup. of LLC245)	
Sample Date			25-Aug-02	12-Aug-02	12-Aug-02	12-Aug-02	12-Aug-02
Temperature	°C		20.81	8.52	10.09	10.09	11.03
pH			7.88	5.8	7.32	7.32	7.55
Alkalinity	mg/L $CaCO_3$		101.6	67.6	88.4	88.4	112.8
DO	mg/L		5.6	8.52	8.62	8.62	11.04
Conductivity	µS/cm		695	5510	2278	2278	2420
Ag	mg/L	0.002	0.0008	<0.0002	<0.0002	<0.0002	0.0003
Al	mg/L	0.01	<0.01	<0.01	0.01	<0.01	<0.01
As	mg/L	0.0004	0.0142	0.0048	0.004	0.0044	0.0046
B	mg/L	0.002	0.086	0.028	0.028	0.041	0.041
Ba	mg/L	0.0001	0.116	0.0197	0.0302	0.0235	0.0243
Be	mg/L	0.0005	<0.0005	<0.0005	<0.0005	<0.0005	<0.0005
Ca	mg/L	0.5	23	420	186	160	79.3
Cd	mg/L	0.0001	0.0019	0.0027	0.001	0.0009	0.001
Co	mg/L	0.0001	0.0008	0.0039	0.0017	0.0019	0.0019
Cr	mg/L	0.0004	<0.0004	<0.0004	<0.0004	<0.0004	<0.0004
Cu	mg/L	0.0006	0.0025	0.0048	0.0069	0.0043	0.0037
Fe	mg/L	0.005	0.012	<0.005	0.014	<0.005	<0.005
Hg	mg/L	0.0001	NA	NA	NA	NA	NA
K	mg/L	0.1	102	42.9	21.4	28.5	14.5
Mg	mg/L	0.01	52.7	790	273	279	138
Mn	mg/L	0.001	0.021	0.172	0.11	0.124	0.063
Mo	mg/L	0.0001	0.99	1.3	0.966	0.417	0.407
Na	mg/L	0.5	19.4	19.1	12.2	10	4.5
Ni	mg/L	0.0001	0.0634	0.467	0.197	0.162	0.156
Pb	mg/L	0.0001	0.0004	<0.0001	0.0001	0.0001	<0.0001
Sb	mg/L	0.0004	0.0431	0.0041	0.0042	0.0043	0.0044
Se	mg/L	0.0004	0.0046	0.0224	0.0045	0.0043	0.0044
Si	mg/L	0.1	3.4	7.1	7.2	7.8	3.9
Sr	mg/L	0.0001	0.709	5.23	2.09	2.04	2.11
U	mg/L	0.0001	0.0004	0.0018	0.0019	0.0027	0.0026
V	mg/L	0.0001	0.0045	0.0022	0.0031	0.002	0.002
Zn	mg/L	0.002	0.011	0.017	0.031	0.012	0.01
NH_3-N	mg/L	0.005	0.999	<0.005	<0.005	<0.005	<0.005
Cl	mg/L	1	74	5	4	5	5
F	mg/L	0.05	0.06	NA	NA	NA	NA
NO_3-N	mg/L	0.006	6.44	80.5	12.8	10.7	10.5
NO_2-N	mg/L	0.002	1.64	0.311	0.012	0.01	0.01
PO_4-P	mg/L	0.001	0.007	0.014	0.013	0.003	0.004
SO_4	mg/L	0.05	234	3300	1440	1050	1340
DIC	mg/L	0.5	17.5	15	19.2	23.4	23.7
DOC	mg/L	0.5	8.9	18.1	14.3	10.7	12.6

August 2002 LLCF Water Analyses (cont'd)

Solution # **Sample**	82 **02-LLEW2** (dup. of LLG245)	83 **02-LLMW2**	84 **02-UBW2**	85 **02-UCW2**	86 **02-UDW2** (dup. of UC245)
Sample Date	12-Aug-02	12-Aug-02	13-Aug-02	17-Aug-02	17-Aug-02
Temperature	11.03	9.61	11.87	11.09	11.09
pH	7.55	7.65	8.11	6.71	6.71
Alkalinity	112.8	79.4	61.6	51.4	51.4
DO	11.04	9.06	11.8	10.82	10.82
Conductivity	2420	3226	529	565	565
Ag	0.0004	<0.0002	<0.0002	<0.0002	<0.0002
Al	<0.01	0.16	0.0036	0.0052	0.006
As	0.0041	0.006	0.00387	0.00301	0.00313
B	0.031	0.026	0.033	0.029	0.032
Ba	0.0321	0.0192	0.112	0.127	0.13
Be	<0.0005	<0.0005	<0.0005	<0.0005	<0.0005
Ca	188	210	15.3	20.2	20.7
Cd	0.0019	0.0023	0.00042	0.00036	0.00037
Co	0.0016	0.001	0.0003	0.0002	0.0002
Cr	<0.0004	<0.0004	0.00055	0.0008	0.00074
Cu	0.0059	0.0047	0.0039	0.0015	0.002
Fe	<0.005	0.007	0.01	0.007	<0.005
Hg	NA	NA	0.00006	0.00005	0.00006
K	21.5	27.5	35.6	32.4	6.41
Mg	276	343	30.2	31.3	32.4
Mn	0.113	0.06	0.0085	0.0023	0.0022
Mo	1.02	1.08	0.22	0.184	0.19
Na	12.3	13.2	8.67	13.3	13.7
Ni	0.196	0.156	0.0223	0.0156	0.0163
Pb	0.0001	<0.0001	0.00009	<0.0001	<0.0001
Sb	0.0043	0.0052	0.0076	0.00758	0.00792
Se	0.0048	0.0054	0.0006	0.0006	0.0006
Si	7.3	6.6	2.4	1.7	0.3
Sr	2.18	2.91	0.307	0.379	0.386
U	0.002	0.0011	0.00013	0.00051	0.00052
V	0.0034	0.0021	0.00133	0.00101	0.00102
Zn	0.03	0.014	0.0054	0.0045	0.0049
NH_3-N	<0.005	0.13	<0.005	0.149	0.151
Cl	4	4	21	48	49
F	NA	NA	NA	NA	NA
NO_3-N	13.3	12.7	1.86	4.49	1.81
NO_2-N	0.006	0.049	0.203	0.131	0.183
PO_4-P	0.012	0.022	<0.001	<0.001	<0.001
SO_4	787	1970	124	111	118
DIC	19	18.7	13.1	12.8	13
DOC	13.6	11.9	14.4	11.9	8.9

C) Field Blank Analyses

Solution #			87	88	89
	units	**d.l.**	**00-FB1**	**00-FB2**	**01-FB1**
Year sampled			2000	2000	2001
Ag	mg/L	0.0001	<0.0001	<0.0001	<0.0001
Al	mg/L	0.0003	0.0054	0.012	0.0139
As	mg/L	0.00003	<0.00003	<0.00003	<0.00003
B	mg/L	0.001	<0.001	<0.001	<0.001
Ba	mg/L	0.00005	0.00053	0.00095	0.00137
Be	mg/L	0.0002	<0.0002	<0.0002	<0.0002
Ca	mg/L	0.004	0.066	0.046	0.08
Cd	mg/L	0.00005	<0.00005	<0.00005	<0.00005
Co	mg/L	0.0001	<0.0001	<0.0001	<0.0001
Cr	mg/L	0.00006	0.00073	0.00076	0.00023
Cu	mg/L	0.0006	<0.0006	<0.0006	<0.0006
Fe	mg/L	0.005	0.039	0.05	0.038
Hg	mg/L	0.00002	<0.00002	<0.00002	<0.00002
K	mg/L	0.005	0.052	0.074	<0.005
Mg	mg/L	0.004	0.135	0.118	0.162
Mn	mg/L	0.0001	0.0006	0.0009	0.0011
Mo	mg/L	0.00006	0.00052	0.00041	<0.00006
Na	mg/L	0.005	<0.005	0.005	<0.005
Ni	mg/L	0.00006	0.00056	0.00084	0.00113
Pb	mg/L	0.00005	<0.00005	<0.00005	<0.00005
Sb	mg/L	0.00003	0.00022	0.00017	<0.00003
Se	mg/L	0.0001	<0.0001	<0.0001	<0.0001
Si	mg/L	0.1	NA	NA	0.2
Sr	mg/L	0.0001	0.0008	0.0006	0.001
U	mg/L	0.00005	<0.00005	<0.00005	<0.00005
V	mg/L	0.00005	<0.00005	0.00005	<0.00005
Zn	mg/L	0.0008	0.0013	<0.0008	<0.0008
NH3-N	mg/L	0.005	<0.005	<0.005	0.114
Cl	mg/L	0.05	<0.05	<0.05	<1
F	mg/L	0.05	<0.05	<0.05	<0.05
NO3-N	mg/L	0.006	<0.006	<0.006	<0.006
NO2-N	mg/L	0.002	<0.002	<0.002	<0.002
PO4-P	mg/L	0.001	<0.001	0.001	0.003
SO4	mg/L	0.05	<0.05	<0.05	0.1
DIC	mg/L	0.5	<0.5	<0.5	<0.5
DOC	mg/L	0.5	<0.5	0.6	0.8

Field Blank Analyses (cont'd)

Solution #	90 **01-FB2**	91 **01-FB3**	92 **02-FB1**	93 **02-FB2**	94 **02-FB3**
Year sampled	2001	2001	Jul-02	Aug-02	Aug-02
Ag	<0.0001	<0.0001	<0.0001	<0.0001	<0.0001
Al	<0.0003	0.0015	0.0005	<0.0003	0.0011
As	<0.00003	<0.00003	<0.00003	<0.00003	<0.00003
B	<0.001	0.005	<0.001	<0.001	<0.001
Ba	0.00016	<0.00005	<0.00005	<0.00005	<0.00005
Be	<0.0002	<0.0002	<0.0002	<0.0002	<0.0002
Ca	<0.004	<0.004	<0.004	<0.004	0.006
Cd	<0.00005	<0.00005	<0.00005	<0.00005	<0.00005
Co	<0.0001	<0.0001	<0.0001	<0.0001	<0.0001
Cr	<0.00006	<0.00006	<0.00006	<0.00006	<0.00006
Cu	<0.0006	<0.0006	<0.0006	<0.0006	<0.0006
Fe	<0.005	<0.005	<0.005	<0.005	<0.005
Hg	<0.00002	<0.00002	<0.00002	<0.00002	<0.00002
K	<0.005	<0.005	0.007	0.008	0.006
Mg	<0.004	<0.004	<0.004	<0.004	<0.004
Mn	<0.0001	0.0003	<0.0001	<0.0001	<0.0001
Mo	<0.00006	<0.00006	<0.00006	<0.00006	<0.00006
Na	<0.005	<0.005	<0.005	<0.005	<0.005
Ni	<0.00006	<0.00006	<0.00006	0.00009	<0.00006
Pb	<0.00005	<0.00005	<0.00005	<0.00005	<0.00005
Sb	0.00003	0.00081	0.00016	0.00041	0.00015
Se	<0.0001	<0.0001	<0.0001	<0.0001	<0.0001
Si	NA	NA	<0.1	NA	NA
Sr	<0.0001	<0.0001	<0.0001	<0.0001	<0.0001
U	<0.00005	<0.00005	<0.00005	<0.00005	<0.00005
V	<0.00005	<0.00005	<0.00005	<0.00005	<0.00005
Zn	<0.0008	0.0009	0.0012	<0.0008	<0.0008
NH3-N	NA	NA	<0.005	0.014	<0.005
Cl	NA	NA	<1	NA	<1
F	NA	NA	<0.05	NA	<0.05
NO3-N	NA	NA	<0.006	NA	<0.006
NO2-N	NA	NA	<0.002	NA	<0.002
PO4-P	NA	NA	<0.001	NA	<0.001
SO4	NA	NA	<0.05	NA	<0.05
DIC	NA	NA	NA	NA	NA
DOC	0.8	NA	<0.5	0.5	NA

Appendix B: Temporal Variation Plots

This appendix contains temporal variation plots for **(A)** processed kimberlite fines pore-water and surface water samples collected from the upstream side of **(B)** Dyke B and **(C)** Dyke C.

A) Suction lysimeter pore-water box-and-whisker plots

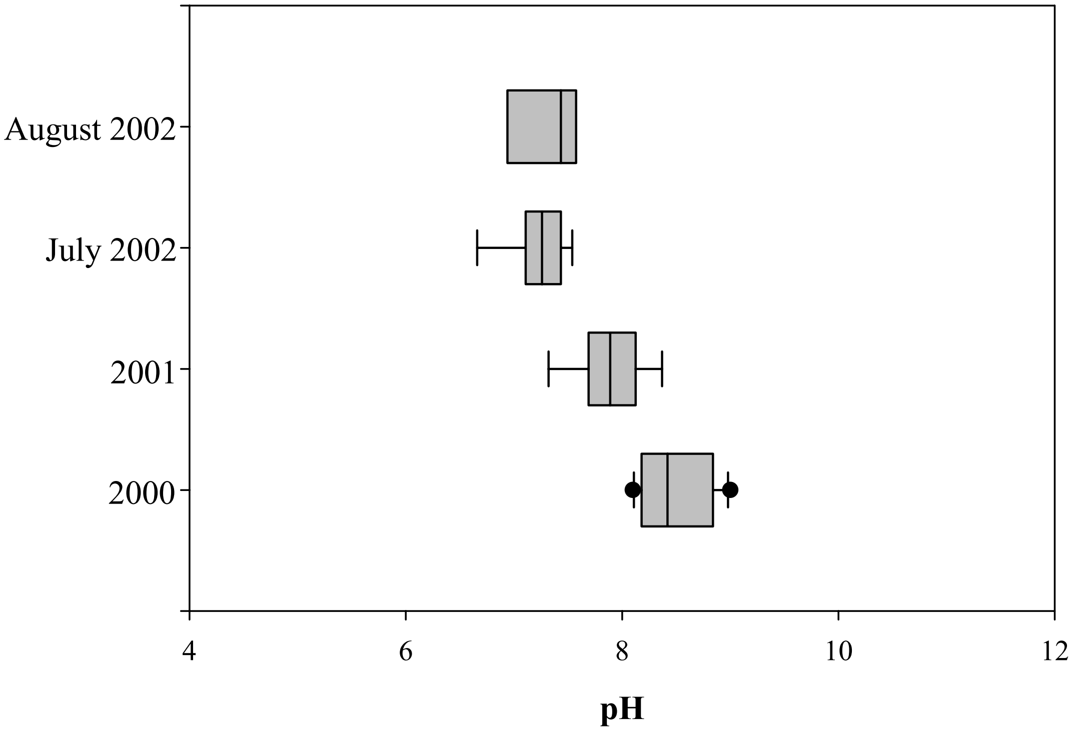

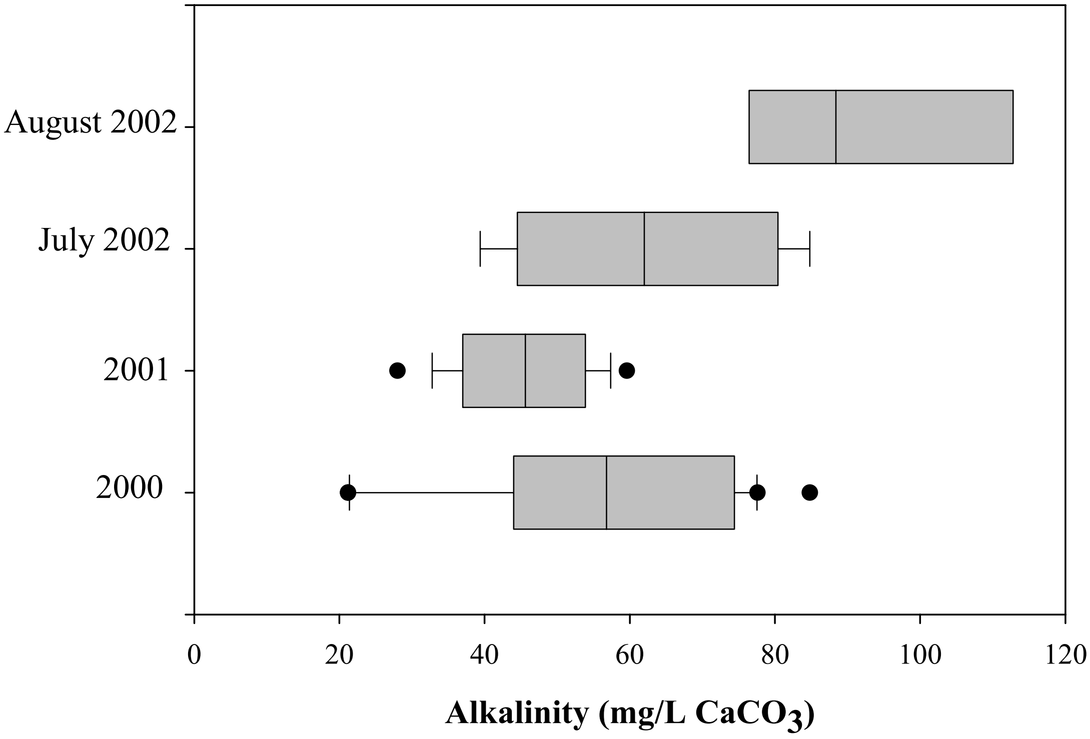

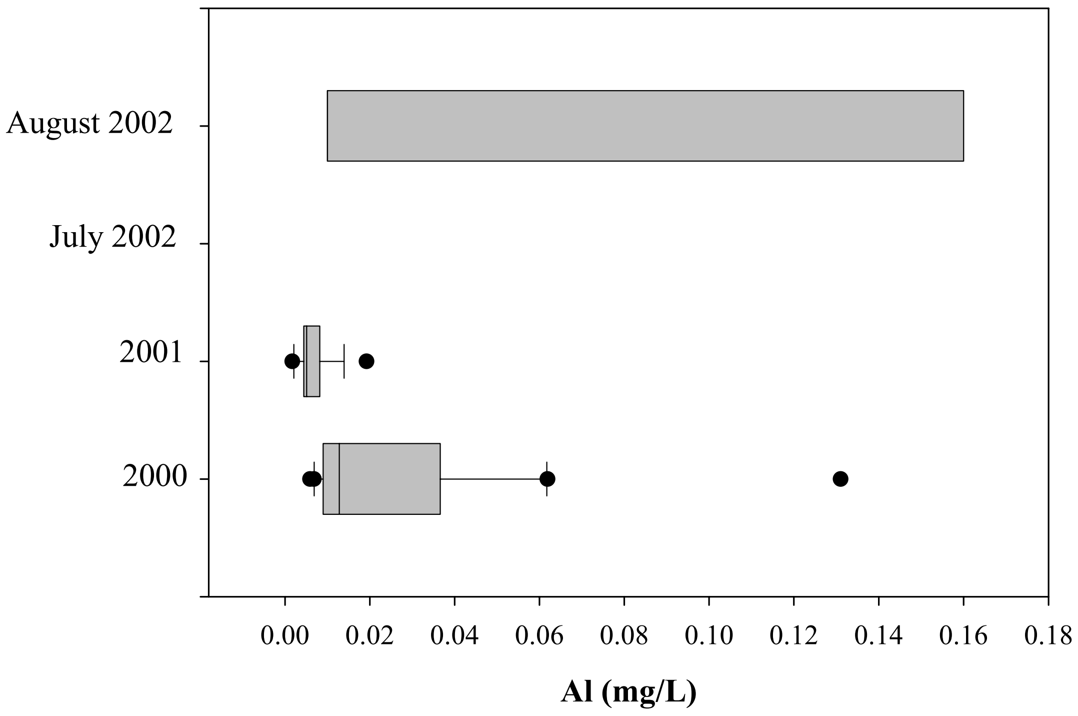
August 2002
July 2002
2001
2000
0.00
0.02
0.04
0.06
0.08
0.10
0.12
0.14
0.16
0.18
Al (mg/L)

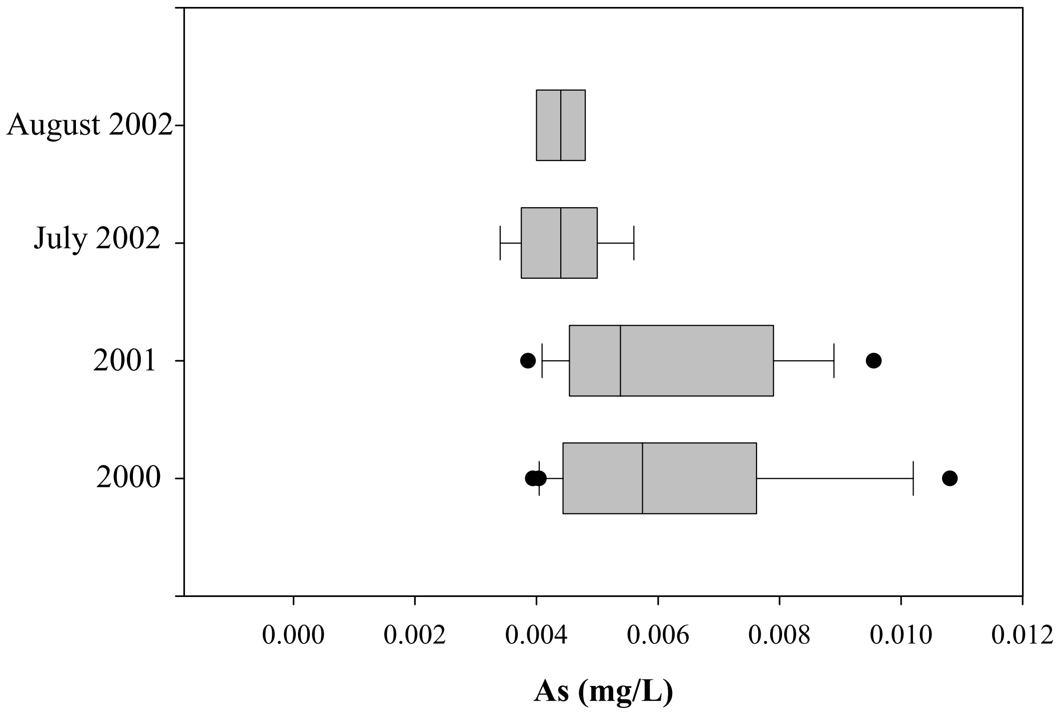
August 2002
July 2002
2001
2000
0.000
0.002
0.004
0.006
0.008
0.010
0.012
As (mg/L)

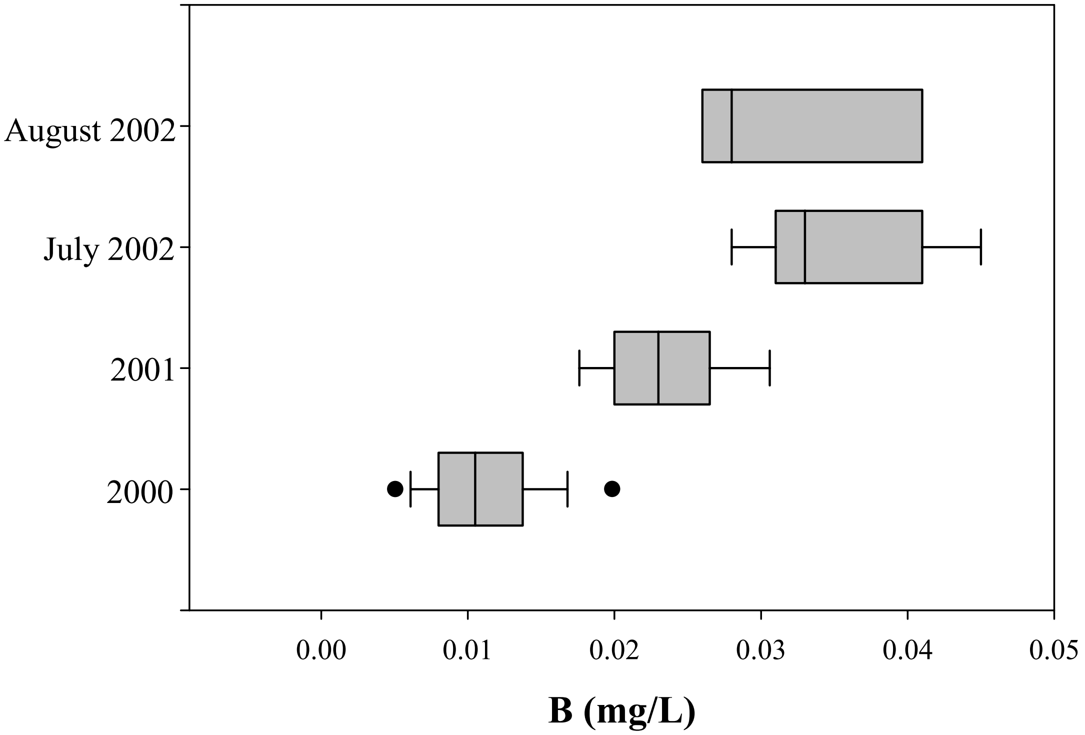
August 2002
July 2002
2001
2000
0.00
0.01
0.02
0.03
0.04
0.05
B (mg/L)

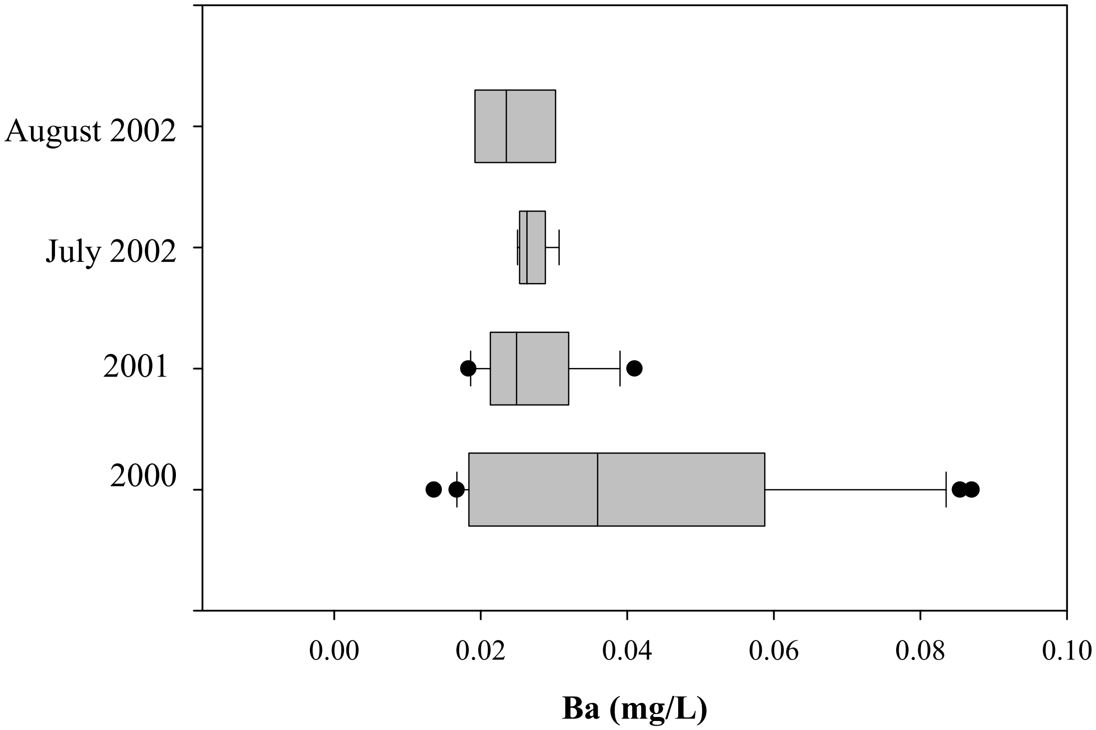
August 2002
July 2002
2001
2000
0.00
0.02
0.04
0.06
0.08
0.10
Ba (mg/L)

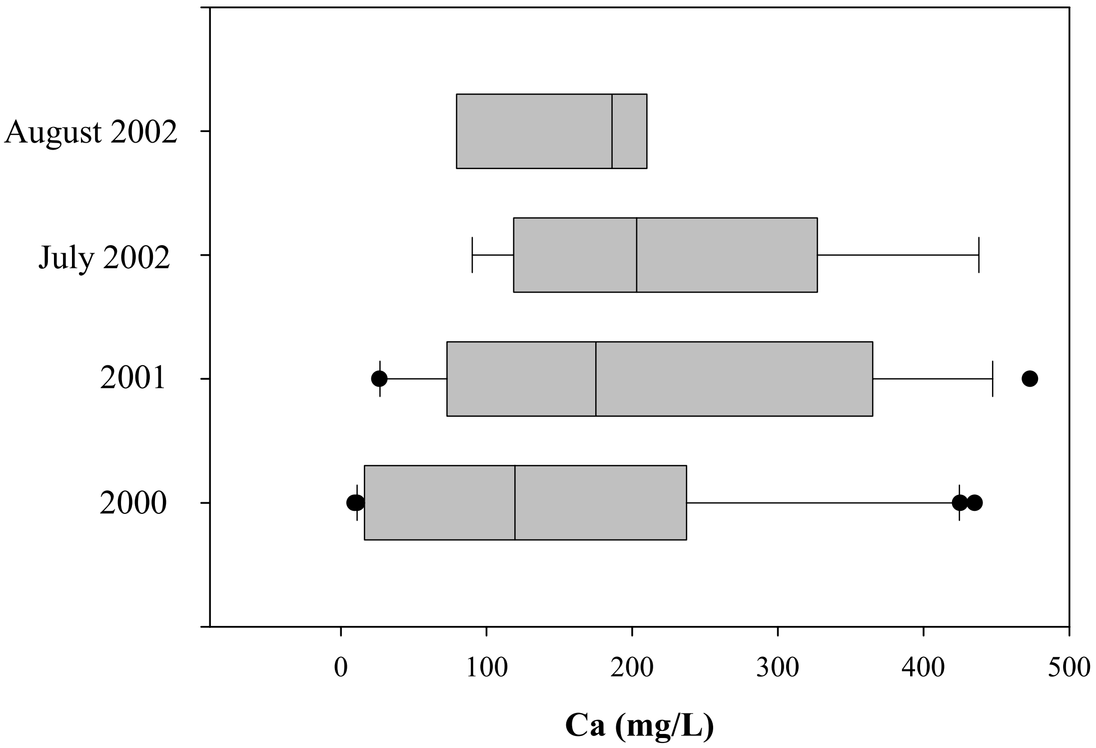
August 2002
July 2002
2001
2000
0
100
200
300
400
500
Ca (mg/L)

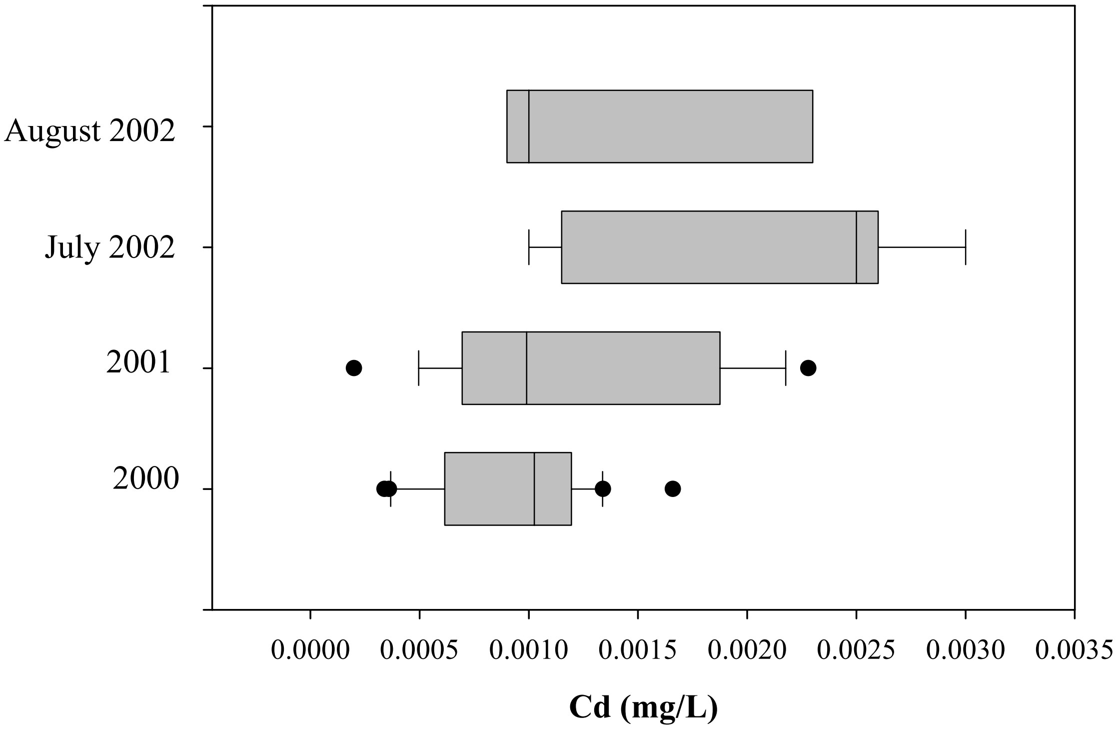
August 2002
July 2002
2001
2000
0.0000
0.0005
0.0010
0.0015
0.0020
0.0025
0.0030
0.0035
Cd (mg/L)

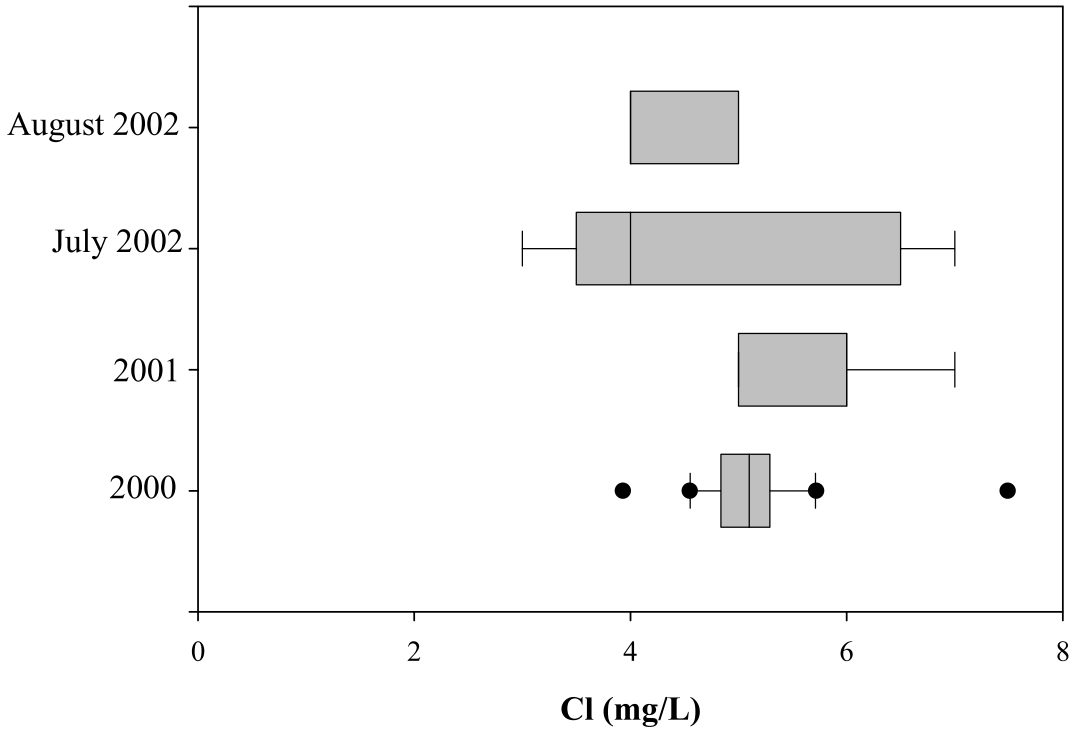
August 2002
July 2002
2001
2000
0
2
4
6
8
Cl (mg/L)

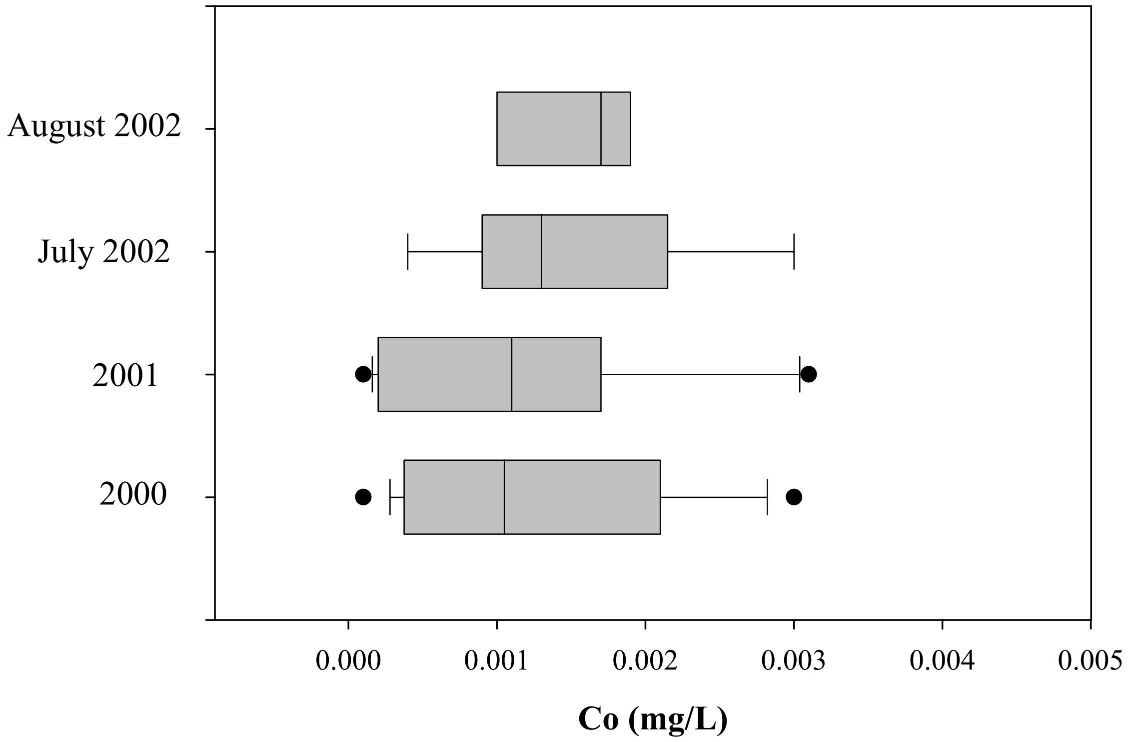
August 2002
July 2002
2001
2000
0.000
0.001
0.002
0.003
0.004
0.005
Co (mg/L)

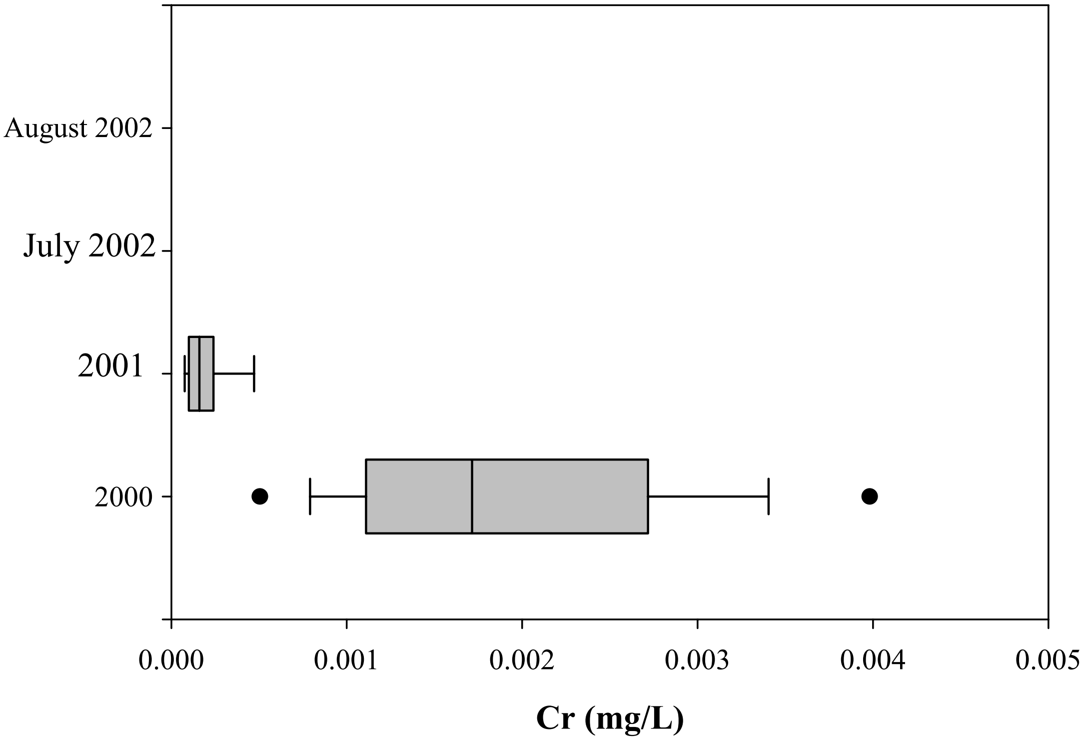
August 2002
July 2002
2001
2000
0.000
0.001
0.002
0.003
0.004
0.005
Cr (mg/L)

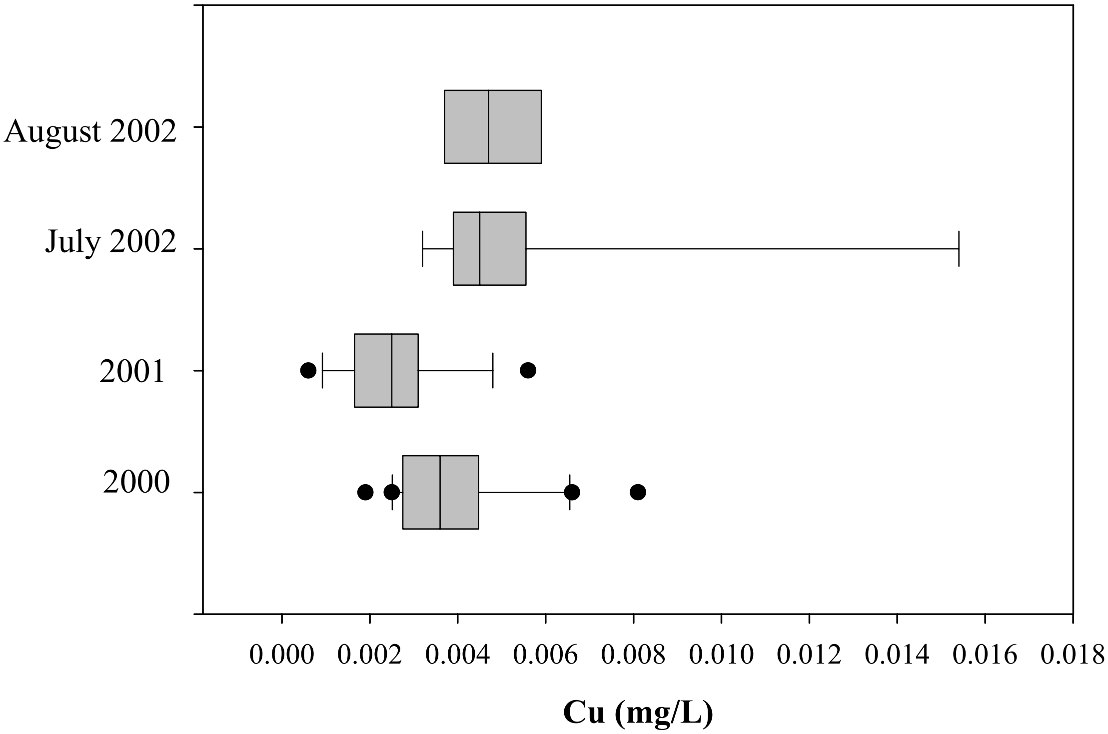
August 2002
July 2002
2001
2000
0.000
0.002
0.004
0.006
0.008
0.010
0.012
0.014
0.016
0.018
Cu (mg/L)

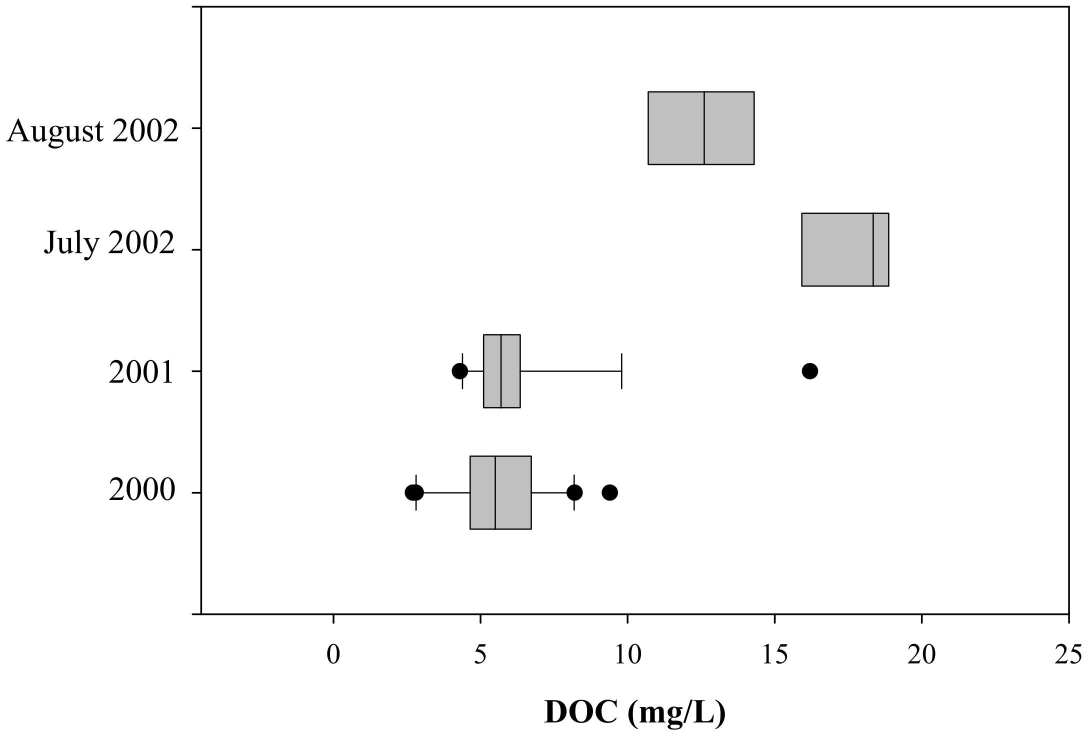
August 2002
July 2002
2001
2000
0
5
10
15
20
25
DOC (mg/L)

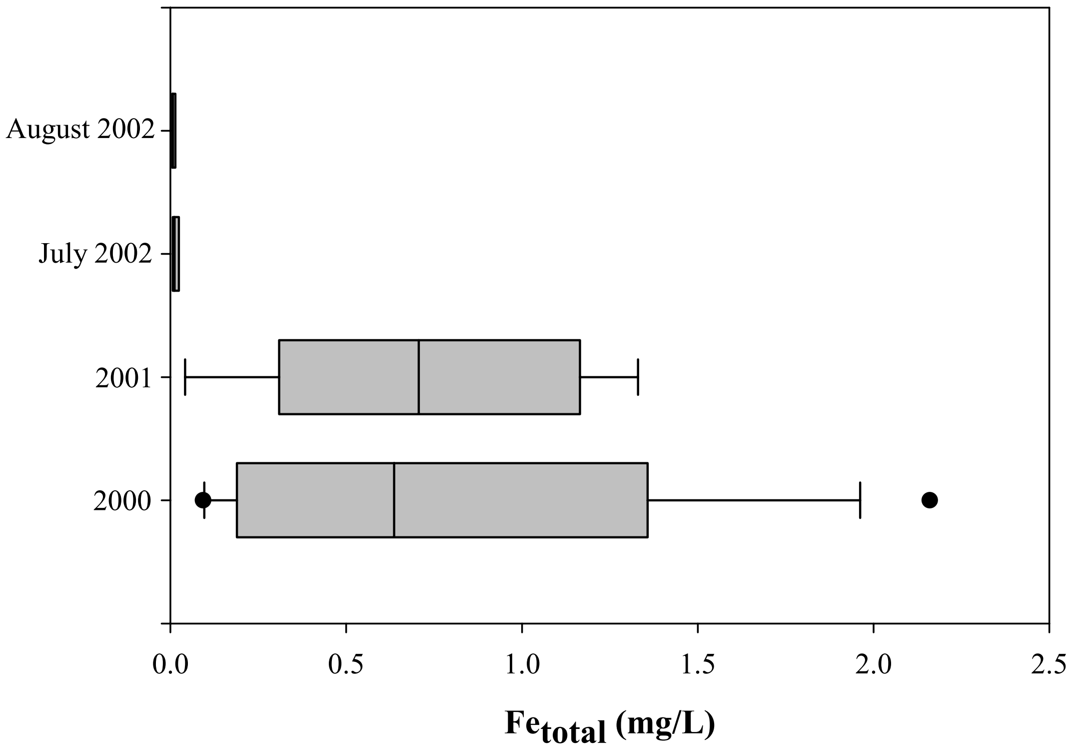
August 2002
July 2002
2001
2000
0.0
0.5
1.0
1.5
2.0
2.5
Fe$_{total}$ (mg/L)

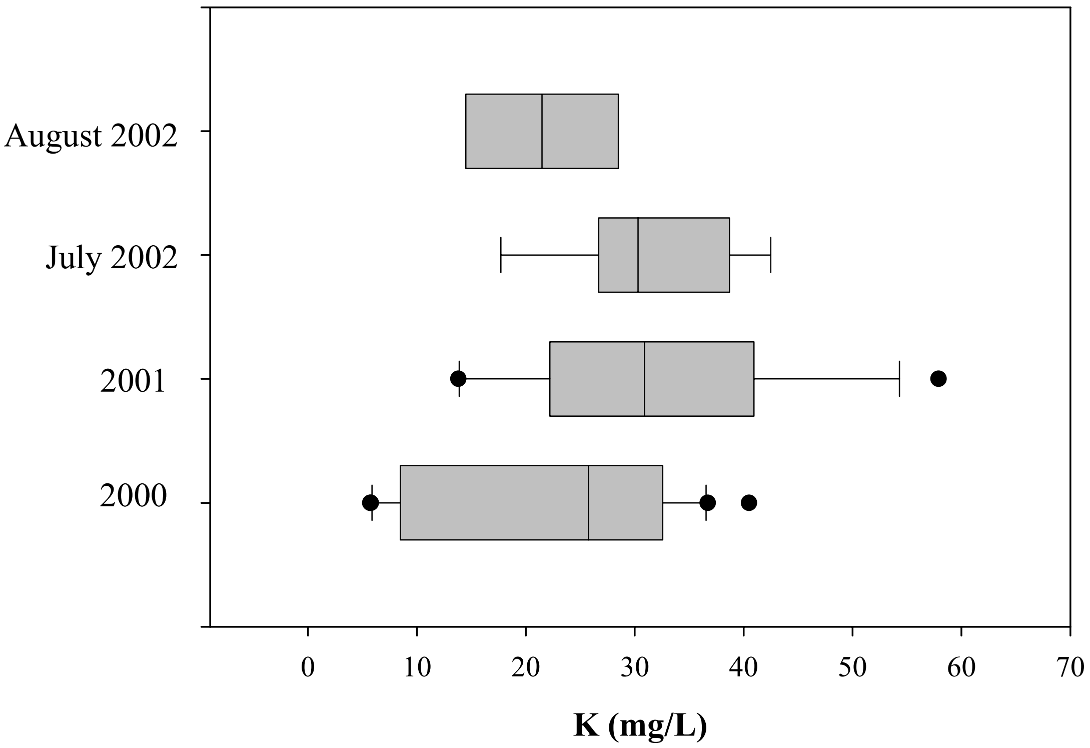
August 2002
July 2002
2001
2000
0
10
20
30
40
50
60
70
K (mg/L)

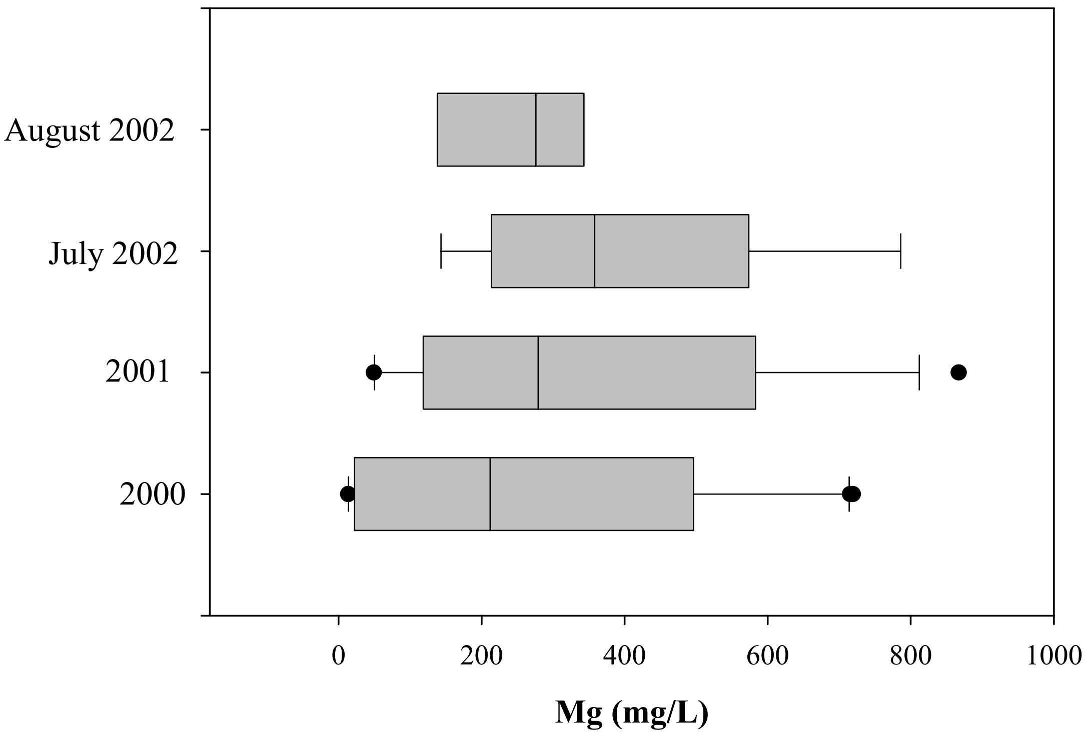
August 2002
July 2002
2001
2000
0
200
400
600
800
1000
Mg (mg/L)

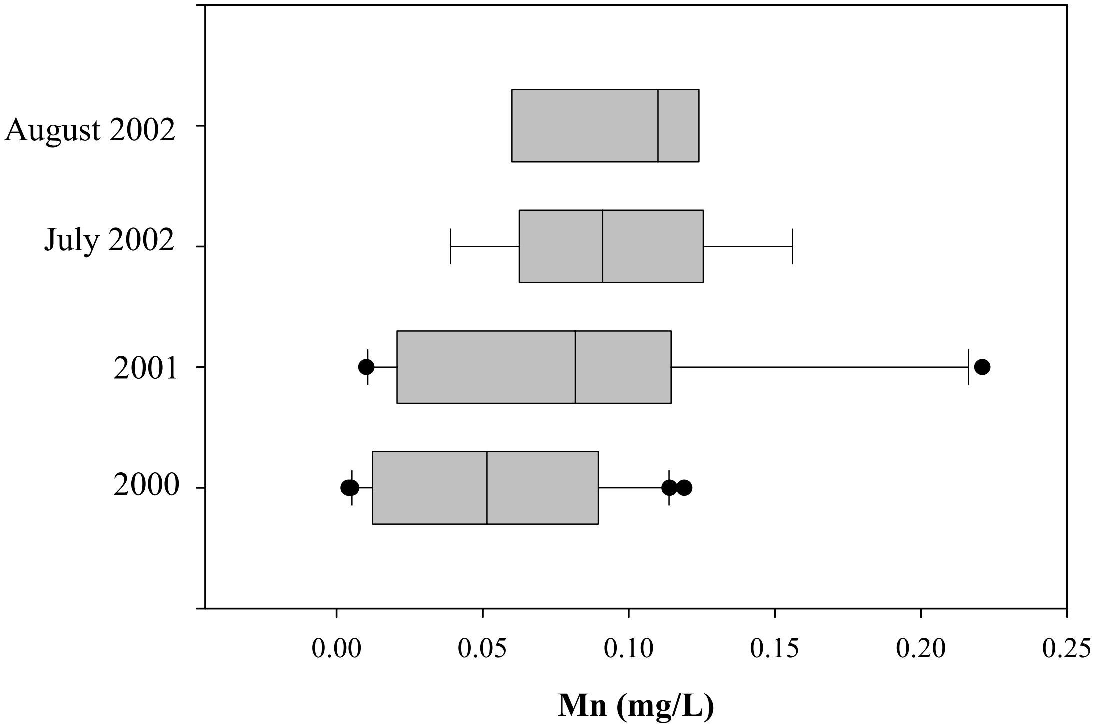

August 2002
July 2002
2001
2000
0.00
0.05
0.10
0.15
0.20
0.25
Mn (mg/L)

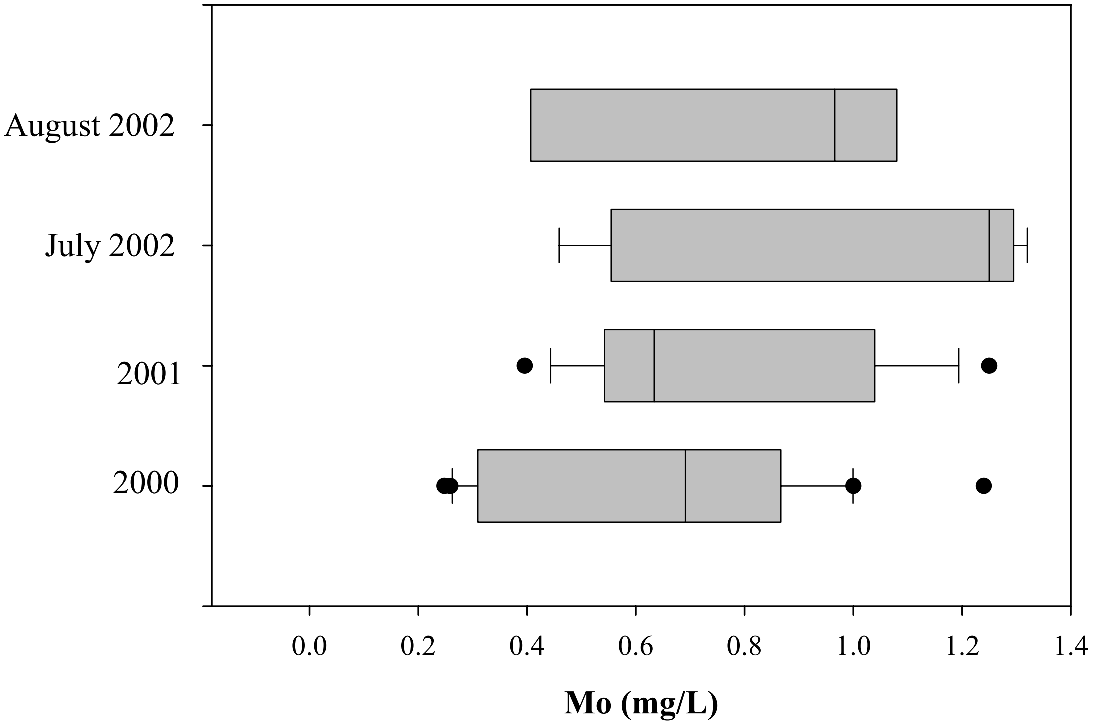

August 2002
July 2002
2001
2000
0.0
0.2
0.4
0.6
0.8
1.0
1.2
1.4
Mo (mg/L)

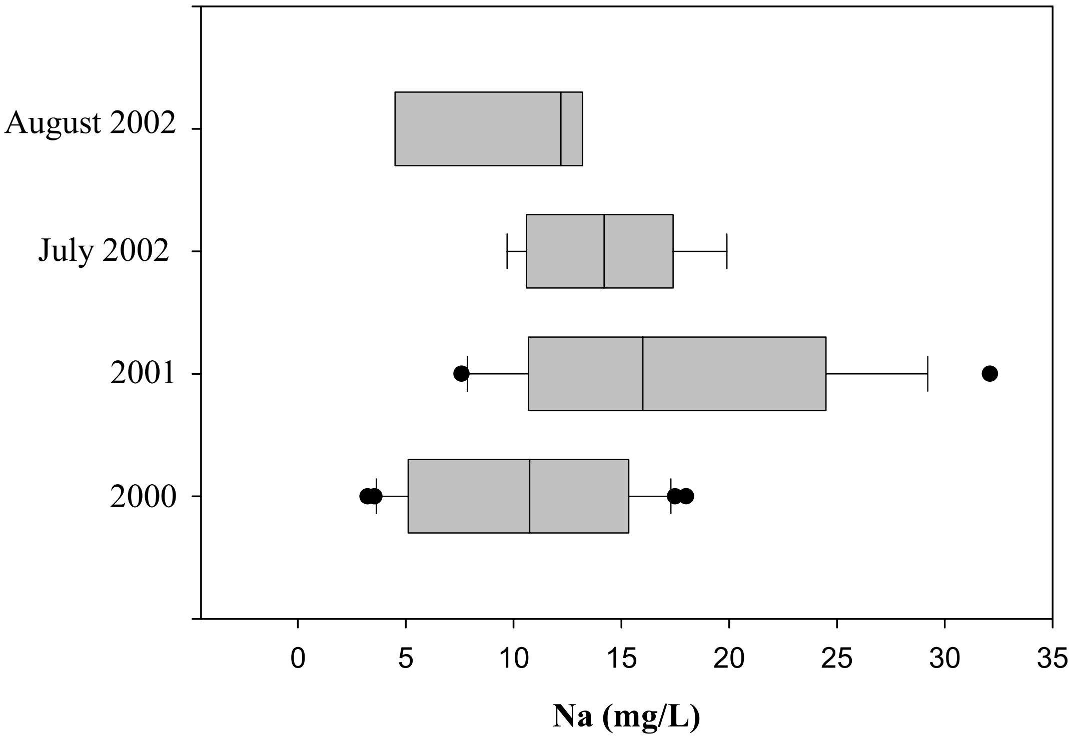
August 2002
July 2002
2001
2000
0
5
10
15
20
25
30
35
Na (mg/L)

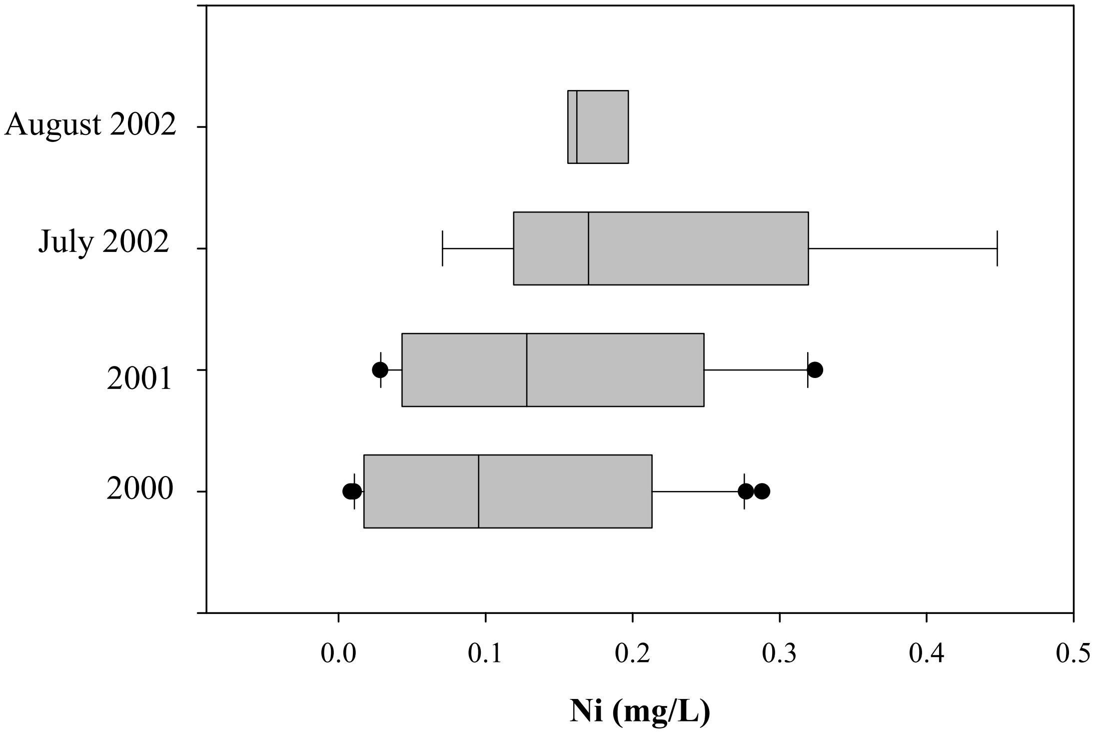
August 2002
July 2002
2001
2000
0.0
0.1
0.2
0.3
0.4
0.5
Ni (mg/L)

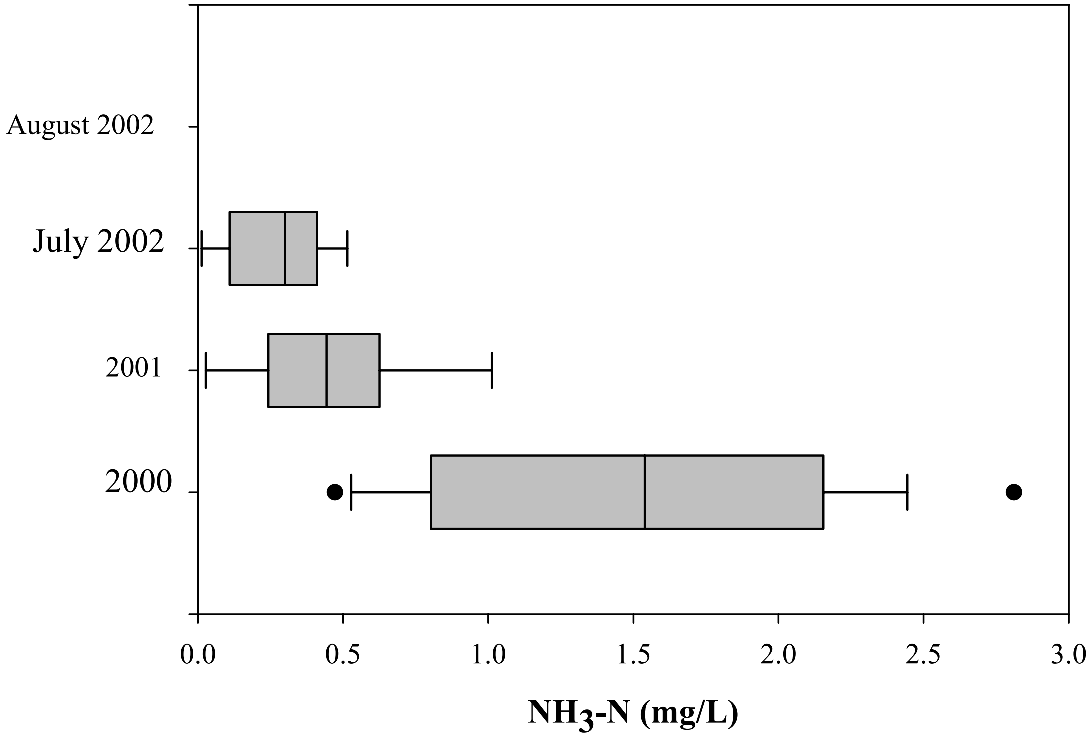
August 2002
July 2002
2001
2000
0.0
0.5
1.0
1.5
2.0
2.5
3.0
NH3-N (mg/L)

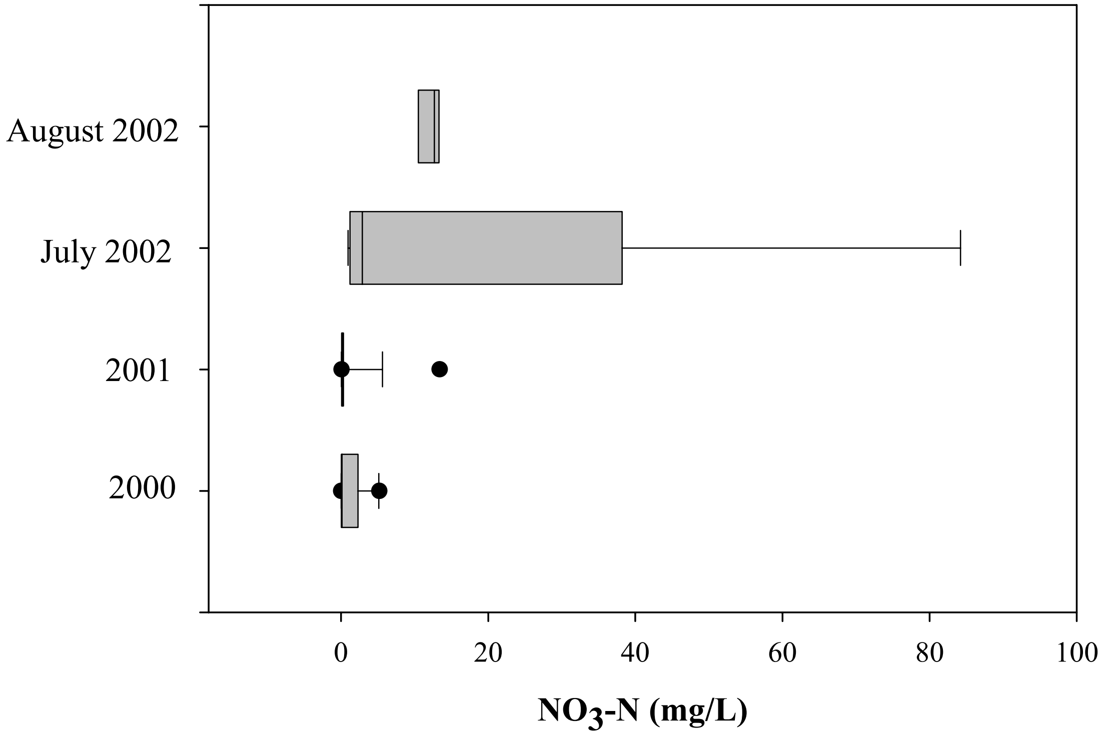
August 2002
July 2002
2001
2000
0
20
40
60
80
100
NO3-N (mg/L)

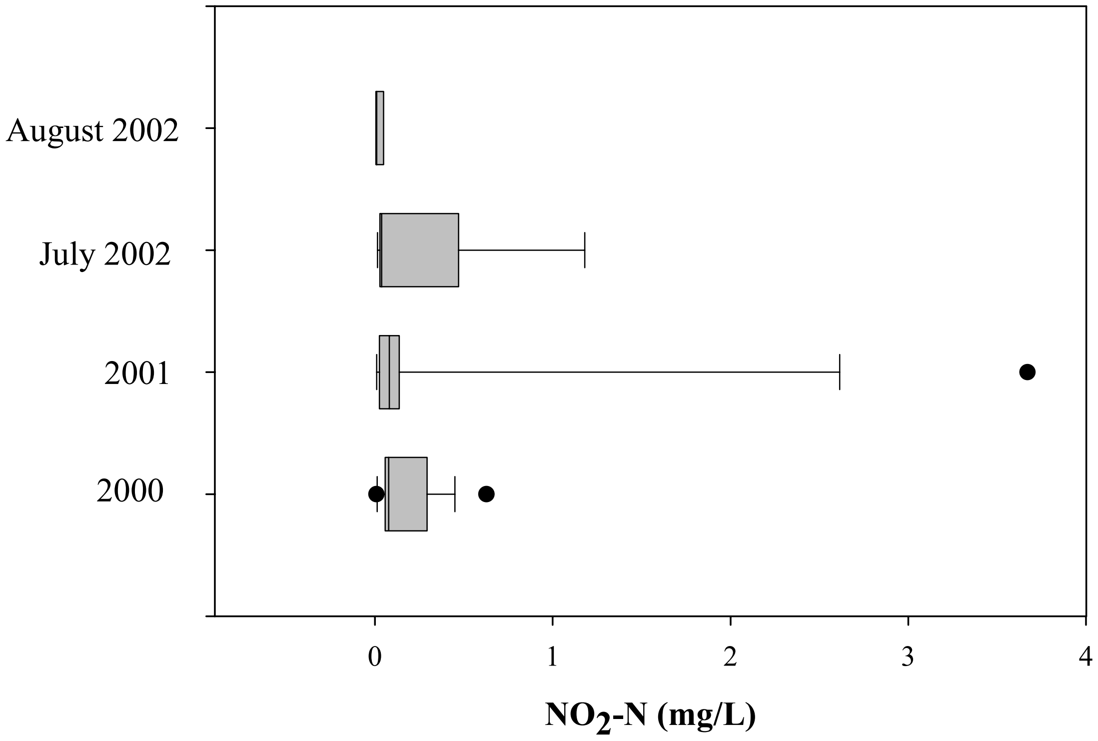
August 2002
July 2002
2001
2000
0
1
2
3
4
NO$_2$-N (mg/L)

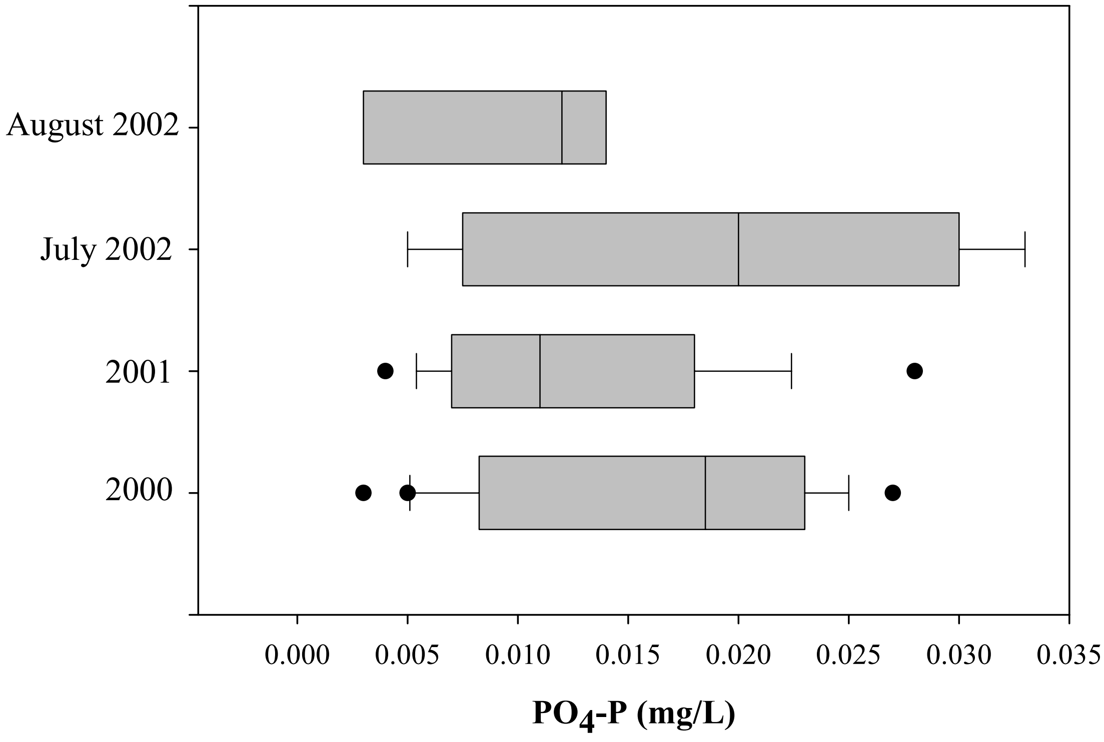
August 2002
July 2002
2001
2000
0.000
0.005
0.010
0.015
0.020
0.025
0.030
0.035
PO$_4$-P (mg/L)

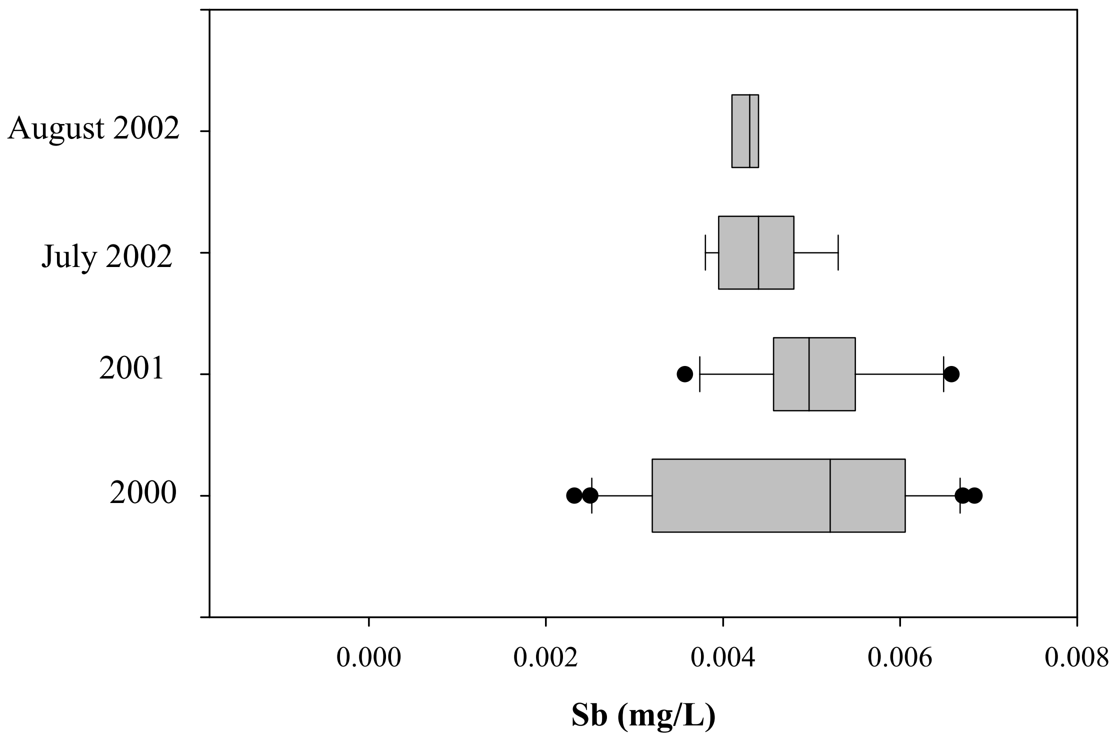
August 2002
July 2002
2001
2000
0.000
0.002
0.004
0.006
0.008
Sb (mg/L)

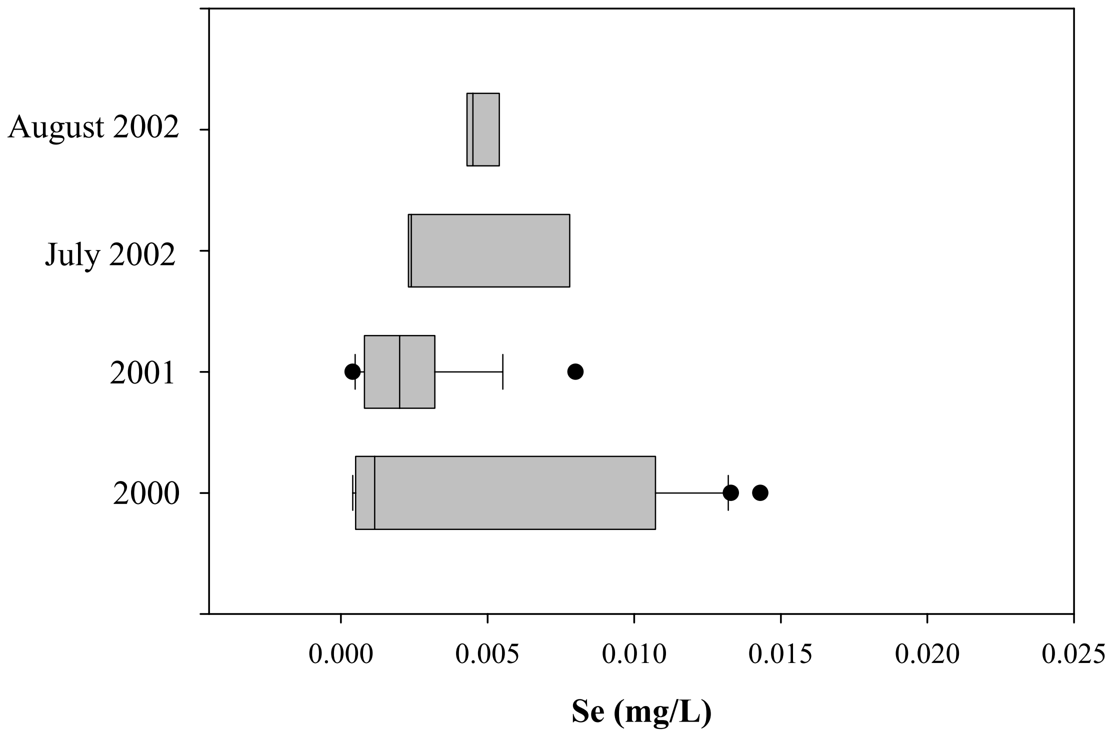
August 2002
July 2002
2001
2000
0.000
0.005
0.010
0.015
0.020
0.025
Se (mg/L)

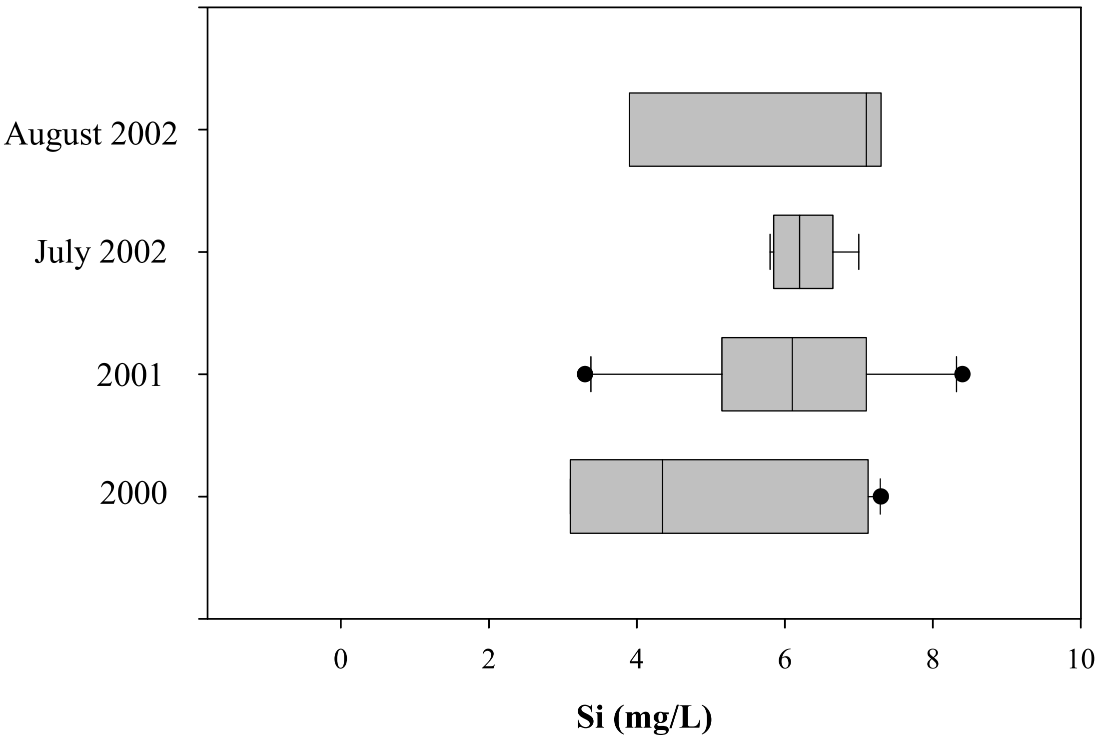
August 2002
July 2002
2001
2000
0
2
4
6
8
10
Si (mg/L)

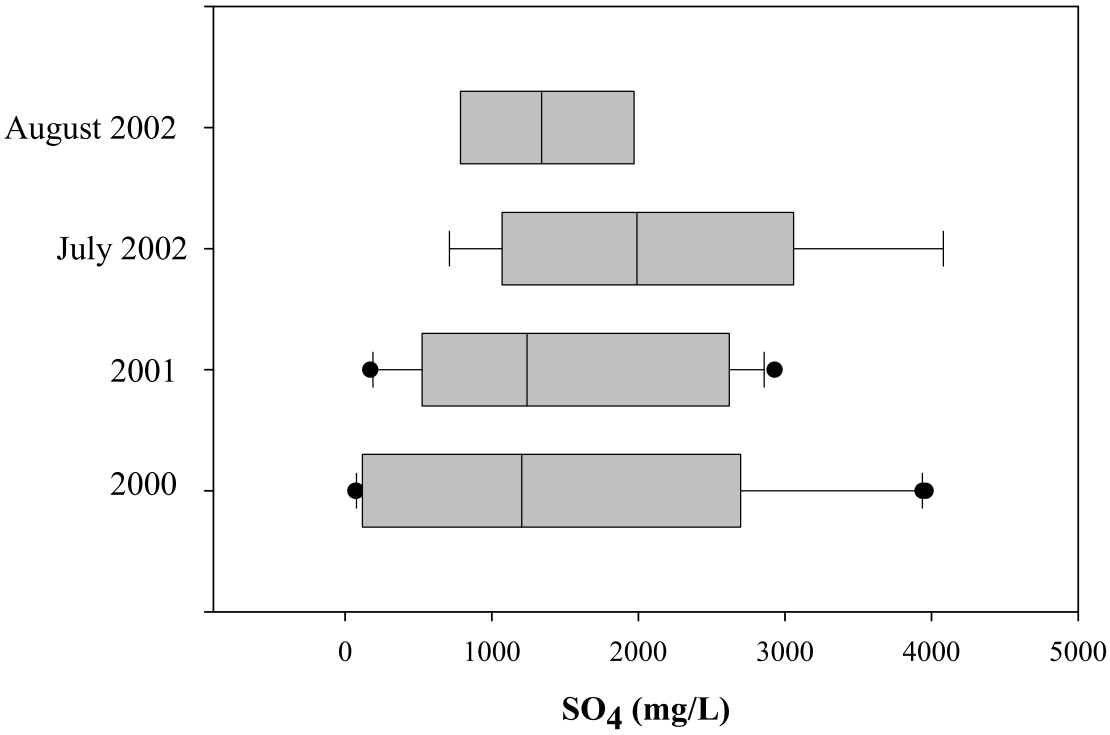
August 2002
July 2002
2001
2000
0
1000
2000
3000
4000
5000
SO4 (mg/L)

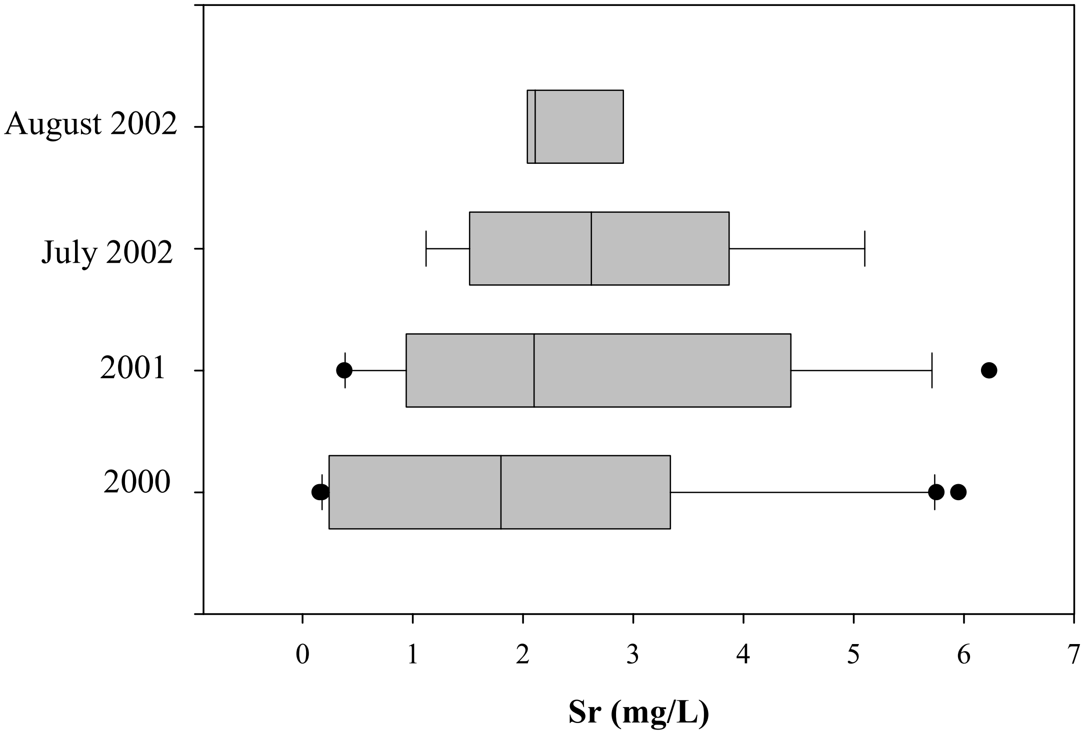
August 2002
July 2002
2001
2000
0
1
2
3
4
5
6
7
Sr (mg/L)

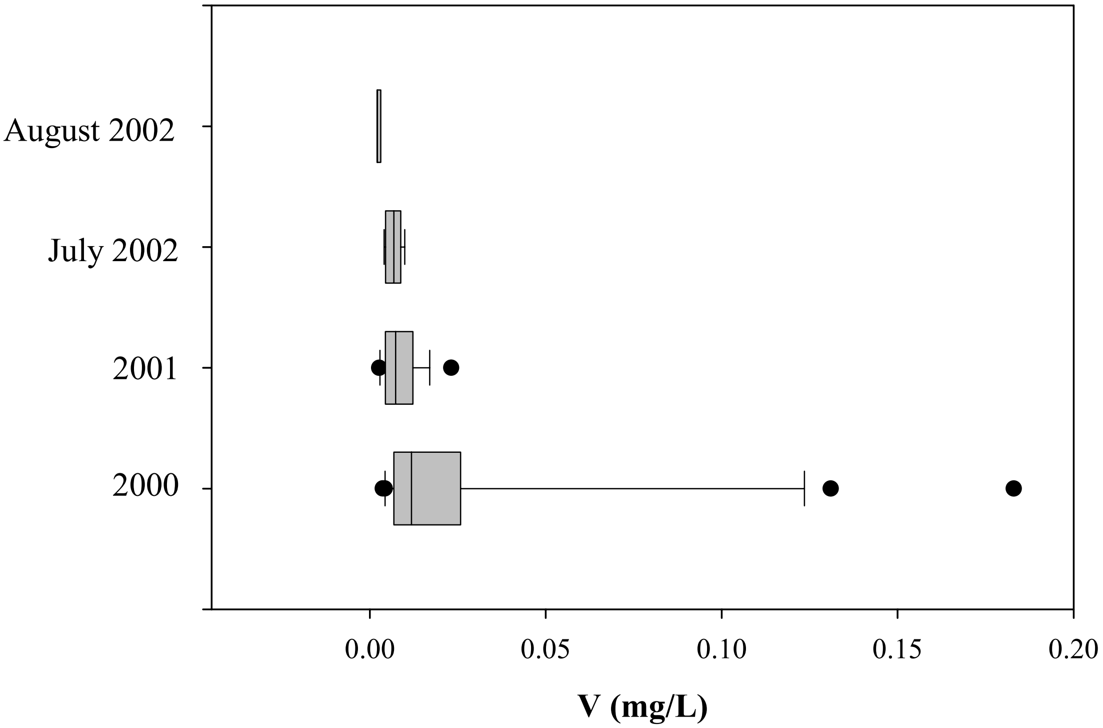
August 2002
July 2002
2001
2000
0.00
0.05
0.10
0.15
0.20
V (mg/L)

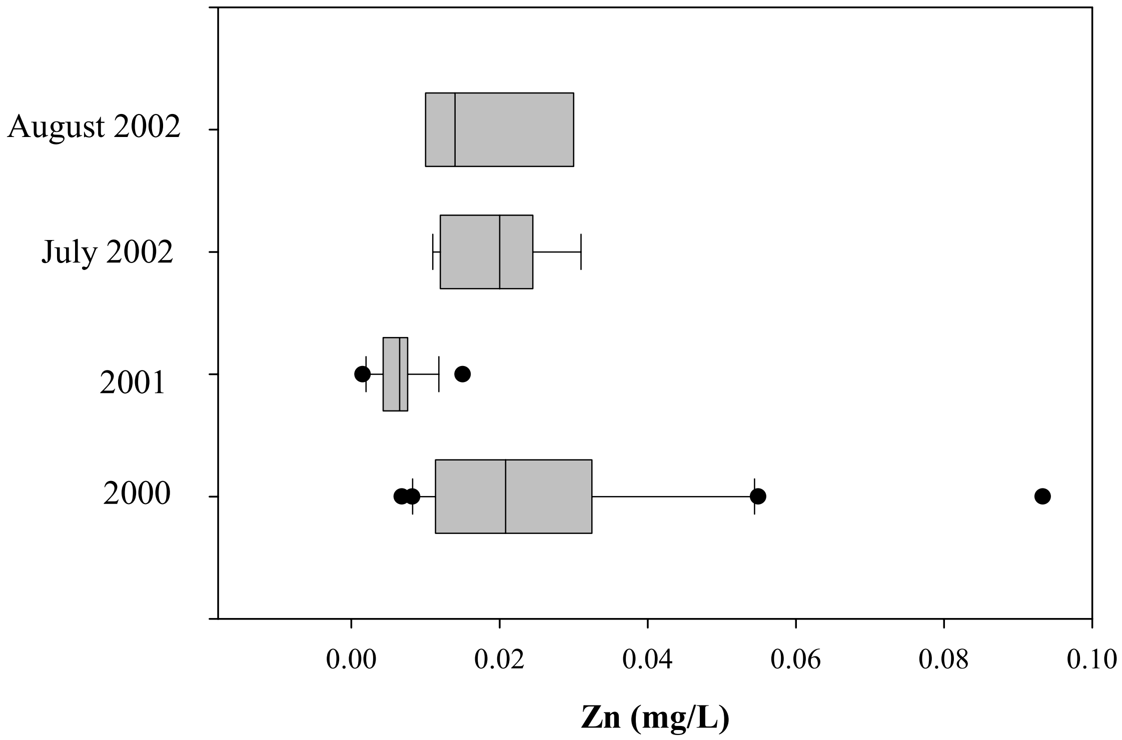
August 2002
July 2002
2001
2000
0.00
0.02
0.04
0.06
0.08
0.10
Zn (mg/L)

B) Dyke B surface water temporal variation plots

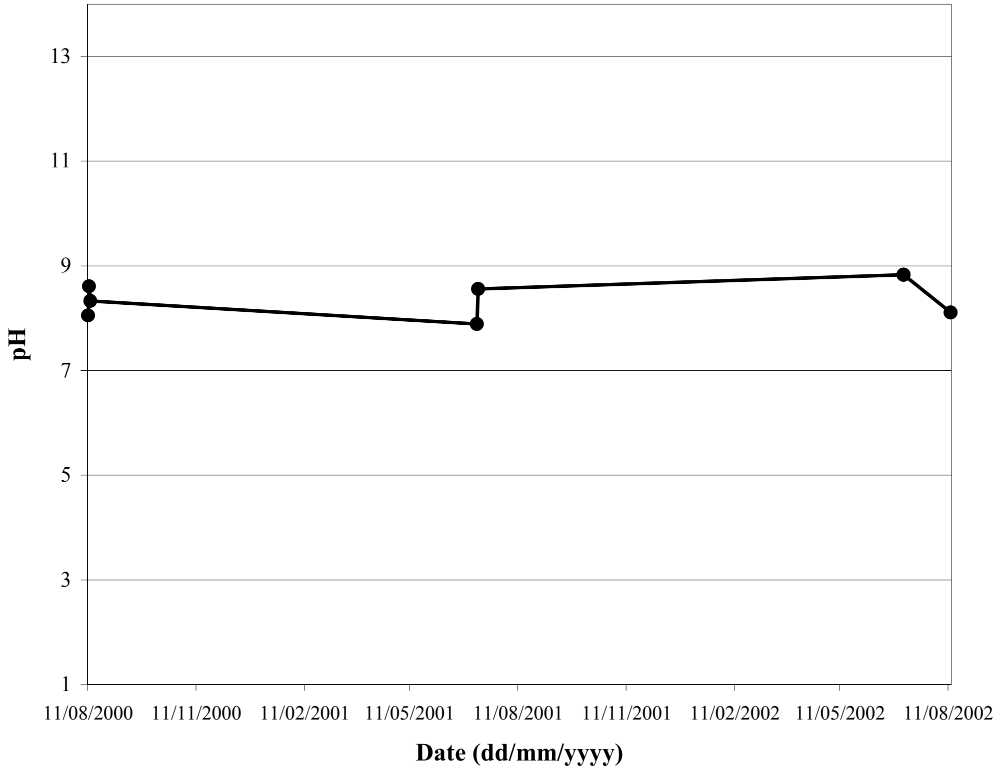

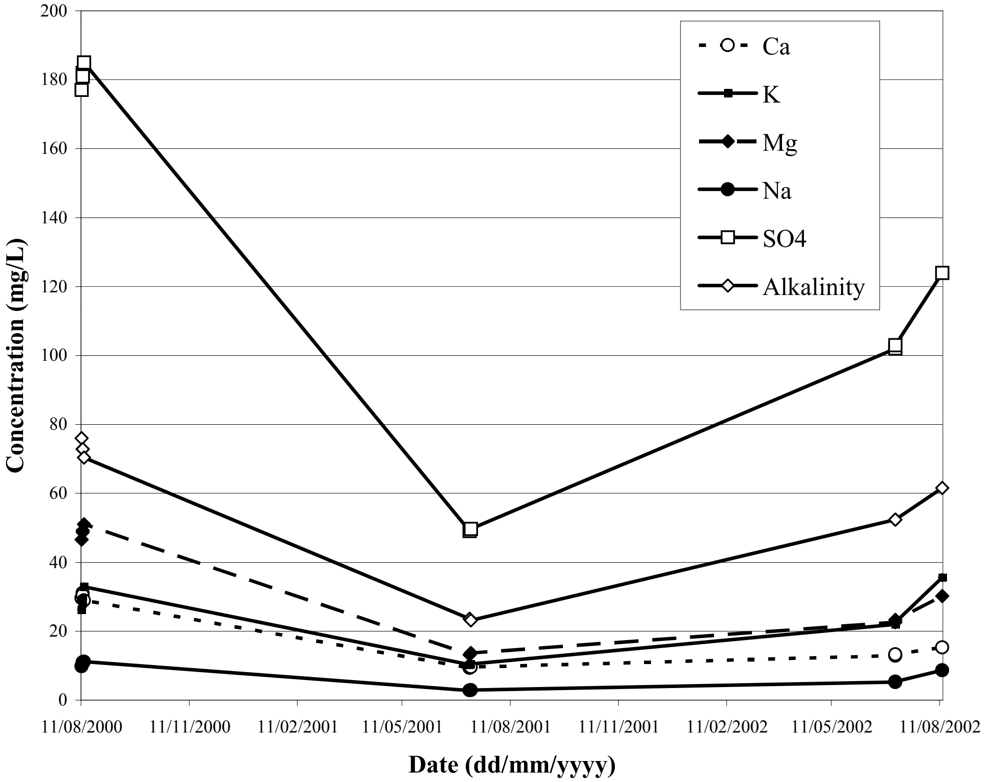

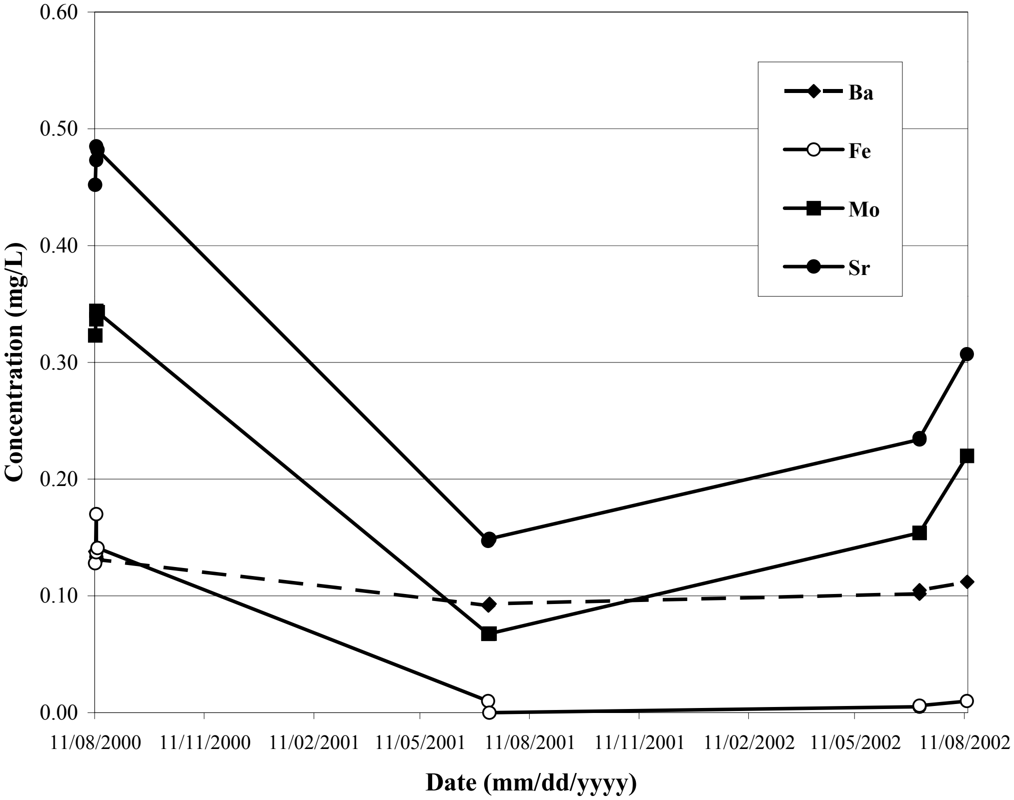
0.60
0.50
0.40
0.30
0.20
0.10
0.00
Concentration (mg/L)
Ba
Fe
Mo
Sr
11/08/2000
11/11/2000
11/02/2001
11/05/2001
11/08/2001
11/11/2001
11/02/2002
11/05/2002
11/08/2002
Date (mm/dd/yyyy)

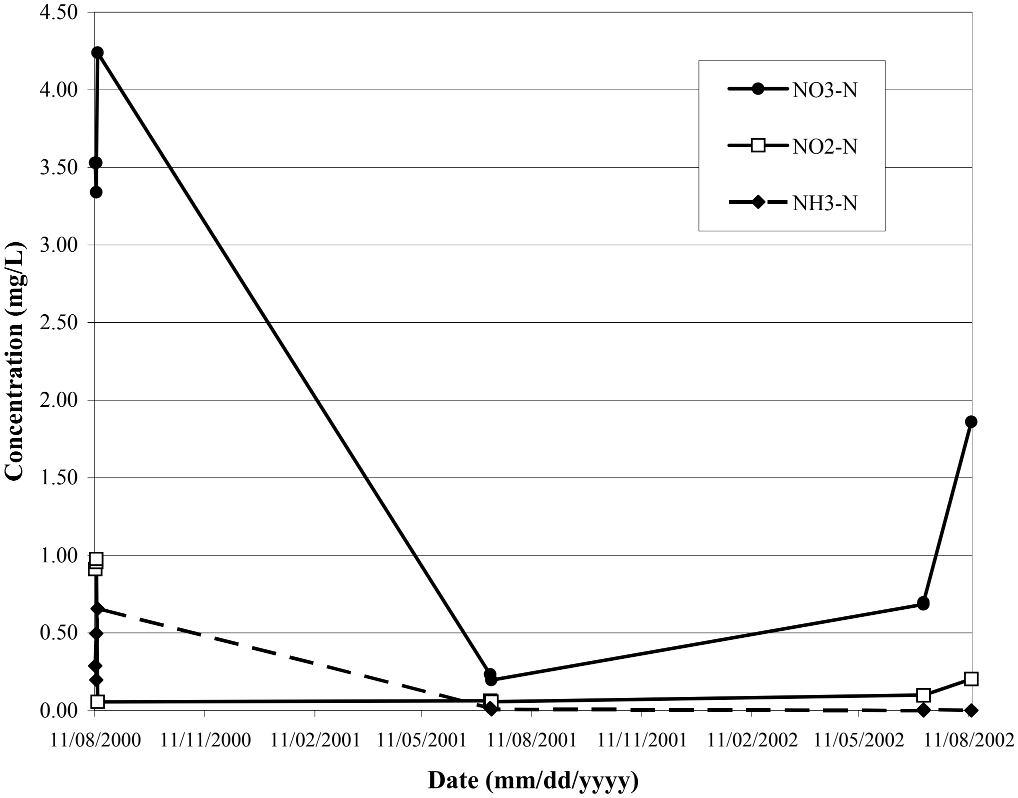
4.50
4.00
3.50
3.00
2.50
2.00
1.50
1.00
0.50
0.00
Concentration (mg/L)
NO3-N
NO2-N
NH3-N
11/08/2000
11/11/2000
11/02/2001
11/05/2001
11/08/2001
11/11/2001
11/02/2002
11/05/2002
11/08/2002
Date (mm/dd/yyyy)

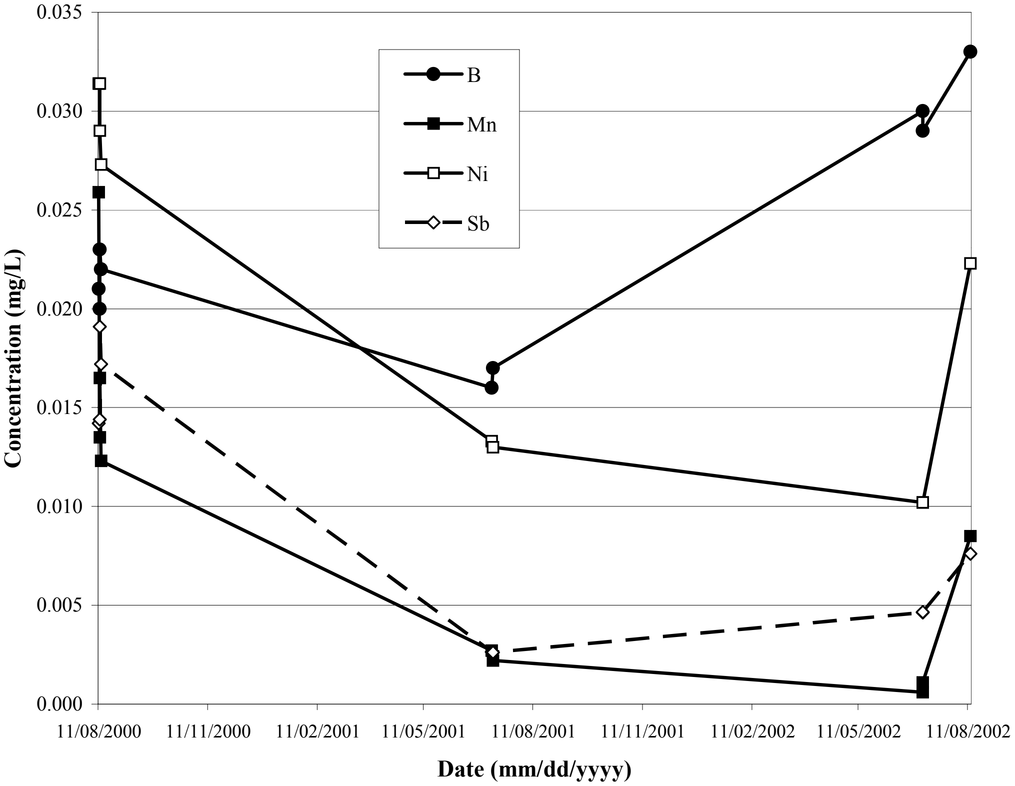

0.035
0.030
0.025
0.020
0.015
0.010
0.005
0.000
Concentration (mg/L)
B
Mn
Ni
Sb
11/08/2000
11/11/2000
11/02/2001
11/05/2001
11/08/2001
11/11/2001
11/02/2002
11/05/2002
11/08/2002
Date (mm/dd/yyyy)

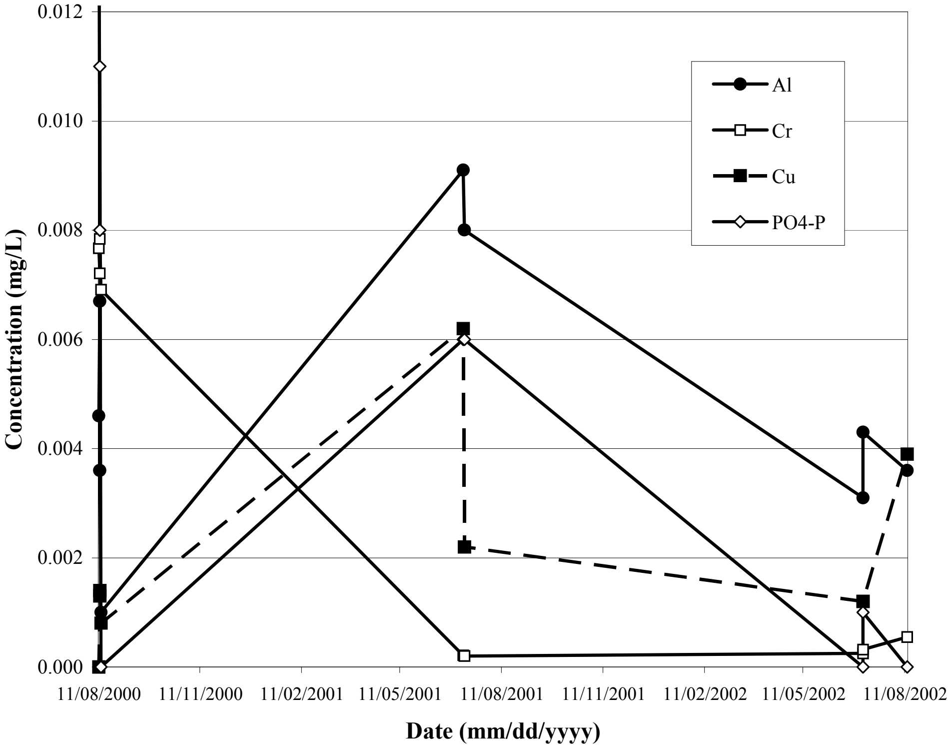

0.012
0.010
0.008
0.006
0.004
0.002
0.000
Concentration (mg/L)
Al
Cr
Cu
PO4-P
11/08/2000
11/11/2000
11/02/2001
11/05/2001
11/08/2001
11/11/2001
11/02/2002
11/05/2002
11/08/2002
Date (mm/dd/yyyy)

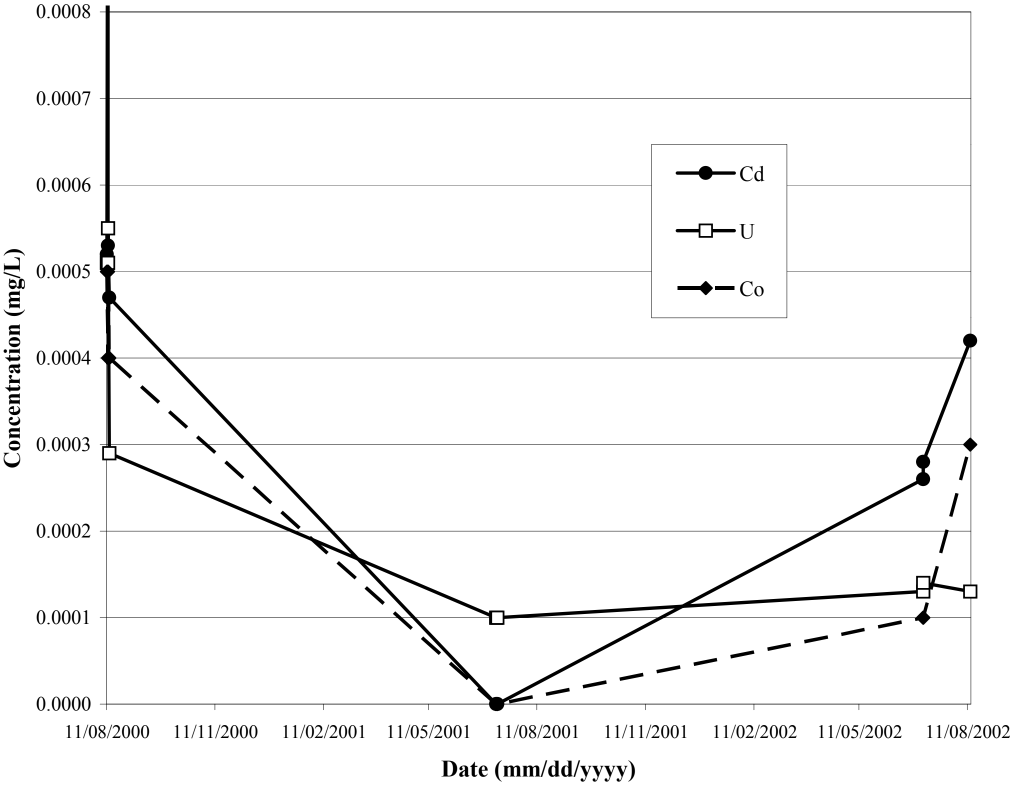
0.0008
0.0007
0.0006
0.0005
0.0004
0.0003
0.0002
0.0001
0.0000
Concentration (mg/L)
11/08/2000
11/11/2000
11/02/2001
11/05/2001
11/08/2001
11/11/2001
11/02/2002
11/05/2002
11/08/2002
Date (mm/dd/yyyy)
Cd
U
Co

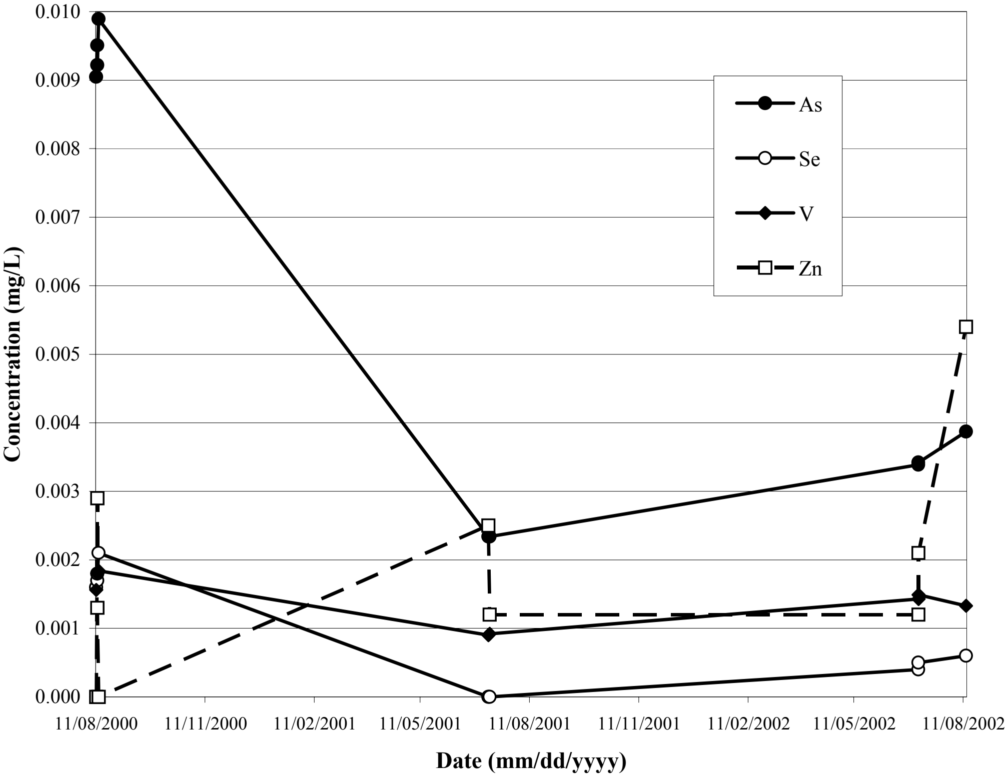
0.010
0.009
0.008
0.007
0.006
0.005
0.004
0.003
0.002
0.001
0.000
Concentration (mg/L)
11/08/2000
11/11/2000
11/02/2001
11/05/2001
11/08/2001
11/11/2001
11/02/2002
11/05/2002
11/08/2002
Date (mm/dd/yyyy)
As
Se
V
Zn

C) Dyke C surface water temporal variation plots

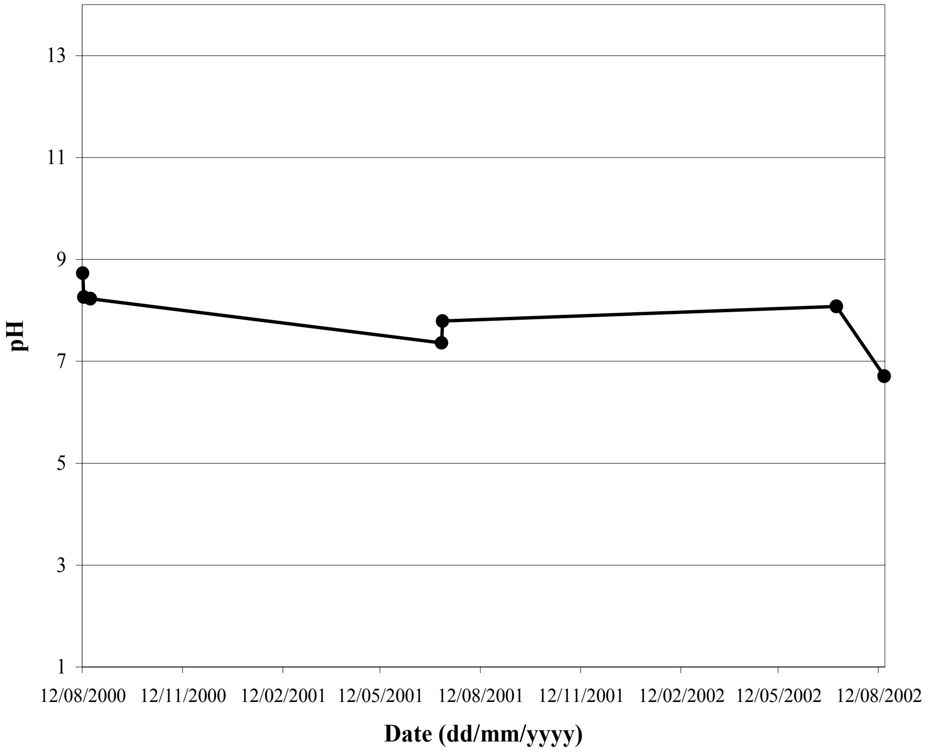

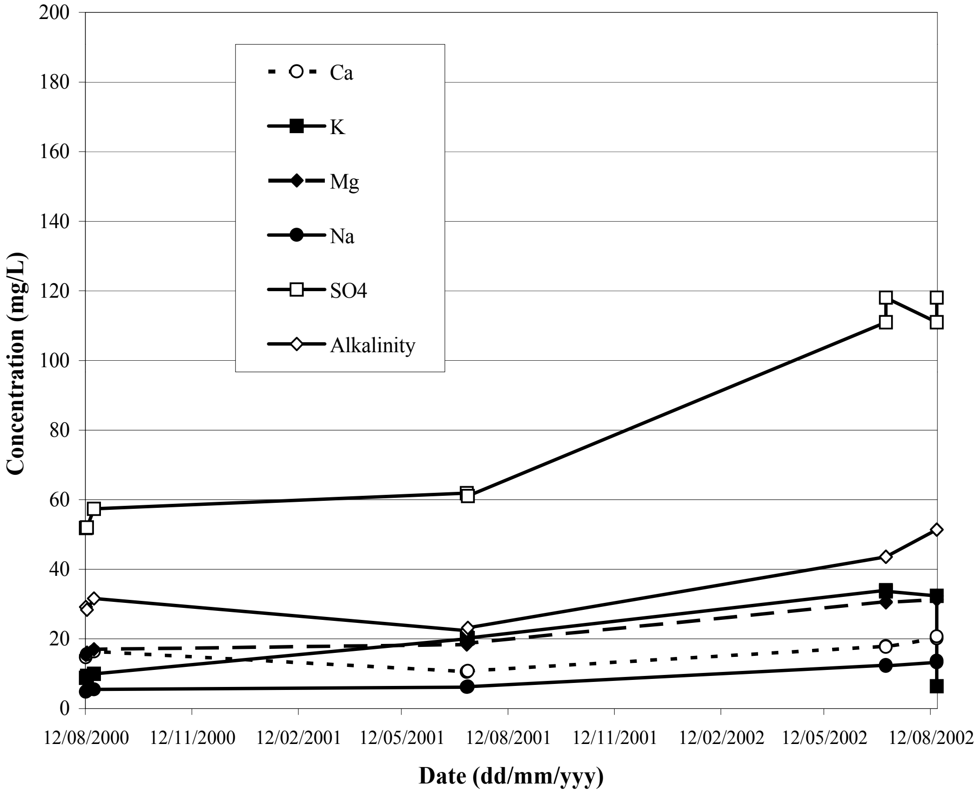

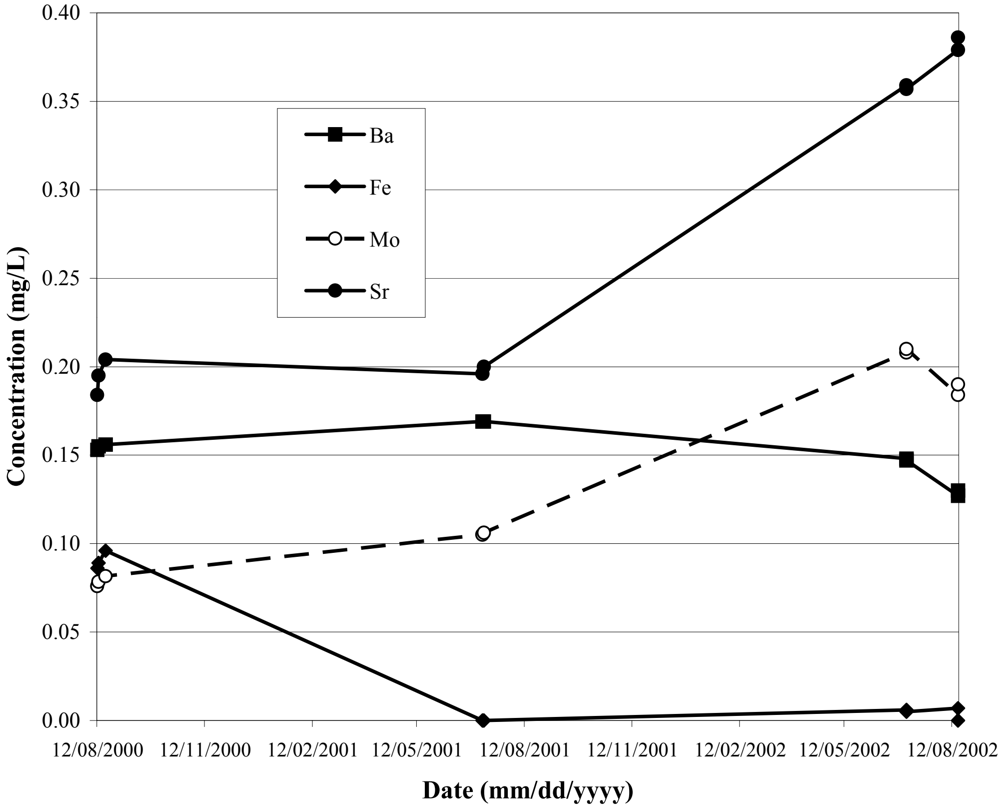
0.40
0.35
0.30
0.25
0.20
0.15
0.10
0.05
0.00
Concentration (mg/L)
Ba
Fe
Mo
Sr
12/08/2000
12/11/2000
12/02/2001
12/05/2001
12/08/2001
12/11/2001
12/02/2002
12/05/2002
12/08/2002
Date (mm/dd/yyyy)

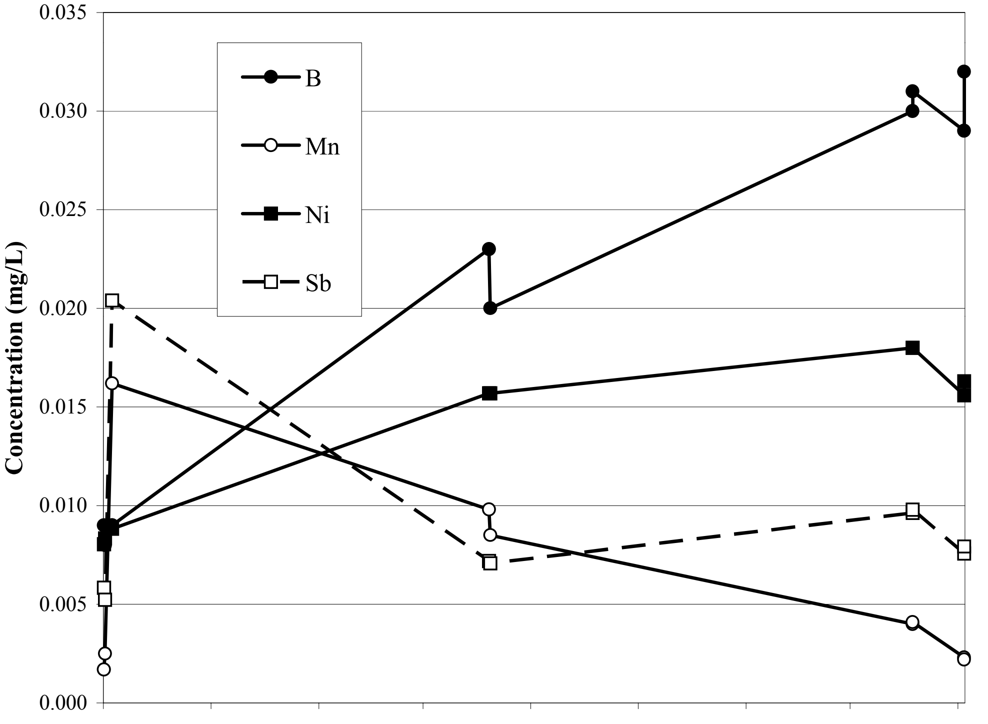
0.035
0.030
0.025
0.020
0.015
0.010
0.005
0.000
Concentration (mg/L)
B
Mn
Ni
Sb
12/08/2000
12/11/2000
12/02/2001
12/05/2001
12/08/2001
12/11/2001
12/02/2002
12/05/2002
12/08/2002
Date (mm/dd/yy)

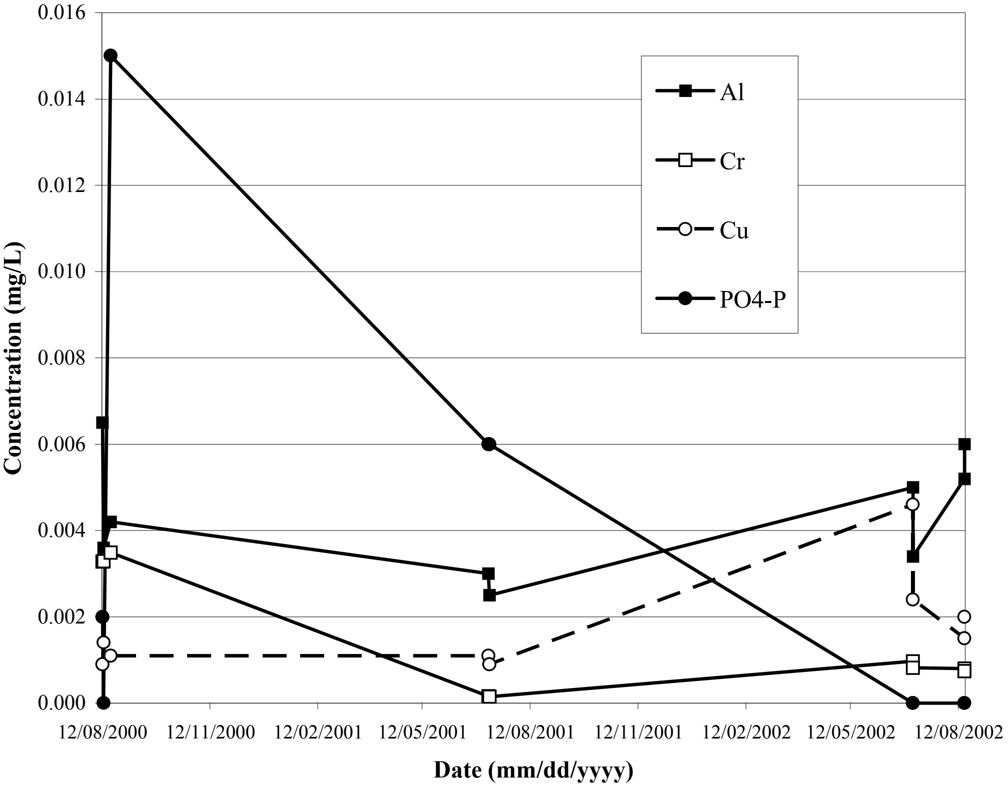
0.016
0.014
0.012
0.010
0.008
0.006
0.004
0.002
0.000
Concentration (mg/L)
Al
Cr
Cu
PO4-P
12/08/2000
12/11/2000
12/02/2001
12/05/2001
12/08/2001
12/11/2001
12/02/2002
12/05/2002
12/08/2002
Date (mm/dd/yyyy)

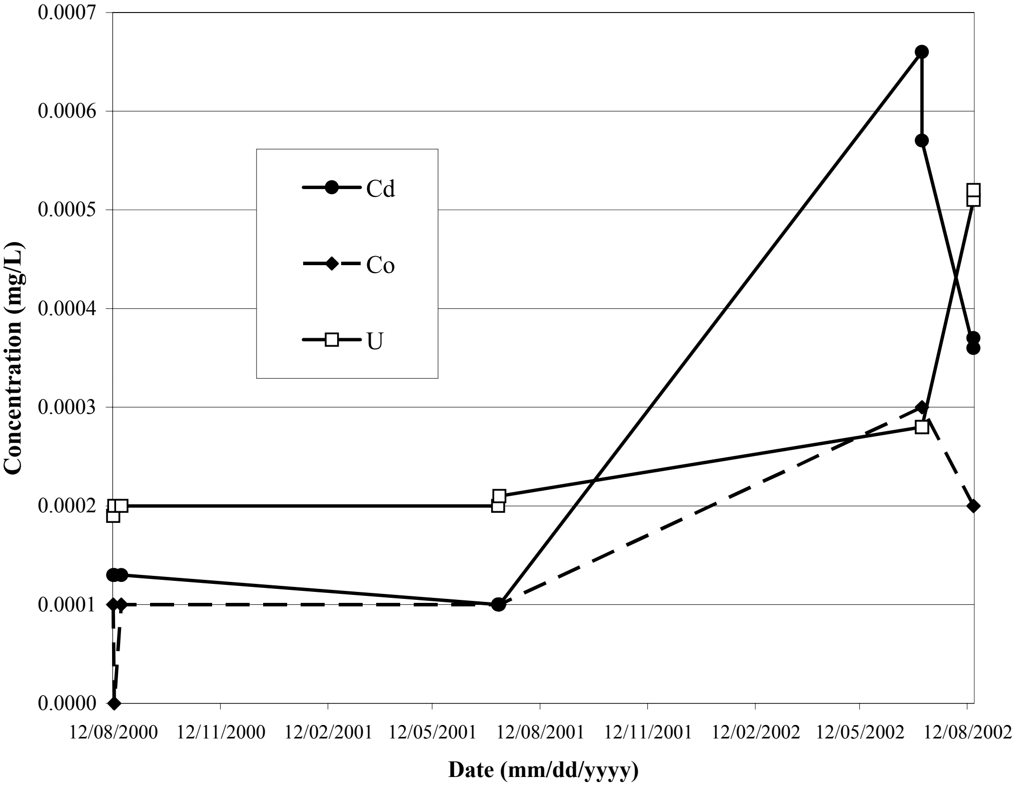
0.0007
0.0006
0.0005
0.0004
0.0003
0.0002
0.0001
0.0000
Concentration (mg/L)
Cd
Co
U
12/08/2000
12/11/2000
12/02/2001
12/05/2001
12/08/2001
12/11/2001
12/02/2002
12/05/2002
12/08/2002
Date (mm/dd/yyyy)

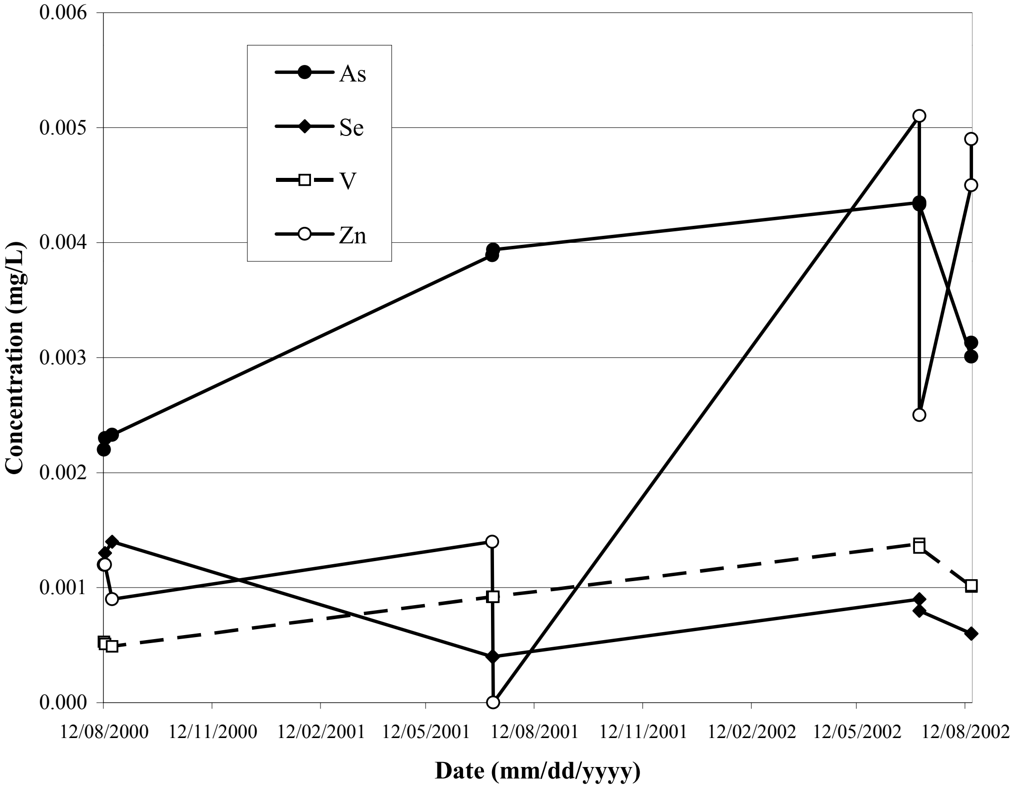

0.006
0.005
0.004
0.003
0.002
0.001
0.000
Concentration (mg/L)
As
Se
V
Zn
12/08/2000
12/11/2000
12/02/2001
12/05/2001
12/08/2001
12/11/2001
12/02/2002
12/05/2002
12/08/2002
Date (mm/dd/yyyy)

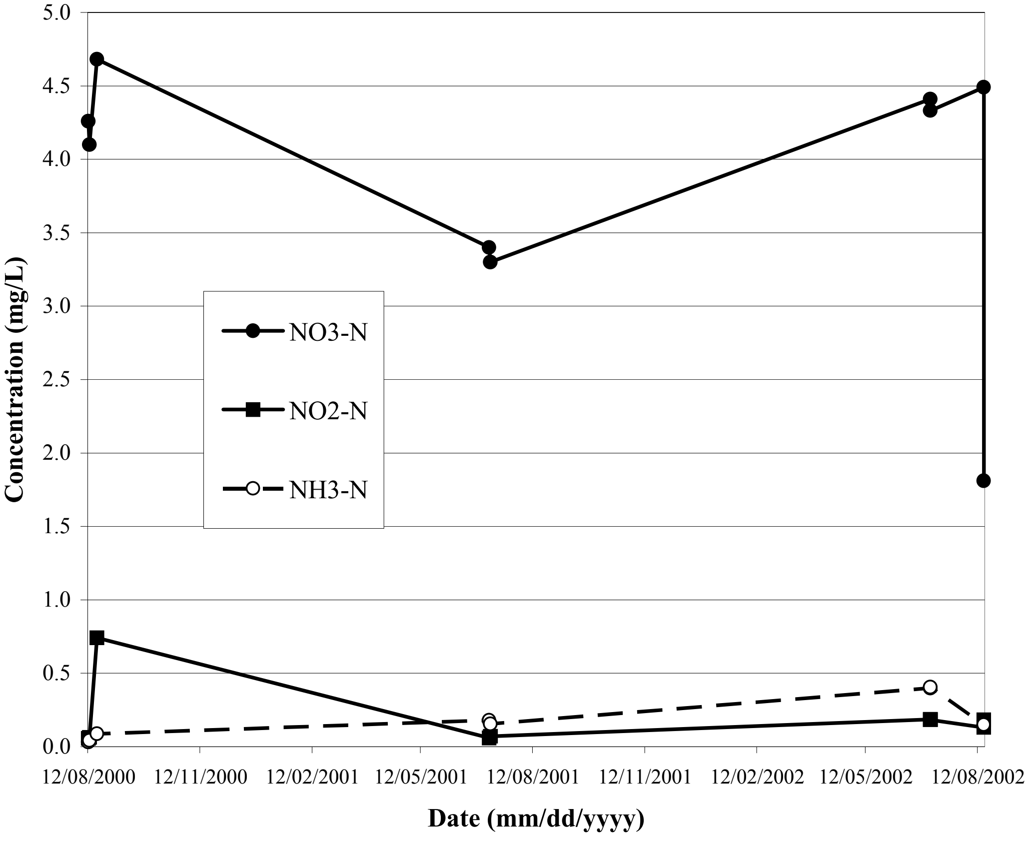

5.0
4.5
4.0
3.5
3.0
2.5
2.0
1.5
1.0
0.5
0.0
Concentration (mg/L)
NO3-N
NO2-N
NH3-N
12/08/2000
12/11/2000
12/02/2001
12/05/2001
12/08/2001
12/11/2001
12/02/2002
12/05/2002
12/08/2002
Date (mm/dd/yyyy)

Appendix C: Electron Microprobe Analyses

This appendix contains electron microprobe analyses for olivine, garnet, and pyroxene from the Panda Kimberlite. All values are reported as weight percent oxides.

Panda Kimberlite Olivine EMPA Analyses (wt. % oxide)

	1	**2**	**3**	**4**	**5**	**6**	**7**
SiO_2	40.47	40.81	40.73	40.75	41.07	40.77	41.16
TiO_2	0.00	0.00	0.00	0.00	0.00	0.00	0.00
Al_2O_3	0.00	0.00	0.00	0.00	0.00	0.00	0.00
Cr_2O_3	0.00	0.00	0.10	0.00	0.11	0.11	0.00
FeO	8.96	7.81	7.98	10.01	8.49	8.60	8.24
MnO	0.18	0.00	0.23	0.00	0.21	0.00	0.15
MgO	50.48	51.56	51.57	49.58	50.61	50.24	51.30
CaO	0.09	0.00	0.00	0.09	0.07	0.00	0.10
Na_2O	0.39	0.61	0.56	0.00	0.00	0.00	0.00
K_2O	0.00	0.04	0.00	0.00	0.03	0.00	0.00
SUM	100.57	100.84	101.17	100.42	100.59	99.72	100.96

	8	**9**	**10**	**11**	**12**	**13**	**14**
SiO_2	41.74	41.04	40.80	40.82	42.25	41.01	41.73
TiO_2	0.00	0.00	0.00	0.00	0.00	0.00	0.00
Al_2O_3	0.00	0.00	0.00	0.00	0.00	0.00	0.00
Cr_2O_3	0.00	0.13	0.00	0.00	0.00	0.00	0.11
FeO	7.13	7.88	9.02	8.32	7.24	8.90	5.92
MnO	0.22	0.33	0.00	0.10	0.17	0.26	0.00
MgO	50.92	50.21	48.68	48.92	51.73	50.37	52.56
CaO	0.06	0.13	0.05	0.11	0.00	0.00	0.00
Na_2O	0.37	0.30	0.27	0.49	0.71	0.65	0.79
K_2O	0.00	0.00	0.00	0.00	0.00	0.00	0.00
SUM	100.43	100.03	98.83	98.76	102.10	101.19	101.11

Panda Kimberlite Garnet EMPA Analyses (wt. % oxide)

	1	2	3	4	5	6	7	8
SiO_2	41.59	41.52	40.82	40.65	40.82	39.82	41.57	40.96
TiO_2	0.62	0.16	0.35	0.10	0.00	0.00	0.51	0.00
Al_2O_3	18.69	17.61	18.85	16.38	14.98	17.58	19.09	17.68
Cr_2O_3	5.30	7.76	5.41	9.15	11.08	6.77	5.02	7.61
FeO	8.21	6.43	8.30	7.00	6.56	11.95	7.79	6.43
MnO	0.22	0.19	0.27	0.42	0.60	0.83	0.47	0.46
MgO	19.99	21.00	18.77	19.89	19.76	15.67	21.40	21.05
CaO	6.93	6.14	7.79	6.70	6.56	7.15	5.02	6.16
Na_2O	0.10	0.00	0.00	0.00	0.00	0.00	0.00	0.00
K_2O	0.00	0.00	0.00	0.00	0.08	0.05	0.00	0.00
SUM	101.63	100.81	100.55	100.28	100.43	99.82	100.87	100.36

Panda Kimberlite Pyroxene Analyses (wt. % oxide)

	1	2	3	4	5	6	7	8	9	10
SiO_2	59.32	58.70	54.42	57.74	57.61	58.74	58.62	58.09	59.53	47.65
TiO_2	0.00	0.00	0.07	0.15	0.15	0.00	0.00	0.00	0.07	0.89
Al_2O_3	0.34	0.38	4.57	0.33	0.32	0.39	0.26	0.29	0.34	7.87
Cr_2O_3	0.33	0.31	0.42	0.42	0.31	0.41	0.21	0.23	0.24	0.00
FeO	4.50	4.50	6.12	4.70	4.75	4.31	5.72	5.29	4.62	14.66
MnO	0.12	0.09	0.00	0.09	0.21	0.12	0.00	0.08	0.08	0.33
MgO	38.40	37.40	31.50	34.84	34.70	35.46	37.11	36.99	38.66	13.22
CaO	0.33	0.51	0.81	0.45	0.52	0.67	0.58	0.72	0.14	12.60
Na_2O	0.34	0.42	0.00	0.00	0.00	0.00	0.30	0.50	0.52	1.05
K_2O	0.00	0.00	0.00	0.00	0.00	0.00	0.00	0.05	0.00	0.62
SUM	103.67	102.31	97.91	98.73	98.57	100.10	102.81	102.24	104.20	98.89

Appendix D: Sulphate-S, Sulphide-S, and Inorganic-C Analyses

This appendix contains total-S, sulphate-S, sulphide-S, and inorganic-C concentrations for mud xenoclast, kimberlite ore, and processed kimberlite fines samples. All sulphur concentrations are reported as weight percent S and inorganic-C data are reported as weight percent CO_2.

Sulphate-S, Sulphide-S, and Inorganic-C analyses

Sample	Type	Total-S (wt. %) d.l. = 0.01	Sulphate-S (wt. %) d.l. = 0.01	Sulphide-S[†] (wt. %) d.l. = 0.01	Inorganic-C (wt. % CO_2) d.l. = 0.2
PP01B	Mud xenoclast	2.84	0.23	2.61	0.4
PP02B*	Mud xenoclast	2.76	0.17	2.59	0.4
PP03B	Mud xenoclast	1.79	0.2	1.59	0.7
PP15B	Mud xenoclast	3.78	0.38	3.4	0.6
PP20B	Mud xenoclast	2.83	0.27	2.56	0.5
PP21B	Mud xenoclast	2.87	0.36	2.51	0.4
PP08	Kimberlite ore	0.32	0.12	0.2	1.1
PP17*	Kimberlite ore	0.36	0.14	0.22	1.1
PP19	Kimberlite ore	0.36	0.16	0.2	2
00-LLC-30	Kimberlite fines	0.41	0.12	0.29	2.9
00-LLC-46	Kimberlite fines	0.27	0.04	0.23	2.4
01-LLC-8	Kimberlite fines	0.45	0.08	0.37	2.9
00-LLG-36	Kimberlite fines	0.32	0.03	0.29	3
01-LLC-19	Kimberlite fines	0.24	0.02	0.22	2.1
01-LLG-16	Kimberlite fines	0.36	0.05	0.31	2.2
01-LLG-33	Kimberlite fines	0.35	0.03	0.32	3.2
01-LLK-25	Kimberlite fines	0.23	0.03	0.2	1.3
01-LLD-25*	Kimberlite fines	0.19	0.04	0.15	1.4
01-LLM-59	Kimberlite fines	0.4	0.05	0.35	2.6
01-LLM-46	Kimberlite fines	0.25	0.03	0.22	2.4
01-LLD-46*	Kimberlite fines	0.25	0.02	0.23	1.8
01-LLM-26	Kimberlite fines	0.3	0.03	0.27	2.8
00-LLG-60	Kimberlite fines	0.26	0.02	0.24	1.8
00-LLD-60*	Kimberlite fines	0.22	0.01	0.21	2.6
01-LLK-51	Kimberlite fines	0.21	0.01	0.2	2.7
00-LLG-21	Kimberlite fines	0.19	0.02	0.17	2.3

*denotes duplicate of the sample immediately above

[†] calculated by subtracting sulphate-S from Total-S (see section 3.4.2.2)

H. Andrew Rollo

Education

2000-2003	M.Sc. Candidate in Geological Sciences Department of Geological Sciences and Geological Engineering, Queen's University, Kingston, ON, Canada. *Thesis title:* Processed Kimberlite-Water Interactions in Diamond Mine Waste, Ekati Diamond Mine, N.W.T., Canada *Supervisor:* Dr. Heather Jamieson
1994-1999	B.Sc. (Honours) in Geological Sciences Department of Earth and Ocean Sciences, University of British Columbia, Vancouver, BC, Canada. *Thesis title:* Mineralogy and Geochemistry of Mica Minerals from the Little Nahanni Pegmatite Group, Northwest Territories. *Supervisor:* Dr. Lee Groat

Teaching Experience

2000-2003	Teaching assistant (Queen's University) ▪ Introductory Geology (APSC 151) ▪ Quaternary Geology (GEOL 323) ▪ Introductory GIS (GEOL 463/863) ▪ Applied Aqueous Geochemistry (GEOL 485/885)
1999-2000	Geology Laboratory Coordinator/Supervisor and Instructor (UBC) ▪ Introductory Geology for Science and Engineering

Professional Experience

July – August 2000	Summer Geochemistry Student, Environment Department, Ekati Diamond Mine, N.W.T., Canada
1998-2000	Mineralogy Laboratory Manager, Mineralogical Research Group, Department of Earth and Ocean Sciences, UBC, Vancouver, B.C. Canada
July-August 1998	Geological Field/Exploration Assistant, Inmet Mining Corporation, Vancouver, B.C., Canada
1997-1998	Geological Information Technician, Tombstone Explorations Co. Ltd., Vancouver, B.C., Canada
July-August 1997	Geological Field/Exploration Assistant, Imperial Metals Corporation, Vancouver, B.C., Canada

Awards

Queen's University

2003	Canadian Water Resource Association Scholarship
2002-2003	NSERC Northern Research Postgraduate Scholarship Supplement
2001-2002	NSERC Northern Research Postgraduate Scholarship Supplement
2001-2002	NSERC Postgraduate Scholarship 'A'

University of British Columbia

1999	NSERC Undergraduate Research Award
1994-1999	UBC Dean of Science Honours List
1998	Aaron Craig Nicholls Memorial Award
1997	Walter D. Frith Scholarship
1996-1998	Thomas and Marguerite MacKay Scholarship
1996	J. Fred Muir Memorial Scholarship

Publications and Technical Reports

Groat, L.A., Mulja, T., Ercit, T.S., Mauthner, M.H.F., Raudsepp, M., Gault, R.A., Rollo, H.A. (2003). Geology and Mineralogy of the Little Nahanni Rare-Element Granitic Pegmatites, Northwest Territories. Canadian Mineralogist, 41(1): 139-160.

Rollo, H.A., Jamieson (2003). Processed Kimberlite-Water Interactions in Diamond Mine Waste, Ekati Diamond Mine, N.W.T., Canada. In: Geological Association of Canada/Mineralogical Association of Canada/Society of Economic Geologists Annual General Meeting, Vancouver, B.C., Abstract Volume, 28: No. 227.

Rollo, H.A., Jamieson (2003). Processed Kimberlite-Water Interactions in Diamond Mine Waste, Ekati Diamond Mine, N.W.T., Canada. In: 8th International Kimberlite Conference, Victoria, B.C., Extended Abstracts Volume: No. 286.

Rollo, H.A., Jamieson, H.E. (2003). Mineral-Water Interactions in Diamond Mine Waste, Ekati Diamond Mine, Canada. In: International Symposium on Environmental Geochemistry, Edinburgh, Scotland, Abstracts Volume (*in press)*.

Rollo, H.A., Jamieson, H.E. (2002). Mineral-Water Interactions in the Long Lake Containment Facility, Ekati Diamond Mine, N.W.T.: Progress Report # 4. Submitted to Ekati Environment Department, 36 pp.

Rollo, H.A., Jamieson, H.E. (2002). Mineral-Water Interactions in the Long Lake Containment Facility, Ekati Diamond Mine, N.W.T.: Progress Report # 3. Submitted to Ekati Environment Department, 38 pp.

Rollo, H.A., Jamieson, H.E. (2001). Mineral-Water Interactions in the Long Lake Containment Facility, Ekati Diamond Mine, N.W.T.: Progress Report # 2. Submitted to Ekati Environment Department, 28 pp.

Rollo, H.A., Jamieson, H.E. (2001). Mineral-Water Interactions in the Long Lake Containment Facility, Ekati Diamond Mine, N.W.T.: Progress Report # 1. Submitted to Ekati Environment Department, 40 pp.

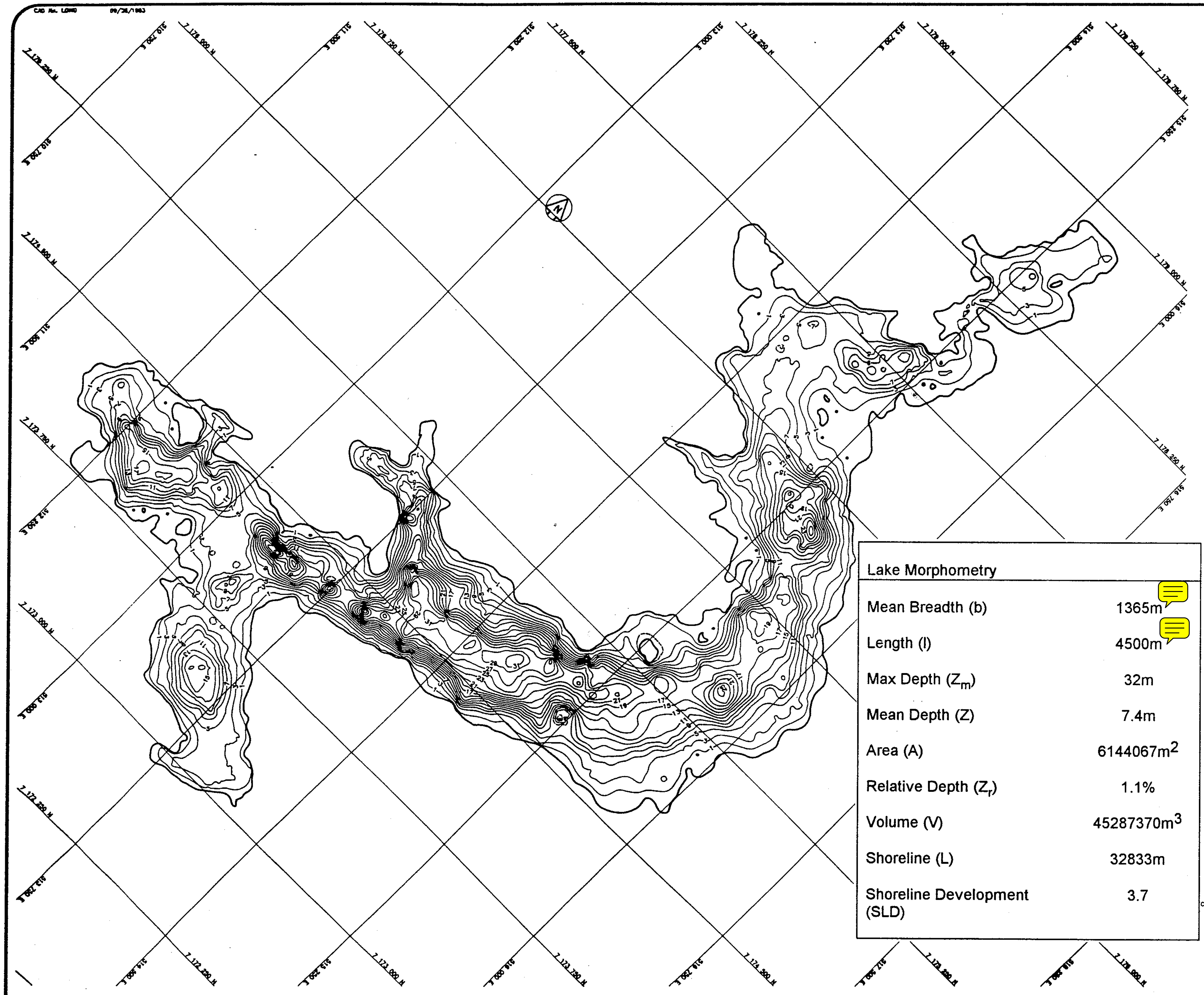

Lake Morphometry

Mean Breadth (b)	1365m
Length (l)	4500m
Max Depth (Z_m)	32m
Mean Depth (Z)	7.4m
Area (A)	6144067m^2
Relative Depth (Z_r)	1.1%
Volume (V)	45287370m^3
Shoreline (L)	32833m
Shoreline Development (SLD)	3.7

DEPTH (m)	PERIMETER (m)	AREA (sq. m.)	VOLUME (cu. m.)
0.00	704.13+29.78+29.78		
0.00	+29.78+29.78+29.78		
0.00	+29.78+63.81+298.83		
0.00	+29.78+29.78+29.78		
0.00	+29.78+29.78+29.78		
0.00	+29.78+29.78+29.78		
0.00	+29.78+29.78+29.78		
0.00	+358.18+172.34+240.86		
0.00	+101.59+44.88+80.19		
0.00	+44.08+153.07+29.78		
0.00	+29067.77	6144068.50	
1.00	23788.59+140.57+80.30		
1.00	+63.86+2302.10+107.44		
1.00	+484.18	4893078.31	5518571.41
2.00	23542.96+104.43+88.35		
2.00	+148.55+1302.11+55.88		
2.00	+239.05	4337180.56	4615133.43
3.00	22583.42+71.38+128.38		
3.00	+117.34+81.13+172.79		
3.00	+1214.57+118.29+273.96		
3.00	+140.37	3846866.82	4091438.73
4.00	2057.04+19845.71+87.33		
4.00	+85.87+154.44+800.08		
4.00	+33.75+481.29+312.10	3270818.71	3558292.32
5.00	1891.53+13443.82+511.05		
5.00	+2855.91+448.86+1423.96		
5.00	+378.43+94.50+365.79	2839037.29	3054929.50
6.00	1525.25+13217.42+368.37		
6.00	+2720.38+342.70+1324.07		
6.00	+362.73	2539723.84	2685380.57
7.00	1396.87+12281.31+182.39		
7.00	+748.85+2406.38+108.35		
7.00	+98.11+1198.08+153.98	2310006.53	2424885.22
8.00	1303.70+11887.83+65.79		
8.00	+468.78+2289.75+1058.11	2118937.86	2214472.22
9.00	1228.18+11810.31+375.84		
9.00	+2200.69+1018.28+79.24		
9.00	+118.65	1948727.81	2032832.83
10.00	1155.82+11334.87+281.78		
10.00	+2148.59+297.08+442.91		
10.00	+180.13	1781382.53	1864040.17
11.00	1031.28+11387.72+115.2?		
11.00	+52.32+388.89+1705.87		
11.00	+89.82+191.80+148.94		
11.00	+114.64	1618700.41	1700028.47
12.00	775.19+889.89+8748.80		
12.00	+179.01+1606.71+70.45		
12.00	+40.82+1770.81	1461364.44	1540042.43
13.00	789.27+1455.53+58.94		
13.00	+1465.88+1702.61+401.98		
13.00	+7348.70	1322500.07	1391942.29
14.00	1068.36+693.39+1394.48		
14.00	+1653.01+302.79+287.24		
14.00	+7445.80	1186594.23	1254547.15
15.00	546.54+973.41+1303.87		
15.00	+1388.34+53.48+36.83		
15.00	+167.81+247.87+7392.66	1042496.28	1114545.25
16.00	24.48+414.93+891.85		
16.00	+136.35+746.50+1460.74		
16.00	+184.09+135.14+218.03		
16.00	+1326.58+5804.36	892514.44	967555.35
17.00	99.18+71.92+787.48		
17.00	+240.03+250.88+237.03		
17.00	+1274.85+4729.52+102.70		
17.00	+187.57+83.18+92.11		
17.00	+807.75+846.89	748536.04	820674.74
18.00	718.70+96.86+72.28		
18.00	+509.35+88.51+1227.35		
18.00	+4869.98+85.49+160.26		
18.00	+141.32+72.54+896.88	650692.90	699713.97
19.00	688.16+457.11+270.41		
19.00	+1212.70+4266.52+132.33		
19.00	+611.28	564776.45	607834.66
20.00	632.58+107.88+58.35		
20.00	+188.80+840.50+240.17		
20.00	+4144.48+102.20+538.95	494318.52	529547.49
21.00	589.71+602.87+178.24		
21.00	+4049.09+66.86+471.81	438799.89	466558.11
22.00	215.27+296.82+420.96		
22.00	+222.83+115.83+3940.79		
22.00	+404.63	383948.20	411374.45
23.00	180.58+233.99+353.58		
23.00	+65.99+53.46+3618.01		
23.00	+335.24	336368.03	360653.82
24.00	144.21+204.47+296.69		
24.00	+253.69+3275.12+205.51		
24.00	+260.24	290085.31	312726.87
25.00	100.13+109.79+140.57		
25.00	+249.28+119.55+186.27		
25.00	+164.12+2780.74+166.06	244896.11	267495.71
26.00	87.13+165.48+77.77		
26.00	+119.21+110.86+2747.52		
26.00	+133.79	206329.67	225812.89
27.00	65.91+122.29+58.73		
27.00	+63.09+2601.50+70.06		
27.00	+106.60	169757.28	188043.46
28.00	48.07+32.80+2571.86		
28.00	+82.51	132096.48	150927.87
29.00	233.22+665.75+1569.70		
29.00	+55.68	89061.96	110673.22
30.00	190.62+408.48+393.88		
30.00	+64.57+433.01+311.06		
30.00	+28.66	41966.89	66510.42
31.00	66.34+284.60+183.46		
31.00	+329.19+221.81	16382.50	29165.69
32.00	142.06+124.89	2599.45	9480.97

Cumulative Volume = 45287370.29 (cu. m.)

0 75 150 300 450 600 750 m

Scale 1 : 22500

BHP

LONG LAKE

NORTHWEST TERRITORIES

Rescan

CAD No. NANCY 10/06/1993

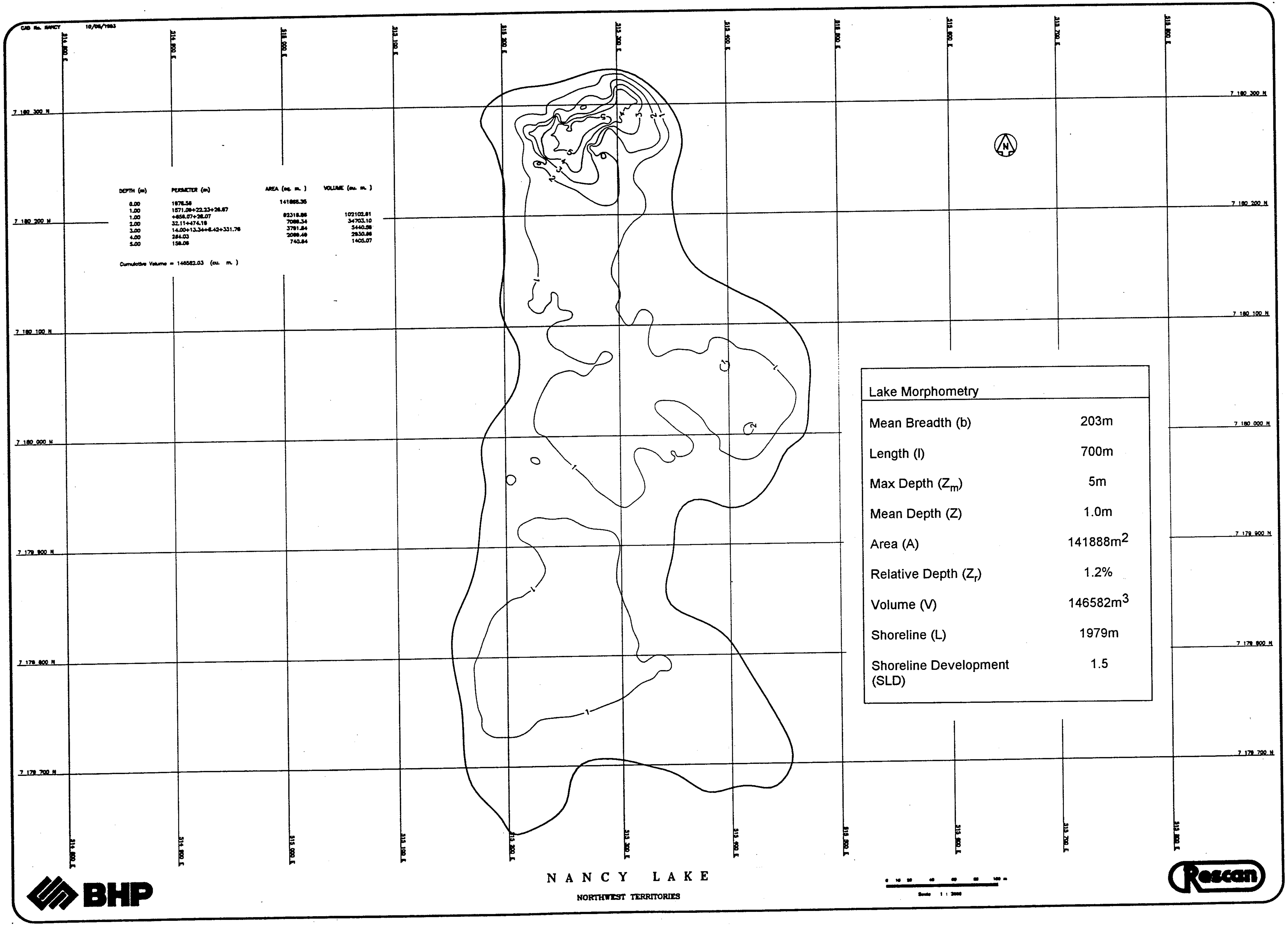

DEPTH (m)	PERIMETER (m)	AREA (sq. m.)	VOLUME (cu. m.)
0.00	1978.58	141888.35	
1.00	1571.09+22.23+26.67		
1.00	+858.07+28.07	82318.86	102102.81
2.00	32.11+474.18	7088.34	34703.10
3.00	14.00+13.34+8.42+331.78	3791.84	5440.58
4.00	284.03	2089.40	2930.86
5.00	158.08	740.84	1405.07

Cumulative Volume = 146582.03 (cu. m.)

Lake Morphometry

Mean Breadth (b)	203m
Length (l)	700m
Max Depth (Z_m)	5m
Mean Depth (Z)	1.0m
Area (A)	141888m^2
Relative Depth (Z_r)	1.2%
Volume (V)	146582m^3
Shoreline (L)	1979m
Shoreline Development (SLD)	1.5

NANCY LAKE

NORTHWEST TERRITORIES

BHP

Rescan